Lipid bilayers and interfaces

Promotoren:

prof. dr. M.A. Cohen Stuart
hoogleraar Fysische chemie met bijzondere aandacht voor de kolloïdchemie
Wageningen Universiteit

prof. dr. ir. F.A.M. Leermakers
persoonlijk hoogleraar bij de leerstoelgroep Fysische chemie en kolloïdkunde
Wageningen Universiteit

Copromotor:

dr. J.M. Kleijn
universitair docent bij de leerstoelgroep Fysische chemie en kolloïdkunde
Wageningen Universiteit

Promotiecommissie:

prof. dr. E.J.R. Sudhölter (Technische Universiteit Delft)
prof. dr. W.J. Briels (Universiteit Twente)
prof. dr. J.A. Killian (Universiteit Utrecht)
prof. dr. A.M.C. Emons (Wageningen Universiteit)

Lipid bilayers and interfaces

Richard A. Kik

Contents

Chapter 1

Introduction

1.1   Introduction

The lipid bilayer membrane is probably the most important structure in living organisms because it separates the protoplasm, i.e., the substance inside the cell where the nucleus and the cell organelles reside, from the extra cellular environment. Inside the cell membranes play also an important role as a highly permeation-selective barrier, which separates the cell organelles and nucleus from the cytoplasm. Moreover, they are actively involved in a large array of metabolic processes. Until approximately 1895 it was unknown what type of molecules form a membrane.

Charles Ernest Overtone was the first who, more or less accidentally, found that non-polar substances have the ability to pass surprisingly quickly across membranes of plant and animal cells [3,4]. From this observation he concluded that the molecules of a membrane are of a special type, which he called lipoids. He discovered that the solubility of the substances in lipoids determined to a large extent the penetration speed of these molecules.

In 1917, Irving Langmuir gained some initial information about the type of molecules. He performed research on oil films [5] by using an improved version of an apparatus originally developed by Agnes Pockels, that later became known as the Langmuir trough. He proved that information could be retrieved on the orientation, shape and size of these molecules by varying the air/water surface area, and he proposed that lipid molecules present on the air/water interface are oriented in such a way that their (hydrophobic) tails were pointing to the air and the (hydrophilic) headgroups reside in the aqueous phase.

In 1925 Gorter and Grendel used the same technique as Langmuir to determine the amount of lipids in erythrocytes (red blood cells) of several different animals [6]. They first isolated the lipids, put them on the air/water interface, and then compressed them to a certain surface pressure in the Langmuir trough and found that the ratio between this lipid area and the erythrocytes surface area was always approximately two. This led them to the conclusion that a membrane consists of two layers of lipids where the lipid tails are oriented towards each other and the
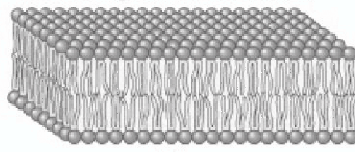
Figure 1.1: Shematic representation of a lipid bilayer. The lipid tails are present at the interior of the lipid bilayer, while the headgroups are oriented to the aqueous solution.

headgroups are exposed on the outside of this bilayer (figure 1.1). It is interesting to note that it was discovered later that this experiment contained two severe errors. The first one was that by far not all lipids were extracted from the erythrocytes, and the second one was that the erythrocytes area was largely underestimated. In retrospect it turned out that these two mistakes most fortunately neutralised each other. The true ratio indeed is of the order of two.

At the time Gorter and Grendell proposed their model, they did not get serious attention from the scientific community, because most scientist focused on another membrane model. In this competing model the membrane was regarded as a impenetrable barrier with some pores in it with some particular size. This model implied a size-dependent transport of molecules across the membrane, i.e., smaller molecules pass faster through the membrane than larger ones. This idea explained some, but not all data, and it was gradually becoming clear that the membrane is not a sheet with small holes.

Almost ten years later the lipid membrane model was accepted by the majority of the researchers, in part because of studies by Danielli and Harvy [7]. These researchers demonstrated that proteins accumulate at the interface between an oil droplet and the protoplasm of mackerel eggs, resulting in a measurable decrease of the interfacial tension. In a following paper [8] Danielli and Davson proposed a membrane structure comparable to that of Gorter and Grendell [6], but with the extra feature that the lipid bilayer is coated on both sides by a densely packed layer of proteins. This sandwich structure was chosen, because at that time it was believed that only proteins could decrease the surface tension.

The model described by Danielli an Davson [8] was accepted by the majority of researchers for a long time, in spite of the fact that there were mounting contradictory pieces of information. For instance, when the proteins were present at the outside on the membrane the hydrophilic headgroups were screened from the aqueous environment. Why then, one could argue, are these headgroups at that specified location? One of the main reasons that the model was not challenged for such a long time was that electron microscope studies confirmed this structure. More specifically it confirmed the estimated dimensions of the structure of Danielli and Davson. The electron microscope also revealed that not only the cell was covered with a membrane, but also the organelles were separated from the cytoplasm

by a membrane. These findings brought Robertson [9] to the conclusion that all membranes in the cell had a similar structure, and that they were all interconnected with each other. He named it the unit membrane.

Until the beginning of the nineteen seventies this model was generally accepted, but with the improvement of the electron microscope, it became evident that there were major differences between the membranes of various organelles. This suggested that the membrane structure was much more complicated than the rather simple description of Robertson and that they can not be all connected to each other. At this stage it was suggested that proteins are more likely anchored into the membrane rather than sitting as a densely packed layer on the outside of the lipid layer. This idea eventually led to two opposing hypotheses in the mid sixties, with the unit membrane of Robertson on one side, and the theory of Green [10], where the lipid bilayer had almost been completely replaced by proteins, on the other side.

Lenard and Singer [11] already found in 1966, when they studied the membrane with optical rotary dispersion (ORD) and circular dichroism (CD), that approximately 33% of the proteins in a lipid bilayer have an α-helix conformation. Understanding that the Danielli-Davson-Robertson model did not maximize the hydrophobic interactions, they introduced yet another model where the proteins, or more specifically the α-helices penetrated the bilayer partly or completely in order to maximize these hydrophobic interactions.

The development of the electron microscope freeze-fracture technique gave new impulses to the membrane research. The freeze fracture technique made it possible to split a membrane into its two leaflets, opening the possibility to study the inside of a membrane. It was found that the centre of the membrane was not entirely flat consistent with the Danielli-Davson-Robertson model. Interestingly, a lot of holes were found which could be attributed to the proteins that were ripped off from the monolayers. The freeze-fracture technique also revealed that the lipid/protein ratio varies between various membranes. Eventually, these studies led to the fluid mosaic model proposed by Singer and Nicolson in 1972 [12], which is shown in figure 1.2. In this model the proteins are present inside the bilayer and not on the outside of the lipid bilayer and the membrane can be regarded as a two-dimensional fluid where lipid and proteins diffuse more or less freely. The driving force stabilising this structure are the hydrophobic interactions between the lipid tails and the hydrophobic parts of the proteins.

Nowadays there is a much better and deeper understanding of biological membranes due to the enormous amount of research that has been done on this subject over the last few decades. In the modern view of the bilayer membrane there still is consensus that the bilayer provides a matrix in which the proteins reside, as proposed in the fluid mosaic model. This is why the fluid-mosaic model is still the leading (first-order) picture. The structural, mechanical and thermodynamical properties of lipid bilayers have been probed by a very broad range of experimental techniques and the membrane structure has been confirmed by various theoretical methods.
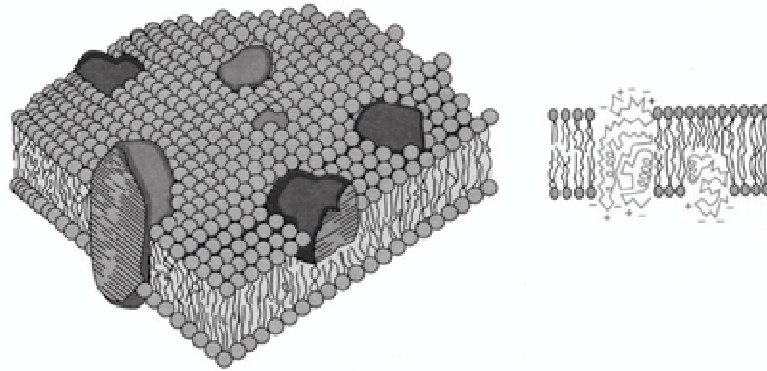
Figure 1.2: Schematic representations of the fluid mosaic model, with proteins floating around in a fluid lipid bilayer. Some proteins completely span the bilayer, while others partly penetrate the lipid bilayer. To the left a 3D picture is shown, to the right a cross-section is presented.

Also the three dimensional structures and the functioning of many membrane proteins are now known in quite some detail. Nevertheless, many questions remain unanswered and research on many branches of membrane science is underway.

In this thesis we focus on the effect of interfaces on lipid bilayers. As we will argue, membranes frequently encounter interfaces. These interfaces can be divided into two separate classes, namely hydrophilic and hydrophobic interfaces. Hydrophilic interfaces are typically present outside the bilayer, for instance an oxide (soil, glass), or in our case a gold surface. Biologically relevant examples are a cell surrounded by other cells or a cell or lipid vesicle that is attached to a substrate. Lipid bilayers in the presence of hydrophobic surfaces often disintegrate and form adsorbed monolayers (as it occurs at the air/water interface). Hydrophobic interfaces with a relatively small area are present in the hydrophobic interior of the lipid bilayer. Examples are the hydrophobic parts of integral proteins or trans-membrane peptides. To get a full understanding of the interactions of proteins with the bilayer membrane is one of the most challeging targets of the years to come.

My thesis can be divided into two parts. In part one a theoretical self-consistent field study is presented aimed to describe the thermodynamical, structural and mechanical consequences of a trans-membrane inclusion in a lipid bilayer. In the second part the adhesion of lipid vesicles to a solid surface is investigated with self-consistent field theory and various experimental methods. In the next few paragraphs I will give a short introduction on a number of membrane issues that are relevant for my thesis. In the first part physical chemical aspects of the formation of the lipid bilayer matrix are discussed. Next, I give some background on the integral membrane proteins. This is followed by a brief introduction of theoretical models that can be used for modelling the lipid bilayer and how the self-consistent field theory is positioned in this field. With a small overview of lipid-protein interactions and vesicle (closed
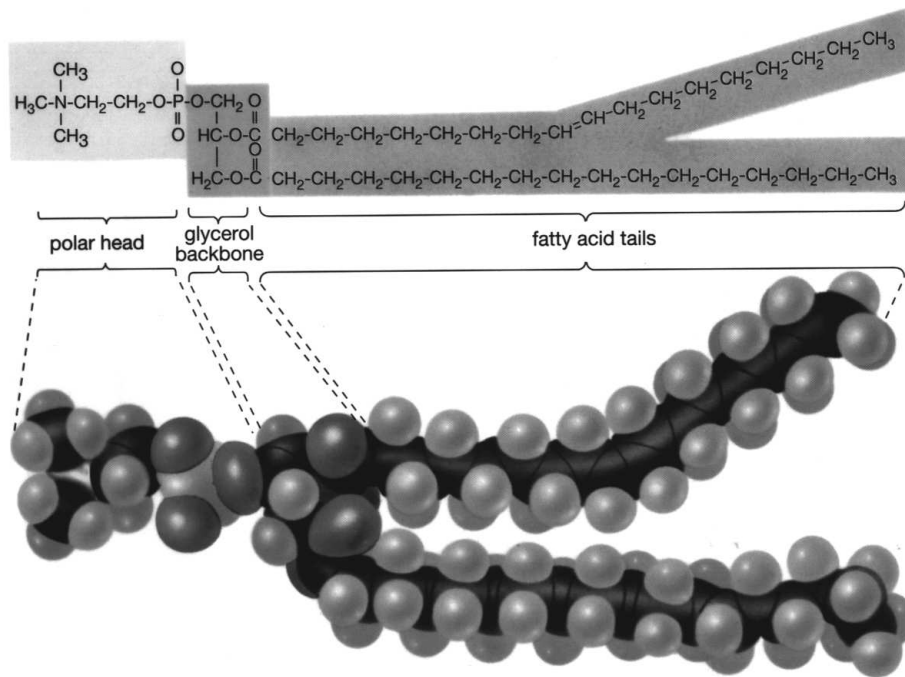
Figure 1.3: Structures of 1-heptadecanoyl-2-oleoyl-sn-glycero-3-phosphocholine. The two hydrophobic tails and the hydrophilic head are indicated both in a space filling (3D) picture (bottom) as well as in the usual chemical language (top).

bilayers) adhesion onto hydrophilic surfaces I will close this introduction.

1.2 The lipid bilayer matrix

It is necessary to explain at this stage what physical chemical aspects are responsible for the lipids to form bilayers. According to the fluid mosaic model the lipids form a flat two-dimensional sheet consisting of two layers of closely packed lipids of which the hydrophobic tails are directed to each other, while the hydrophilic headgroups are oriented towards the aqueous phase. It has to be noted that biological membranes consist of many different types of lipids. The most abundant ones are the phospholipids. These phospholipids have two hydrophobic fatty acyl tails and a hydrophilic headgroup connected to a glycerol backbone (figure 1.3). Lipids are members of a larger class of molecules that share the common property that they have two distinct sides, called amphiphiles or surfactants (a name that refers to the surface activity of these molecules). In an aqueous solution, all amphiphiles and thus also the lipids spontaneously cluster together into multi-molecular aggregates.

The formation of such self-assembled structures only occurs above a certain threshold concentration, called generally the critical micelle concentration (CMC). For most lipids this already occurs at very low concentrations, ranging from approximately 10^{-12} to 10^{-8} M, depending on the tail length, headgroup charge and

ionic strength. It is not self-evident that self-assembling amphiphiles form a two-dimensional sheet. It is well-known that that alternative structures can form such as spherical micelles, cylindrical micelles, etc. The geometry of such aggregates can be predicted from a dimensionless number (surfactant packing parameter) $P \equiv v/al$, where v is the total volume of the surfactant, l is the effective length of the surfactant tail(s) and a is the effective area of the surfactant headgroup. For example, the surfactant cethyl trimethylammonium bromide (CTAB), with $P < 1/3$, has a larger headgroup area compared to the average tail area. These surfactants prefer to group themselves in spherical micelles thereby minimising packing frustration. The many lipids in the bilayer membrane must have an other shape in order to form a flat bilayers. Effectively, the lipids have a cylindrical shape with a headgroup area a comparable to the average tail area v/l and in this case $P \approx 1$.

Limiting ourselves to self-assembled objects of the bilayer type, there are interesting transitions that can be observed by changing the temperature of the system. The bilayer phase behaviour is rich and complex and by now well documented. In a concentrated (pure) lipid solution, the lipid layers can basically be divided into four distinguishable states. Going from a high temperature T to lower T, we find the fluid phase denoted as L_α-phase and three liquid crystalline or solid phases, denoted as $P_{\beta'}$, $L_{\beta'}$ and L_c-phases (figure 1.4). The first two low-T phases are known as the gel phase and the $P_{\beta'}$-phase is referred to as the rippled phase, because of its wavy appearance as schematically illustrated in figure 1.4. The gel-to-liquid phase transition temperature T_m depends mainly on the chain length and the number of double (unsaturated) bonds in the acyl chains. It increases with increasing chain length. For example, for the saturated 1,2-dimyristoyl-sn-glycero-3-phosphocholine (DMPC), 1,2-dipalmitoyl-sn-glycero-3-phosphocholine (DPPC) and 1,2-distearoyl-sn-glycero-3-phosphocholine (DSPC) bilayers the transition temperatures T_m are 24°C, 42°C and 54°C, respectively. The increase of unsaturated bonds in the acyl chain results in a strong suppression of T_m, because double bonds induce kinks in the conformations of the tails and such bended chains organise less easily in a crystalline way. The effect is very large indeed: a single double bond in 1,2-dioleoyl-sn-glycero-3-phosphocholine (DOPC) decreases T_m by 20° compared to DSPC which has no double bonds.

In biological systems the majority of bilayers is in this fluid phase, albeit that usually the lipid composition is selected in such a way that the system is not very far from the gel-to-liquid transition temperature. In this thesis we will therefore limit ourselves to the fluid phase.

1.3   Membrane proteins

An important aspect of the fluid-mosaic model and of course in biomembranes is that there are proteins in the membrane. Proteins are molecules constructed by a long sequence of amino acids. Amino acids may be divided into hydrophilic and
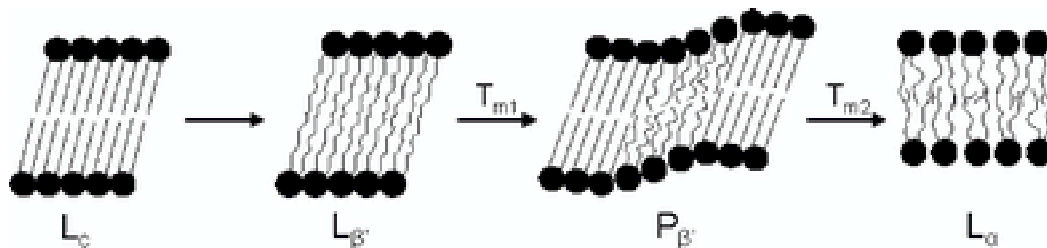
Figure 1.4: The four different bilayer phases of phospholipid bilayer. The three left structures are in the liquid crystalline phase. The phases of the two central bilayers ($L_{\beta'}$ and $P-\beta'$ are also called gel phase. The bilayer on the right L_α is in the liquid phase.

hydrophobic ones. Through the same driving forces as discussed for the self-assembly of the lipids into bilayers, in water the hydrophobic amino acids cluster together in such a way that the proteins are compact entities with little water inside. In this process the hydrophilic segments remain on the water-side. In a way a protein is thus a unimolecular micelle. Due to the high density inside the protein, and the unique sequence of polar and apolar amino acids, it appears that a protein molecule often assumes a unique three-dimensional structure. Within this structure one can typically distinguish structural motives such as helices, or parallel sheets, etcetera.

As proteins have the intrinsic polar-apolar duality, they can be seen as huge surfactants and as such they are often membrane-active species. With this we mean that they can easily be inserted or they insert themselves spontaneously in the bilayer membrane. In the bilayer, the apolar regions of the protein can find an apolar medium as these parts can interact with the acyl tails of the lipids. In a transmembrane configuration, the more hydrophilic amino acids can be organised such that these remain hydrated by placing them at the membrane periphery. The transmembrane configuration is therefore a natural consequence of minimising solvation frustration of such inserted protein molecule. Membrane proteins typically need the lipid bilayer environment to assume their active three-dimensional configuration. This means that the conformation of such protein in the aqueous solution is expected to differ fundamentally from that in the bilayer. It is believed that most membrane proteins remain compact objects inside the bilayer. This means that the swelling of these proteins with lipids is limited. Apparently, the packing efficiency of amino acids with each other does not tolerate the intercalation of many lipids. Effectively the surface acts as a surface to the lipids.

Not all membraneproteins span the bilayer. There exist a second class, the so-called peripheral membrane proteins. These are attached to the membrane temporarily, with electrostatic, covalent and other interactions. They reside on the outside of the membrane. In this thesis we will consider models of proteins in bilayer membranes, but we will focus on the trans-membrane configuration only.

The numbers and types of proteins in the bilayer determine its biological function. For example, two very important energy conversion processes in biological systems, i.e., photosynthesis and oxidative phosphorylation, are carried out by membrane proteins. Membrane proteins also play an important role in the transport of molecules across the membrane. The transport of these molecules by means of these proteins can be regulated in various ways, for instance by the hydrophobic mismatch, i.e., the difference between the hydrophobic length of the inclusion and the hydrophobic bilayer thickness. Examples are the activity of Ca^{2+}-ATPase [13], (Na^+,K^+)-ATPase [14, 15] and the channel lifetime of dimeric gramicidin [16]. One application of our investigation is thus that our results may be used to understand how these complicated biological processes can be regulated.

1.4   Self-consistent field theory

In the above we have several times hinted in the direction of theoretical modelling. Indeed, the generic structure of the amphiphiles and their self-assembling behaviour may lead one to think that it should be feasible to design a theoretical framework that explains most of what is known about the bilayer membrane, starting from the fundamental laws of physics. There are however major challenges that present themselves. First of all one should have a sufficiently powerful method that relates molecular properties to observable quantities and secondly one should be able to apply such theory to a sufficiently accurate molecular model of the bilayer membrane to explain why one amphiphile behaves differently from the other, and to unravel the phenomena that occur when lipid bilayers are next to hydrophilic surfaces or experience protein-like inclusions.

The first problem is to find a sufficiently powerful theoretical machinery that is suitable for us. Very fundamental is that we like to understand not just the properties of a single molecule in space, but the collective behaviour of a large set of such molecules. Theories that do this make use of the laws of averages, i.e., statistics. Here we thus enter the intricate domain of statistical mechanics, or statistical thermodynamics. Indeed, the route to be followed for a given model to predict the expected macroscopic properties, is explicitly specified by the statistical thermoydnamical machinery. A target is to compute the so-called partition function. The partition function exactly specifies in how many relevant states our system can be in. Through further manipulations (differentiations etc.) we then can extract measurable quantities from such partition function, such as the membrane structure, or details regarding the lipid ordering around a protein inclusion. The problem is, however, that there is no known route to obtain this partition function for the complex systems we study here.

With the invention of the digital computer an interesting idea appeared, which allowed huge progress in this field. The key idea is to take a suitable molecular model and generate relevant realisations by brute force. Even though the total partition

function is not computed, the averaging over these relevant realisations then gives an idea about the expectation for a given observable. Although this route is generally applicable, there remain problems. One of these is that one needs to find the relevant realisations from an immense set of not-so-relevant ones. How can we do this? It appears possible to solve Newton's equations of motion for all the movable parts in the system. This is called molecular dynamics MD simulations. Indeed, all we want to know about the lipid bilayer membrane on the nanosecond and nanometre length scale can be computed with this method. To find predictions for systems on a longer time and larger length scale we need coarse, less detailed models. Other strategies to generate relevant realisations (such as Monte Carlo simulations) suffer the same problem that only small systems can be studied.

Even before the invention of the digital computer, people came up with other solutions to this problem. The idea is that when the exact partition function can not be evaluated one should try to find the best approximate partition function for a particular model. These approximate partition functions invariably make use of approximations of the mean-field type.

One of the special difficulties in the evaluation of the partition function is that each molecule interacts with many other molecules and that for each particular realisation of the system the number and type of these interactions differs. Through the many interactions, all molecules are intimately coupled to each other. All these couplings should be accounted for. In a mean field approximation, a pre-averaging of these relevant interactions is carried through. The pre-averaging leads to a decoupling of the molecules and suddenly the problem becomes significantly less involved. For a long time only for molecularly very simple models real progress was possible. From this we know when a mean-field theory is reasonably accurate and under which conditions the theory will fail.

In short, when a particular molecule has, at each given instance, many interactions of the same type with other molecules, it will be clear that the average of these many interactions will not deviate much from an actual, continuously fluctuating, value. As a result the pre-averaging is reasonable and we may expect some good results. On the other hand, when there are few interactions the actual interactions will fluctuate wildly and the pre-averaging is poor. An application of mean-field modelling to the dense packing of lipid molecules in bilayers is an example for which the mean-field theory is expected to hold in many cases. The reason is that each lipid molecule continuously interacts with many neighbours, simply because the density in the bilayer is very high.

Until the introduction of the digital computer it was impossible to implement mean-field theories for molecularly complex systems. During the last two decades or so, the theory, which is known as the self-consistent field (SCF) theory, has developed as a computational technique which can be seen as a method that complements computer simulations. Even though the method is not exact, there are good reasons to develop such models. This is not only due to the fact that SCF models are

computationally extremely inexpensive. One other reason is that the method solves (unlike in simulations) its partition function. Through this partition function one can obtain thermodynamic and mechanical properties of bilayers (we will return to this below).

Due to the dense packing of lipid molecules in the bilayer membrane it is well-recognized that the accuracy of the predictions heavily depends on the molecular model used; this model must be molecularly realistic. Implicitly this has already been discussed in the context of the surfactant packing parameter P introduced above. In a molecularly realistic model for lipid self-assembly there are two important aspects. The first one is that the (excluded) volume, molecular architecture of a given molecule must be accurately represented. The second one is that both the strength as well as the range of the interactions between various parts of the molecule and its surroundings must be accounted for. Both issues are efficiently implemented in a lattice model.

The molecules that are used in our self-consistent field modelling are coarse-grained and consist of segments. All segments have the size of a lattice site. These lattice sites are used to discretise the space. We are not directly interested in the placing of a segment of a specified molecule in a particular conformation on the lattice site, but more in the average result of all the possible conformations. Such average behaviour results in some probability that lattice site are filled, resulting in an average volume fraction per segments per lattice site. Typically, we introduce subsequent approximations. By making use of the symmetry in particular systems, we may design lattices with cylindrical, spherical or flat geometry and consider only density gradients in a direction in the radial or normal direction. This idea can be used to study laterally homogeneous bilayers or spherically or cylindrically shaped vesicles. In other cases our interest is in laterally inhomogeneous systems, e.g., when inclusions in bilayer membranes of integral membrane proteins is studied. In such a case the lattice geometry is adapted to the problem and in homogeneities in two directions is accounted for.

Within a lattice model it is never possible to exactly represent the size and shape of the lipid molecules. For example, it is difficult to account for the size differences between a CH_2 and a CH_3 group. Nevertheless in first order the shape can be represented rather well. For example, our lipid molecules were taken to have two apolar tails and a hydrophilic headgroup as a side-group, in between the two apolar tails.

As already mentioned, another important feature of the SCF theory is that the pair interactions of a segment with all other segments is replaced by the interaction of this segment with an external potential field $u_A(z)$ (for segment with name A at position z). This potential field has the meaning of the work needed to bring a segment from the bulk (where the potential is zero) to the specified coordinate. Without going into detail we mention that we usually take a number of contributions to this work into account. First of all, we need a contribution to create space for

the segment at coordinate z. This work is proportional to the size of the segment, and this contribution is linked to the compressibility relation used. Next there are short-range interactions, which are implemented using Flory-Huggins parameters. These parameters account for the likelihood that two segments of different type are sitting next to each other. For example, the hydrocarbon tail does not like the water phase and thus the interactions between tail segments and water molecules are taken to be repulsive. Finally, there are contributions that account for the electrostatic interactions in the system.

Once the potentials are known for all the segments, it is possible to evaluate the probabilities of finding the various segments in the system. For this we need to evaluate all the statistical weights of all possible and allowed conformations. In general this is a huge task, but we simplify this procedure by introducing a Markov approximation. This approximation implies that we focus on so-called freely-joined chains in a potential field. Once the combined statistical weights of all possible conformations of all molecules are found, we have the mean-field partition function. From this we can extract the measurable quantities of the membrane system.

The application of this theory to the lipid bilayer membrane has a relatively short history. The focus first was on the structure of the lipid bilayers, namely how exactly the lipid tails are packed, what the conformation is of the headgroup and how much the chains of oppositely faced bilayers interdigitate [17]. In recent years the focus is also on the thermodynamic and mechanical properties of the pure lipid bilayers [18]. We have used this approach to investigate bilayer membranes and interfaces. As explained we focus on two cases. In one case we consider the lipid bilayer next to hydrophilic surfaces. In the other case we consider lipid bilayers with protein-like inclusions. The latter problems are models for lipid-protein interactions.

1.5   Thermodynamics

A central thermodynamic potential relevant for the stability of the lipid bilayer membrane, that is directly available from the SCF calculations, is the (excess) grand potential given by Ω and defined by

$$\Omega = U - TS - \sum_i \mu_i n_i + pV = \gamma A \tag{1.1}$$

Here U is the total energy of the system, S is the entropic contribution, T the temperature, $\sum_i \mu_i n_i$ are the chemical work terms of all molecules and pV is the volume work, with V the volume of the lipid vesicle and p the pressure difference on both sides of the lipid bilayer. The area of the bilayer is denoted by A. This bilayer grand potential Ω has contributions from three different bilayer regions, i.e., the hydrophobic tail, the interfacial and the headgroup region. The grand potential of the hydrocarbon tails Ω_t is determined by two counteracting contributions, which are the attractive van der Waals interaction and a repulsive contribution resulting

from the conformational loss of the aligned and extended chains in the bilayer. The grand potential of the headgroup region Ω_h depends on several factors, but in general a repulsive contribution dominates. Indeed the headgroup repulsion is regarded as the stopping mechanism of the self assembly. The stopping force depends on the charge of the headgroups, the hydrophilicity of headgroups, type of counter ions, etc. The interfacial contribution to the bilayer grand potential Ω_s is the effective surface tension of the hydrocarbon-water interface. This effective surface tension differs somewhat from a 'normal' oil-water surface tension, because in the bilayer case there are also headgroups and counter ions in the interfacial region present and the alkanes are far from isotropic. The geometrical dimensions of a lipid bilayer, i.e., the area per lipid molecule a_0 and the bilayer thickness d_l^0, are a result of minimising the Helmholtz energy. In the case of a tensionless planar bilayer the surface tension $\gamma = 0$ and the grand potential of the bilayer $\Omega = 0$.

1.6 Elasticity theory

From the above it is clear that a molecularly realistic model of the lipid bilayer should obey the equilibrium constraints specified by the general thermodynamics. As such the modelling provides a molecular picture behind the thermodynamical framework. A fruitful route to make progress in the understanding of the bilayer model extends the thermodynamics and considers the bilayer as an elastic sheet. Statistical mechanical methods, such as the SCF theory, can provide a molecular interpretation for the elastic properties of the bilayer.

Helfrich showed [19] that the lipid bilayer can be treated with a continuum-mechanical description, i.e., the bilayer is seen as a thin elastic sheet that undergoes three classical modes of deformation, namely stretching, shearing and bending. However, in the case of the fluid lipid bilayer in rest the shearing contribution must vanish and the equilibrium mechanical properties are primarily determined by stretching and bending. The deformation due to stretching of a lipid bilayer is only very limited, because the bilayer area can only increase a few percent. The surface tension γ of a compressed or expanded planar bilayer can be described as a function of the relative change of the bilayer area $\Delta A/A$

$$\gamma = \gamma_0 + k_a \frac{\Delta A}{A} \tag{1.2}$$

Here k_a is the compression-expansion modulus which describes the surface tension change $\Delta \gamma$ in terms of the relative bilayer area change, as shown in equation 1.3

$$k_a \equiv \left(\frac{\partial \gamma}{\partial \ln A} \right)_{\gamma=0} \tag{1.3}$$

There is little experimental information about the value of k_a. Sackmann [20] reported k_a values of approximately $40k_BT$ nm^{-2} for a bilayer in the L$_\alpha$-phase and k_a increases several times when the bilayer is in the L$_\beta$-phase.
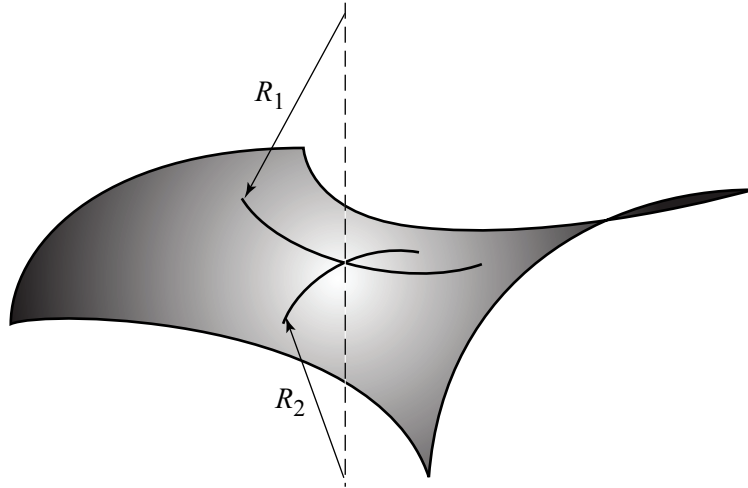
Figure 1.5: The two principal radii of curvature R_1 and R_2 of a surface.

The bilayer tension is expected to change when the bilayer is curved. The second order Taylor expansion of the surface tension γ in the mean curvature J and the Gaussian curvature K reads [18]

$$\gamma(J,K) = \gamma_0 + \frac{1}{2}k_c(J - J_0)^2 + \bar{k}K \tag{1.4}$$

with

$$J = \frac{1}{R_1} + \frac{1}{R_2} \tag{1.5}$$

and

$$K = \frac{1}{R_1 R_2} \tag{1.6}$$

where R_1 and R_2 are the principal radii of curvature as shown in figure 1.5.

As given by equation 1.4 the bilayer's mechanical parameters are the spontaneous curvature of the bilayer J_0, the mean bending modulus k_c and the saddle splay modulus $\bar{k}$. The spontaneous curvature J_0 is the bilayer's curvature for which the free energy (of the cylindrically curved layer) is minimised. Even though the individual monolayers in general have a spontaneous curvature $J_0^m \neq 0$, the spontaneous curvature of most bilayers vanish for symmetry reasons. Although in an undisturbed symmetric bilayer the effect of a spontaneous monolayer curvature is not manifest, it (most likely) has an effect on how a bilayer deals with a perturbation, for example when a trans-membrane peptide or protein is inserted into the bilayer [21].

The mean bending modulus k_c, which is necessarily positive, determines the free energy cost of the bending of the bilayer. The k_c's of phospholipid bilayers have been determined in basically two ways, which can be used individually or in combination. In the first method one measures the response of a bilayer to an applied

force and in the second method the amplitudes of the thermally excited membrane fluctuations are measured. The mean bending modulus was found to be in the range $10k_BT < k_c < 30k_BT$ in the case of fluid phospholipid bilayers [22]. Lee *et al.* [23] studied the variation of the bending rigidity of a DPPC bilayer of the phase transition range from a fluid state bilayer to a gel state bilayer and found that k_c of an L_β-phase bilayer ($k_c \approx 200k_BT$) was approximately ten times the k_c of the L_α-phase bilayer ($k_c \approx 20k_BT$). Experiments also indicate that the addition of cholesterol in the bliayer increases the rigidity [22]. The saddle-splay modulus $\bar{k}$ determines the topology rather then the rigidity of the bilayer. When $\bar{k}$ is negative the bilayer has a preference for spherically curved deformations and when $\bar{k}$ is positive the bilayer has a preference for saddle splay shapes. Although it may seem that this might be an important issue for vesicle fusion, endocytosis and exocytosis, there is no or hardly any experimental information about its value let alone whether it is positive or negative. Recent efforts by Waugh *et al.* [24] failed to give a consistent picture.

Lipid bilayers in solution will, in most cases, close forming so-called vesicles. The reason for vesicle formation is easily understood. The central point is to eliminate the unfavourable edge. The minimum vesicle size where this happens depends on the interplay between the bending energy and the free energy gain when the edge around the bilayer patch is removed. Using Eqn 1.5 the bending energy of a bilayer Ω obeys to

$$\Omega = A\gamma(J, K) = 4\pi(2k_c + \bar{k}) \tag{1.7}$$

It is obvious that this Ω is independent of the vesicle size and is only determined by k_c and $\bar{k}$. If both parameters are positive this would mean that vesicles should always be instable and have a tendency to fuse. However when $\bar{k} \approx -k_c$ the entropic contributions such as undulations, polydispersity and translational entropy might be ably to compensate Ω and stabilise the vesicle against fusion, adhesion and the formation of a multilamellar phase [25].

As freely floating bilayers are free of tension, the physics of lipid layers is determined in large by the mechanical parameters. It is therefore not a surprise that elasticity theory is fundamentally present in the problem of lipid bilayers and interfaces.

1.7 Lipid-protein interaction

The effect of inclusions on the lipid bilayer structure and its thermodynamics has been investigated in a number of theoretical studies, and in this thesis I try to contribute to this discussion. Many of these studies used the elasticity theory developed by Helfrich [19] or microscopic models [26–28]. The two most important findings of these studies were i) the parabolic dependence of the insertion free energy on the hydrophobic mismatch and ii) the deformation of the lipid bilayer as a result of this trans-membrane inclusion being an exponential decaying wave. Many extensions of

this elasticity theory were introduced over the years, for instance the dependence of monolayer equilibrium curvature [21], the variation of the mean bending modulus and the saddle splay modulus at different curvatures [29] as well as the effect of the conformational restrictions of the tails adjacent to the inclusion [30, 31]. However, the latter led to small adaptations in the energetically favourable hydrophobic mismatch and the parabolic width. Another important aspect that was investigated with these theoretical methods was the fact that multiple inclusions could interact with each other, caused by the overlap of the deformed bilayer around these inclusions [32–36].

Using our SCF model, it is possible to provide the molecular picture behind these models. In fact, our SCF model is able to test the underlying approximations in the elastic membrane theory in relation to the incorporation on inclusions. This is one of the targets elaborated on in this thesis.

1.8 Vesicle adhesion

The adhesion of lipid vesicles to a (hydrophilic) surface is a very complicating, but interesting process, which is studied in this thesis. Several scenarios exist, because a large number of parameters influence this process. Basically one would like to understand whether a lipid vesicle adsorbs and remains intact or whether an adsorbed vesicle ruptures and transforms into a supported lipid bilayer. The type of substrate determines to a large extend the strength of adsorption. For instance on oxidised Au, oxidised Pt and TiO_2 fluid phospholipid vesicles do adsorb intact, while on Si_3N_4, SiO_2 and mica the adsorbed vesicles form a flat supported lipid bilayer. This difference can be attributed to differences in the adsorption energy and as a consequence the deformation of the adsorbed vesicles [37]. We may distinguish various contributions to the interaction energy. Almost always the van der Waals interaction, the hydration layer, the electrostatic interactions and local short range chemical interactions, play together to determine the interaction between the lipids and the surface. To date it is still unknown which contribution makes the decisive difference between the various substrates. In some studies the electrostatic contribution appears to dominate. The problem in these type of studies is, however, that besides charge variation also other parameters are varied and this makes it difficult to certify whether the difference in adhesion can be attributed to electrostatic variation only. Other methods are known of transforming intact adsorbed vesicles into supported lipid bilayers. For instance, osmotic pressure between the vesicle content and the aqueous environment can induce vesicle rupture. There are also reports wherein Ca^{2+} ions are used to induce vesicle fusion. Again, the bilayer rigidity and the temperature (which influences the bilayer rigidity) are important parameters. Finally, the surface coverage with lipid vesicles appears a relevant parameter whether vesicles stay intact or form a supported bilayer. The need to have a high coverage before the supported bilayer is formed is evidence that in some cases vesicle-vesicle

interaction is needed before the vesicle layer can/will transform.

In this thesis we not only study the adhesion of vesicles using the SCF model, but we also experimentally investigate lipid vesicle adhesion onto a gold substrate.

1.9   Experimental methods

We used two different methods to follow the adsorption of the lipid vesicles to a gold surface. These methods are the surface plasmon resonance (SPR) method and the quartz crystal microbalance (QCM). The former measures the change of the refractive index near the surface, which is a measure for the adsorbed lipid bilayer mass, while the latter measures the frequency change of a quartz crystal coated with gold, which tells something about the adorbed mechanical mass. We have chosen for these methods because they complement each other to some extent and give us the possibility to get detailed information about the manner of adsorption of the lipid vesicles. Secondly, the use of gold as a substrate is ideal for both methods. In the next two paragraphs I will discuss the methods individually.

1.9.1   Surface plasmon resonance

With surface plasmon resonance the intensity of the reflected light of a p-polarised monochromatic incident beam is measured at various angles (see figure 1.6). Depending on the angle of the incident beam, a small or large part of the light energy interacts with the delocalised electrons in the metal film (plasmon) which results in a reduced reflected light intensity at a typical angle, i.e., the critical angle. This angle, at which most energy is lost, depends on multiple parameters. Important ones are the thickness of the adsorbed layer and the refractive index of the adsorbed layer and the bulk solution. When the thickness of the gold layer, the refractive index of the bulk solution and that of the adsorbed film are known, it is possible to reveal the thickness and/or the total mass of the adsorbed film.

In our case the interpretation of the data is rather complex, because there is not a single thin adsorbed film, but instead a layer of lipid vesicles with a diameter of tens of nanometres is adsorbed to the surface. As a result the decaying sensitivity at larger distance from the gold has to be taken into account. This means that the size and deformation of the adsorbed vesicle influence the critical angle shift, i.e., the change of the critical angle upon adsorption of the vesicles. Considering these complications we also used the QCM method.

1.9.2   Quartz crystal microbalance

With the quartz crystal microbalance QCM the adsorbed mechanical mass can be determined by measuring the change of the frequency of the piezoelectric crystal, when adsorption occurs (figure 1.7).
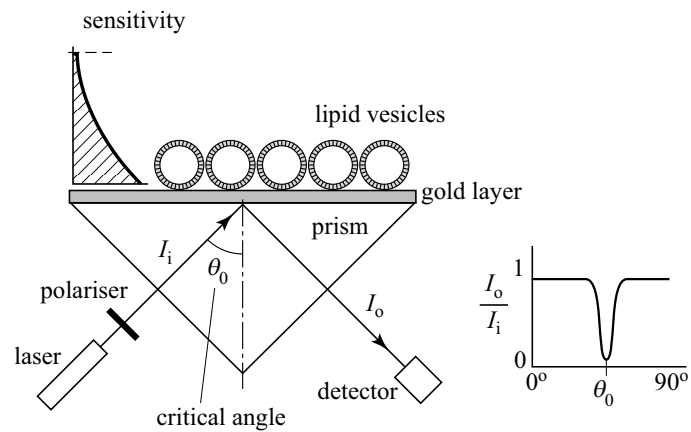
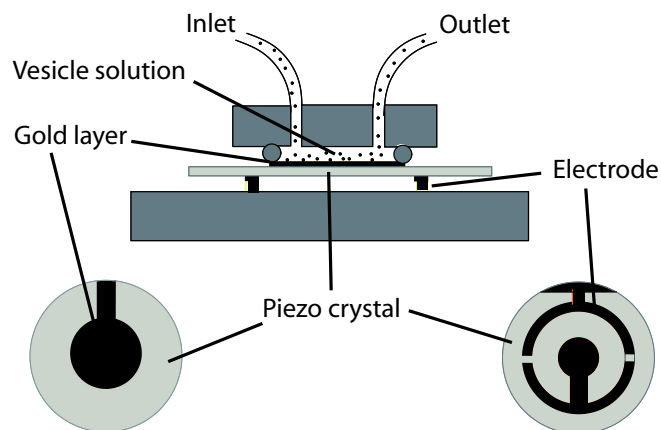Figure 1.6: Schematic representation of the surface plasmon resonance method.

Figure 1.7: Schematic representation of the quartz crystal microbalance. The change of the lateral frequency of the piezo-electric crystal is a measure for the adsorbed mass.

An important advantage of this technique is that the frequency shift can be measured very accurately. As a result the adsorbed mass is also precisely known. The adsorbed mass Γ_m shows a linear relation with the frequency change Δf and can be revealed with the Sauerbrey relation [38].

$$\Gamma_m = -C_0 \Delta f \qquad (1.8)$$

where $C_0 = 17.7 \times 10^{-6}$ mg m^{-2} s. C_0 is determined by the density of the quartz, the shear modulus of the quartz and the fundamental frequency of the quartz plate. The drawback of the QCM is that the Sauerbrey can only be used for rigid thin films. Thus, in the case of lipid vesicles, which are relatively large and soft, the frequency shift is affected. This results in an underestimation of the adsorbed mass. In the literature there are reports where the dissipation was also measured, which gives information about this damping. However there is still a lot unknown about it, because also the vesicle concentration in the bulk solution has an effect on QCM measurements. By combining QCM and SPR results, we are able to draw conclusions about the dependence of the lipid vesicle adhesion on vesicles size, pH and ionic strength.

1.10 Outline of this thesis

This thesis deals with the interactions between lipid bilayer and interfaces and can be divided in two different main parts. The first part comprises chapters three and four, which are self-consistent mean-field studies on the insertion of trans-membrane hydrophobic inclusions, while the second part, which consists of chapters five and six, are theoretical and experimental studies on the adhesion of unilamellar vesicles to a solid surface.

In previous studies it has already been shown how the mechanical properties, such as bending modulus and saddle splay modulus of the modelled lipid bilayer can be determined using SCF theory. In chapter two we will show that it is also possible to determine the bending modulus, the saddle splay modulus and the spontaneous curvature of the individual monolayers in the lipid bilayer.

In chapter three the insertion of a hydrophobic trans-membrane rod into a lipid bilayer is modelled with self-consistent field theory. An effort is made to compare elasticity theory with the results obtained with this microscopic model. We have focussed on the effect of the hydrophobic length mismatch between the inclusion and the lipid bilayer in relation with thermodynamical, structural and mechanical properties.

In chapter four we studied the lipid mediated interactions between two inclusions. In multiple literature studies the lipid-mediated interaction between various trans-membrane inclusions have been investigated. In these studies it was always assumed that there were only steric hindrances of the lipid molecules adjacent to the inclusion. In our study we investigated the consequences of adsorbing/depleting interactions

between the lipid tails and the inclusion on the lipid-mediated interaction between the inclusions at various separations

The fifth chapter reports on a combined experimental and theoretical study. Here the topological and conformational properties of adsorbed lipid vesicles are investigated. Especially the local conformational adjustments of the bilayer are studied. Special attention is directed to the effect of the vesicle size, the adhesion energy and the elastic properties of the lipid bilayers.

In the sixth chapter the importance of electrostatic interactions for the adhesion of lipid vesicles to a solid interface is investigated both experimentally and theoretically. To attempt to understand/predict whether adsorbed vesicles stay intact or transform into a flat supported bilayer. We studied the adhesion of vesicles to a gold surface and tuned the electrostatic interactions by varying the pH, ionic strength of the solution, or by applying an external potential. We tried to get insight into the adsorption mechanism by modelling this system with the SCF theory.

Even though progress has been made, it is evident that there remains a lot to do. One conclusion of my work is that lipid bilayer membranes and surfaces are a complicated combination of research topics, which will undoubtelly attract attention to many researchers in the years to come.

Chapter 2

Bending moduli and spontaneous curvature of the monolayer in a surfactant bilayer

Abstract

We developed a method to evaluate the mechanical properties of the monolayers in symmetric surfactant bilayers using self-consistent field theory. A specific boundary condition is used to impose the same curvature onto the two opposing monolayers at the surfactant chemical potential equal to that of the corresponding homogeneously curved bilayer. Typically the spontaneous monolayer curvature $J_0^m \neq 0$ and its value depends on the surfactant architecture. This is of importance for the thermodynamics and topology of lamellar surfactant phases. Furthermore, it may be relevant in processes involving biological membranes, e.g., the fusion and budding of vesicles and the incorporation of proteins in lipid bilayers.

2.1 Introduction

Surfactants of appropriate structure self-assemble spontaneously in aqueous media to form lamellar structures. The surfactant tails of two opposing monolayers form the core of the bilayer and the surfactant heads form the coronas such that the core is shielded from the water phase. The biological bilayer composed of lipids is one of the most important structural elements in living cells. As a consequence it receives attention from many areas of science.

Unconstrained flat bilayers remain tensionless [121]. Helfrich [19] realized that the physics of tensionless bilayers is controlled by their bending moduli. Introducing the mean $J = 1/R_1 + 1/R_2$ and the Gaussian $K = 1/R_1 R_2$ curvature, where R_1 and R_2 are two principle radii of curvature, the surface tension for a weakly curved bilayer is given by:

$$\gamma(J, K) = \gamma(0, 0) + \frac{1}{2}k_c(J - J_0)^2 + \bar{k}K. \tag{2.1}$$

Symmetry considerations indicate that the flat bilayer is the lowest in free energy and the spontaneous curvature $J_0 = 0$. As a result Eqn 2.1 may be simplified for symmetric bilayers. The mean bending modulus k_c determines the shape fluctuations, whereas the Gaussian bending modulus $\bar{k}$ is important for the topological stability: closed bilayers (vesicles) are stable when $-2k_c \leq \bar{k} \leq 0$. Only the mean bending modulus is (reasonably straightforwardly) experimentally accessible [122]. Many mesoscopic descriptions of amphiphilic systems take the bending moduli as input parameters [21]. In addition one is often interested in the mechanical properties of the individual monolayers. Typically it is assumed that one can apply Eqn 2.1 also to the monolayer. As the monolayer is asymmetric, we should anticipate that (in general) there is a finite value for the preferred curvature $J_0^m \neq 0$, where the super index m refers to the monolayer. One may argue that when J_0^m deviates much from zero, one has a frustrated bilayer, with subsequent consequences for, e.g., the incorporation of proteins into such bilayers [21]. At present we do not know a method to directly determine J_0^m. However, we believe that the value of J_0^m can be deduced from experimental results, e.g., by fitting these to a detailed model in which the spontaneous curvature has an important contribution. Such procedures will always be delicate and therefore it is of extreme importance that there are reliable predictions for this quantity.

To relate the molecular structure of the amphiphiles to the mechanical properties of the resulting monolayer and/or bilayer is the realm of molecular modeling. There are relatively few routes known in the literature to evaluate the mechanical properties of symmetric bilayers. There are predictions for the mechanical properties of densely packed hydrocarbon-like tails end-grafting to a (curved) surface by analysing the conformational entropy of homogeneously packed cores as a function of imposed curvature [123, 124]. In this approach head groups were not included and the strong repulsive interactions with the solvent were omitted. These authors discuss both

monolayer and bilayer systems. However it is clear from the details of their method, that the monolayer is not the monolayer in the bilayer configuration. Consequently they do not find that the mechanical properties of the monolayer could be related to those of the bilayer. This also implies that the spontaneous curvature of the monolayer (next to some oil) may not necessarily be related to that of the monolayer in the bilayer configuration.

In a more complete model one not only should account for the entropy of densely grafted chains, but also for the energetic interactions that drive the self-assembly (hydrophobic effect) and stops the aggregation of the surfactants (head group repulsion). Using a molecular realistic self-consistent field (SCF) approach one can realistically model surfactant self-assembly in systems wherein these aspects are incorporated and where only the curvature of the bilayer as a whole is imposed [18,25]. Again it is possible to obtain the partition function with high precision. As a result the bending moduli of symmetric bilayers are evaluated systematically and accurately. One can identify two major problems that prevented the application to evaluate the mechanical properties of the constituting monolayers. The first problem is how to embed the apolar side of the monolayer. As argued above it is not realistic to put the tails next to vacuum. One may suggest to use an appropriate alkane phase. However the interdigitation of the alkanes into the monolayer strongly depends on their molecular weight, which renders the mechanical properties of the monolayer to be an undesired function of this choice (explaining the result of Szleifer et al [124], where the bending moduli of the monolayers was not half that of the bilayer). The second problem is to know the appropriate number of surfactants per unit area corresponding to tensionless layers. This number may depend on the imposed curvature. Small errors in this quantity will imply some stretching or compression of the monolayer leading to large errors in the predictions. We will suggest solutions for both problems. First, we will go into some more detail how the mechanical properties of the bilayer can be determined using our SCF theory.

2.2   Self-consistent field theory

Oversteegen [18] showed that one can accurately determine the bending moduli from the fitting of the surface tension $\gamma(J, K)$ by Eqn 2.1 or, alternatively, from the curvature dependence of the lateral pressure profile $\omega(r)$. It is convenient to introduce the jth moment over the lateral pressure profile $\omega^0(x)$ of the flat bilayer: $\mathcal{P}_j^0 = \int x^j \omega^0(x) \mathrm{d}x$, where x is the co-ordinate parallel to the membrane normal and $x = 0$ is at the symmetry plane in the bilayer. Unconstrained bilayers have no tension and thus $\gamma = \mathcal{P}_0^0 = 0$. The bending moduli are found from

$$-k_c J_0 = \mathcal{P}_1^0 + \left(\frac{\partial \mathcal{P}_0}{\partial J} \right)_{T,K}^0 \tag{2.2}$$

$$k_c = 2 \left(\frac{\partial \mathcal{P}_1}{\partial J} \right)_{T,K}^0 + \left(\frac{\partial^2 \mathcal{P}_0}{\partial J^2} \right)_{T,K}^0 \tag{2.3}$$

$$\bar{k} = \mathcal{P}_2^0 + \left(\frac{\partial \mathcal{P}_0}{\partial K} \right)_{T,J}^0. \tag{2.4}$$

These equations show that the mechanical properties cannot be derived from the flat bilayer alone. The fundamental reason for this is that in general the grand potential density $\omega(r)$ cannot be defined uniquely [125]. One has to make a choice of how to do the bookkeeping for the non-local interactions. For example in the literature [126] one often finds $\bar{k} = \mathcal{P}_2^0$. The extra term in Eqn 2.4 corrects for the ambiguity in how the bookkeeping is implemented. When the binary interactions are split evenly over the coordinates that are involved, one can write the SCF result for the grand potential density as:

$$\omega(r) = k_B T \sum_i \frac{\varphi_i(r) - \varphi_i^b}{N_i} - \sum_A \varphi_A(r) u_A(r)$$
$$- \frac{k_B T}{2} \sum_A \sum_B \chi_{AB} \left(\varphi_A(r)(\langle \varphi_B(r) \rangle - \varphi_B^b) - \varphi_A^b(\varphi_B(r) - \varphi_B^b) \right) \tag{2.5}$$

Here $k_B T$ is the thermal energy, i the index to the molecule types, A and B are indices running over all segment types, φ is the volume fraction (super index b refers to the homogeneous bulk in equilibrium with the bilayers) and u the self-consistent potential, and χ_{AB} the Flory-Huggins exchange energy parameter that quantifies the nearest-neighbor interactions. Finally, the angular brackets give the geometry-dependent local average of the volume fraction (to be specified below), which comprises the non-local contributions to the grand potential density (that depend on the bookkeeping) [125].

In this paper we will use the SCF model with the discretisation Ansatz of Scheutjens and Fleer [127]. This implies a lattice with layers composed of lattice sites with characteristic length l and surfactant chain molecules of the nonionic type with spherical united atoms and volume that fits on the lattice sites. It is convenient to introduce chain architecture operators $\delta_{i,s}^A$ which obtain the value $\delta_{i,s}^A = 1$ when segment s of molecule i is of segment type A and zero otherwise. These operators are fixed because the segments along the chain in the nonionic molecule have known segment types given by the input data. The SCF model comprises a segment potential for each segment type which is a functional of the volume fractions. For uncharged surfactants, only excluded volume and short-range nearest-neighbor contacts are accounted for and $u_A(r) = u'(r) + \sum_B \chi_{AB} \left(\langle \varphi_B(r) \rangle - \varphi_B^b \right)$, where $u'(r)$ is a Lagrange potential coupled to the incompressibility constraint $\sum_B \varphi_B(r) = 1$. The volume

fraction profiles are also a functional of the potentials. Using a Markov approximation it is possible to formulate an efficient scheme to compute the volume fraction profiles [127]. In short, it is possible to come up with the statistical weights of all possible and allowed conformations and collect them in various Green's functions,

$$G_i(r, s|1; N) = G_i(r, s|1)G_i(r, s|N)/G_i(r, s). \tag{2.6}$$

Here $G_i(r, s|1; N)$ is the statistical weight that segment with ranking number s of molecule i is at coordinate r with the constraint that it is connected by intermediate segments (via all possible walks) to the two terminal segments $s = 1$ and $s = N_i$. The Green's function $G_i(r, s|1)$ gives the statistical weight of of all possible conformations of a chain fragment from $s' = 1, \cdots, s$, where over all coordinates of the end-segment $s = 1$ is integrated over. A comparable definition applies for the complementary Green's functions $G_i(r, s|N)$. This set of Green's functions are generated by a forward and backward propagator, respectively, which are discrete versions of a diffusion equation:

$$G_i(r, s|1) = G_i(r, s) \langle G_i(r', s - 1|1) \rangle = G_i(r, s) \sum_{r'} \lambda(r, r')G_i(r', s - 1|1) \tag{2.7}$$

$$G_i(r, s|N) = G_i(r, s) \langle G_i(r'', s + 1|N) \rangle = G_i(r, s) \sum_{r''} \lambda(r, r'')G_i(r'', s + 1|N) \tag{2.8}$$

which defines the angular brackets also used in Eqn 2.5. Here the sum over r' runs over all possible neighboring coordinates of segment s, i.e., the distance $r - r'$ is the lattice length l. The same applies to summation over r''. The weighting factor $\lambda(r, r')$ gives the *a priori* statistical weight to step from r' to r and obeys the constraint that $\sum_{r'} \lambda(r, r') = 1$. This weight depends on the local geometry, i.e., the curvature of the lattice layers [66] as specified below.

In both equations 2.6 and 2.8 the free segment distribution occurs, i.e., $G_i(r, s) = \sum_A G_A(r)\delta_{i,s}^A$, where $G_A(r) = \exp(-u_A(r)/k_BT)$ is the Boltzmann weight featuring the segment potential. After normalisation of $G_i(r, s|1; N)$ one obtains the volume fraction profiles $\varphi_i(r, s)$ from which the segment type dependent profiles $\varphi_A(r)$ follow, i.e., $\varphi_A(r) = \sum_i \sum_s \varphi_i(r, s)\delta_{i,s}^A$. Below we will discuss the normalisation in more detail. A computer algorithm is used to find the solution for which the segment potentials and segment distributions are consistent with each other while the incompressibility constraint is obeyed [127]. For more details we refer to the literature [66, 127].

A slice normally through an infinitely long tubular vesicle leads to a radial distribution function of the (excess) surfactant density. The first moment over this distribution determines the radius of the vesicle R. Other definitions of the radius can be envisioned, however, for large values of the radius R, all reasonable definitions give identical results. This means that in the limit of large radii the curvature is uniquely defined. The same applies for a spherically curved bilayer (vesicle). In the

inner monolayer the head groups are compressed leading to a relatively high head group density. The tails of the inner monolayer have relatively much space. We will choose the curvature for this monolayer to be negative $J = -1/R$ (cylindrical geometry). The outer monolayer has relatively compressed tails and expanded head groups and the curvature is positive $J = 1/R$. For sufficiently large R there is little ambiguity about the assignment of the curvatures to the two monolayers. In the SCF model we have a radial coordinate counting from the center in units of lattice sites: $r = 1, \cdots, R, \cdots, M$. When $1 << R << M$ the system boundaries $r = 1$ and $r = M$ do not influence the curved bilayer and at both boundaries the homogeneous bulk is present. In general it is expensive (in terms of computer time) to choose the computational volume to be large; instead we may introduce new coordinates $z = 1, \cdots, M_z$ where $r = z + R_l$ and typically $M_z + R_l < M$ and still have the condition that at $r = R_l < R$ and $r = R_l + M_z > R$ bulk conditions apply.

The boundary conditions are chosen such that between layers $z = 0$ and $z = 1$ as well as between layers $z = M_z$ and $z = M_z + 1$ all gradients in u and φ vanish. In more detail, for all segment potentials we set $u(0) = u(1)$ and $u(M_z + 1) = u(M_z)$. In the propagator procedure the gradients in end-point distribution functions vanish at the system boundaries, i.e., $G(0, s|1) = G(1, s|1)$, $G(0, s|N) = G(1, s|N)$, $G(M_z + 1, s|1) = G(M_z, s|1)$, $G(M_z + 1, s|N) = G(M_z, s|N)$ and also $G_i(0, s|1; N) = G_i(1, s|1; N)$ and $G_i(M_z + 1, s|1; N) = G_i(M_z, s|1; N)$. As a result also the volume fractions on either side of the boundaries are identical. This symmetry boundary condition in the curved lattice geometry is used below to calculate the mechanical parameters of the monolayers. The boundary condition has minimal consequences for the conformational entropy of the chains as these can freely cross the boundary.

In the cylindrical coordinate system $L^c(z) = \pi (2(z + R_l) - 1)$ is the number of lattice sites (per unit length) in layer z and the total grand potential (per unit length) of the tubular vesicle) is found by $\epsilon^c = \sum_z L^c(z) \omega^c(z) \approx 2\pi R \gamma(J, 0)$ (c = cylindrical geometry and $J = 1/R$). In spherical geometry we have $L^s(z) = 4\pi ((z + R_l)^2 - (z + R_l) + 1/3)$ and the grand potential of the spherical vesicle is given by $\epsilon^s = \sum_z L^s(z) \omega^s(z) \approx 4\pi R^2 \gamma(J, K)$ (s = spherical geometry and $J = 2/R$ and $K = 1/R^2$). The internal balance for the chain statistics dictates that $L(z')\lambda(z', z) = L(z)\lambda(z, z')$. Using this we find that the transition probabilities are given by $\lambda(z, z - 1) = A(z)/L(z)/3$, $\lambda(z, z + 1) = A(z + 1)/L(z)/3$ and $\lambda(z, z) = 1 - \lambda(z, z - 1) - \lambda(z, z + 1)$ where $A(z)$ is the dimensionless contact area (i.e., the area normalised by l^2) between layers z and $z - 1$. For the cylindrical coordinates we have the area per unit length $A^c(z) = 2\pi(z + R_1)$, whereas for the spherical coordinate system the area is given by $A^s(z) = 4\pi(z + R_1)^2$.

2.3 Parameters

Nonionic surfactants ($i = 1$) of the type $C_n E_m \equiv C_n(OC_2)_m O$ are used where C stands for CH_2 or CH_3 and O is for the oxygen in the ethylene oxide moiety and
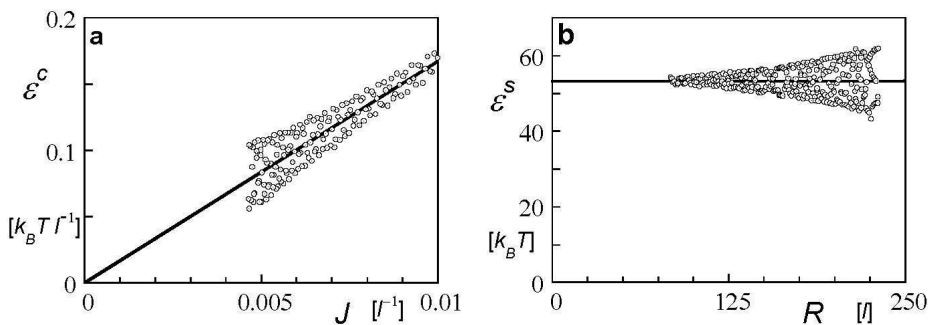
Figure 2.1: The thermodynamics of $C_{14}E_4$ bilayers curved in a) cylindrical and b) spherical geometry. In view graph a the grand potential per unit length of the tubular vesicle ϵ^c is plotted as a function of the radius of curvature $J = 1/R$. The points scatter symmetrically around the linear trend line. In view graph b the grand potential of the spherical vesicle ϵ^s is plotted as a function of the radius of the vesicle R. Again the data points scatter symmetrically around the horizontal trend line.

also for OH as the terminal segment in the head group. Thus all chain architecture operators for this molecule are fixed, i.e., $\delta_{1,1}^C = 1, \cdots, \delta_{1,n+3m+1}^O = 1$. Here we choose to represent the solvent ($i = 2$) by a (compact) cluster of five W units where there is a central one surrounded by four neighbors so that the solvent (water) is somewhat larger than a C atom. There are three FH interaction parameters which we choose such that the known critical micellisation concentration is reproduced: $\chi_{CW} = 1.1$, $\chi_{CO} = 2$ and $\chi_{OW} = -0.6$. These parameters are close to those used in previous studies [128]. Careful comparison of spherical, cylindrical and lamellar topologies of various members of the C_nE_m family show that, in line with experimental data [129], the $C_{12}E_5$ forms stable bilayers only at very high surfactant concentration. The bilayers of $C_{14}E_4$, however, appear more stable than spherical or cylindrical micelles. This is remarkable because the two surfactants differ just by one O atom. Using this information we focus below on the subset C_nE_4 of bilayer forming surfactants with $14 \leq n \leq 18$.

2.4 Results and discussion

2.4.1 Mechanical properties of symmetric bilayers

The determination of the bending moduli of symmetric bilayers starts with the evaluation of the structural properties of the flat bilayer [18]. The tensionless bilayer is characterised by an area per surfactant molecule a_0. This quantity increases with increasing tail length (for given head group size). Using a_0 one can estimate the number of surfactant molecules n_s per unit length of a tubular vesicle with radius R, i.e., $n_s = 4\pi R/a_0$. In this case the volume fraction profiles are found from:
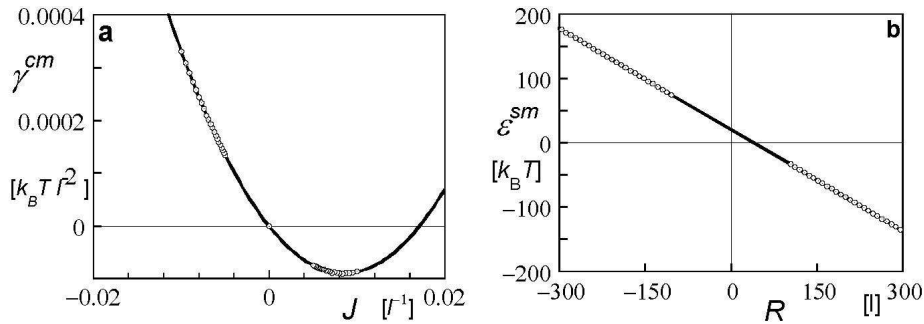
Figure 2.2: The thermodynamics of $C_{14}E_4$ monolayers (in the bilayer configuration) curved in a) cylindrical and b) spherical geometry. In view graph a the surface tension γ^{cm} of the monolayer in a tubular vesicle is plotted as a function of the radius of curvature $J = 1/R$. In view graph b the grand potential of a monolayer in spherical geometry ϵ^{sm} is plotted as a function of the radius of the vesicle R.

$$\varphi(z,s) = CG(z,s|1;N) = \frac{n_s}{\sum_z L(z)G(z,s|1;N)}G(z,s|1;N). \qquad (2.9)$$

The normalisation constant C is also related to the volume fraction of surfactant in the bulk surrounding the bilayer, φ^b. As in the bulk phase all Green's functions are unity it follows that $C = \varphi^b/N$ [127] and thus $\varphi^b = n_s N/(\sum_z L(z)G(z,s|1;N))$. From such an analysis one obtains the grand potential of the cylindrically curved bilayer $\epsilon^c(R)$ from which $\gamma^c(R)$ follows by division by $2\pi R$. As $J = 1/R$ and $K = 0$ we can use Eqn 2.1 to evaluate k_c. It is essential to realize that the bulk volume fraction of surfactants is a weak function of the radius of the tubular vesicle as well, i.e. $\varphi^{bc}(R)$ is not a constant. We may repeat the procedure for spherical coordinates and find that the grand potential of the spherically curved vesicle $\epsilon^s = 4\pi(2k_c + \bar{k})$ [19]. Using the k_c from the analysis of the tubular vesicle (cylindrical coordinates) we can thus extract the Gaussian bending modulus $\bar{k}$ [18].

An example of this procedure for the curved bilayer of $C_{14}E_4$ is given in figure 2.1 where ϵ^c is plotted as a function of the curvature. In fig. 2.1a we have imposed the cylindrical geometry. The data points should ideally fall on the linear trend line. Instead they scatter around this line where the amplitude of the deviations increases with decreasing J. The fundamental reason for this scatter is the fact that the bilayers feel the underlaying lattice somewhat. Because of this the SCF solution results in bilayers that have not only curvature energy but also a tiny bit of stretching energy (either negative or positive) caused by the lattice-induced perturbations. These lattice artifacts average out when a large set of vesicles of different sizes is generated as is easily seen in fig. 2.1. One can also envisage a numerical procedure to search automatically for vesicles that feel very little of this lattice pressure. We do not show this here. The trend line of fig. 2.1a crosses the origin convincingly.

This shows that the symmetric bilayers do not have a preferential curvature and that the bilayers are tensionless. From the slope we obtain directly the value of the mean bending modulus k_c. In fig. 2.1b we present similar results for bilayers ($\epsilon^s(R)$) onto which a spherical geometry is imposed. Again, ideally for vesicles that have only curvature energy the points would fall on the horizontal trend line. The spread of the points increase with increasing radius of the vesicle, showing that the small positive or negative lattice pressure also affects the energetics of spherically curved bilayers. The horizontal line corresponds to the grand potential $\epsilon^s = 4\pi(2k_c + \bar{k})$ and the results convincingly show that for symmetric bilayers $J_0 = 0$.

2.4.2 Mechanical properties of a monolayer in the bilayer configuration

The key ideas to compute the mechanical parameters of the monolayers are: (i) to shift the boundary $z = 1$ (i.e., $r = R_l + 1$) to the coordinate $r = R + 1$ and force the curved bilayer to have its symmetry plane at the lower system boundary and (ii) to normalise the volume fraction profiles with the known $\varphi^b(R)$ values. The symmetry boundary condition (i) forces a curved monolayer to interact with a similarly curved monolayer (its mirror image). Again, due to the imposed symmetry the numbers of chains that (partially) exit and enter the system are identical. As a result the curved monolayer feels in good approximation the same environment as if it was in the unperturbed bilayer. By imposing the normalisation with the known bulk volume fraction (ii), we force the surfactants in the curved monolayer to have the same chemical potential as the surfactant in the homogeneously curved (tubular or spherical) vesicle. The number of surfactants per unit area can adjust so that the monolayer remains unstretched. Hence, we do no longer expect to find noise in the data points due to some residual lattice-induced lateral tension. Indeed, now the grand potential of the monolayer only contains bending work. (iii) Next, we shift the symmetry plane of the bilayer to the upper system boundary such that $z = M_z$ is at the center of the bilayer, i.e., to $r = R$. Again $\varphi^b(R)$ is used to normalise the volume fraction profiles.

For the cylindrical geometry we thus obtain $\epsilon^{cm}(J)$ (and related to that $\gamma^{cm}(J)$) both for negative and positive values of J as is shown for an example in figure 2.2a. In this graph we combined the data of the positively and negatively curved monolayers. In the limit of $J \to 0$ the two branches meet at the value $\gamma^{cm}(0) = 0$; the symmetric uncurved bilayer has no membrane tension. Fitting $\epsilon^{cm}/(2\pi R) = \gamma^{cm}(R)$ to equation 2.1 gives k_c^m and J_0^{cm} straightforwardly. The results obtained following the same procedure for the spherical coordinate system are shown in fig. 2.2b. In this graph we show the grand potential of the monolayer $\epsilon^{sm}(R)$ both for positive and negative R. As expected a linear dependence of $\epsilon^{sm}(R)$ is found. From the slope we find the combination k_c^m and J_0^m. Using k_c^m from the cylindrical geometry we can accurately find J_0^{sm} (here the super index s is added to show that this value of the
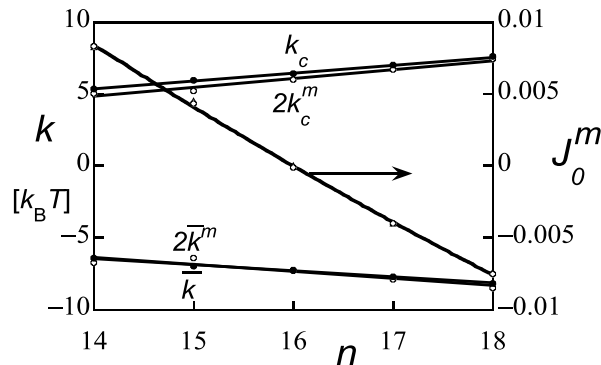
Figure 2.3: The bending moduli of the bilayer k_c and $\bar{k}$ (open spheres) and twice that of the constituent monolayers $2k_c^m$ and $2\bar{k}^m$ (closed spheres) in units of $k_B T$ (left ordinate) and the spontaneous curvature J_0^m (in units $1/l$) as found from cylindrically (open triangles) and spherically (open spheres) curved monolayers (right ordinate), as a function of the length n of the tail of the $C_n E_4$ surfactant. The lines are drawn to guide the eye.

spontaneous curvature is found from the analysis of spherically curved monolayers). From $\epsilon^{sm}(0) = 4\pi(2k_c^m + \bar{k}^m)$ we may find $\bar{k}^m$ because k_c^m is known.

In figure 2.3 we show a compilation of the mechanical properties of the bilayer as well as of the monolayers for a series of alkyl ethylene oxide $C_n E_4$. The mean bending modulus k_c is found to increase linearly with the chain length and the Gaussian bending modulus is negative and decreases linearly (becomes more negative) with increasing length of the tail of the surfactant. The corresponding quantities for the monolayers are about half of those of the bilayer. This is accurately the case for the Gaussian bending modulus, but there appears to be a small systematic deviation between the mean bending modulus of the bilayer and (twice) that of the monolayer. This difference is close to the numerical noise of our method. The value of J_0^m computed from the tubular shaped monolayers are identical to those found from spherically shaped monolayers. This internal consistency of the data inspires confidence in the proposed method. We find that J_0^m is positive for $n < 16$ indicating that for small values of n spherical micelles will become a feasible alternative geometry for self-assembly, whereas for $n > 16$ the reversed curvature may be considered by the surfactants (and the reversed hexagonal phase is anticipated). This is largely in line with expectations based on packing considerations [130].

In the SCF modeling there are no constraints on the surfactant assemblies other than the curvature of the bilayers or monolayers. The head groups or tail segments choose positions such that the free energy is optimized; we not only account for conformational entropy in the molecule, but also for all relevant interactions in the molecule and with the solvent. As a result the surfactants partition between the bulk (where the concentration is close to the critical micellisation concentration) and the densely packed surfactant layers. In the same way the solvent is free to partition

somewhat into the bilayer, albeit that the tails force most of the solvent (water) out of the bilayer because of the unfavourable interactions. Our curved bilayer and monolayers are free of any lateral tension as the area per molecule is always optimized. Therefore the grand potential of our curved bilayers and monolayer can safely be assigned to the curvature energy in the system. Moreover the tails can and will cross the symmetry plane in the bilayer [67] such that the free energy is minimized.

Physically one expects that the bending modulus for the monolayer k_c^m and $\bar{k}^m$ are just half the values of the full bilayer. The good correspondence observed between the bilayer rigidity and twice that of the monolayer (cf. fig. 2.3) is in line with this expectation. The small deviations observed are attributed to minor details regarding the interdigitation of tails into the opposite monolayer (just a tiny little bit different using the symmetry boundary condition than in the real situation). This directly proves that the correct embedding of the monolayer is of utmost importance.

Our predictions complement corresponding results in the literature [123,124,126]. In the work of Szleifer et al. [123,124] only the tail contribution to the bending moduli is considered. These authors tether short semi-flexible hydrocarbon chains to a plane at fixed curvature. They enforce some ad hoc (albeit justifiable) assumptions regarding the homogeneity of the chain packing. It is necessary to mention that these authors discuss both bilayers and monolayers. In the bilayer case they implement a constant density throughout the layer, whereas in the monolayer system the packing density may vary. The argument is that a reduced tail density is supplemented by (unspecified) oil molecules. From this it is clear that their monolayer is not the monolayer in the bilayer configuration. Therefore, it is not surprising that the bending modulus of their bilayers is not twice that of their monolayer at corresponding area per surfactant molecule. It is difficult to compare our predictions with those by Szleifer et al [124]. This is because they keep the area per molecule as a variable in the problem and it is impossible to extract what area per molecule corresponds to a tensionless bilayer. Such direct comparison would already be complicated because in the Szleifer papers there are no head groups, there are no positional fluctuation of the grafting point (representing the fluctuation on the head group position), there is no solvent penetration, and there are some doubts regarding the way interdigitation is allowed for in their bilayer calculations.

From a statistical mechanical point of view the method of Szleifer et al. [123,124] has many aspects in common with our SCF theory. For example, they need a local pressure $\pi(x)$ (they use the x coordinate in the normal direction of the bilayer), which is linked to the compressibility constraint (constant tail density). This pressure can be compared to our Lagrange field $u'(r)$. This pressure profile $\pi(x)$ is used to evaluate the bending moduli using equations similar to our eqns 2.2 - 2.4. In fact they can simplify these equations because their lateral pressure $\pi(x)$ is local; there is no bookkeeping issue because they do not account for non-local interactions. In our case $u'(r)$ is also part of the grand potential density $\omega(r)$ (which may be interpreted

as a lateral pressure), but we have several additional contributions to this pressure profile. We put no constraints on the value of $u'(r)$, however Szleifer et al force $\pi(x) \geq 0$. This has important consequences. As they compute $\bar{k} = -\int x^2 \pi(x) \mathrm{d}x$, it is clear that they will always find $\bar{k} < 0$. We know that this can not be generally true, which seriously questions the Szleifer approach. Our predictions of the mechanical parameters of the monolayer in a bilayer configuration are therefore expected to be more accurate that those found in the literature [123, 124, 126].

In the SCF method there are two operational ways to evaluate the mechanical properties of surfactant mono- and bilayers. The first one is using Eqns 2.2 - 2.4. The second one is to evaluate the overall grand potential as a function of J and K and fit the results to the Helfrich eqn 2.1. Oversteegen [18] showed that these two ways give identical results. Computationally the evaluation of the bending moduli from integrals over moments of the grand potential density profiles (and their derivatives) is tedious and, as it turns out, less accurate. In our case it is far more easy, and computationally much more efficient, to use the route of fitting the overall grand potential to Eqn 2.1, as used above. From this fitting procedure we can also filter out the effects of, e.g., the lattice-induced tension. Our method is computationally extremely efficient as the mechanical parameters for a particular surfactant mono- or bilayer can be performed in the order of a few seconds CPU on a desktop PC. Consequently, our method may be used also for other more complex systems, e.g. block copolymers, mixtures of surfactant, etc. [131]. The result that it is possible to accurately evaluate the spontaneous curvature of the monolayer, when it is embedded in the bilayer, is important for obtaining a deeper understanding of self-assembling systems.

2.5   Outlook and conclusions

Using a symmetry boundary condition in curved geometry and placing such boundary at the midplane of a surfactant bilayer is a useful way to analyse the mechanical properties, including the spontaneous curvature, of the monolayers constituting a symmetric bilayer. This idea is implemented in a molecularly realistic self-consistent field model. It is possible to choose the surfactant architecture such that the spontaneous curvature of the monolayer is close to zero and the bilayer is without frustration. In general this is not the case and the monolayers have non-zero spontaneous curvatures. We note that this does not immediately result into loss of thermodynamic stability of the bilayer. Indeed it may be thermodynamically stable even when the monolayers have a significant non-zero spontaneous curvature. The method is not limited to non-ionic systems as discussed in this paper. Corresponding results for (models of) phospholipids in biological membranes may be found elsewhere [79]. It is also possible to evaluate the spontaneous curvature in surfactant layers swollen by an apolar compound, i.e., a suitable oil. This offers the possibility to smoothly go from a Helfrich-type of analysis of swollen surfactant layers to that of micro-

emulsion systems. The finite J_0^m values in the surfactant bilayers are expected to be biologically relevant [132]. More specifically, the spontaneous curvature of the monolayer is expected to be important in processes such as incorporation of protein molecules in lipid bilayers [21], fusion and budding of vesicles, nucleation of pores in bilayers and transport of macromolecules across bilayers.

Chapter 3

Molecular modelling of lipid bilayers and the effect of protein-like inclusions

Abstract

We examined the effect of the insertion of a trans-membrane peptide or protein on the thermodynamic, structural and mechanical characteristics of a lipid bilayer using self-consistent field (SCF) theory. The peptide or protein is modeled as a rigid cylindrical body with a hydrophobic surface and two hydrophilic end caps. We first characterise the properties of the undisturbed bilayer consisting of lipids with a hydrophilic phosphatidylcholine-like head group of 9 segments and two identical tails ranging from 8 to 19 alkyl segments. The structural properties are given in terms of thickness of the hydrophobic core d_l^0 and the area a_0 per lipid. The mechanical or elastic properties are characterised by the mean bending modulus k_c, the saddle splay modulus $\bar{k}$ and the area compression-expansion modulus of the bilayer k_a and its monolayers. Furthermore we calculated the spontaneous curvature J_0^m of the individual monolayer, which can be positive or negative depending on the tail length. Subsequently, we focus on the effect of hydrophobic mismatch between the bilayer and inclusion. The free energy of insertion is parabolic in the mismatch. The minimum is at a small negative mismatch, i.e., when the hydrophobic thickness of the rod is smaller than that of the bilayer. This is attributed to conformational restrictions of the lipid tails close to the rod. This results in a positive curvature of the bilayer adjacent to it, even if the hydrophobic thickness of the rod is larger than that of the bilayer. The bilayer deformation has a wave character which decays exponentially. We show that the decay length of this perturbation is the same as the elastic length $(k_c(d)^2/k_a)^{\frac{1}{4}}$, provided that for the thickness d of the bilayer d_l^0 is used.

3.1 Introduction

The incorporation of peptides and proteins in lipid bilayers or membranes is an important issue in biological systems. Membrane proteins are involved in many cellular processes, acting as receptors, enzymes, channels and so on. Protein moieties that interact with membranes can adopt a surface orientation, partially penetrate the hydrophobic interior or span the hydrophobic core of the lipid bilayer completely. In this study we model the latter configuration, i.e., the inserted or trans-membrane orientation. Membrane-bound proteins that have at least one membrane-spanning domain are called integral membrane proteins. In order to associate with the membrane there has to be a certain degree of hydrophobic match between the membrane-spanning parts of these proteins and the hydrophobic region of the membrane. Hydrophobic mismatch plays an important role in the thermodynamics of the lipid-protein interactions; it perturbs the structure of the surrounding bilayer and as a consequence there will be a deformation free energy cost. This free energy cost depends largely on geometrical characteristics of the proteins membrane-spanning domain, on the structure and mechanical properties of the unperturbed bilayer and on the interaction between the inclusion and the bilayer. It has to be noted that besides this membrane perturbation also the protein might adjust its structure or orientation [39], but we will not go into that in this study.

Hydrophobic (mis)match is an important factor in the functioning and activity of many integral membrane-bound proteins and peptides. For example, mitochondrial cytochrome c oxidase [40], Ca^{2+}-ATPase [13, 14, 41, 42] and (Na^+, K^+)-ATPase [15] have maximum enzymatic activity in phosphatidylcholine lipid bilayers with mono-unsaturated C_{18} tails (di(18:1)PC bilayers). There are also proteins and peptides for which there is no clear optimum bilayer thickness, but of which the functioning is (gradually) lost above or below a particular thickness. An example is the dimeric gramicidin channel [16]. Also the acetylcholine receptor function is correlated with membrane thickness [43]. Also the effect of mismatch on synthetic peptides has been investigated and it was shown that the amount of incorporation of the WALP-peptide in the membrane decreases with increasing negative mismatch [44] and that the way of aggregation is also influenced by the mismatch [45].

Besides many experimental studies, various theoretical models and theories have been used to get more insight into bilayer-protein interactions. Especially the effect of hydrophobic mismatch between the bilayer and the trans-membrane protein parts has been studied extensively. A number of these studies [46–50] can be categorised as phenomenological Landau theories. In all of these theories the effect of a trans-membrane protein is modeled by using a rigid boundary condition for the lipid order parameter. A disadvantage of these theories is that parameters are used that are difficult to relate to measurable physical properties. Furthermore, since a homogeneous dispersion of proteins in the bilayer is assumed, lateral phase separation is excluded. Another Landau type theory that has been used is the so-called mattress model,

which is a two-component theory that allows for lateral phase separation [51]. The two components are the inclusions and the lipids, the basic geometrical variables are the thickness of the hydrophobic region of the lipid bilayer and the hydrophobic length of the inclusion. The model accounts for the elastic properties of the bilayer and that of the inclusion, the hydrophobic mismatch effect, as well as van der Waals interactions. A disadvantage is that microscopic details like the decay of perturbations near individual proteins cannot be described.

Another theory that has been used extensively to describe lipid-protein interactions is the elasticity theory [21,29,31,33,52–58]. It has been developed originally for smectic liquid crystals and later also for the elastic description of lipid bilayers [19]. In a smectic-A type liquid crystal the molecules are arranged parallel to each other, with their principle axes perpendicular to the surface layer. This is comparable to the interior of symmetric lipid bilayers where the arrangement of the tails is on average parallel. An advantage of this model is the use of experimentally accessible elastic parameters of the lipid bilayer. Huang was one of the first researchers who described protein-lipid interactions using a (liquid-crystal) elastic model [52]. He described the free energy of deformation of a solventless membrane with a splay term, a layer-compression term and a surface tension term, although the last one turned out not to be important for perturbation wavelengths in the order of the bilayer thickness. Later this theory has been extended for solvent containing bilayers [53, 54], where the contribution of the surface tension term to the undulation energy turned out to be significant. The effect of the spontaneous curvature J_0 of the monolayer on the insertion energy and the bilayer perturbation profile was first investigated by Ring [54]. It is also argued that when the monolayer's curvature is very large it has to be taken into account that the lipids are capable of tilting away from the normal of the hydrocarbon - water interface and therefore an additional modulus, namely the tilt modulus has to be introduced [19, 31]. The decay length and the periodicity of the perturbation have also been determined with help of elasticity theory by making use of mechanical and geometrical bilayer characteristics [33, 55] and later this has been extended to include the tilt modulus [31].

Detailed microscopic statistical mechanical models have also been used to investigate lipid-protein interaction energies [26, 59–61]. In these models molecular interaction forces and the hydrocarbon chain conformation are taken into account. Marčelja was the first to use a molecular field theory to describe nonspecific lipid-protein interactions [59]. In Marčelja's model the protein is introduced as a rigid cylindrical boundary condition on the lipid orientational order. With this model he describes lipid-mediated interactions between membrane integral proteins which could lead to protein aggregation. Fattal and Ben-Shaul used a molecular model to calculate the free energy and the decay length of membrane perturbations caused by an insertion [60]. The free energy of the lipid tails is calculated using the rotational isomeric state scheme and the interfacial free energy contribution is calculated using a phenomenological expression, which accounts for head group repulsion and

hydrocarbon-water interfacial tension. The main difference with Marčelja's model is the connection between the segments with gauche vs trans energy, while in Ben Shaul's model the chains are entirely flexible. The flexibility turned out to be of negligible importance. More important for the structural and thermodynamical properties are the presence of a well-defined interface and a constant density of chain segments in the hydrophobic interior [62, 63].

In the present study a molecularly realistic self-consistent field (SCF) theory is used to obtain thermodynamical, mechanical and structural characteristics of bilayers and the effect of protein or peptide insertion into such bilayers. The SCF model has been described in detail [64] and has been used for the description of the thermodynamical and structural characteristics of bilayers [65]. It is in spirit similar to the model of Ben Shaul and coworkers, however it is more complete as it imposes no a priori positional constraints on the individual lipids. Besides these characteristics it is also possible to determine mechanical bilayer characteristics like the bending modulus, the saddle splay modulus [18] and the monolayer spontaneous curvature [2]. Furthermore, the area-compression modulus can be determined as will be shown in this paper. The determination of these mechanical characteristics makes it possible to compare the microscopic model with the liquid-crystal elasticity theory. This will be done in this study by comparing the perturbation decay length retrieved from the microscopic SCF segment density profiles with the elastic length that is calculated from bilayer mechanical and structural characteristics.

3.2 Molecular modelling of laterally inhomogeneous lipid bilayers

The basic approximation in mean-field partition functions as in SCF models is that excluded-volume interactions between pairs of molecules (atoms) are replaced by the interaction of a single molecule (united atom) with external potential fields. The latter potential fields are not chosen arbitrarily, but their magnitude reflects the average behavior of all molecules in space and because of this they are known as the self-consistent potential fields $u_A(\mathbf{r})$, where A is the segment type. Here $\mathbf{r}$ is pointing to a discrete coordinate defined by the system.

The first step of a self-consistent field theory is thus to define a suitable coordinate system. The basic idea is that in this coordinate system we are going to apply some symmetry considerations to reduce the 3-dimensional problem into a lower dimensional one. The various geometries used below are illustrated in fig. 3.1. In laterally homogeneous bilayers we can in first order assume that parallel to the membrane surface there are planes in which the local densities of various molecular entities will fluctuate only marginally. In these planes we assume that the potential field is homogeneous. This will result in homogeneity of the density in these planes as well. Perpendicular to these planes the density will vary and thus the potential will
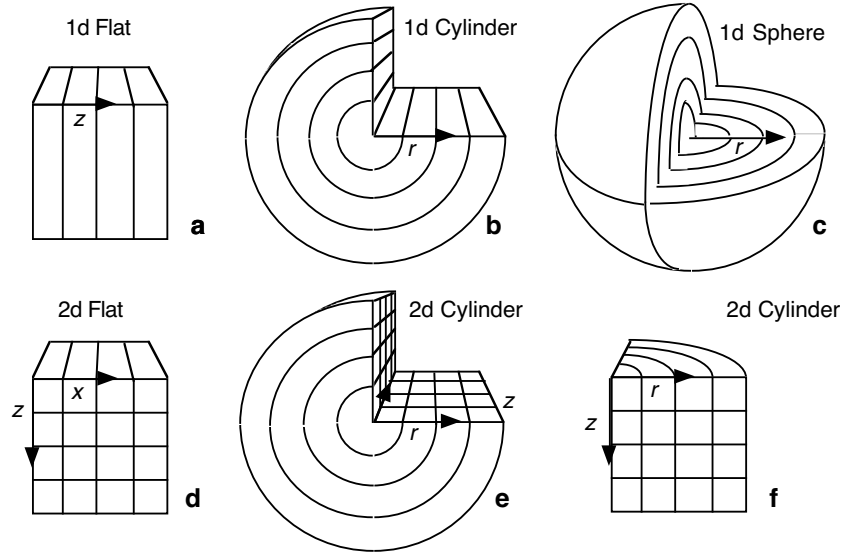
Figure 3.1: Schematic illustration of the lattice geometries used in this paper. In a,b and c the three dimensional space is reduced to a system with only one gradient in density (1d) where the mean field approximation is applied in flat layers (a), cylindrical planes (b) and spherical shells (c). For inhomogeneous bilayers we need to reduce the three dimensional space into two gradients in density as in d, e and f. If the inhomogeneity occurs on one side of the system, we may use a 2d flat system of coordinates (d). If there is a spherical domain in the bilayer matrix a 2d cylindrical geometry is appropriate (e,f). The generalised coordinate will be given by $\mathbf{r}$. In the 1d theory either the z or the r coordinate is used in the flat and cylindrical or spherical geometry, respectively. In the 2d model we use (x, z) in the flat case and (z, r) in the cylindrical case. The arrows point in the directions of the gradients in density and gradients in potential.

be inhomogeneous as well. As a result we reduce the problem to a 1-gradient theory. Below we will apply such 1-gradient (1d) theory to characterise the unperturbed bilayers in terms of their mechanical and structural parameters. In figures 3.1a, b and c we have flat, cylindrical and spherical geometries, respectively. The non-flat geometries are needed to obtain the bending moduli of the bilayers. Inhomogeneous bilayers, i.e. bilayers in which there is a line of perturbation, or one with a local spherical symmetry, should be modeled in a 2-gradient theory using the 2d flat or 2d cylinder geometry given in fig. 3.1d and figures 3.1e and f, respectively.

The target of the theory is to compute the optimal segment density profiles, i.e., for each segment type A the density must be determined at all coordinates $\mathbf{r}$. At this point it must be realised that segments are the building units of the molecules. Let us denote the molecules by the index i. Below we refer to water as $i = 1$, the lipid as $i = 2$, and the protein-like inclusion as $i = 3$. As we will work in a compressible system, we allow for vacant sites on the lattice. For making the equations a bit more symmetric we may think of the existence of a fourth species $i = 4$ which 'occupy' the vacant sites. At this stage it is sufficient to mention that the primary sequence of segments and the way they are connected (chain architecture) are key ingredients of the model. For computational reasons we will apply a coarse grained model for the lipid molecules roughly on the level of united atoms, i.e. a CH_2 or CH_3 group will be represented by one segment (see parameter section below).

As in MD simulations where Newton's law is the governing equation that determines how the evolution of the system takes place after a detailed initial 'guess', the partition function method has a relatively simple governing equation. The mean-field simplification mentioned above allows the calculation of the partition function $Q(n, V, T)$, where n represents the fact that the total number of molecules of each type n_i is known, the volume V of the system is fixed and the temperature T is given. From statistical thermodynamics the partition function is linked to the Helmholtz energy $F = -k_B T \ln Q(n, V, T)$ where $k_B T$ is the thermal energy. Generically this Helmholtz energy can be expressed as a functional of all potentials u and volume fractions φ:

$$F[u, \varphi] = k_B T \sum_i n_i \ln \frac{C_i}{Q_i[u]} - \sum_{\mathbf{r}} \sum_A u_A(\mathbf{r}) \varphi_A(\mathbf{r}) + F^{int}[\varphi] \qquad (3.1)$$

In this equation the first two terms represent the entropic contribution, with the normalisation constant C_i [66] and the single chain partition function Q_i [66], whereas the third therm is the enthalpic contribution to the Helmholtz energy. In the latter term we are going to implement the local compressibility condition that $\varphi_4(\mathbf{r}) = 1 - \sum_{i=1}^{3} \varphi_i(\mathbf{r})$. The first term is a functional of the potentials only, whereas the interaction part can be computed once all volume fractions are known. The second term is the signature of the self-consistent field theory. It shows that the segment potentials and the segment densities are conjugated quantities. Eqn 3.1 should only be used for the condition that the free energy is optimised with respect to these two
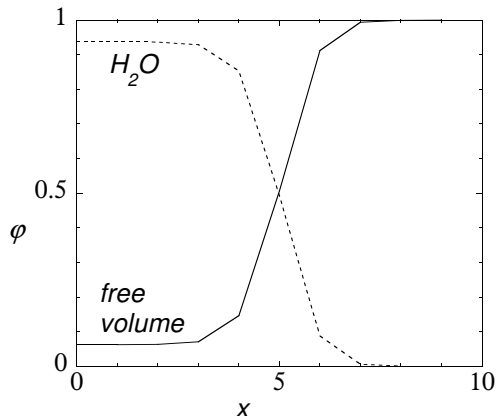
Figure 3.2: The segment-density profile of water and free volume across the air-water interface.

types of distributions, i.e.,

$$\frac{\partial F}{\partial u_A(\mathbf{r})} = -\sum_i \frac{n_i k_B T \partial \ln Q_i}{\partial u_A(\mathbf{r})} - \varphi_A(\mathbf{r}) = 0 \qquad (3.2)$$

$$\frac{\partial F}{\partial \varphi_A(\mathbf{r})} = -u_A(\mathbf{r}) + \frac{\partial F^{int}}{\partial \varphi_A(\mathbf{r})} = 0 \qquad (3.3)$$

for all coordinates r and segments types A. This set of equations forms the basis of any self-consistent field theory. It exactly specifies how to compute the segment volume fractions from the segment potentials and how the segment potentials follow from the segment volume fractions. When these two complementary computational routes are consistent with each other, the free energy of Eqn 3.1 is optimised and the structural properties can be found from analysing the detailed volume fraction profiles and the thermodynamic quantities follow directly from differentiation of the Helmholtz energy [67]. Here we will continue with the precise definition of the system used and discussing the parameters of the model.

3.3 Parameters

To present realistic equilibrium hydrated lipid bilayers one should realise that lipids self-assemble due to the fact that the tails want to escape from the water phase. From this point of view it is natural to pay attention to both the lipid bilayer as well as the aqueous medium. The simplest model is that the water phase is considered to be composed of simple monomers and the second component is an amphiphile with a series of polar segment connected to a string of apolar segments.

Such a primitive model suffers from a series of shortcomings. The major one is due to the translational entropy of the monomeric water units. Water partitions in the bilayer in very significant amounts if the interaction parameters are

chosen such that the critical micelle concentration (CMC) has a reasonable value. Alternatively, by using extreme values for the repulsion between tail segments and water dehydration of the bilayers core is possible. This however will set the CMC at a concentration that is orders of magnitude too low compared to experimental estimates.

We solve this problem in first order by considering water to be present as clusters consisting of five water segments and allow only translational entropy for the cluster. The cluster is build from one central and four surrounding units. In this model the water content in the bilayers core is less than 1 volume percent.

The second major parameter in bulk water is its overall volume fraction, or alternatively, the amount of free volume in the bulk. The Flory-Huggins interaction parameter between free volume V and water W units was fixed to $\chi_{VW} = 2.3$. This value has been chosen in such a way that the surface tension of the calculated air-water interface, which is shown in fig. 3.2, is of the same order of magnitude as the surface tension of a real air-water interface. In passing we note that $\chi_{VV} = \chi_{WW} = 0$ by definition and only one parameter sufficies. Here; $\chi_{VW} = \frac{Z}{2k_BT}[2U_{VW} - U_{VV} - U_{WW}]$, where Z is the lattice coordination number, and U_{XY} is the interaction energy between units X and Y. In free volume theories one can realise that all interactions with vacancies should be identical to zero and thus $U_{VW} = U_{VV} = 0$. As a result one finds the one-to-one relation that $\chi_{VW} = -\frac{Z}{2k_BT}U_{WW}$. So, without loosing generality we can use the FH parameters even in a free volume theory. This parameter is sufficient to generate an interface between a water-rich and a free-volume-rich phase. In fig. 3.2 we show the profile of the 'air'-water interface. According to experimental facts, the interface is sharp and extends over just a few water molecule lengths. From this equilibrated interface we extract the saturated amount of free volume in the water phase. This value is given by $\varphi_V^b = 0.051396$ and was fixed in subsequent calculations.

The lipid molecules have a branched structure. On the branch point two identical apolar tails with length t are coupled to a hydrophilic head group. The head group is a mimick of phophatidylcholine, having two hydrophilic fragments, each consisting of three segments, spaced by a pair of apolar units. See fig. 3.3 for a pictorial representation of the molecular entities used in the calculations.

Below we will specify the interaction for the various segments in the lipid molecule both with the water molecules as well as with the free volume. By choosing the tails of the lipids to have a higher affinity for free volume as for water, we anticipate that some free volume will accumulate in excess with respect of the water phase in the bilayer. As soon as these parameters are fixed we have no free variables left to model the adsorption of lipids on the air-water interface. In this paper we will not go into these details and only mention that in such calculations it found that the tails are oriented towards the free volume phase and the head groups remain hydrated.

In table 3.1 we have collected the full set of Flory-Huggins parameters used in our calculations. The most important one which drives the self-assembly of the
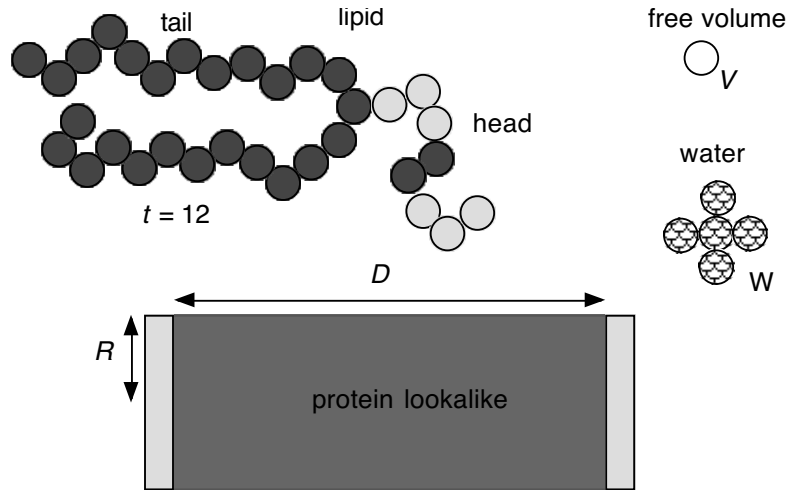
Figure 3.3: Structure of molecules that are used in the calculations.

	C	W	X	V	S	E
C	0	1.1	2.5	1.5	−1.0	2.0
W	1.1	0	−0.5	2.3	2.0	0
X	2.5	−0.5	0	2.3	2.0	0
V	1.5	2.3	2.3	0	1.5	2.3
S	−1.0	2.0	2.0	1.5	0	0
E	2.0	0	0	2.3	0	0

Table 3.1: The Flory-Huggins interaction parameters

lipids is $\chi_{WC} = 1.1$. The value of this parameter is chosen such that the tail length dependence of the CMC of a surfactant molecule was accurately reproduced. Moreover the CMC values of the lipids are close to the experimental ones. The amount of mixing of head and tail segments in the bilayer is governed by $\chi_{XC} = 2.5$ where X is a hydrophilic head group unit. The high positive value is necessary to avoid too much overlap between the profiles of these chain fragments. Finally there are the hydrophilic water contacts χ_{XW} for which a value close to zero is chosen. The equilibrium membrane thickness results from a balance of forces: the hydrophobic driving force and the crowding of hydrated head groups on the membrane surface which gives a stopping force. The conformational stretching-entropy loss of the apolar tails is another stopping mechanism. Thermodynamic analysis of free floating membranes that can adjust their area shows that their surface tension vanishes. This quantity follows from the Helmholtz energy by subtracting all the chemical work terms (including the contribution of the vacancies, which may be interpreted as the volume work):

$$\gamma = \frac{F - \sum_i \mu_i n_i}{A} \tag{3.4}$$

where A is the membrane surface area. As for the Helmholtz energy the surface tension is found as a functional over the segment volume fractions and the segment potentials and can be evaluated accurately after the SCF solution is found.

Using the 1d coordinate systems, we can evaluate the structural and mechanical parameters of the bilayers. In the first part of the results section we will do this as a function of the tail length of the lipids. These results will serve as the reference for the study of bilayers containing protein-like inclusions. In this paper we will focus on the effects of the inclusion of a simple, solid cylinder-like object (see fig. 3.3) and we will explicitly ignore all internal degrees of freedom of the protein-like inclusion. In future work we will allow for various internal degrees of freedom of the inclusions. Now the focus is on the lipids rather than on the protein. The central part of the inclusion is composed of units S with an apolar character. This part is very well solvated by the lipid tails. The entropy loss of the tail units near the impenetrable inclusion is compensated by assigning a finite value of χ_{SC}, namely -1. The rod-length is fixed to 7, 8 or 9 lattice units and both sides of the rod have an hydrophilic end-cap composed of units E. The radius of the rod is fixed to 6 lattice units.

The membrane thickness is varied by considering lipids with different tail length. In this way the mismatch between the membrane core and the apolar part of the protein-like inclusion can be varied. The last part of the discussion is completely devoted to the membrane perturbations. The effect of the interaction of the tails with the hydrophobic inclusion, the radius of the membrane inclusion and the interaction between two membrane inclusions will be topics of a forthcoming paper.
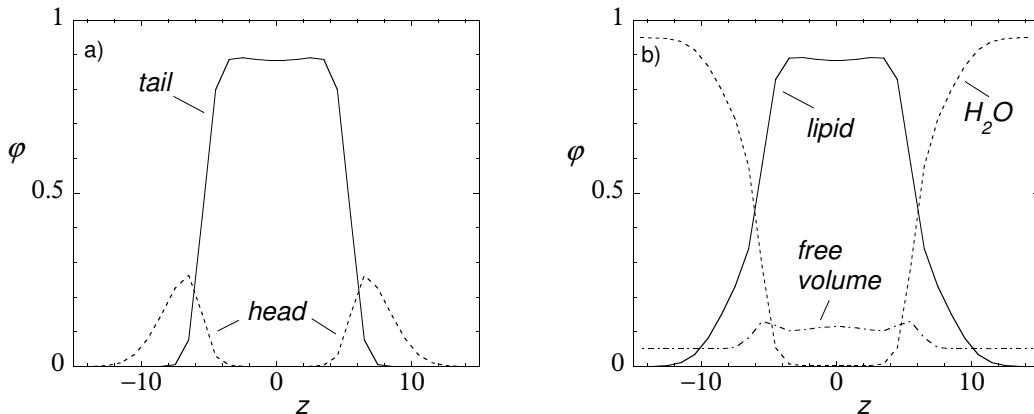
Figure 3.4: Volume-fraction profiles across a tensionless planar lipid bilayer with $t = 18$. a) Lipids tail and head segments. b) Lipid, water and the free volume segments.

3.4 Results and discussion

3.4.1 Structural properties of the bilayer

We evaluated several bilayers composed of lipids with tails ranging from 8 to 19 segments. It has to be noticed that all bilayers are tensionless and in the fluid state. Volume fraction profiles across a planar bilayer consisting of lipids with 18 segment tails are shown in fig. 3.4. Fig. 3.4a shows the volume fractions of the lipid tail and head segments and fig. 3.4b gives the overall volume fractions of the other segments in the system, namely free volume and water. In the hydrophobic interior the volume fraction of the tails is approximately 0.89, while that of the free volume and water is approximately 0.11 and less than 0.005, respectively. At the bilayers exterior the volume fraction of hydrophilic heads does not exceed 0.30. This implies that the corona interface of the bilayer consists mainly of water that is trapped between the hydrophilic head groups. The hydrophobic thickness of the bilayer is arbitrarily taken as the distance between the positions where the volume fraction of the tails equals 0.5. This hydrophobic bilayer thickness d_l^0 is for this particular bilayer 10.62 lattice layers l and the area per lipid a_0 is 8.38 l^2. In the next calculations we assume that $l = 0.2$ nm, which is an approximation from the volumes of the various atomic groups represented by the different segments in our system. This lattice spacing gives a d_l^0 of 2.12 nm and an a_0 of 2*0.34 = 0.67 nm^2. The multiplication of the lipid area with 2 is to correct for the fact that the lattice sites are not isotropic [64]. Comparison of these calculated geometrical dimensions with those of a fluid 1,2-dioleoyl-sn-glycero-3-phosphocholine (DOPC) bilayer shows that they are in good agreement. The experimentally determined d_l^0 of a DOPC bilayer is 2.6 nm [68] and a_0 is 0.72 nm^2 [69]. The fact that the calculated d_l^0 is smaller than the experimentally determined hydrophobic thickness can be largely attributed to the fact that in the calculations the lipid tails are fully flexible in contrast to the semi-flexible acylchains of DOPC.
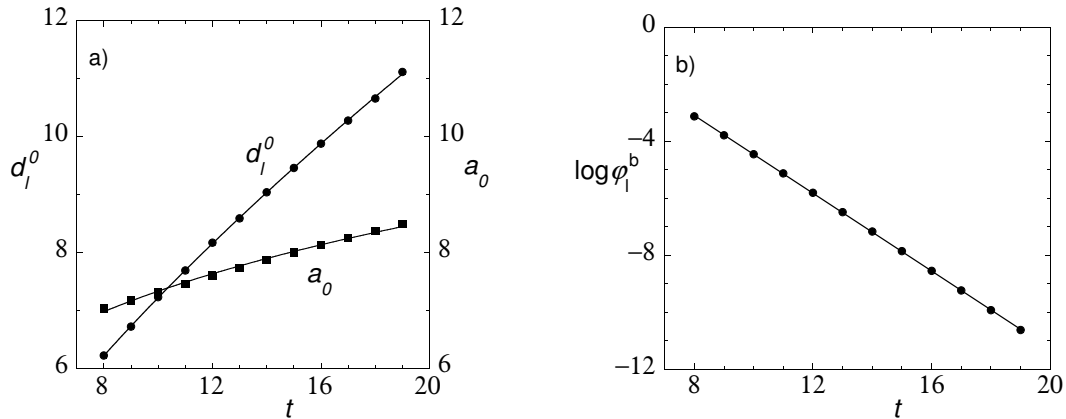
Figure 3.5: Characteristic dimensions of bilayers with tail length t ranging from 8 to 19 segments. a) Bilayer hydrophobic thickness d_l^0 in lattice layers l and the area per lipid a_0 in square lattice layers l^2. b) The bulk volume fraction φ_l^b of the freely dispersed lipids coexisting with the tensionless bilayers.

It is important to mention that the membrane characteristics, such as the packing densities of the chains in the core and the head group region, do in first order not depend on tail length t. Only the dimensions of the bilayer, such as the hydrophobic thickness d_l^0 and the area per lipid a_0, vary with the length of the acyl chains. In fig. 3.5a the hydrophobic thickness and the area per lipid molecule are presented as a function of t. As expected both parameters increase with increasing t. When we calculate from this the hydrophobic volume per lipid molecule v_l, i.e., by multiplying d_0^l with a_0, it is clear that there is an almost linear relation between the chain length and the hydrophobic volume per lipid.

The bulk volume fraction of the freely dispersed lipids, φ_l^b, coexisting with the tensionless bilayer shows a logarithmic dependence on t as is shown in fig. 3.5b. About every three segments increase of the tail length, φ_l^b decreases by two decades. This dependence is a result of the fact that when t increases the number of possible unfavorable interactions between the tail and the water molecule increases and consequently the lipids have a higher tendency to form aggregates in which the tails are screened from the water molecules [70]. In the calculations where a protein-like inclusion perturbs the bilayer we have fixed φ_l^b to the value of the unperturbed bilayer. By doing so we make sure that far from the inclusion the membrane tension vanishes.

3.4.2 The mechanical properties of the lipid bilayer

Helfrich showed that the physics of tensionless bilayers is dictated by the mechanical parameters [19], i.e., the bending modulus k_c and the saddle splay modulus $\bar{k}$, which is also called the Gaussian bending modulus. The k_c is a measure for the rigidity of the bilayer and has necessarily a positive value because any deformation with respect to the equilibrium state increases the free energy of the bilayer. The Gaussian

bending modulus $\bar{k}$ on the other hand can be negative or positive and determines the topology of the bilayer. If $\bar{k}$ is negative spherical deformations are preferred and if $\bar{k}$ is positive the free energy is lowered by saddle splay surface formation. The mechanical parameters k_c and $\bar{k}$ can be obtained unambiguously from SCF calculations using the Helfrich equation, when homogeneously curved geometries are used [18]. The Helfrich equation describes the curvature dependence on the surface tension of lipid bilayers [19].

$$\gamma(J, K) = \gamma_0 + \frac{1}{2}k_c(J - J_0)^2 + \bar{k}K \qquad (3.5)$$

The surface tension γ of the lipid bilayer is zero in the case of a flat symmetric bilayer. The total curvature, $J = 1/R_1 + 1/R_2$ and the Gaussian curvature $K = 1/(R_1R_2)$ are determined by the local radii of curvature R_1 and R_2. The spontaneous curvature J_0 corresponds to the minimum in the interfacial free energy and is zero in the case of symmetric bilayers. Because the geometry of the coordinate system is an input constraint, the variation in bilayer curvature can be achieved by changing the number of lipid molecules in non-flat geometries [18, 25]. Both cylindrical and spherical vesicles can be used to elucidate $\bar{k}$ and k_c. In the case of a cylindrical geometry $K = 0$, $J = 1/R$ and the bilayer area $A = 2\pi Rh$, where R is the radius and h the length of the aggregate. Now eqn 3.5 can be reduced to

$$\epsilon^c \equiv \gamma(J)A = \pi k_c Jh \qquad (3.6)$$

which defines the grand potential of the cylindrical bilayer. The mean bending modulus k_c can now be determined by plotting ϵ^c vs J. A spherical vesicle can subsequently be used to determine $\bar{k}$. When the bilayer is placed in a spherical geometry it is clear that $J^2 = 4K = 4/R^2$ and $A = 4\pi R^2$, and this means that eqn 3.5 can be written as

$$\epsilon^s \equiv \gamma(J)A = 4\pi(2k_c + \bar{k}) \qquad (3.7)$$

which defines the grand potential of a spherical vesicle. It is obvious that in the case of a symmetric bilayer ϵ^s is not a function of R. Because k_c is known from the cylindrical geometry it is now easy to calculate $\bar{k}$.

With the methods described above k_c and $\bar{k}$ have been determined for bilayers consisting of lipids with varying tail length t. The results are shown in fig. 3.6a. k_c values of the bilayers are proportional to t and they are in the order of 10-20 k_BT, which is comparable with experimental bending moduli of phospholipid bilayers [71–73]. The $\bar{k}$ values have a very weak dependence on t and are negative in all cases. The $\bar{k}$ values are in the same order of magnitude as $-k_c$. From these k_c and $\bar{k}$ values it can be concluded that all the bilayers are capable of forming stable lipid vesicles because $2k_c + \bar{k} > 0$.

Besides the k_c and $\bar{k}$, which give information about the rigidity and topology of the lipid bilayer, another parameter, namely the area compression-expansion mod-
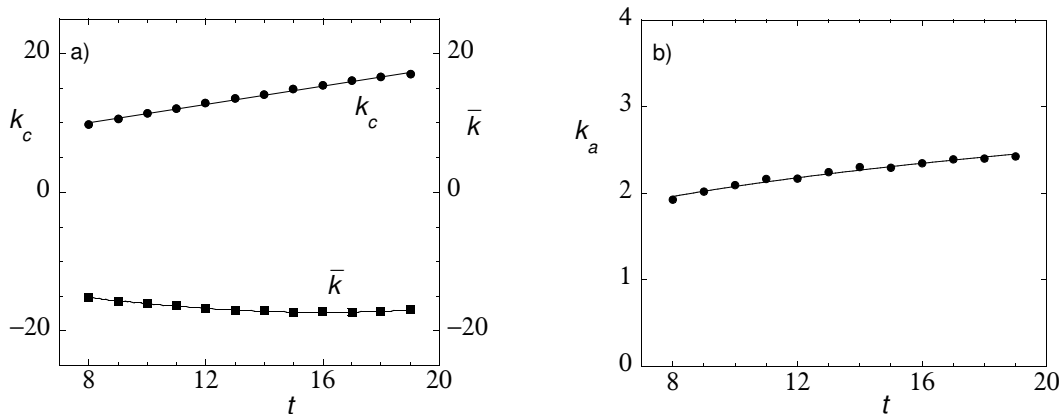
Figure 3.6: a) k_c and $\bar{k}$, both expressed in units of $k_B T$, as a function of lipid tail length t. b) The area compression-expansion modulus k_a given in units $k_B T/l^2$ as a function of t.

ulus k_a, has been determined. This k_a gives the surface tension change by relative expansion or compression of the bilayers surface area.

$$k_a \equiv \left(\frac{\partial \gamma}{\partial \ln a} \right)_{\gamma=0} \tag{3.8}$$

The k_a of the bilayer has been determined by calculating the surface tension for fixed numbers of lipid molecules per unit area in a flat geometry. The k_a values are depicted in fig. 3.6b. The plot shows that k_a increases weakly with increasing t. The values are of the same order as experimentally determined values of fluid phosphatidylcholine bilayers [74, 75]. Occasionally one finds in the literature [76, 77] the suggestion that $k_c \propto k_a (d_l^0)^2$. This relation follows from the assumption that the two leaflets of the bilayer slide against each other upon bending the bilayer. We cannot find evidence for this from our SCF analysis proving that curving the bilayer cannot be simply mimicked by a sliding / expansion-compression process.

3.4.3 The mechanical properties of the lipid monolayer

We also developed a method to determine the elastic properties of an individual monolayer that makes up half of a bilayer. This method has been described in detail elsewhere [2] and therefore only a short description is given here. The basic idea is to place the monolayer directly next to a reflecting boundary in a 1-dimensional cylindrical and spherical geometry. By doing so the curved monolayer feels a similarly curved monolayer (it's mirror image) just outside the system. Concentrating on the grand potential of just one of the monolayers, it is possible to derive the bending modulus k_c^m, the saddle splay curvature $\bar{k}^m$ and also the spontaneous curvature J_0^m of the monolayer in more or less the same way as shown for bilayers. Referring to fig. 3.7 we define positive curvatures when the monolayer is expanded in headgroup and compressed in the tail region. It has to be noticed that J_0^m is not zero in most
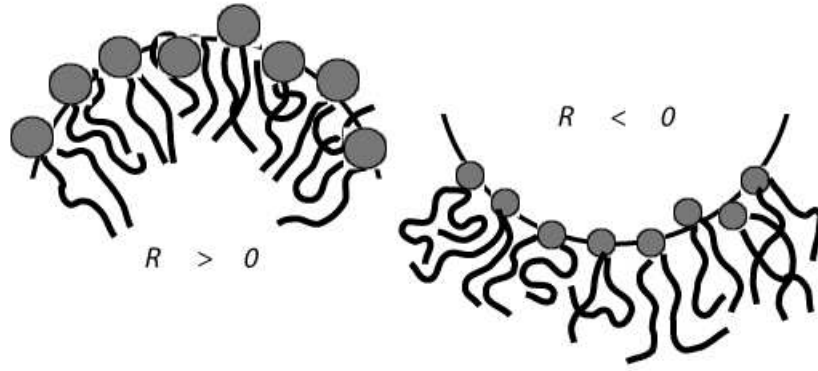
Figure 3.7: Two monolayers with a positive (left) and negative (right) radius of curvature.

cases and this means that equation 3.5 can be written as :

$$\gamma(J, K) = \gamma_0^m + \frac{1}{2}k_c^m J^2 - k_c^m J J_0^m + \frac{1}{2}k_c^m J_0^{m2} + \bar{k}^m K \qquad (3.9)$$

Because the surface tension of the flat bilayer is zero, it is also zero for the two identical opposing flat monolayers. This means that $\gamma_0^m + \frac{1}{2}k_c^m J_0^{m2}$ is also zero and that these terms can be excluded from eqn 3.9. If the monolayer is now placed in a cylindrical lattice eqn 3.9 can be written as:

$$\epsilon^{cm} \equiv \gamma(J)A = -2\pi k_c^m J_0^m h + \pi k_c^m J h \qquad (3.10)$$

which defines the grand potential of the cylindrical monolayer aggregate ϵ^{cm}. From eqn 3.10 it is possible to retrieve k_c^m and J_0^m by plotting ϵ^{cm} against J. By subsequently placing the monolayer in a spherical lattice geometry eqn 3.9 can be changed to

$$\epsilon^{sm} \equiv \gamma(J)A = 4\pi(2k_c^m + \bar{k}^m) - 8\pi k_c^m J_0^m R \qquad (3.11)$$

which defines the grand potential of the spherical monolayer aggregate ϵ^{sm}. Since k_c^m is known it is possible to retrieve $\bar{k}^m$ from this equation.

To determine the monolayer's mechanical parameters it is further necessary that φ_l^b is the same as in the case of the homogeneously curved bilayer to ensure the same chemical potential of the lipids. The mechanical parameters of monolayers consisting of lipids with $t = 8$, 9, 13, 14, 17, 18 and 19 were determined with this method and the results are shown in fig. 3.8.

In fig. 3.8a k_c^m and $\bar{k}^m$ are shown. Both parameters were determined for the inner as well as the outer monolayer, which gave the same result. The calculated k_c^m and $\bar{k}^m$ values are in good agreement with the bilayer properties, i.e., practically equal to $\frac{1}{2}k_c$ and $\frac{1}{2}\bar{k}$, respectively. The very small deviations observed are probably due to very small details regarding the interdigitation of tails into opposite monolayers. However, the close agreement shows that the followed procedure gives a very good
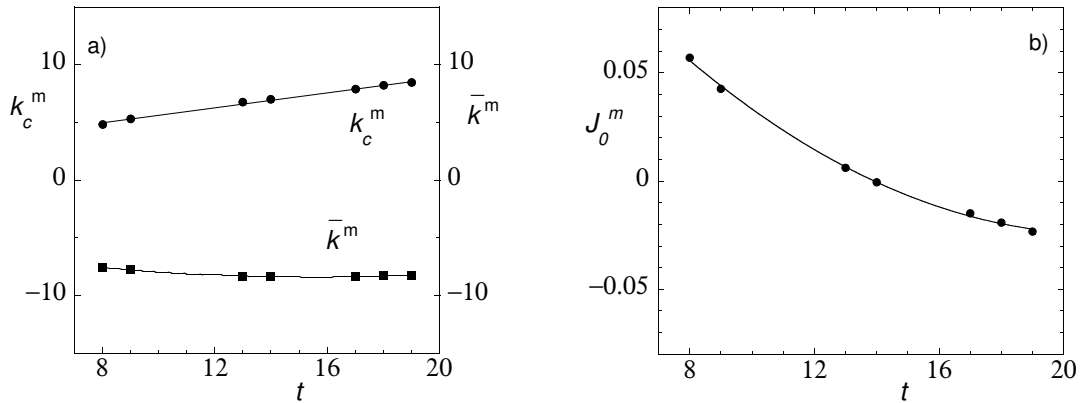
Figure 3.8: a) The bending modulus of the lipid monolayer k_c^m and its saddle splay modulus $\bar{k}^m$ as a function of t. Both moduli are given in units $k_B T$. b) The dependence of the spontaneous curvature J_0^m of the monolayer on t.

approximation of the mechanical properties of the monolayer. More importantly, the spontaneous curvature of the monolayer J_0^m is shown in fig. 3.8b. According to intuition J_0^m decreases with increasing t, because the volume and the area of the tails increase while the head group packing is more or less constant. Lipids with very short tails therefore tend to have a high positive spontaneous curvature and have a tendency to form spherical micelles instead of lamellar bilayers. Lipids with long tails on the other hand have a negative spontaneous curvature and they have a tendency to form hexagonal phases. Interestingly, the monolayer consisting of lipids with $t = 14$ has a J_0^m of approximately zero. This means that these lipids are the most suitable for arrangement in a flat tensionless bilayer.

3.4.4 The insertion of a hydrophobic rigid rod

Now that the bilayers have been fully characterized an inclusion with a hydrophobic body is incorporated into these bilayers. In the remainder of this paper we will see how the bilayers adjust to this protein-like inclusion. The rod, with a hydrophobic length D, is inserted as shown in fig. 3.9. The hydrophobic mismatch Δd is defined as $\frac{1}{2}(D - d_l^0)$ and is varied by changing the bilayer thickness at three values of D.

In fig. 3.10a the normalized insertion free energy $f = \frac{F}{2\pi R k_B T}$ is plotted for several lengths of the rod D. It can be seen that f is parabolic in Δd and the curves shift to higher values as D is larger. The minimum ranges from $f = 3.1$ when $D = 7$ to $f = 3.4$ when $D = 9$ and occurs at a negative mismatch $\Delta d \approx -0.7$ in all cases. It has to be mentioned that the value of Δd is somewhat arbitrary, because it depends on the choice of the bilayer's interface, which is at $\varphi_C = 0.5$ in our case. However, the minimum insertion energy remains at a negative Δd till $\varphi_C \approx 0.73$.

The normalised insertion free energy f can be regarded as a sum of four contributions, which are not completely separable. These are (i) the bilayers deformation energy caused by the mismatch, f_d, (ii) the entropy loss and bilayer deformation

top view   side view

Figure 3.9: Schematic representation of the insertion of a hydrophobic rod with hydrophilic end caps in a bilayer.

energy caused by conformational restrictions of the tails adjacent to the inclusion, f_c, (iii) the direct contact interaction energy of the inclusion and the tails, f_i and (iv) the interaction energy of the inclusion end caps with their environment, f_h.

The parabolic dependence of f with Δd is thought to mainly result from two of these contributions. The first one is the deformation energy of the bilayer f_d, because the bilayer adjusts its structure to minimize the contact of the hydrophobic regions with the aqueous solution. If this was the only contribution, the minimum of the parabolic function would have been at $\Delta d = 0$. However, due to the conformational restrictions in close proximity of the rigid inclusion the tails tilt away. Since the bilayer density in the core remains constant, deformation of the bilayer occurs even in the case that $\Delta d = 0$.

The third contribution to the insertion free energy, f_i, is negative because it results from the attractive interaction between the inclusion and the tails. It has only a very weak dependence on Δd, because the density of the tail in the first layer adjacent to the inclusion is practically the same in all cases. The variation in this density is less than 5 percent.

Finally, the interaction energy of the inclusion's end caps with the lipids and the bulk solution, f_h, is rather complex and not only results from direct interactions between the caps and their environment but also from the entropic loss of the lipids adjacent to this cap. The total contribution is rather large but has marginal dependence on the mismatch. In our calculations it is approximately 1.74 $k_B T$.

Now let us focus on the deformation of the bilayer caused by the embedded inclusion. Fig. 3.11 shows the profile of the lipid tails density in the case that $D = 8$ and $t = 8$, i.e., $\Delta d = 0.86$. In this figure it is easily seen that the bilayer adjusts itself to minimize contact of the hydrophobic regions with the aqueous solution. One can measure several physical membrane properties as a function of the r-coordinate. For example one can measure the membrane thickness, the area per molecule, the perturbation of the packing density in the core etc. We choose the area per molecule for our futher analysis, because it can be determined very accurately. Fig. 3.12a shows profiles of the area per lipid relative to that in an unperturbed bilayer, $a(r) - a_0$. For $D = 8$ and t ranging from 8 to 19 the mismatch varies from $\Delta d = -1.50$ to
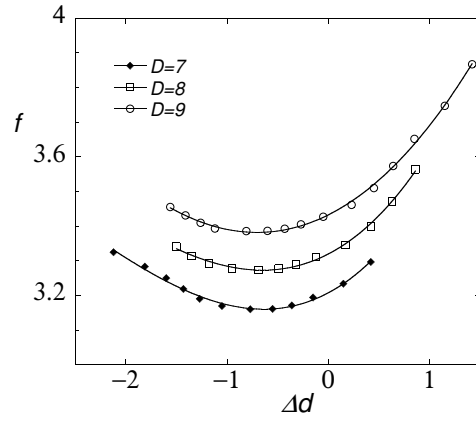
Figure 3.10: The dependence of the insertion free energy of the inclusion in the bilayer f on Δd.
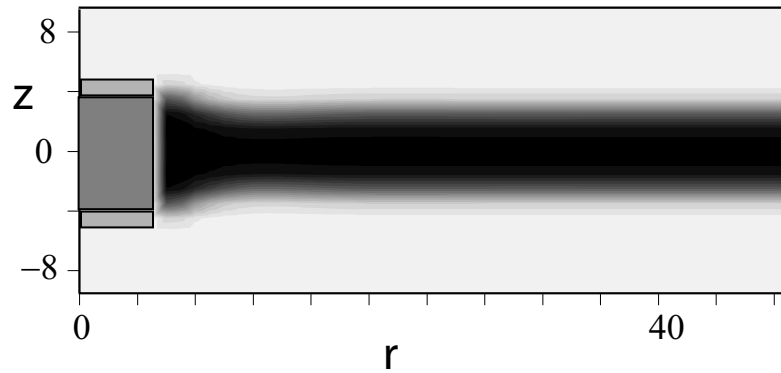

Figure 3.11: Tail volume fraction density profile of a bilayer. In this case a rod with $D = 8$ is inserted in a bilayer consisting of lipids with $t = 8$.
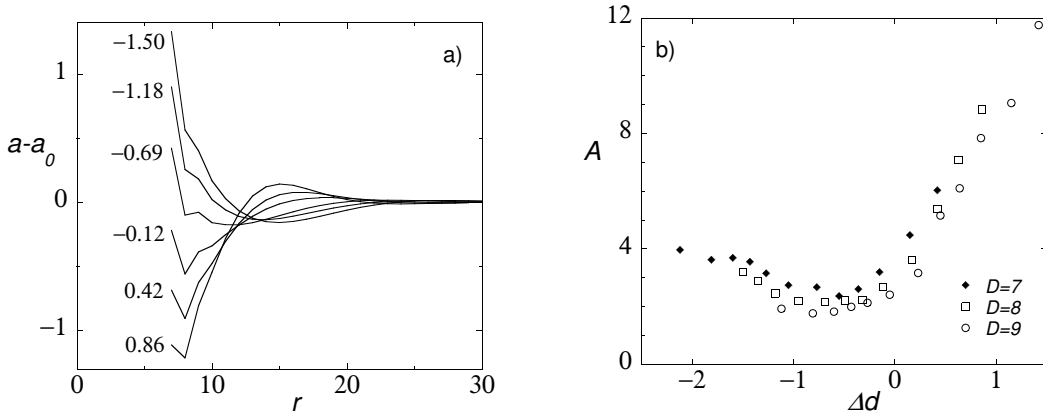
Figure 3.12: a) The lipid area perturbation profile for different Δd (see figure) when $D = 8$. b) The dependence of the perturbation amplitude A on Δd.

0.86. The perturbation profile has a wavelike appearence and decay exponentially. However, the onset of the exponential decay is approximately at $R + \frac{1}{2}d_l^0$. One may describe this profile by

$$a(r) - a_0 = A \exp\left(-\frac{r}{\xi}\right) \sin(2\pi(\frac{r - \delta}{\lambda})) \tag{3.12}$$

The equation accurately describes the deformation of the bilayer only for $r > R + \frac{1}{2}d_l^0$, because at shorter distances the orientation and conformation of the tails is directly affected by the rigid inclusion. In equation 3.12 δ represents the first position from the centre of the inclusion where $a(r)$ is equal to a_0 and where $\frac{\mathrm{d}a(r)}{\mathrm{d}r} > 0$.

In fig. 3.12b the dependence of A, which we will call the perturbation amplitude, on Δd is plotted. A exhibits a minimum at $\Delta d \approx -0.7$, in line with the the position of the minimum in insertion free energy (fig. 3.10). This suggests that the parabolic dependence of f is related to the bilayer deformation.

The parameters A and δ are determined by D and t. The decay length ξ and the wavelength λ, which are retrieved from fitting, are determined entirely by bilayer characteristics, i.e., they are independent of D. The decay length ξ is proportional to the tail length as is shown in fig. 3.13a and it ranges from 3.5 l to 5.5 l. With $l = 0.2$ nm, ξ ranges between 0.99 nm and 1.56 nm. There are a couple of reasons that could account for the difference with the decay lengths determined by Fattal and Ben Shaul [60] who reported values ranging from 0.3 to 0.6 nm. An important difference is that they preassumed an exponential decay starting adjacent to the inlcusion, while we did not put any constraints on the profile and find that the decay has an onset at approximately half the hydrophobic thickness of the bilayer

Beside microscopic models also elasticity theory has been used to determine the decay length of bilayer perturbations. In several studies the decay length was retrieved by using the Euler-Lagrange equation for the minimization of monolayer perturbation energy. This is described with the area compression-expansion modulus of the monolayer, k_a^m, which is $\frac{1}{2}k_a$, the monolayer's bending modulus, k_c^m, which is
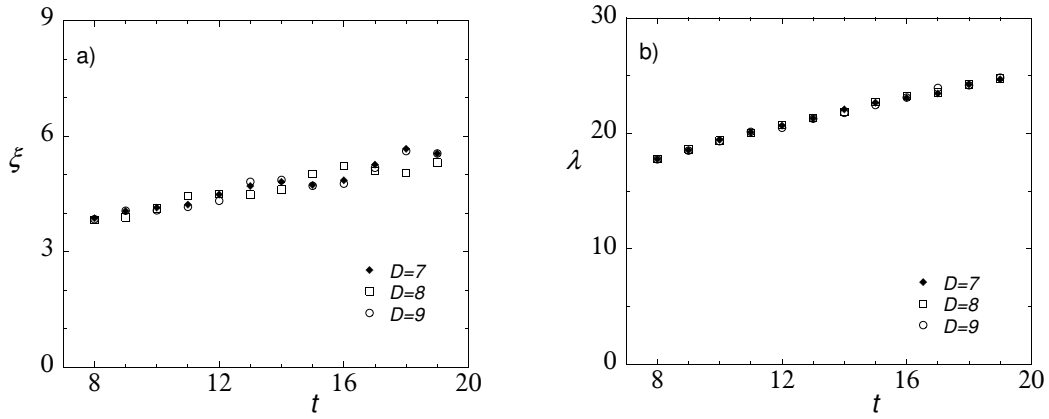
Figure 3.13: The decay length and the wavelength (both in units l) vs t.

$\frac{1}{2}k_c$ and the bilayer thickness, d_l^0, as shown in [33, 55].

$$F = \frac{1}{2}\int_R^\infty k_a^m \frac{u^2}{(\frac{1}{2}d_l^0)^2} + k_c^m(\frac{\partial^2 u}{\partial r^2})^2 \mathrm{d}r \qquad (3.13)$$

The elastic decay length that is retrieved from this equation is also a function of the bilayer thickness d_l^0 and the monolayer's mechanical moduli k_c^m and k_a^m:

$$\xi_e = \sqrt[4]{\frac{(d_l^0)^2 k_c^m}{k_a^m}} \qquad (3.14)$$

May extended the formula for the determination of the elastic decay length by introducing the tilt modulus and proposed a decay length [31], which we will call the elastic tilt decay length, ξ_t, described by

$$\frac{1}{\xi_t} = \frac{\sqrt{k_a^m}}{d_l^0}\sqrt{\frac{d_l^0}{\sqrt{k_c^m k_a^m}} + \frac{1}{k_t^m}} \qquad (3.15)$$

For the calculation of ξ_t, tilt moduli, k_t^m, have been used that were calculated simply by analysing the orientational fluctuations of the tails in the equilibrium bilayer (for details see the appendix). The results of this exercise are presented in in fig. 3.14a. This figure shows that the tilt modulus decreases with tail length, which is easily explained because longer tails fluctuate more easily away from the membrane normal. Fig. 3.14b shows our microscopic decay length ξ, which is an average of results for the three inclusion sizes, D = 7, 8 and 9, the elastic decay length ξ_e and the elastic tilt decay length, ξ_t. From this it is clear that our decay length within numerical precision, is the same as ξ_e, while ξ_t is significantly smaller. Also if the tilt modulus proposed by May [31] is used, ξ_t is still significantly smaller. Only for infinite k_t^m, i.e., when tilt is ignored, the decay lengths become equal, i.e, $\xi = \xi_e = \xi_t$. The resemblance between the microscopic and the elastic decay length shows that the relevant bilayer thickness for the elastic length scale is the hydrophobic core dimension. Finally we note that in the calculation of ξ_e the monolayer spontaneous

62
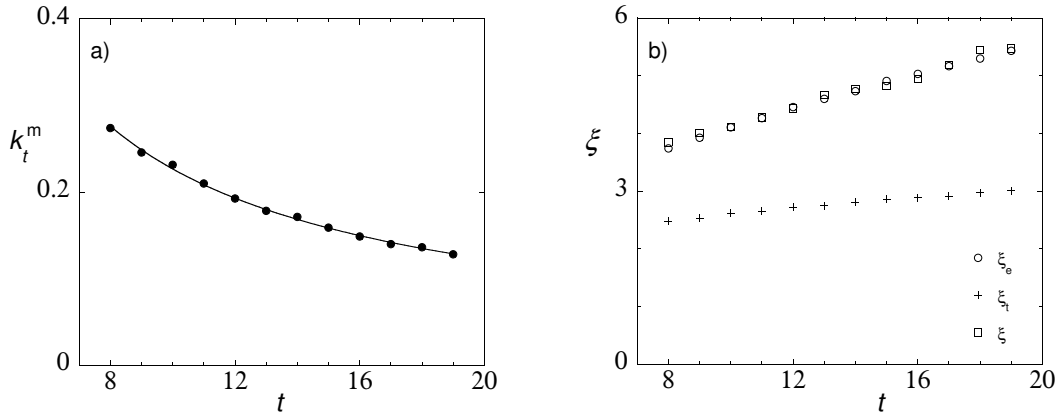
Figure 3.14: a) The tilt modulus k_t^m vs t. b) Comparison of the different decay lengths vs t. ξ_e is determined from elasticity theory, ξ_t is determined from elasticity theory with tilt and ξ is determined with microscopic theory.
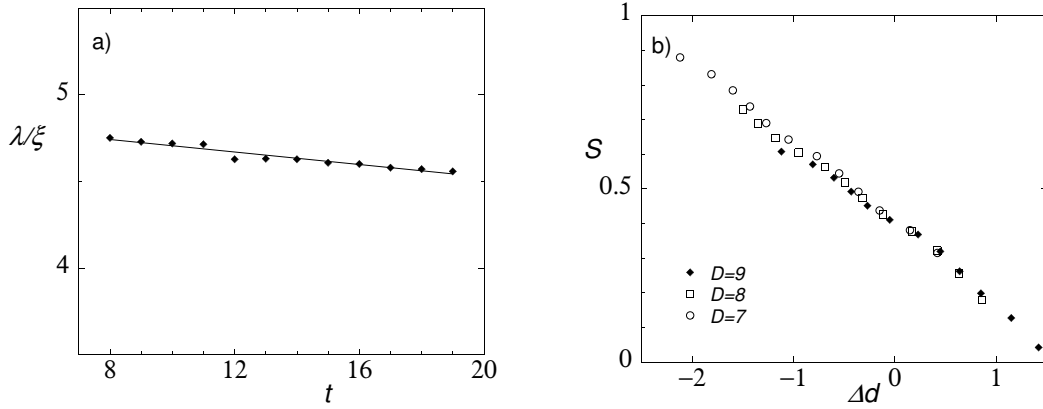
Figure 3.15: a) The correlation between the perturbation wavelength λ and the decay length ξ for different tail lengths. b) The slope S of the bilayers at $r = R$

curvature was assumed to be zero. Apparantly, this spontaneous curvature is of negligible importance in determining the elastic length scale. However, in the case of the wavelength λ, the spontaneous curvature may have a minor contribution, because there is a small decrease of the ratio λ / ξ with increasing tail length as shown in fig. 3.15a.

Finally, another interesting property of the perturbation profile, is the contact slope S of the bilayer surface at $r = R$. S is defined as $(\frac{\partial d_l(r)}{\partial r})_{r=R}$. In our case S is determined as the slope of the bilayers surface in the first layer adjacent to the inclusion. Fig. 3.10a shows that S is proportional to Δd. One can also see that S is the same for all inclusion lengths. The linear dependence has been discussed within the framework of bilayer elasticity theory [21] where S minimizes f and where $\frac{\partial f}{\partial S}$ = 0. Although both our model and the bilayer elasticity theory show this linear dependence, there are some differences. For instance $\frac{\partial S}{\partial \Delta d}$ in the elasticity model is -1 nm^{-1}, while in our case this is much lower, namely -0.16 nm^{-1}. Another

important difference is that our results show that $S > 0$ when $\Delta d = 0$, while in the elasticity model $S = 0$. These difference can be attributed to the conformational restrictions of the tails caused by the rigid inclusion explicitly accounted for in our approach, while in the elasticity theory these conformational restrictions are not included. Another interesting aspect is that the linear dependence of S with Δd is approximately the same for all D. From this it can be concluded that S is mainly determined by the mismatch and the conformational restrictions of the tails. The spontaneous curvature of the monolayer, which varies with t, seems to be of minor importance.

3.5 Conclusions

Using a molecularly realistic self-consistent field (SCF) theory we have analysed the structrural perturbations and corresponding thermodynamic effects of inserting rod-like inclusions (mimicking trans-membrane proteins or peptides) into tensionless lipid bilayers. We found that the free energy of insertion is at its minimum at a small negative mismatch, i.e., when the hydrophobic thickness of the inclusion is somewhat smaller than that of the bilayer. That the minimum is not precisely at zero mismatch, is due to conformational restrictions of the lipid tails near the inclusion. This results into a tendency of the tails to tilt away from the rod, which, in turn, gives rise to a positive curvature of the bilayer/solution interfaces adjacent to the inclusion. The spontaneous curvature of the individual monolayer halves of the bilayer, which we showed to depend on the lipid tail length, seems to be of minor importance for this phenomenon. As a function of distance from the inclusion the bilayer perturbation has a damped-wave character. The decay length as derived from our microscopic SCF model equals the decay length computed using elasticity theory, provided that in the latter theory for the bilayer thickness the dimension of the hydrophobic core is used. The ratio between the period and the decay length of the perturbation is rather constant, showing that the periodicity also largely depends on the elasticity of the bilayer. This ratio only slightly decreases with increasing lipid tail length, which is tentitavely attributed to the decreasing spontaneous curvature of the monolayers. In a forthcoming paper we will look into the effect of the inclusion's radius and the lipid-mediated interaction between two or more membrane-spanning peptides.

3.6 Appendix: Tilt modulus

As explained above the SCF theory features for each segment type two conjugated profiles. There is the segment potential $u_A(\mathbf{r})$ which operates as an external potential to obtain the probability distribution of conformations of molecules. From the information of the statistical weight of all possible and allowed conformations one can extract the volume fraction profiles $\varphi_A(\mathbf{r})$. This means that the volume

fractions are a functional of the potentials. In short we write $\varphi[u(\mathbf{r})]$, where we have dropped the indices to the segment types for convenience. The potentials are known as self-consistent potentials because the potentials are made a functional of the volume fraction profiles. In short, this may be expressed as $u[\varphi(\mathbf{r})]$. We solve for a self-consistent solution of these equations numerically upto high precision (at least 7 significant digits), without the need to put positional constraints on the molecules. All lipid molecules may either choose to self-assemble in the bilayer structure or to remain in the aqueous solution. In the bilayer the solvation energy is low, but in solution the entropy is high. At equilibrium the chemical potentials of each of the molecules are the same everywhere in the system. Furthermore, the total number of lipid molecules in the system is adjusted such that the membrane tension vanishes (for the unperturbed bilayers).

Once a self-consistent field solution is obtained one can analyse various properties of the lipid molecules. For example it is straightforward to measure the thickness of the bilayer the orientational order of the tails and the head group, the average position of each of the segments as well as the fluctuations of it. Moreover one can evaluate the bond order profile which is experimentally accessible. One of the properties we have computed is the level of interdigitation of the lipid tails of one monolayer into the other layer [78]. For symmetric bilayers one has to unravel the distribution of the tails of lipids belonging to one monolayer from those belonging to the other monolayer. This is routinely been done by computing density-density correlation functions. To compute the tilt modulus we need to make again use of these conditional distribution functions. In short the goal is to find the statistical distribution function of tail ends away from the normal.

In a two-gradient SCF model we have a coordinate system as given in fig. 3.1d. The z-coordinate is in the normal direction, the bilayer is in the x-y-plane. In the unperturbed bilayer the probability to tilt in the x-direction is the same as in the y-direction. It suffices to analyse the tilt in the x-direction. Lets assume that the equilibrium membrane exists in the x-y-plane. Of all lipid conformation we concentrate on the subset of lipids that have the branching unit, given by the segment $s = s^*$ (where the two alkyl tails meet with the head group) at any z-position (referred to by z_{s^*}), but constrained on a given x-coordinate which is far from the system boundaries, we choose to name this coordinate $x = 0$. The full set of conformations of this subset of molecules is characterised by the volume fraction profile $\varphi(z, x, s|z_{s^*}, 0, s^*)$. Our special interest is in the distribution of the tail ends with ranking numbers $s = s_1$ and $s = s_2$. Because of symmetry reasons in the molecule these two segments have exactly the same distribution. Let us therefore focus on one of them, i.e. s_1. We are interested in the probability that segment s_1 is at a coordinate x. To obtain this probability distribution we have to integrate over all possible coordinates of the tail end, i.e. z and the coordinates of the branch point z_{s^*}:

$$p(x) = \frac{\sum_z \sum_{z_{s*}} \varphi(z, x, s_1 | z_{s*}, 0, s^*)}{\sum_z \sum_{z_{s*}} \sum_x \varphi(z, x, s_1 | z_{s*}, 0, s^*)} \tag{3.16}$$

where the denominator is used to normalise the probability distribution to unity. This probability distribution has a peak at $x = 0$, is symmetric, i.e. $p(-x) = p(x)$ and falls off for larger values of $|x|$ to zero. Near $x = 0$ it is Gaussian. This means that $\ln p(x)$ is parabolic

$$-\ln p(x) = k_t^m x^2 + C \tag{3.17}$$

The steepness of the parabola is given by k_t^m which may be identified as the tilt modulus and has dimensions $1/l^2$. The larger the tilt modulus the harder it gets for the tails to wonder away from the normal.

Chapter 4

Molecular modelling of peptide-like inclusions in lipid bilayers: Lipid-mediated peptide-peptide interactions

Abstract

The trans-membrane peptide-lipid bilayer interaction is investigated with a self-consistent field theory. The peptide is modelled as a rigid cylindrical (with radius R) or flat inclusion with a hydrophobic surface and two hydrophilic end-caps. The lipids are modelled as a hydrophilic phosphatidylcholine-like head group linked to two hydrophobic tails both with length t. Three different aspects are investigated. We show that the insertion free energy Ω is strongly regulated by the short-range interaction energy between the hydrophobic surface of the inclusion and the lipid tails and that this parameter controls the best match of the hydrophobic length of the inclusion with that of the lipid bilayer. Furthermore, we show that the line-tension $\tau = \Omega/2\pi R$ decreases linearly with the curvature $J_p = 1/R$ of a cylindrical inclusion. These results are used to analyse how the boundary lipids around the inclusions influence the colloidal stability of the inclusions. The free energy of interaction between two inclusions (with curvature $J_p = 0$) is strongly non-monotonic as a function of the distance between the inclusions. There are three different length scales, namely (i) the long-range elastic interaction, which is an exponentially decaying oscillation. In some situations this elastic interaction can be strong enough to play a role in the lateral organisation of proteins in the bilayer. (ii) The intermediate length scale repulsive interaction is a consequence of the conformational restriction of the tails between two inclusions and is only weakly influenced by the hydrophobic mismatch and the tail-peptide interaction. (iii) The characteristics of the short-range interaction, which typically also has a oscillatory and/or a depletion-induced attractive contribution, is largely determined by the tail-peptide interaction.

4.1 Introduction

The functioning and organisation of trans-membrane peptides and proteins in a membrane is determined by many factors. A well studied and important aspect, which we investigated in an earlier paper [79], is the hydrophobic mismatch between the inclusion and the lipid bilayer. A hydrophobic mismatch is defined as $\frac{1}{2}(D - d_l^0)$, with D the hydrophobic peptide length and d_l^0 the unperturbed hydrophobic bilayer thickness. When there is a difference in these lengths, the bilayer can adapt itself to avoid contact between hydrophobic parts and water. However, there is a free energy penalty associated with such adaptation. The mismatch issue is of key importance for the functioning and activity of various integral membrane-bound proteins and peptides, as is shown in several experimental studies [13–16, 40–45]. Besides experimental work, a significant theoretical effort is underway to gain insight into the physical aspects of peptide insertion. Some of these studies extend the elasticity theory developed by Helfrich [19] to get phenomenological insights into the energetically and structural consequences of hydrophobic mismatch [21, 52–55, 58]. An important extension of this elasticity theory was the introduction of the chain directors model by May, which accounts for the conformational restrictions of the lipid chains in the vicinity of the inclusion that determine local deformations of the bilayer [31]. Other studies analyse detailed microscopic statistical mechanical models [60, 79]. In these models molecular interaction forces and the hydrocarbon chain conformations are taken into account. The models that have been used by Fattal and Ben-Shaul [60] and by the present authors [79] have much in common. However, the approach taken by us is somewhat more advanced as we impose no *a priori* positional constraints on the individual lipids. Besides a hydrophobic mismatch, also the structural properties of the inclusion, such as the curvature, and more general the shape and its size affect peptide insertion. Dan and Safran [56] studied the effect of various inclusion geometries on the structural spatial perturbations of the bilayer and found that a given lipid will favour a particular protein conformation over another one.

In biological membranes a typical trans-membrane peptide conformation is the α-helix conformation, which has a radius of approximately 0.5 nm. This dimension is comparable to the cross-section of a lipid molecule. Larger trans-membrane structures such as magainin-pores, $R = 4.5$ nm and alamethicin pores, $R = 2.0$ nm, are known to have a set of trans-membrane α-helical structures. Another well-known example is a small pore protein called gramicidin, which consists of two $\beta^{6.3}$-helices that span half the bilayer each and have a radius of approximately 0.9 nm. One can pose significant questions regarding this size range, whether the range of curvatures observed of these peptides have some physical underpinning and whether there is a thermodynamically most favourable size. Lagüe et al. [27, 28] used molecular dynamics in combination with statistical mechanical integral equation theory. They investigated the incorporation of rigid cylindrical inclusions with a radius of 0.25,

0.5 and 0.9 nm into lipid bilayers of various thickness and consisting of saturated or unsaturated lipids. They found two different bilayer perturbation oscillations around the inclusions, each having a different length scale. Besides an exponentially decaying oscillation with a wavelength of 1 nm, they also found a less pronounced oscillation with a much longer wavelength. They furthermore showed that this long-wavelength oscillation becomes more obvious when the radius of the inclusion increased. These complex results call for complementary approaches directed to unravel this. Our self-consistent field (SCF) method is suitable to do such job, especially for the properties on the nanometre length scale and above. We will study the effect of the inclusions curvature on the bilayer perturbation around the inclusion and its effect on the free energy of insertion.

Intuitively, one would expect that there might be (free) energy interactions involved when the lipid tails are forced to be near the hydrophobic part of the inclusion. There is not much known about the consequences of such interactions. In most theoretical studies it is assumed that the lipids freely adjust their conformation to overcome any 'interaction' mismatch and leave possible nearest-neighbour interactions tactically out of the analysis. However, it is clear that such interactions between the inclusion and the bilayer must exist simply because the protein-like bodies and the lipids have different chemical constituents. For example, the outside of a α-helix will be rich in CH_3 groups especially when only alkyl groups point outwards. Below we will allow for some various interactions between the inclusion's surface and the lipid tails and show that the hydrophobic mismatch is not purely a geometric quantity, but that a hydrophobic interaction between the inclusion and the lipid tails should be included in the analysis as well. We will further show that the overall free energy of inclusion insertion into the bilayer is largely determined by the interaction energy of lipid-tails with the inclusions and that these interactions also influence the lipid perturbations. The effect of the curvature of the inclusion and the non-ideal hydrophobic interaction are in this paper studied with a rather primitive model for the protein-like inclusion, namely the cylindrical rod with a hydrophobic surface, covered on both sides by a hydrophilic cap.

The main focus of this paper is however on understanding how the lipids mediate the interaction between these inclusions. In general this problem is very complex as in experimental systems the peptide-peptide interactions have, e.g., electrostatic, van der Waals, hydrogen bonding, etc. contributions. Our simple model for the limiting case that the protein-like inclusions are flat (curvature of the inclusion is ignored) reduces this problem significantly, albeit that it still is a very rich system.

In the past a number of studies has been performed concerning lipid-mediated protein-protein interaction [26–28, 30, 32–36, 50, 80–82]. Most of these studies used the elasticity theory [32, 33, 35, 36, 81], but also a molecular field theory [26, 30], the phenomenological Landau theory [50], some Monte Carlo [34] and Molecular Dynamics simulations [27, 28] have been directed to this problem. From all these studies three different length scales have been found for bilayer-induced peptide-peptide

interaction: (i) the oscillating and exponentially decaying (mesoscopic) long-range interaction caused by the overlap of the inclusion-induced mesoscopic structural bilayer perturbations. The wavelength and decay length of this interaction profile is determined by the structural and elastic properties of the bilayer [32, 33, 79]. (ii) The intermediate length scale where another interaction contribution becomes important, namely a repulsive interaction [27, 30, 34]. This is caused by the overlap of the domains in which the inclusions induce a tilt of the lipids. This results in conformational restrictions of the lipid tails in the confined space between the inclusions. (iii) When the inclusions approximate each other very closely, i.e., on the (segmental) short-range length scale, a depletion-induced attraction between the inclusions starts to play a role as is shown by a couple of studies [27, 28, 30, 34]. In all of these studies there was no effective adsorption of the lipid tails to the inclusion's surface. However, in this paper we also consider non-ideal interactions between tails and the inclusions and will show that they play an important role in the short-range interaction between inclusions. If the adsorption of the lipid tails on the inclusions surface increases, the depletion-induced attraction disappears and is replaced by a large oscillating and strongly decaying interaction. Our method is computationally inexpensive and numerically very accurate so we can obtain systematic predictions for these complex problems.

The remainder of this paper is as follows. First we will outline the SCF model and discuss the parameters used for the modelling. In our results section we will discuss basically three types of problems. The first is related to the influence of non-ideal interactions between tails and the inclusion on the structural properties of the lipid bilayer. The second aspect is related to the effect of the curvature of the inclusions and finally we consider the lipid-mediated interactions between inclusions. In the last sections we will discuss some implications of our result and formulate our conclusions.

4.2   Theory and methods

4.2.1   Self-consistent field theory

The current SCF theory has been successfully used to study self-assembling structures, like bilayers, micelles and vesicles [64, 83, 84]. The theory is formulated using a discrete lattice. This allows us to accurately and efficiently account for the different conformations of chain-like and branched molecules. The lattice represents a three-dimensional system, but a mean-field approximation allows us to use two- or one coordinate lattices, depending on the number of gradients present in the system. These lattices can have a spherical, cylindrical or flat geometry, depending on the system that is modelled. The advantage of this reduction in dimensions is that the calculation time remains very low. A drawback is that the aggregates are forced to adopt a preset geometry. In our calculations two-dimensional flat and cylindrical
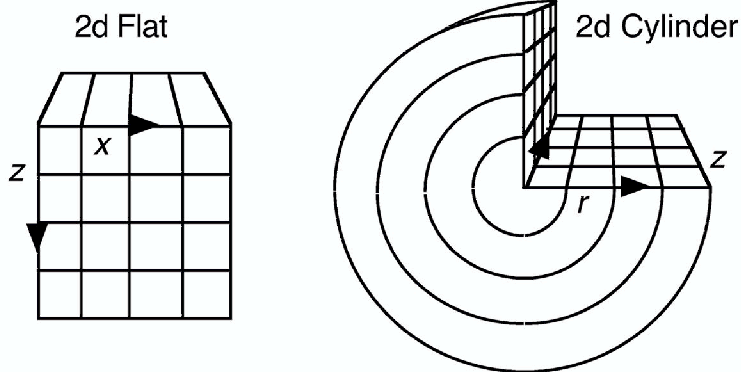
Figure 4.1: Schematic illustration of the two lattice geometries used in this paper. Both are systems where two volume fraction gradients are present. If the inhomogenity occurs in two perpendicular directions, we may use a 2d flat system of coordinates (a). If there is a spherical domain in the bilayer matrix a 2d cylindrical geometry is appropriate (b). We use $\mathbf{r} = (x, z)$ in the flat case and $\mathbf{r} = (z, r)$ in the cylindrical case. The arrows point in the directions of the gradients in the densities and potentials.

systems are used as shown in figure 4.1, which makes it possible to study laterally inhomogeneous bilayers. The two gradients in the molecular structure are perpendicular to the bilayer's surface and perpendicular to the inclusion's surface. For inclusions with radius R the cylindrical coordinates are used. In the limit $R \to \infty$ this coordinate system is identical to the 2d flat one.

The molecules present in the system are coarse-grained on the united atom level, i.e., they consist of segments, which are the basic building blocks. All segments are uniform in size and have the same volume as a lattice site. The basic idea in this theory is that instead of keeping track of exact positions of the segments the focus is on average density at a given position, i.e., at a given lattice site.

In mean-field partition functions the excluded-volume interactions between pairs of molecules are replaced by the interaction of a single molecule with external potential fields. These potential fields reflect the average behaviour of all molecules in space. The physical meaning of this potential field $u_A(\mathbf{r})$ is that it contains all the potential energy contributions to bring a segment A from bulk to position $\mathbf{r}$, with $\mathbf{r} = (z, x)$ in 2d flat and $\mathbf{r} = (z, r)$ in 2d cylindrical geometry. The potential energy of a segment A at position $\mathbf{r}$ can be written as

$$u_A(\mathbf{r}) = u'(\mathbf{r}) + k_B T \sum_B \chi_{AB}(<\varphi_B(\mathbf{r})> - \varphi_B^b) \tag{4.1}$$

The $u'(\mathbf{r})$ is the excluded-volume potential which arises from the incompressibil-

ity constraint $\sum_A \varphi_A(\mathbf{r}) = 1$. In other words, it is the energy needed to generate a vacant site at position $\mathbf{r}$ to insert segment A. The second term accounts for the non-ideal interactions of segment A with all other segment types, denoted by B. The Flory-Huggins nearest-neighbour exchange energy parameter is denoted by χ_{AB}. It describes the interaction energy between segment A and segment B. The parameter is negative when the AA and BB interactions are energetically unfavourable compared to the AB interactions and positive when it is the other way around. The parameter φ_B is the volume fraction of B and the superscript b refers to the bulk solution, i.e. the aqueous solution at infinite distance from the bilayer. The angular brackets represent a local average.

$$< \varphi_B(\mathbf{r}) >= \sum_{\mathbf{r}'} \varphi_B(\mathbf{r}')\lambda(\mathbf{r},\mathbf{r}') \tag{4.2}$$

where $\lambda(\mathbf{r},\mathbf{r}')$ is the *a priori* step probability to go from coordinate $\mathbf{r}$ to $\mathbf{r}'$ [64]. It is non-zero when $\mathbf{r}$ and $\mathbf{r}$' are neighbouring sites. These *a priori* step probabilities depend on the type of lattice used and implement the difference in lattice geometry. This site-averaging thus account for the gradients in the distribution which are geometry-dependent. In the most simple case, i.e., a one-dimensional flat lattice where $\mathbf{r} = z$, this local average can be written as $< \varphi(z) >= \lambda_{-1}\varphi(z-1)+\lambda_0\varphi(z)+ \lambda_1\varphi(z+1)$, with $\lambda_{-1} + \lambda_0 + \lambda_1 = 1$.

From the potential $u_A(\mathbf{r})$ it is possible to retrieve the distribution and thus the volume fraction $\varphi_A(\mathbf{r})$ of a *free* segment A on coordinate $\mathbf{r}$.

$$n_A(\mathbf{r}) \propto G_A(\mathbf{r}) = \exp\left(\frac{-u_A(\mathbf{r})}{k_B T}\right) \tag{4.3}$$

Here k_B is the Boltzmann constant and T is the temperature. The number of segments A at position $\mathbf{r}$ is given by $n_A(\mathbf{r})$, which is proportional to the Boltzmann factor $G_A(r)$. The computation of the volume fraction $\varphi_i(\mathbf{r},s)$ of segment s of molecule i on coordinate $\mathbf{r}$ is more complex. Here the ranking number s of the segments ranges from 1 to N_i, where N_i is the total number of segments in molecule i. To evaluate this it is necessary to generate all possible configurations of each molecule i. Here, a possible configuration is defined by the set of coordinates $\{\mathbf{r}_s^c\}_i$ for all segments of molecule i. The degeneracy of conformation c, can be enumerated by

$$\omega_i^c = L(\mathbf{r}_1^c) \prod_s^{N_{i-1}} \lambda(\mathbf{r}_s^c, \mathbf{r}_{s+1}^c) Z \tag{4.4}$$

Here $\lambda(\mathbf{r}_s^c, \mathbf{r}_{s+1}^c)$ is the *a priori* step probability when going from segment s at $\mathbf{r}_s^c$ to segment $s+1$ at $\mathbf{r}_{s+1}^c$. The other parameter $L(\mathbf{r}_1^c)$ is the number of lattice sites at coordinate $\mathbf{r}$ where segment $s = 1$ of molecule i in conformation c is placed. The parameter Z is the coordination number of the lattice and determines the total number of neighbour sites. As transition probabilities obey the detailed balance

equation $\lambda(\mathbf{r}_s, \mathbf{r}_{s+1})L(\mathbf{r}_s) = \lambda(\mathbf{r}_{s+1}, \mathbf{r}_s)L(\mathbf{r}_{s+1})$ it is possible to show that ω^c does not depend on direction of the walk along the chain, i.e., the inversion symmetry is obeyed.

Assuming now that all $u_A(\mathbf{r})$ are known (equation 4.1), it is rather easy to evaluate the overall potential u_i^c of a molecule i in conformation c.

$$u_i^c = \sum_{s=1}^{N_i} \sum_A u_A(\mathbf{r}_s^c)\delta_{i,s}^A = \sum_{s=1}^{N_i} u_i(\mathbf{r}_s^c) \tag{4.5}$$

where the chain architecture operator $\delta_{i,s}^A$ is unity when segment s of molecule i is of type A and zero otherwise. The right-hand side of equation 4.5 shows that if the potentials of the individual segments are known it is just a matter of adding up all these segment potentials $u_i(\mathbf{r}_s^c$ to obtain the overall segment potential u_i^c of a molecule i in conformation c. From this overall potential it is possible to determine the statistical weight of this conformation by determining the Boltzmann weight:

$$n_i^c = C_i\omega_i^c \exp\left(\frac{-u_i^c}{k_B T}\right) \tag{4.6}$$

where n_i^c is the number of molecules i in conformation c and C_i is the normalisation constant [66]. After summation over all conformations c the volume fraction profiles are found.

It is in principle straightforward to generate for a given molecule all possible self-avoiding conformations on the lattice. However, in practice for systems containing many molecules this approach becomes exceedingly time consuming. There exist very efficient schemes to sum-up the statistical weights of a set of conformations if the chains need not be self-avoiding; these schemes are known as Markov chains. In this paper we have implemented a first-order Markov approximation which has the property that for a fixed chain architecture segments along the chain occupy neighbouring sites, but that excluded volume correlations along the chain are not exactly obeyed. This means that the chain can fold back on previously occupied sites. These intra-chain excluded volume problems are very similar to inter-chain excluded volume problems inherent in a SCF analysis which are treated on the same footing.

Thus far we have shown that there are potentials $u_A(\mathbf{r})$ that are a function of the volume fractions (eqn 4.1), and that in turn these potentials determine the volume fractions (eqn 4.6). A numerical algorithm is used to find the corresponding system, better known as the self-consistent field (SCF) solution. For such SCF solution it is possible to compute the free energy and various other thermodynamic potentials such as the grand potential [18], which can be defined with

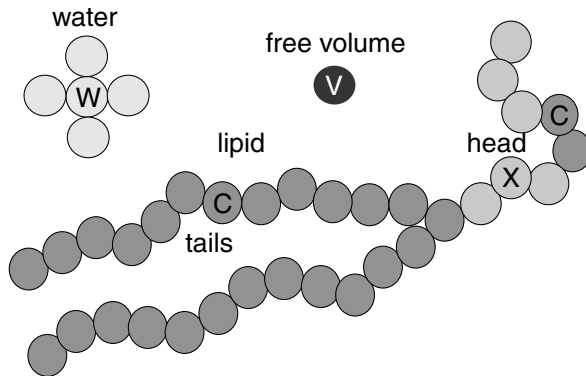$$\Omega = \sum_z \sum_r L(r)\omega(z, r) \tag{4.7}$$

Figure 4.2: The molecules that are used in the calculations are coarse-grained on a molecular level. The water molecule is a cluster of five identical W-segments, while the free volume is a single hydrophobic V-segment. The most complex molecule in the system is the lipid that consists of two tails of length t. The tail segments are hydrophobic and each segment represents a CH_2- or a CH_3-group. The lipid head comprises two hydrophilic regions consisting of three segments which are spaced by two hydrophobic segments that are identical to the tail segments.

with $L(r)$ the number of lattice sites at coordinate (z, r) and $\omega(z, r)$ is the grand-potential density at each lattice site [64]. The number of lipid molecules in the bilayer (area per molecule) is used in a subsequent numerical optimisation step to find the bilayer that is tensionless (equilibrium for freely-floating unsupported bilayers), i.e., $\gamma(r) = 0$, with $\gamma(r)$ the local surface tension, which is given by

$$\gamma(r) = \sum_z \omega(z, r) \tag{4.8}$$

4.2.2   Parameters and summary of previous results

At the basis of our analysis we consider tensionless bilayers. The modelling and characterisation of these have been discussed in a previous paper in detail [79] and will be briefly reviewed. The structure of the molecules is presented in figure 4.2 and the relevant interaction parameters are collected in table 4.1. The branch point in the lipid couples two hydrophobic tails of length t to a hydrophilic head group. The head group mimics phosphatidylcholine, containing two hydrophilic fragments of three segments spaced by two hydrophobic segments. Lipids freely distribute between being dispersed in the aqueous solution and being densely packed in the bilayer. The concentration of the freely dispersed lipids, the critical micellisation concentration (c.m.c.), is determined to a large extent by the Flory-Huggins parameter χ_{WC} for the interaction between the tail segments (C) of the lipids and the water segments (W). We use $\chi_{WC} = 1.1$, which gives the correct tail length dependence for the c.m.c. for surfactants. This means that C and W repel each other and this drives

	C	W	X	V	S	E
C	0	1.1	2.5	1.5	−1.0	2.0
W	1.1	0	−0.5	2.3	2.0	0
X	2.5	−0.5	0	2.3	2.0	0
V	1.5	2.3	2.3	0	1.5	2.3
S	−1.0	2.0	2.0	1.5	0	0
E	2.0	0	0	2.3	0	0

Table 4.1: The Flory-Huggins interaction parameters between the different segments. A positive value means that the interaction is repulsive and a negative value represents an attractive interaction with respect to the interaction between identical segments.

the self-assembly of the lipids. On the other hand, the lipid head group contains six hydrophilic (X) segments that contribute to the stopping force for self-assembly. This suggests that the interaction between these segments and water is attractive. We choose $\chi_{XW} = -0.5$ as in our previous paper [79].

From experiments it is known that water is almost completely absent in the hydrophobic core. For this reason we have implemented water as a small compact cluster of 5 segments as shown in figure 4.2. Such clusters of water will not easily partition in the core, i.e., the water content in the bilayers core is less than 1 volume percent. Furthermore, like in the previous paper [79], we account for some volume fraction of vacant sites (V) in the system. The Flory-Huggins parameter $\chi_{VW} = 2.3$ has been chosen in such a way that the surface tension of the calculated V-W interface is of the same order of magnitude as experimentally determined values. The bulk volume fraction of free volume in the aqueous solution is $\varphi_V^b = 0.051396$ which is fixed throughout all calculations. Previous studies on the membrane formation by such model lipids in an aqueous solution revealed that the head groups should not mix well with the lipid tails. Again in line with previous calculations, the demixing of the lipid tails and heads is established with $\chi_{XC} = 2.5$. The hydrophobic segments (S) and the hydrophilic end-cap segments (E) of the peptide will be discussed in a later section.

The structural and mechanical properties of the bilayers are a result of the balance between the hydrophobic driving force and the stopping mechanisms, like the crowding of the hydrated head groups and the stretching of the lipid tails. In figure 4.3 an example is shown of a segment density profile across a bilayer composed of lipids with $t = 18$. In this figure it is seen that water solvates the head group but not the tails, the free volume partitions more in the bilayer than in the aqueous solution, the size of the bilayer head group region is comparable to the hydrophobic region and the segment density in the core of the hydrophobic region is homogeneous. Many features in figure 4.3 follow quantitatively corresponding MD results as was shown a number of years ago [67].

From our previous results [79] we know that in this model the bilayer thickness
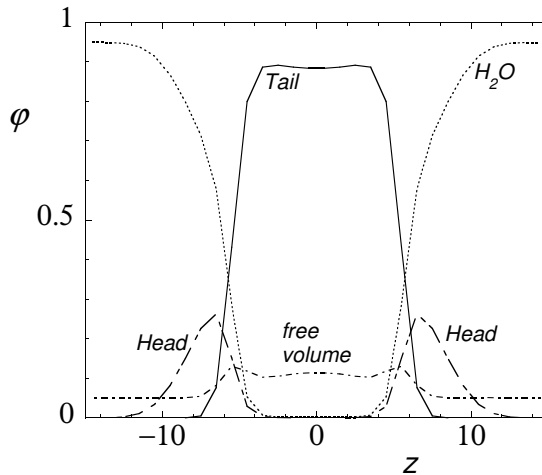
Figure 4.3: Volume fraction profile across a tensionless planar lipid bilayer with tail length $t = 18$. Volume fraction of the tail segments and the head segments are depicted, but also the free volume and the water volume fraction profiles are shown.

d_l^0 in units of l, the size of a lattice site, and area per lipid molecule a_0 (in units l^2) in a tensionless bilayer show a linear dependence on t.

$$d_l^0 = 2.86 + 0.437t \tag{4.9}$$

$$a_0 = 5.99 + 0.133t \tag{4.10}$$

The bending modulus k_c, the area compression-expansion modulus k_a and the elastic length scale ξ_e show a linear dependence on t. The bending modulus $k_c \equiv \partial\gamma/\partial J^2$ (in units k_BT) is a measure for the bilayer rigidity. Here γ (k_BTl^{-2}) is the surface tension of the bilayer and J (l^{-1}) the bilayer curvature, i.e., $J = 1/R_1 + 1/R_2$ with R_1 and R_2 the local radii of bilayer curvature.

$$k_c = 4.69 + 0.668t \tag{4.11}$$

The area compression-expansion modulus $k_a \equiv (\partial\gamma/\partial \ln a)_{\gamma=0}$ (in units k_BTl^{-2}), with a the bilayer area in units l^2 is a measure for the energy to stretch a bilayer.

$$k_a = 1.65 + 4.31 \times 10^{-2}t \tag{4.12}$$

The elastic length scale $\xi_e = ((d_l^0)^2 k_c)/k_a)^{1/4}$ (in units l) [33, 55], which is a characteristic bilayer property that gives information about the decay of bilayer perturbations.

$$\xi_e = 2.64 + 0.150t \tag{4.13}$$

In the remainder of this paper we are going to discuss three different aspects of peptide incorporation in the bilayer. In all cases the hydrophobic length of the
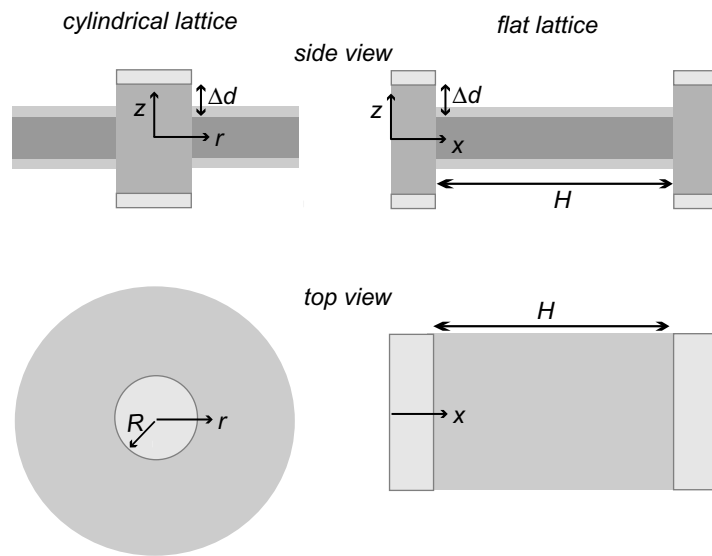
Figure 4.4: Schematic representation of the insertion of inclusions (top: side views, bottom: top views). The cylindrical two-dimensional lattice (left) is used when a single inclusion is incorporated into the bilayer. When two inclusions are inserted in the bilayer a two-dimensional flat lattice (right) is needed. The distance H between the hydrophobic surface of these inclusions can be varied. The hydrophobic mismatch Δd is defined as $\frac{1}{2}(D - d_l^0)$, with D the hydrophobic length of the inclusion and d_l^0 the hydrophobic thickness of the unperturbed bilayer.

inclusion is $D = 8l$ and the two hydrophilic end caps have a length of $1l$. The interactions between the end-caps and the lipid head group segments $\chi_{EX} = 0$ and with the water $\chi_{EW} = 0$ for simplicity. For the interaction of the rigid hydrophobic surface with hydrophilic segments we choose the interaction to be unfavourable, i.e., $\chi_{SW} = \chi_{SX} = 2$. The interaction of the rigid hydrophilic head with the hydrophobic lipid tails must be unfavourable and again for simplicity reasons the same value as the latter two, i.e., $\chi_{EC} = 2$ was selected. For the interaction with the vacancies $\chi_{EV} = \chi_{VW} = \chi_{VX} = 2.3$, which implies that the V segments are strongly repelled by the polar segments. Recall that the interaction between C and V is also repulsive, i.e., $\chi_{CV} = 1.5$. The interaction of the hydrophobic surface of the inclusion and the hydrophobic tails is attractive, i.e., $\chi_{SC} = -1$, unless stated otherwise. The interactions of the hydrophobic surface with the V units are in between the interactions with the hydrophilic and the hydrophobic segments, i.e., $\chi_{SV} = 1.5$.

In the previous paper [79] we incorporated a cylindrical inclusion with radius $R = 6l$ and $\chi_{SC} = -1$ and varied its hydrophobic length D. The free energy of insertion may be normalised by the circumference of the cylindrical inclusion to obtain $\tau = \Omega/2\pi R$, which may be called the line tension as it has the dimension $k_B T/l$. This line tension has a parabolic dependence on the hydrophobic mismatch between the inclusion and the bilayer $\Delta d = \frac{1}{2}(D - d_l^0)$.

$$\tau = W(\Delta d - \Delta d_{min})^2 + \tau_{min} \tag{4.14}$$

with W the width of the parabola, τ_{min} the minimum line tension and Δd_{min} the optimal hydrophobic mismatch, i.e., the mismatch of the lowest free energy. We showed that variation of D only influences τ_{min} significantly, which can be attributed to the increased interaction area between the inclusion's hydrophobic surface and the bilayer. However, $W \approx 0.1$ and $\Delta d_{min} \approx 0.7$ were not significantly affected by varying D.

For the investigation of the influence of the hydrophobic interaction between the lipid tails and the inclusion χ_{SC} and the inclusion's curvature $J_p = 1/R$ on the free energy of insertion and on the bilayer structure we make use of a two-dimensional cylindrical lattice (fig. 4.4a). The system size is chosen large enough so that in the r-direction the effect of the inclusion has vanished and in the z-direction the bulk becomes homogeneous. In the first case the radius of the inclusion is fixed at $R = 6l$ and χ_{SC} is varied between -2 and 1. In the second case R is varied between $1l$ and $30l$ and χ_{SC} is fixed at -1. In both cases Δd is varied between $-1.50l$ and $0.86l$ by varying the length of the lipid chains t and thus d_l^0. The dependency of Δd on t for $D = 8$ is given by

$$\Delta d = 2.57 - 0.218t \tag{4.15}$$

At the end of this paper we investigate the lipid-mediated interaction between two peptide-like inclusions. These calculations have been done in a two-dimensional flat lattice (fig. 4.4b). In this case we examine the effect of Δd and χ_{SC} on the
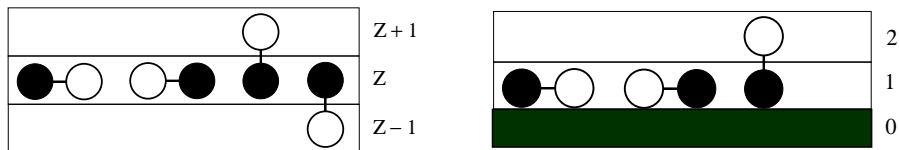
Figure 4.5: Schematic two-dimensional illustration of the entropy loss of dimers adjacent to a rigid surface. The white spheres of the dimers in the bulk (left) can obtain four different positions, whereas the white spheres of the dimer adjacent to a rigid surface (right) can only sit at three different positions. The bond between the black and white sphere has lost conformational entropy when the dimer is near a surface.

interaction energy as a function of the distance between the inclusions H. The interaction energy F is defined as $F(H) = \Omega(H) - \Omega(\infty)$.

4.3 Results and discussion

4.3.1 Affinity between the inclusion and the lipid tails.

There is little known about the consequences of the contact interaction between the hydrophobic part of the inclusion and the lipid tails. Typically it is assumed that the lipids adjacent to the inclusion experience only steric hindrance by the inclusion's rigid wall, while interactions between the wall and the lipid tails are not considered. Because of this steric hindrance the lipids around the inclusion experience conformational entropy loss compared to the lipids that are present in an unperturbed bilayer. As a consequence the lipid tails will to some extent avoid the surface. Calculations show that the tail segments compete with the V units for the surface sites. This means that if the tail segments deplete from the inclusion and the V units take their place. We note that the interaction parameter between these V units and the surface S is kept constant $\chi_{SV} = 1.5$.

In contrast to our cylindrical inclusions, the surface of a real membrane inclusion like a peptide is not smooth and rigid, but molecularly rough with several groups attached to it that have different affinities to the lipid tails. As a result we should seek a correction to compensate for the somewhat unrealistic conformational entropy loss suffered by the tails in our model. This issue is well known in polymer adsorption theory, where the concept of a critical adsorption energy is introduced [85, 86]. Referring to figure 4.5, where the different conformations of dimers are shown (in a two-dimensional system), it can be seen that there are four white spheres in the bulk (left), whereas there are only three near the surface (right). The entropy loss for a bond (between black and white) near the surface therefore amounts, in the general case that one out of Z directions is blocked by the surface, to $\Delta S = -k_B \ln(1 - 1/Z) \approx 1/Z \equiv \lambda_1$. As a segment C next to the inclusion has
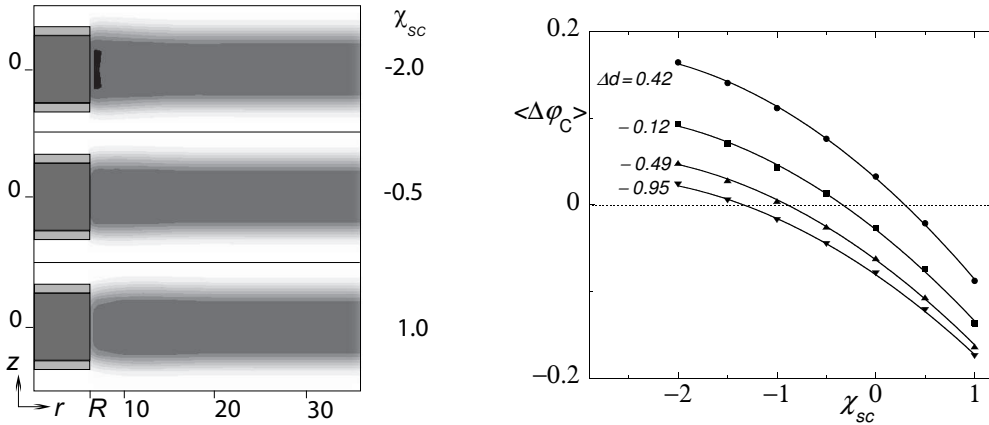
Figure 4.6: a) Volume fraction profiles of the lipid tails when $\Delta d = -0.12l$. The lipid tails volume fraction increases from white to black. The inclusion is shown on the left side of each plot. From up to down χ_{SC} is -2, -0.5 and 1. b) The dependence of $< \Delta\varphi_C > \equiv < \varphi_C^{R+1} > - < \varphi_C^{\infty} >$ on χ_{SC} is shown for various values of Δd.

$\lambda_1 \chi_{SC}$ contacts, the exchange with V gives an energy effect, $\Delta u = \lambda_1(\chi_{SC} - \chi_{SV})$. This means that $\chi_{SC} - \chi_{SV} \approx 1$, in order to compensate for this entropic loss, resulting in a homogeneous distribution of C and V perpendicular to the surface. When the enthalpic contribution is larger there will be an excess of C near the surface, and when it is lower C will deplete. However, this analysis does not account for the fact that the tails are strongly aligned in the z-direction, parallel to the inclusion. We therefore have no accurate evaluation of the true critical adsorption energy. In particular we expect this also to depend on the hydrophobic mismatch.

In figure 4.6 three two-dimensional volume fraction profiles of the lipid tails next to an inclusion are plotted in cylindrical coordinates (z, r). In all three cases $t = 12$, i.e., $\Delta d = -0.12l$, but χ_{SC} has different values, i.e., $\chi_{SC} = -2, -0.5$ and 1. The inclusion with a radius $R = 6l$ and hydrophobic length $D = 8l$ is present at the left side of each contour plot. The lipid tail volume fraction φ_C increases from white to black. The profile on the top where $\chi_{SC} = -2$ exhibits an increased φ_C adjacent to the inclusion, represented by the dark area. Furthermore it can be seen that the bilayer thickness d_l in the first layers next to the inclusion is increased with respect to the unperturbed bilayer far from the inclusion. These two features implicate that apparently the enthalpic contribution is larger than the conformational entropic loss. The profile for $\chi_{SC} = -0.5$ shows that it is possible that φ_C and d_l are approximately constant in the r-direction, indicating that in this case the lipid-peptide interaction energy counterbalances the entropic loss of the lipid tails. The profile at the bottom, where $\chi_{SC} = 1$, is the opposite of the first profile. Now χ_{SC} does not compensate for the entropic loss, resulting in an decreased d_l and φ_C nearby the inclusion. Besides a gradient in d_l resulting from the unbalanced contributions, the bilayer can deform in order to minimize its free energy. As a result it is difficult to determine the

exact interaction energy that just compensates for the conformational entropic loss. To quantify this issue, we have evaluated the average volume fraction at a given r coordinate.

$$< \varphi_C^r > = \frac{1}{D} \sum_{z=-\frac{1}{2}D}^{\frac{1}{2}D} \varphi_C(r,z) \qquad (4.16)$$

In fig 4.6b we present $< \Delta\varphi_C > \equiv < \varphi_C^{R+1} > - < \varphi_C^\infty >$ as a function of χ_{SV} for several values of Δd. The figure shows that, irrespective of Δd, $< \Delta\varphi_C >$ decreases when χ_{SC} increases, i.e., when the strength of the attractive interaction decreases. It furthermore shows that χ_{SC}^{cr}, i.e., the χ_{SC} where $< \Delta\varphi_C > = 0$, is a function of Δd. A closer look reveals that there is a linear dependence of χ_{SC}^{cr} on Δd which can be described by $\chi_{SC}^{cr} = -0.23 + 1.24\Delta d$. In the case where $\Delta d = 0$ and $\chi_{VS} = 1.5$, the value $\chi_{CS}^{cr} - \chi_{VS} \approx -0.23 - 1.5 = -1.73$. This value is significantly more negative than -1, which was found for polymers adsorbing on a rigid wall. In the case of a positive Δd the bilayer thickness adjacent to the inclusion is larger than d_l^0 and an increase in bilayer thickness increases the tail density with respect to the unperturbed bilayer. This increase in tails density caused by the bilayer deformation opposes the effect of entropic loss of the tails, resulting in a decreased tail density near the rigid wall and as a consequence χ_{SC} has to be less attractive compared to an isotropic solution in order to keep $< \Delta\varphi_C > \approx 0$. In the case of a negative Δd the situation is just the opposite, i.e., the bilayer thickness adjacent to the inclusion is decreased, which results in an extra depletion contribution on top of the conformational entropic loss.

The adsorption energy χ_{SC} influences not only the bilayer structure but also the free energy of insertion of the inclusion into the bilayer. As the partition function is accurately available, we can compute this free energy of insertion straightforwardly. There are at least four interconnected contributions. These are (i) the bilayer perturbation contribution which is a result of some hydrophobic mismatch, (ii) the conformational entropy loss of the annular lipid chains caused by the rigid inclusion, (iii) the direct contact interaction energy between the inclusions hydrophobic surface and the bilayer core, and finally (iv) there are the interactions between the inclusion end-caps and their environment, but these have been chosen in such a way that their contribution to Ω is negligible.

It is found that the dependence of τ on Δd has a parabolic form for all values of χ_{SC} (eqn. 4.14). Again, the width of the parabola W is not affected much by χ_{SC}. This means that energetically comparable structural changes take place in the bilayer by varying Δd. In figure 4.7a the strong dependence of the minimal line tension τ_{min} on χ_{SC} is shown. To a good approximation τ_{min} is proportional to χ_{SC} and increases with $2.03k_BT$ when χ_{SC} is increased by one unit. This means that the total insertion energy $\Omega = 2\pi R\tau$ increases with $76.5k_BT$ ($R = 6l$) when χ_{SC} is increased with one unit. From this we can understand that the affinity of the
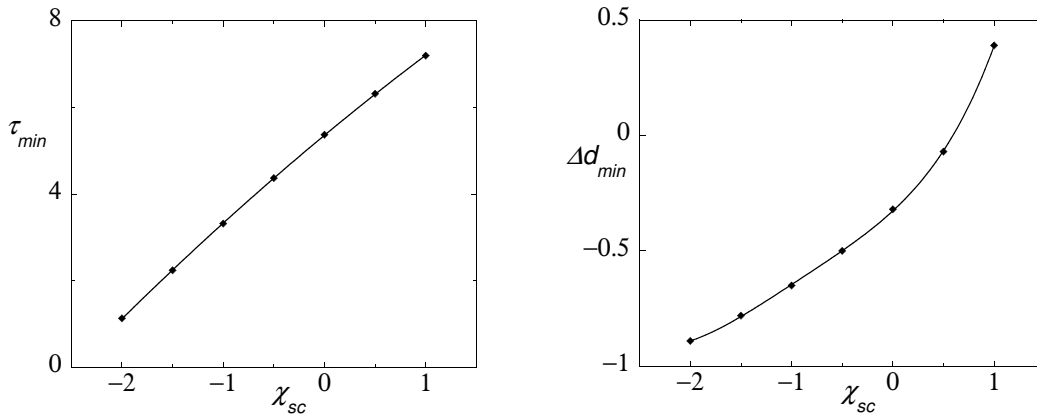
Figure 4.7: a) The dependence of the minimal line tension τ_{min} on the Flory Huggins interaction parameter χ_{SC} between the surface and the tail segments. b) The dependence of the hydrophobic mismatch Δd_{min} at minimal line tension τ_{min} on χ_{SC}.

amino acid residues in a trans-membrane peptide that interact with the hydrophobic core in the lipid bilayer have to be selected carefully in order to avoid excessively large values of the insertion free energy. Indeed most of the residues should have a hydrophobic character and in line with the experimental data the number of non-apolar residues largely determines whether the peptide is inserted in the bilayer or not. Close inspection of figure 4.7a reveals that there is a small deviation from the linearity between τ_{min} and χ_{SC}, that must be attributed to entropic effects, i.e., there are small changes in the packing or the average tilt of the lipid tails adjacent to the inclusion. The dependence of Δd_{min}, i.e., the mismatch at τ_{min}, on the adsorption energy is presented in figure 4.7b. It is of interest to mention that Δd_{min} increases more than linear with χ_{SC} especially for $\chi_{SC} > 0$. This exemplifies the non-trivial variations of the lipid distributions around the inclusion as discussed previously in this section. We conclude that both the hydrophobic length of the peptides as well as the hydrophobic interaction between the peptides and the bilayer play a role in the organisation of these trans-membrane peptides.

4.3.2 The curvature of the inclusion

In the introduction some examples have been given of trans-membrane proteins and peptides that illustrated the possible variations of the radius of biological inclusions. Here we will investigate the consequences of the inclusion's curvature J_p, with $J_p = \frac{1}{R}$, on the conformational properties of the surrounding lipids as well as at the free energy effects. When an inclusion is incorporated, far from this inclusion ($r \to \infty$) the bilayer is unperturbed and the local surface tension γ vanishes. However, near the inclusion this is no longer the case. Below we like to present the membrane tension as a function of the distance to the inclusion. In principle, how-
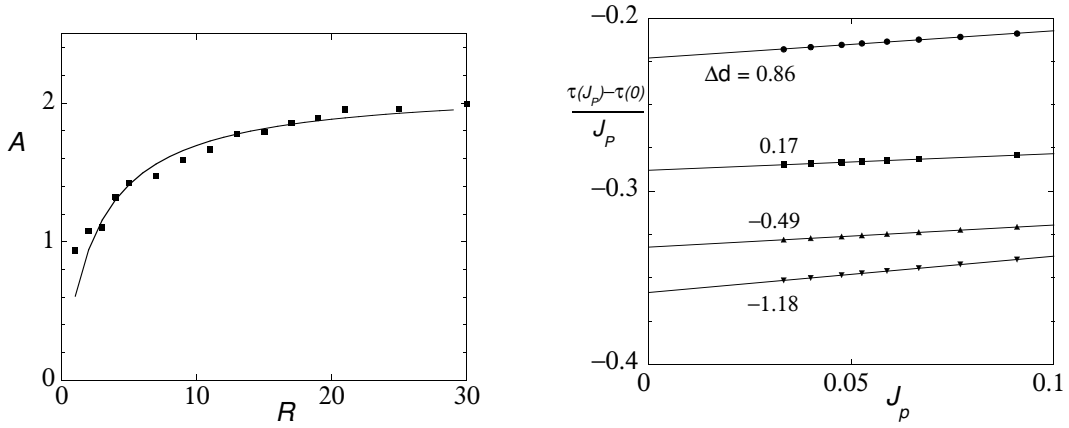
Figure 4.8: a) The dependence of A $(/10^{-4}k_BT)$ on R in units l b) The relation between $(\tau(J_P) - \tau_0)/J_P$ and J_P, with τ en J_P in units k_BT/l and $1/l$, respectively. The slope gives information about the curvature modulus.

ever, the local surface tension cannot unambiguously be defined. The reason is that binary interactions make the surface tension non-local. Here we take the approach to compute $\gamma(r)$, such that non-local interactions are evenly distributed over the segments that are involved in the interaction. It is found that such local surface tension $\gamma(r)$ is a function of the distance from the inclusion's surface $\Delta r = r - R$ which phenomenologically can be fitted by

$$\gamma(\Delta r) = A \exp -\frac{\Delta r}{\xi} \sin\left(2\pi\frac{\Delta r - \delta}{\lambda}\right). \tag{4.17}$$

In this equation ξ is the decay length and λ the wavelength. The offset of the damped waves is denoted by δ and A is the extrapolated maximum amplitude at the inclusion's surface. It has to be mentioned that this equation only describes the dependence of the local surface tension accurately in the elastic region, i.e., the region where $\Delta r > d_l^0$. The coefficients ξ and λ are fully determined by the mechanical parameters of the bilayer. When Δr becomes smaller than d_l^0 the molecular bilayer properties of the lipids become the dominant factor. In the remainder of this section we discuss the surface tension profile when $\Delta d = 0.86$, i.e., the tail length $t = 8$, because in this case the variation of γ with Δr is relatively large. The qualitative tendencies that we will discuss are the same for other Δd.

As told above, in the limit $\Delta r \to \infty$ the bilayer is unperturbed and tensionless, i.e., the surface tension $\gamma = 0$. However, when the bilayer thickness and lipid tail density are reduced with respect to the unperturbed bilayer the surface tension $\gamma > 0$ and when the bilayer thickness and the lipid tail density are larger than the unperturbed bilayer $\gamma < 0$.

It appears that both the wavelength λ and the decay length ξ do not depend on J_p. Both quantities are a function of the mechanical parameters of the bilayer and correlated with the elastic length ξ_e given in equation 4.13. Moreover the offset of the

83

oscillation δ does not depend much on J_p either. The only parameter that shows a significant dependence on J_p is the extrapolated maximum amplitude A as is shown in figure 4.8a. When the radius of the inclusion is increased, i.e., the curvature J_p is decreased, the amplitude A increases to a limiting value of $2.19 \times 10^{-4} k_B T/l^2$ in the case of a flat surface, i.e., $R = \infty$. These results are in agreement with the results shown by Lagüe et al. [27, 28], who showed that the long-range oscillations become more pronounced when the inclusion's radius increased.

The total insertion energy Ω has almost a linear dependence on R which is mainly due to the increased interaction area between the inclusion and the bilayer. Again there is a small deviation from this linearity. This suggest a small curvature dependence of τ, which is a response of the structure of the bilayer around the inclusion. It is possible to expand τ up to a second order Taylor series in J_p

$$\tau(J) = \tau(0) + \frac{\partial \tau}{\partial J_p} J_p + \frac{1}{2} \frac{\partial^2 \tau}{\partial J_p^2} J_p^2 = \tau(0) - k_2 J_0 J_p + \frac{k_2}{2} J_p^2 \qquad (4.18)$$

here $\tau(0)$ is the line tension at $J_p = 0$. Equation 4.18 defines the curvature modulus k_2 as $\frac{\partial^2 \tau}{\partial J_p^2}$ at $J_p = 0$ and J_0 is the curvature where the line tension has an extreme (either maximum or a minimum depending on the sign of k_2).

In figure 4.8b we present $\frac{\tau(J) - \tau(0)}{J_p}$ as a function of J_p for several values of Δd. The slope of the lines corresponds to $\frac{1}{2} k_2$ which appears to be small and positive, i.e., approximately $0.1 < \frac{1}{2} k_2 < 0.2$. The intercept is given by $-J_0 k_2$ and is negative showing that J_0 is positive and of order unity. From this it can be concluded that $\tau(J)$ does not depend strongly on J_p and that $\tau(0)$ is a reasonable measure for the free energy of insertion also for small values of R. We will use this result below when we consider the interaction between two inclusions in the bilayer.

4.3.3   Lipid-mediated interaction between peptides

To insert peptides and proteins into the bilayer membrane is one of the prime fundamental steps for the functioning of bio membranes. The control over the degree of organisation of the inclusions in a bilayer is another one. To obtain information on how inclusions interact with each other in the plane of a bilayer is a hard task. The analysis of the interaction between inclusions with radius R in the bilayer generally calls for a 3-gradient SCF analysis. For the time being this exceeds our computing facilities. In the limit of $R \to \infty$ however, it is possible to reduce the problem to a 2-gradient SCF analysis. Above we showed that there are relatively few effects of the radius R on the bilayer perturbation. For this reason we believe we can get useful information from such 2-gradient analysis about the bilayer induced interaction between two inclusions (see figure 4.4). This is also supported by studies where the interaction between inclusions of different sizes is investigated [28, 34].

We will once again consider the effects of the hydrophobic mismatch Δd and the hydrophobic interaction between the inclusion and the bilayer (χ_{SC}) on this lipid-mediated interaction.
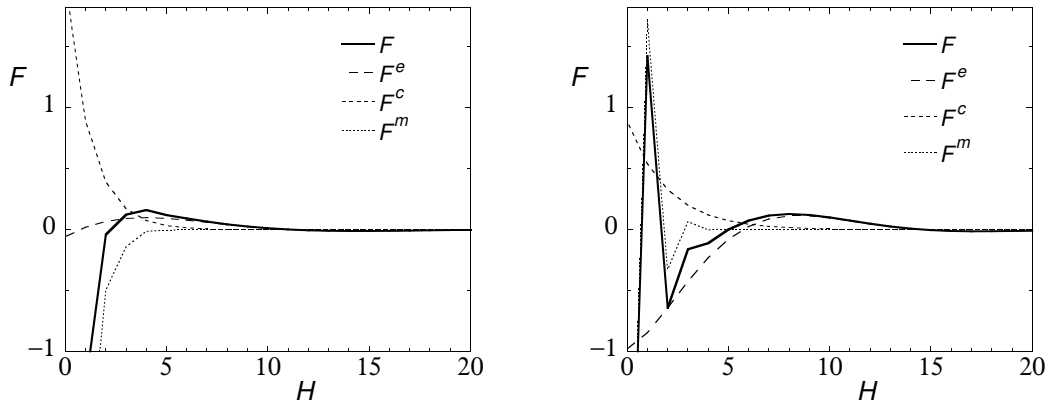
Figure 4.9: The total interaction energy F/k_BT per unit length l between two hard flat inclusions as a function of the separation between the wall edges H (thick solid line). The interaction energy at a certain separation is a result of three contributions, namely the short-range segmental contribution F^m (dotted line), the intermediate conformational contribution F^c (short dashed line) and the long-range elastic contribution F^e (long dashed line).
a) For the case of a small hydrophobic mismatch ($\Delta d = -0.12$) and no effective interaction between lipid tails and inclusion, i.e, $\chi_{SC} = \chi_{SV}$. b) For large mismatch ($\Delta d = 0.86$) and attractive interaction ($\chi_{SC} = -1$).

It appears that for the lipid-mediated interaction free energy F, which is defined as $F(H) = \Omega(H) - \Omega(\infty)$, with H the distance between the two inclusions, it is possible to identify three different regimes each having its own length scale in the interaction profile. First, there is the long-range interaction F^e, which is dominant at distances $H > d_l^0$. In this regime the free energy of interaction $F(H)$ manifests itself as an exponentially decaying oscillation. It is a result of the overlap of the inclusion-induced bilayer perturbations and is retrieved by fitting $F(H)$ with a equation similar to eqn 4.17. At the intermediate length scale, i.e., $2\sqrt{a_0} < H < d_l^0$, a second contribution becomes evident, namely a repulsive interaction F^c. In all cases we found that $F^c(H)$ decays approximately exponentially with H as illustrated in fig 4.9. This $F^c(H)$ dependence is retrieved by subtracting F^e from F. For $2\sqrt{a_0} < H < d_l^0$ the intermediate contribution is easily fitted. We believe that this interaction contribution is a consequence of the confinement of the lipid tails by the inclusions. At even smaller separations between the inclusions, i.e., $H < 2\sqrt{a_0}$, the situation becomes more complex. We define the contribution F^m, $F^m(H) = F(H) - F^e(H) - F^c(H)$. This contribution is non-universal as it strongly depends on the interaction of the tails with the inclusions' surfaces. It can consist of a depletion-induced [87] attractive interaction F^d and/or a strongly oscillating and exponentially decaying interaction F^s. Similar forces are seen for polymer melts confined between to solid surfaces which are believed to be related to the finite compressibility in the system.

Two rather extreme cases of interaction profiles are shown in figure 4.9. Both figures show F as a function of H and also its contributions, i.e., F^e, F^c and F^m, are depicted. Figure 4.9a shows F as a function of H and also its different contributions when there is almost no hydrophobic mismatch, i.e., $\Delta d = -0.12$, and no effective lipid tail-inclusion interaction, i.e., $\chi_{SC} = \chi_{SV}$. It shows a repulsive barrier at intermediate separation and a depletion-induced attraction at short separation. A similar interaction profile has been shown in several other studies in which inclusion-induced interaction without mismatch and effective tail-peptide interaction were studied [27, 30, 34].

In figure 4.9b the dependence of F, F^e, F^c and F^m on H are depicted in the case of strong attractive lipid tail-inclusion interaction, i.e., $\chi_{SC} = -1$, and a large positive mismatch, i.e., $\Delta d = 0.86$. In this case also strong oscillations are present in the short-range regime. This situation has not been discussed before, but it exemplifies the importance of the tail-inclusion interaction at short separations. Below, we discuss the findings for the three different length scales separately.

Long-range interaction

In this region the lipid-mediated interaction is a consequence of the overlap of the structural bilayer perturbations. These perturbations result in a local variation in, e.g. the membrane thickness $d_l(r)$, or the area per molecule $a(r)$. These perturbations follow the same functional form as the surface tension $\gamma(r)$ given in eqn. 4.17. The wavelength λ and the decay length ξ of these perturbations are set by the structural and elastic properties of the bilayers [79]. Figure 4.10 shows the energy of interaction $F(H)$ for $H > d_l^0$, where $F^e(H) \approx F(H)$. As the force f between the $f = -\frac{\partial F}{\partial H}$, the result shows that there are attractive or repulsive forces depending on the distance H. In figure 4.10a the dependence of F on the hydrophobic mismatch Δd is shown, whereas the dependence of χ_{SC} is shown in figure 4.10b.

When $H > d_l^0$ all the profiles that are shown in figure 4.10 can be fitted by

$$F(H) = A^F \exp\left(-\frac{H}{\xi^F}\right) \sin\left(2\pi\left(\frac{H - \delta^F}{\lambda^F}\right)\right) \tag{4.19}$$

Here δ^F is the offset of the interaction profile and λ^F is it's wavelength, which is equal to the wavelength λ found for the local surface tension variations discussed above. Also the interaction decay length ξ^F coincides with the decay length ξ discussed above. The fact that the wavelengths λ, λ^F and the decay lengths ξ, ξ^F are similar indicates that they have the same origin. The oscillatory free energy curve may be rationalised using the elastic length scale concept. Whether attraction or repulsion is found at some distance H depends on the match or mismatch of integer number of elastic lengths between the surfaces. The extrapolated maximum amplitude A^F at $H = 0$ of the interaction energy profile shows the same dependence on Δd and χ_{SC} as A. For example when $\chi_{SC} = -1$, both A^F and A show a minimum at $\Delta d \approx -0.65$ [79].
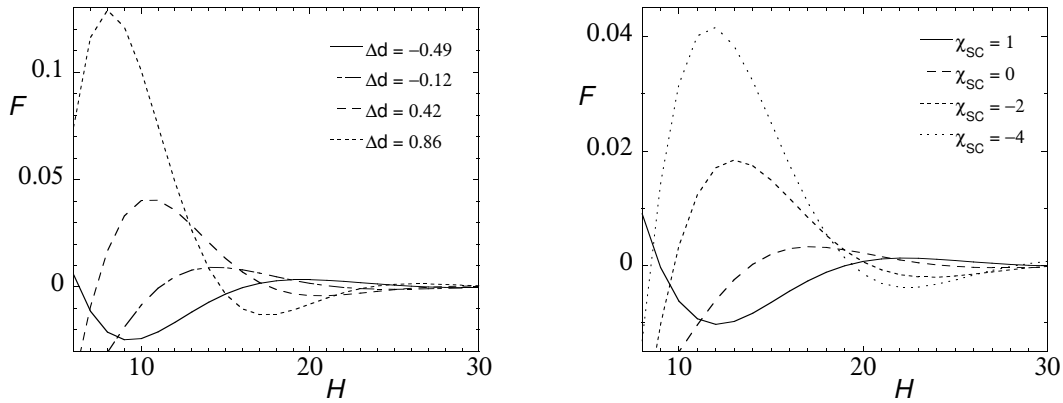
Figure 4.10: The interaction energy F/k_BT per unit length l between two hard flat inclusions as a function of the separation between their surfaces H. The distance H is varied between 6 and 30l a) For several Δd when $\chi_{SC} = -1$. b) For various χ_{SC} when $t = 12$ and $\Delta d = -0.12l$.

Figure 4.10a shows the dependence of F on H for several values Δd. The distance H and the amplitude A^F of the first maximum and minimum are determined by Δd. The amplitude of the maxima and minima decreases exponentially with increasing H and there is a parabolic dependence on Δd. In fig 4.10a, the largest maximum is found for $\Delta d = 0.86$, amounting to approximately $0.12 k_B T/l$. When $l = 0.2 nm$ this energetic barrier is large enough to easily overcome the thermal energy (approximately $1 k_B T$), even for inclusions with a biologically relevant size. This means that in this situation and maybe also for the case of $\Delta d = 0.42l$ the energetic barriers are sufficient to prevent the inclusions from coming closer to each other. The first elastic minima are relatively small compared to the maxima. However, when a minimum appears at relatively small values of H, it may be deep enough compared to the thermal energy to localise these inclusions at this distance. This is for example the case for $\Delta d = -0.49l$, where $F^{min} \approx -0.04 k_B T/l$. It can be concluded that for relatively small hydrophobic mismatches the first elastic maximum or minimum can be large enough to play a role in the organisation of peptides or proteins in a bilayer. In these cases such molecules will either remain freely dispersed in the bilayer or become ordered with many lipids between them.

In figure 4.10b the dependence of F on H is depicted for several values of χ_{SC}. In all cases the mismatch between the inclusion and the bilayer is kept small, i.e., $\Delta d = -0.12l$. The position of the maxima and the minima is clearly affected by χ_{SC} as well as their amplitudes. In the case were $\chi_{SC} = -4$ the height of the first elastic maximum is approximately $0.04 k_B T/l$, which can in some cases be high enough to prevent inclusions from approaching each other closely. Thus even when the mismatch is small the elastic interaction can be an effective energetic barrier. The first elastic minima in the studied cases are probably to small to accommodate the inclusions at this distance from each other.

Overall it can be concluded that the elastic minima and maxima can play a role in the organisation of proteins and peptides even in the case of a relatively small hydrophobic mismatch and these elastic minima and maxima may prevent the aggregation of proteins.

Intermediate-range interaction

When the inclusions are separated at intermediate distance from each other, i.e., $2\sqrt{a_0} < H < d_l^0$, the interaction free energy F cannot be described only by F^e. In this region another contribution must be taken into account, namely an interaction energy F^c that decreases exponentially with increasing H. This exponentially decaying F^c can be attributed to the conformational restrictions of the lipid tails as a consequence of the restricted volume between the two inclusions. As already shown in previous sections the lipid tails do experience conformational entropic loss when they are close to the inclusion's surface and as a consequence the lipid tails try to avoid this surface, resulting in an average lipid tilt with respect to the normal of the bilayer surface. Strong confinement interferes with this tilt; i.e. it is destroyed by confinement and this results in a repulsive force. This contribution has also been discussed by May and Ben-Shaul [30], who used a simple director model as well as a molecular-level mean-field model. They showed that, in the case of the mean-field model, the interaction profile was not affected by the constraints on the head group distribution. This repulsive contribution results in some cases in a barrier at the intermediate range that is large enough to prevent the inclusions from approaching each other closely.

As discussed above, to retrieve F^c we subtracted $F^e(H)$ from $F(H)$ in the intermediate range. As expected $F^c(H)$ shows an exponential dependence on H.

$$F_c(H) = A^c \exp\left(-\frac{H}{\xi^c}\right) \tag{4.20}$$

Here A^c is the extrapolated value at $H = 0$ and ξ^c the decay length. In figure 4.11a the dependence of the decay length ξ^c is depicted as a function of χ_{SC} in the cases of a small hydrophobic mismatch, i.e., $\Delta d = -0.12$. The figure shows that in first order $\xi^c \approx 2l$. A reason that ξ^c decreases somewhat with χ_{SC} might be that in the case of strong attractive tail-inclusion interaction close to the inclusion the density of the tails and their average tilt is larger than for weaker tail-inclusion interactions.

In figure 4.11b the relation between ξ^c and the lipid tail length is shown. It appears that there is a nonmonotonic dependence. However, we attribute this to a minor lattice artefact. Apart from this ξ^c tends to increase with increasing tail length. This is consistent with the interpretation that this contribution is due to the confinement of tilt conformations. A longer tail length results in a larger length scale of the conformational interaction.
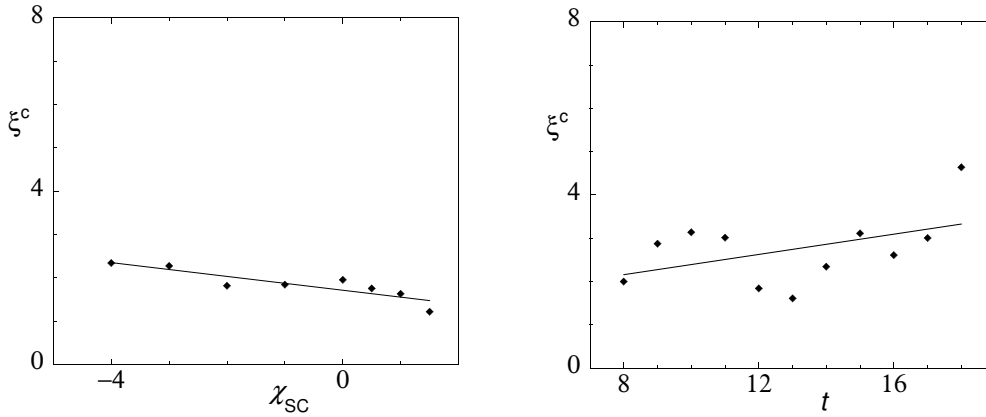
Figure 4.11: a) The dependence of the decay length ξ^c in units l on χ_{SC} for $\Delta d = -0.12l$. b) ξ^c as a function of t for $\chi_{sc} = -1$.

Short-range interaction

When two inclusions are at very close proximity two different effects can occur. There can be a depletion-induced attraction as shown first by Asakura and Oosawa [87] in a system of colloidal particles in a polymer solution. Our system is intrinsically the same regarding the inclusion as a colloid and the lipid tails as a two dimensional polymer solution. The depletion effect is found for those cases in which the tails are not strongly interacting with the inclusion. If there is a strong attraction we observe a pronounced oscillatory force curve which decays rapidly. The origin of this behaviour is not so clear. However, this type of interactions is also seen in polymer melts in strong confinement situations. We therefore expect that they result from the finite compressibility of the lipid core.

In figure 4.12 the short-range interaction energy F^m is plotted as a function of H for different systems. F^m is defined as $F^m(H) = F(H) - F^e(H) - F^c(H)$ where the profiles of $F^e(H)$ and $F^c(H)$ have been extrapolated to $H = 0$. Typically we expect that $F^m(H) = F^s(H) + F^d(H)$.

In figure 4.12a the dependence of F^m on H is shown for several values of Δd. In all these cases $\chi_{SC} = -1$. F^m shows a large exponentially decaying oscillation with a wavelength of $2l$. Apparently F^m is not affected by the hydrophobic mismatch. In this case F^m only consists of F^s and no depletion-induced attraction is present in these cases. This is in contrast with results shown in figure 4.12b where F^m profiles are depicted for $\Delta d = -0.12l$ and various values of χ_{sc}. It shows clearly that $F^m(H)$ is strongly influenced by χ_{SC}. In the case of strong attractive interaction, i.e., $\chi_{SC} = -1$, there is a large oscillation and no depletion-induced attraction. In the case where $\chi_{SC} = \chi_{SV} = 1.5$, the large oscillation has completely vanished and $F^m(H)$ only consist of the depletion-induced attraction $F^d(H)$.

One of the consequences of the strong non-monotonic interactions at strong confinement is that when the separation between the inclusions becomes small a
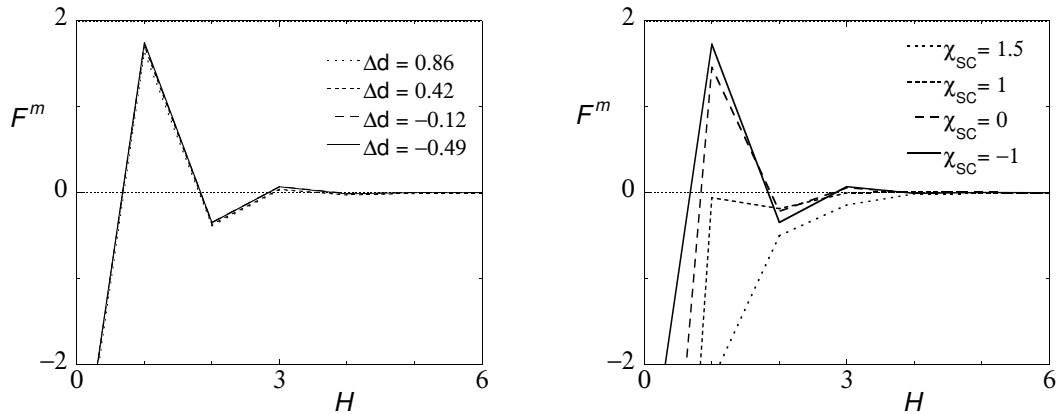
Figure 4.12: The short-range interaction energy F^m/k_BT. It can consists of an entropic part F^s and a depletion contribution F^d a) For different values of Δd (in units l) with $\chi_{SC} = -1$. b) For several values of χ_{SC} with $\Delta d = -0.12l$.

monomeric lipid layer can stay in between them. Whether this will be the case depends entirely on χ_{SC}. This means that χ_{SC} is not only important for the inclusions to reside in the bilayer, but this interaction is also important to understand how proteins can pack densely in a lipid bilayer.

4.4 Conclusions

Lipid membranes can host inclusions like proteins and small peptides. We modelled the lipid bilayer structure around these inclusions using a molecular level self-consistent field theory. We focussed on three different aspects, namely the interaction between the lipid tails and the inclusion, the curvature of the inclusion and the lipid-mediated interaction between two inclusions. The tail-inclusion interactions determine to a large extent the total energy of inserting an inclusion into a bilayer. Furthermore the packing of the lipid tails adjacent to the inclusion and the perturbation of the bilayer are affected by these interactions and as a consequence the energetically most favourable hydrophobic mismatch is also influenced by this interaction. The curvature of the inclusion has only a minor effect on the density of the lipids adjacent to the inclusion. However, an increase of the inclusion's radius results in larger bilayer oscillations. The line tension between the inclusion and the bilayer decreases with increasing inclusion radius. There are three distinct length scales for the lipid-mediated interaction between two flat inclusions. When the distance between the inclusions is larger than approximately the bilayer thickness the interaction is determined by elastic properties of the bilayer and an exponentially decaying oscillating interaction profile is found. In some situations the interaction on the elastic length scale can be strong enough to play a role in the organisation of proteins and peptides in bilayers. At intermediate separation the conformational restriction

of the lipid tails starts to play an important role resulting in an exponentially decaying repulsive interaction. This repulsive interaction is only weakly influenced by the hydrophobic mismatch and the tail-inclusion interactions. When the inclusions do approach each other closely the interaction between the inclusion and the tails becomes important. In the absence of a strong attractive tail-inclusion interaction a depletion-induced attraction is found. In the case of strong tail-inclusion interaction a strong oscillating and decaying interaction is found which is attributed to the finite compressibility of the apolar core of the lipid bilayer. We conclude that the tail-inclusion interaction can play an important role in the organisation of proteins and peptides in the bilayer and this interaction should be considered together with the hydrophobic mismatch.

Chapter 5

Effect of size, rigidity and bilayer-surface interaction on the adsorption of lipid vesicles: experimental study and self-consistent field model calculations

Abstract

In this study we address the effects of vesicle size, bilayer-surface interaction energy and bilayer elasticity on the adsorption of lipid vesicles. This is done both experimentally, by studying the adsorption of dioleoylphosphatidylcholine (DOPC) vesicles to a gold surface, and theoretically, by using a self-consistent field (SCF) modelling. The adsorption of vesicles has been studied with a quartz crystal microbalance (QCM), which gives the adsorbed mechanical mass, and with surface plasmon resonance (SPR) experiments, in which the adsorbed lipid mass is measured. By combining these two techniques we show that the deformation of the adsorbed vesicles increases with increasing vesicle size. Adsorption of DOPC vesicles with a radius R larger than about 40 nm results into a fully covered gold surface, while below this radius the surface is only partly covered, because the vesicles' curvature limits the interaction area with the surface and therefore the adsorption is energetically less favourable. These size-effects are confirmed by the SCF calculations. The calculations further show that there are three regimes for adsorption, depending on the balance between bilayer-surface interaction energy and bilayer elasticity: i) the interaction with the surface is too weak to deform the vesicle and no adsorption takes place; ii) moderate interaction leading to adsorption of intact vesicles (surface partly or completely covered); in this regime the interaction energy

and the penalty for deformation are balanced in such a way that the total adsorption energy is independent of the bilayer bending modulus k_c; iii) a strong interaction regime in which an adsorbed bilayer patch is more favourable than an adsorbed vesicle, resulting in the tendency of vesicles to fuse or to rupture at the surface.

5.1 Introduction

Nowadays, vesicle adsorption is used frequently as a primary step in the formation of supported lipid bilayers, i.e., lamellar bilayers attached to a solid substrate. As a consequence the formation of such a supported bilayer has been studied rather extensively, while only a limited number of studies has been directed specifically to the adhesion of intact vesicles. Insight into the conditions for intact vesicle adhesion can be beneficial for various applications, for example, for studying membrane proteins embedded in adsorbed vesicles using surface techniques (like total internal reflection fluorescence, electrochemical methods and scanning probe techniques). Another example is the use of adhered vesicles in sensor and immunoassay applications [88]. A major advantage of the use of adsorbed vesicles in a sensor device is that the internal volume of a vesicle can store a large number of (e.g., fluorescent) reporter molecules, which gives the possibility of strong signal amplification. Our interest in the adsorption of lipid vesicles is generic, but also motivated by the idea that if one succeeds to concentrate vesicles at a surface, with minimal interaction between lipids and surface, it should be possible to study processes like vesicle rupture and fusion as a response to changes in the aqueous environment using surface techniques. In addition, the effect of bilayer-surface interactions could be studied by varying these, e.g., by changing the pH (if the surface has a pH-dependent electric potential) or an externally applied potential.

As mentioned above the adhesion of intact vesicles to a solid substrate has been investigated in a limited number of studies. Keller et al. [89] were the first who showed the intact adhesion of small unilamellar fluid eggPC vesicles onto oxidized gold without subsequent rupture and fusion and the formation of a supported lipid bilayer. They used QCM-D, i.e., a quartz crystal microbalance in which not only the frequency shift upon adsorption is measured but also the dissipation by the adsorption layer, giving the adsorbed mechanical mass as well as the viscoelastic properties of the adsorbed layer. Reimhult et al. [37, 90, 91] studied the adsorption of small unilamellar lipid vesicles on SiO_2, TiO_2, platinum and gold. They showed that these surfaces facilitate the adsorption of intact vesicles at varying surface coverage, over a large temperature range and also over a broad osmotic pressure range. Furthermore, they found that the degree of deformation of adsorbed eggPC vesicles on TiO_2 increases when the vesicle size (radius) is increased from 12.5 nm to 100 nm. The same vesicles adsorbed to SiO_2, before they form a single bilayer, are much more deformed compared to vesicles on TiO_2. Obviously, the strength of the substrate-bilayer interaction is an important factor determining whether adsorbed vesicles stay intact, but it is still unclear why fluid lipid vesicles are stable on gold, platinum or TiO_2 and why they rupture and fuse to form supported bilayers on similar hydrophilic surfaces like SiO_2, S_3N_4, glass and mica.

Besides experimental studies a number of theoretical studies have been performed to gain insight into the parameters that determine the adsorption of lipid vesicles.

Seifert and Lipowsky [92,93] elaborated a model in which the lipid bilayer is regarded as a macroscopic sheet with a certain curvature-dependent free energy [19]. In their model the structure of the lipid bilayer does not play a role and the Gaussian bending modulus $\bar{k} = 0$. They introduced an effective contact potential that, together with the interaction area between the vesicle and the substrate, determines the total adhesion energy. In addition some constraints for the volume and area of the vesicle were applied. Based on the assumption that when a vesicle adsorbs to a surface the total adsorption energy $W 4\pi R^2$ has to be equal or larger than the elastic bending energy $4\pi 2k_c$, they defined a minimal adhesion radius $R_a = (2k_c/W)^{1/2}$. If the pressure difference over the bilayer $P = 0$ and k_c and W are taken to be constant, this means that for $R < R_a$ the vesicle will not adsorb and for $R > R_a$ it is favourable to be bound to the surface.

Besides this minimal adhesion radius Seifert and Lipowsky introduced a crossover length R_c. If the radius of the vesicle $R > R_c$, the adhesion is determined by thermally excited shape fluctuations and thus the entropy. Below this R_c the adhesion is an energetically driven process and can described by the above-mentioned contributions. According to Seifert and Lipowsky the value of R_c is approximately 200 nm for unilamellar phospholipid vesicles. A drawback of their theory is that it excludes strong bilayer curvature because of the use of extremely large bending energies. In reality however the lipid molecules in the bilayer can reorganise making a strong curvature conceivable. Blokhuis and Sager [94,95] avoided this problem by studying cases where the vesicles are very large which makes it possible to neglect the bending rigidity of the bilayer. Their model is however not suitable for the adhesion of small vesicles to a surface.

In the first part of the present study we experimentally address the effect of vesicle size on the adhesion of vesicles to gold, using the surface plasmon resonance (SPR) technique and a quartz crystal microbalance (QCM). With SPR the adsorbed lipid mass is determined whereas the QCM measures the total adsorbed mass, i.e., the mass of the lipid bilayers plus the solution present in the interior of adsorbed intact vesicles. Combination of the results of these two techniques allows drawing conclusions regarding the surface coverage and deformation of the vesicles. We used unilamellar vesicles made of the zwitterionic phospholipid DOPC (dioleoylphosphatidylcholine). At room temperature DOPC bilayers are in the fluid state. We varied the size of the vesicles from $R \approx 25$ nm to $R \approx 125$ nm.

In the second part of this study the influence of vesicle size, bilayer bending elasticity and bilayer-surface interaction on the adhesion of a single vesicle is studied by self-consistent field (SCF) modelling. The theory allows investigating the thermodynamics of the adsorption process as well as the structural changes in the vesicle, i.e., the overall deformation of the vesicle and the structural adjustments in the bilayer while using a molecularly realistic model.

5.2 Materials and methods

5.2.1 Vesicle preparation

The lipids used in this study are 1,2-dioleoyl-sn-glycero-3-phosphocholine (DOPC) and 1,2-dipalmitoyl-sn-glycero-3-phosphocholine (DPPC) purchased from Avanti Polar Lipids (Alabaster, AL). KNO_3 was obtained from Merck (Darmstad, Germany) and water was purified with a Milli-Q water purification system (Millipore, Sweden) and had a resistance > 17 MΩ/cm.

The lipids were dissolved in chloroform, which was evaporated under nitrogen or in the roto-evaporator, and subsequently dried for at least 2.5 hours in vacuum. The lipids were re-dispersed in an aqueous KNO_3 solution to a lipid concentration of approximately 12 mg/ml. The resulting polydisperse multilamellar vesicle dispersion was freeze-thawed three to five times in order to dissolve all the lipids and to make unilamellar vesicles. Subsequently the dispersion was pushed 41 times trough a polycarbonate filter, using a mini-extruder (LiposoFast, Avestin, Ottawa, Canada). Filters with pore diameters of 50, 80, 100, 200, 400 and 800 nm were used, resulting in mean vesicle radii of 35, 45, 50, 70, 100, and 125 nm respectively, as determined by dynamic light scattering (DLS) measurements and using cumulant analysis and Contin fit to analyse the results. Smaller vesicles (mean radius 20 nm) were made by sonication in a water bath.

5.2.2 QCM measurements

To monitor the adhesion of the lipids to gold, a quartz crystal microbalance was used from Maxtek, Inc (Santa Fe Springs, California USA), with plano-plano AT-cut polished quartz plates (1 inch in diameter) with a fundamental resonance frequency of 5 MHz, on both sides coated with an inner layer of chrome and an outer layer of gold (149273-1). The quartz plates were placed in a Teflon crystal holder (CHT-100), the cell holder was connected to a plating monitor (PM-710). We used a homebuilt flow cell provided with an inlet and an outlet that allow for the supply of blank solutions and vesicles dispersions.

Before the measurements the plates were rinsed extensively with chloroform, ethanol and millipore water, followed by cleaning in a plasma cleaner PDC-32G from Harrick (Ithaca, New York) for at least 3 minutes. Then the plates were placed overnight in the same solution (without vesicles) as used during the adsorption measurements. Prior to each measurement a plate was shortly rinsed with millipore water and dried under nitrogen. Subsequently, it was placed in the Teflon cell holder with the flow cell. The flow of solutions was established by using gravity, because using a pump resulted in an oscillating flow that interfered with the measurements.

The QCM measures the change in frequency of the gold-coated quartz piezo crystal as a result of adsorbed mass. The frequency shift Δf is related to the adsorbed mass Γ_m according to the Sauerbrey relation [38]

$$\Gamma_m = -\frac{(\rho_q \mu_q)^{\frac{1}{2}}}{2 f_0^2} \Delta f \qquad (5.1)$$

where the density of the quartz $\rho_q = 2.648 \times 10^{-9}$ mg m^{-3} and the shear modulus of quartz $\mu_q = 2.947 \times 10^{15}$ mg m^{-1} s^{-2}. The fundamental frequency of the quartz plate $f_0 \approx 5 \times 10^6$ s^{-1}. This gives $\Delta m = 17.7 \times 10^{-6} \Delta f$, with Γ_m in mg m^{-2} and Δf in s^{-1}. It should be mentioned that the Sauerbrey relation only accounts for the adhesion of thin rigid films. When the deposit is a relatively thick (visco)elastic layer (so that it dissipates the vibrational energy), the mass calculated with this equation is an underestimation of the actual adsorbed mass. This deviation can be corrected for by applying the viscoelastic model described by Voinova et al. [96] and can only be determined when the dissipation by the adsorbed layer is measured. Our QCM does not have this ability. However, we can estimate the effect of dissipation on the basis of earlier studies [37, 90] where the dissipation has been measured. In these studies the actual adsorbed mass for several vesicle sizes (on TiO$_2$) was calculated with the above-mentioned viscoelastic model. The results show that when the vesicle radius is approximately 20 nm the adsorbed mass calculated with the Sauerbrey relation and with the viscoelastic model of Voinona are equal. For a radius of around 100 nm the "Sauerbrey mass" is approximately 15 percent lower than the "Voinova mass". In this paper we will use the Sauerbrey equation to calculate the adsorbed mass and keep possible corrections in mind.

5.2.3 Surface plasmon resonance experiments

The adhesion of lipid vesicles to gold was also measured with a surface plasmon resonance (SPR) instrument (Autolab ESPRIT SPR, Ecochemie BV, Utrecht, The Netherlands). It uses a laser with a fixed wavelength of 670 nm. Commercially available gold-coated glass disks (Ecochemie BV, Utrecht, The Netherlands) with a diameter of 25 mm and a gold layer thickness of 48 nm, were cleaned in the same way as the QCM crystal plates. The instrument contains two cuvettes that were used simultaneously to study vesicle adsorption, which was done by injecting 100 μl of the vesicles solution into the cuvettes. During the measurements the solutions were stirred continuously by aspirating and dispensing 30 μl of the solution with a flow of 33 μl/s.

The SPR technique is sensitive to changes in the refractive index near the gold/solution interface, which provides information about interfacial events like binding of molecules to the gold surface. At a certain angle, the so-called SPR angle, where the reflection of the incident monochromatic p-polarized light beam on the gold surface is minimal, the energy of the incident monochromatic light beam is coupled into a surface-plasmon wave travelling along the gold/solution interface. This SPR angle is determined by several factors like the wavelength of the incident light beam, the thickness of the gold layer and the refractive index of the solu-

tion. This dependency on the refractive index provides the possibility to measure variations in the solution with the following equation.

$$\Delta\Theta = \kappa n_s \tag{5.2}$$

Here $\Delta\Theta$ is the change of the SPR angle and n_s is the refractive index of the solution. The sensitivity of the measurements is given by κ, which was determined by measuring the SPR angle for several water/ethanol mixtures with n_s ranging between 1.333 and 1.348 and was found to be $7.2 \times 10^{-6}/\text{m}°$. When a single adsorption layer with a thickness d and a refractive index n_l is present at the surface, in equation (5.2) the refractive index of the solution should be replaced by an effective refractive index. In the calculation of such an effective refractive index it should be taken into account that the sensitivity of the SPR exponentially decreases with increasing distance from the surface. This results into the following equation [97]

$$n_{eff} = 2/l_d \int_0^\infty n_z \exp(-2z/l_d)\mathrm{d}z \tag{5.3}$$

where l_d is the characteristic decay length of the exponentially decaying evanescent electromagnetic field into the medium. The value of n_z equals the refractive index of the adsorption layer n_l for $z = 0$ to $z = d$ and from $z = d$ it is equal to n_s. From the experimentally obtained value for $\Delta\Theta$ the effective refractive index is obtained, and using the refractive index increment of the adsorbing component it is possible to derive the adsorbed amount per unit area. For this we use a program called Huygens (Dullware Software, Wageningen, The Netherlands), which is based on the Abeles' method [98, 99].

For the adsorption of intact vesicles the situation is more complicated, because a heterogeneous adsorption layer, consisting of a solution fraction and a lipid bilayer fraction, is attached to the gold surface. The ratio of these fractions depends on the degree of surface coverage and on the deformation of the adsorbed vesicles. We assume that when a vesicle deforms in order to gain adsorption energy, the bilayer area remains the same while the volume is adjusted. As a first approximation we further assume that the vesicles deform to oblate spheroids with a radius $R_{||}$ parallel to the surface and a radius $R_\perp$ perpendicular to the surface, which is half the height H of the deformed vesicle. Now, the ratio of the lipid mass per surface area for the deformed vesicles, Γ_l, and for spherical vesicles of radius R, Γ_l^s, can be calculated with

$$\frac{\Gamma_l}{\Gamma_l^s} = 0.45(\frac{H}{2R})^2 + 0.035\frac{H}{2R} + 0.5 \tag{5.4}$$

With equations (5.3) and (5.2) and using the Huygens program it is now possible to calculate the shift of the SPR angle for a complete monolayer of adsorbed vesicles as a function of the degree of deformation. It is noted here that lipid bilayers are optically anisotropic and in the case of DOPC the p-polarized refractive index

99

$n^p = 1.450$ and the s-polarized refractive index $n^s = 1.435$, as determined with plasmon-waveguide resonance spectroscopy [100]. However, for the adsorption of intact vesicles the bilayer adopts all kind of orientations relative to the surface and therefore we use the average refractive index $n = 1.44$.

5.2.4 Self-consistent field theory

The self-consistent field (SCF) theory is a powerful tool to study association colloids, like micelles, bilayers and vesicles [2, 64, 83, 84]. We refer for most of the details to these papers and references therein. In short, the theory makes use of a mean-field approximation and uses a discrete lattice consisting of layers wherein the volume fraction φ of the molecules represents the (local) average concentration of components. The molecules that are used in the model are coarse-grained and consist of segments which represent small atom groups, for instance a CH_2 or CH_3 group in a lipid tail. All segments have the same size and occupy one lattice site. The lattice allows for one or two concentration (volume fraction) gradients implying an averaging over two or one direction, respectively. Most of the results discussed below make use of a two-gradient cylindrical coordinate system next to an impenetrable surface (c.f. figure 5.1). A drawback of this approach is that the geometry of the self-assembled structures is constrained and in some way pre-proposed. However, this geometry perfectly fits our requirements, because adsorbed vesicles are expected to be deformed in such a way that they can be rotated along an axis that runs through the center of the vesicle and is perpendicular to the surface.

An important feature of the SCF model is that the pair interactions of, e.g., a segment with label A with all other segments, is replaced by the interaction of this segment with an external potential field $u_A(\mathbf{r})$ given by

$$u_A(\mathbf{r}) = u'(\mathbf{r}) + k_B T \sum_B \chi_{AB}(<\varphi_B(\mathbf{r})> -\varphi_B^b) \tag{5.5}$$

where $u'(\mathbf{r})$ represents the energy that is needed to generate a vacant site at position $\mathbf{r}$ to insert a segment A, with $\mathbf{r} = (z, r)$ in the two-dimensional cylindrical case (figure 5.1). The second term represents the non-ideal interactions between segment A and all other segments, with φ_B the volume fraction of the other segments and the superscript b refers to the bulk solution. The angular brackets represent a local average. The Flory-Huggins nearest-neighbour exchange energy parameter is denoted by χ_{AB}. If this parameter is negative the AB interaction is energetically favourable over the AA and BB interactions. The volume fraction of a free segment, that is a monomeric entity) $\varphi_A(\mathbf{r})$ can directly be retrieved from the potential $u_A(\mathbf{r})$:

$$n_A(\mathbf{r}) \propto G_A(\mathbf{r}) = \exp \frac{-u_A(\mathbf{r})}{k_B T} \tag{5.6}$$

Here $G_A(\mathbf{r})$ is the Boltzmann factor, which is proportional to the number $n_A(\mathbf{r})$ of segments A at position $\mathbf{r}$, which in turn is trivially related to the volume fraction

$\varphi_A(\mathbf{r})$. When a segment is not free, but part of a chain-like molecule, the possible conformations of the chain have to be taken into account. By generating all possible self-avoiding walk conformations one can retrieve the statistical weight of all these possible chain conformations. However, this is a very time consuming job, especially for larger chains. Therefore we make use of a first order Markov approximation which permits, in principle, the positioning of a chain segment on a site aready preoccupied by another segment of the same chain. The excluded-volume problems is in part compensated by enforcing that on average each site is filled exactly once (as explained already). Within the first-order Markov approximation there exists a very efficient method to generate the volume fraction distribution for given set of segment potentials.

In short the SCF formalism thus allows to compute the volume fractions of the components once the segment potentials are avaiable, which symbollically may be abbreviated by $\varphi[u(\mathbf{r})]$. Morover Eqn 5.5 shows that the potentials can be computed from the segment distributions, or symbolically $u[\varphi(\mathbf{r})]$. Numerically a fixed point of this system is found routinely using an iterative procedure. The solution is known as the SCF solution obeys together with the vacancies an incompressibility constraint, i.e. $\sum_A \varphi_A(\mathbf{r}) = 1$ for all coordinates.

As at the basis of the SCF formalism there is an expression for the Helmholtz energy of the system, it is straightforward to accurately compute thermodynamic variables from this as soon as the SCF solution is available. These results are used below to analyse adsorption energies etc. for the interfacial vesicles.

Parameters

Referring to fig. 5.1, our system consists of two type of molecules, i.e., lipids and water, shown in figure 5.1. The lipid molecule has two tails, each consisting of $t = 12$ to 18 hydrophobic segments. Its headgroup consists of nine segments, i.e., two fragments of three hydrophilic segments spaced by a fragment of three hydrophobic segments. Water is present as a cluster of five segments, i.e., one central W surrounded by four others. The motivation for this water-model is that it suppresses (in line with experimental data) the amount of water in the bilayers as compared of using monomeric water species. Besides these two molecules there is also a single unit entity V, which represents free volume and allows for the compressibility of the system. The choice of the Flory-Huggins interaction parameters between the different segments has been discussed in a previous paper [79] and are shown in table 5.1.

We will briefly review the most important parameters. The repulsive interaction parameter $\chi_{CW} = 1.1$ between the hydrophobic tail segments and water drives the self-assembly of the lipid molecules to supramolecular structures. It has been chosen in such a way that the critical micelle concentration (c.m.c.) of the lipid is in the same range as the experimentally determined c.m.c. and shows comparable dependence on the tail length. The interaction between the hydrophilic head seg-
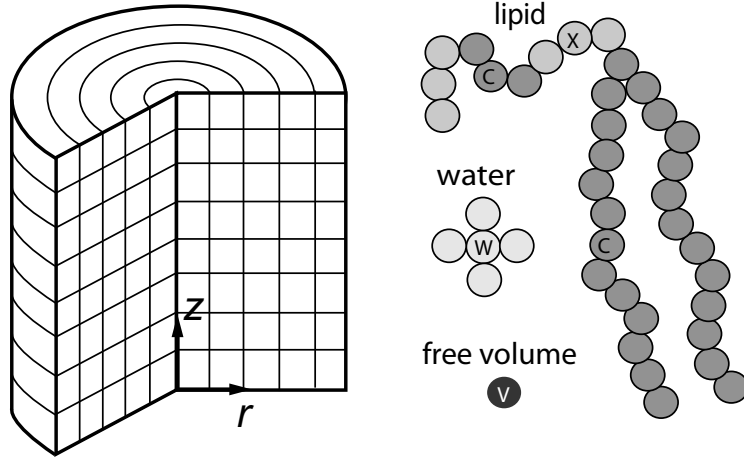
Figure 5.1: On the left side a two-dimensional cylindrical lattice. The z direction runs perpendicular to the surface ($z = 1$ is the first layer next to the surface - not indicated). The r coordinate is parallel to the surface. Note that the number of lattice sites $L(r, z)$ in a coordinate (r, z) is proportional to r. This coordinate system is used to study isolated adsorbed vesicles. For further explanation see the text. On the right the molecules that were used in the calculations. The head and two-tail structure of the lipid, and the water molecule assumes 5 sites as indicated. We further allow for free volume sites which may be represented by a monomeric species V. The names of the segment types of the components are indicated.

	C	W	X	V	S
C	0	1.1	2.5	1.5	0.5
W	1.1	0	−0.5	2.3	0
X	2.5	−0.5	0	2.3	−2.0
V	1.5	2.3	2.3	0	2.3
S	0.5	0	−2.0	2.3	0

Table 5.1: The Flory-Huggins interaction parameters between the various segments. A positive value means that the interaction is repulsive and a negative value represents an attractive interaction with respect to the interaction between identical segments. The parameter set is an extended (for the surface interaction) one from ref. [2]
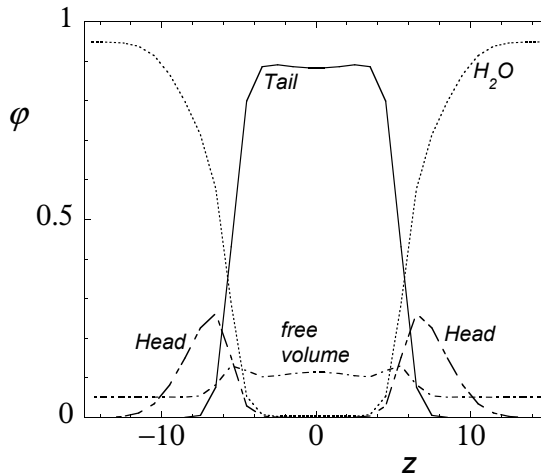
Figure 5.2: Volume fraction profile across a tensionless planar lipid bilayer with lipid tail length $t = 18$. Volume fraction profiles of the tail segments and the head segments are depicted, as well as those of the free volume and the water molecules.

ments and water is attractive ($\chi_{XW} = -0.5$), which determines, together with the repulsive interaction parameter between the head segments and the tail segments ($\chi_{XC} = 2.5$), the typical orientation of the lipids in the bilayer. It furthermore functions as a stopping mechanism in the self-assembly of the bilayer. In figure 5.2 the volume fraction profile of head, tail, water and free volume segments across a typical bilayer ($t = 18$) is depicted. It shows the high density of the lipid tails in the core of the bilayer and the water-rich headgroup region on the outside of the bilayer.

In previous studies [79] we have determined several structural and mechanical properties of these bilayers as a function of the tail length t. It was found for example that for a tensionless bilayer the thickness d_l^0 in units l (i.e., the size of a lattice site), and the area per molecule a_0 in units l^2 depend on the tail length of the lipids t according to the following equations:

$$d_l^0 = 2.86 + 0.437t \tag{5.7}$$

$$a_0 = 5.99 + 0.133t \tag{5.8}$$

For the mechanical bilayer properties, i.e., the bending modulus $k_c \equiv \frac{\partial^2 \gamma}{\partial J^2}$ (in units $k_B T$) and the area compression-expansion modulus $k_a \equiv \left(\frac{\partial \gamma}{\partial \ln a}\right)_{\gamma=0}$ (in units $k_B T/l^2$), the dependence on t is given by

$$k_c = 4.69 + 0.668t \tag{5.9}$$

$$k_a = 1.65 + 4.31 \times 10^{-2}t \tag{5.10}$$

103

where γ is the grand potential per unit area of the bilayer which is equivalent to the membrane tension.

As told, in all calculations presented in this paper a two-dimensional cylindrical lattice (figure 5.1) is used and the adsorbing surface is placed at $z = 0$. The vesicles consist of $N = 1000$ to $N = 2000$ lipids, which means that in the free state (not interacting with a surface) they have a radius ranging from $R \approx 18l$ to $25l$ (here l respresents the size of a lattice site). This radius is defined as the distance from the centre of the vesicle to the centre of the lipid bilayer leaflet. The modelled vesicles are rather small (R is in the order of 5 - 10nm) and in this size range the thermal fluctuations discussed by Seifert and Lipowski [92,93] are not relevant. In this study we will further look at the effects of bilayer elasticity and the interaction between the lipid headgroups and the surface on the structure of the adsorbed vesicles and the thermodynamics of the adhesion. This is achieved by varying the tail length from $t = 12$ to $t = 18$ and the interaction parameter between the hydrophilic headgroup segments and the surface χ_{XS} from -3 to 0, which appears to be the relevant range to find weakly adsorbed vesicles. Even though not all head group segments experience the favourable interactions with the surface (only the X-ones have this), below we refer to this adsorption energy as $\chi_{HS} \equiv \chi_{XS}$ for simplicity.

5.3 Results and discussion

5.3.1 Experiments

Figure 5.3a shows the relation between the total adsorbed mass Γ_m on gold as measured by the QCM and the radius of the (DOPC) vesicles in solution, R, for 250 mM KNO_3 and pH 3. The total DOPC concentration in solution was 1 g l^{-1}. The black dots represent the average adsorbed mass of at least three measurements and the error bars show the standard deviation of these measurements. The radius of the DOPC vesicles was varied from $R = 25$ nm to $R = 120$ nm. The total adsorbed mass consists of the adsorbed vesicles including their aqueous interior and any water enclosed between the vesicles. As already mentioned the adsorbed mass is calculated with the Sauerbrey relation [38], which means that in particular for the larger vesicles the adsorbed amount Γ_m is an underestimation (see Materials and methods section / QCM measurements).

The dashed line in figure 5.3a indicates the adsorbed mass Γ_m^s for the theoretical case of (hexagonally) close packed rigid spheres with a density of 1 g ml^{-1}. This density is chosen because the overall density of the vesicles including their content is approximately the same as the density of the aqueous environment. The mass Γ_m^s is an indication of the maximum possible adsorbed mass for intact vesicle adsorption and is proportional to the vesicle radius. Obviously, this results from the fact that the mass of each sphere scales with R^3, while the occupied area at the surface scales with R^2. Comparison of Γ_m with Γ_m^s shows that they diverge with increasing R. For
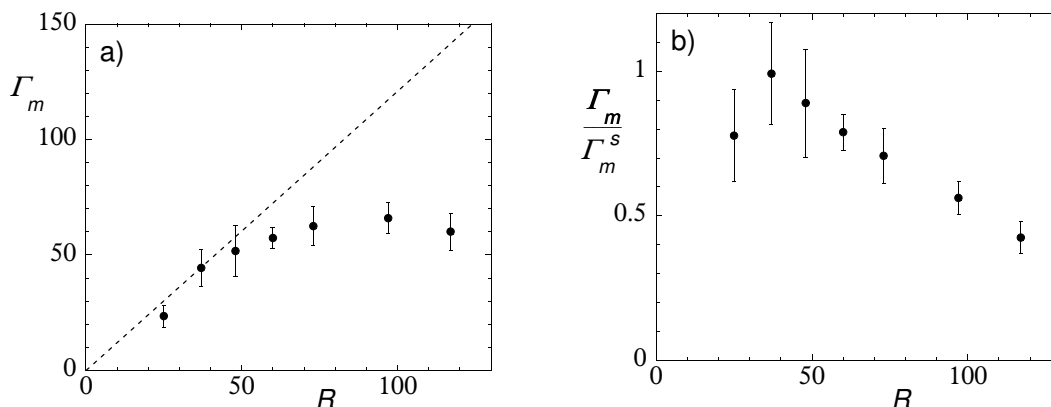
Figure 5.3: a) The total adsorbed mass Γ_m (mg/m^2) measured with the QCM as a function of the vesicle radius R. b) The ratio between Γ_m and the theoretical adsorbed mass for the case of a monolayer of hexagonally packed spheres with the density of water, Γ_m^s, as a function of R. (250 mM KNO$_3$, pH 3.)

the larger vesicles this may be partly due to the dissipation effect, but this effect is expected not to be larger than approximately 15 percent (see Materials and methods section / QCM measurements). Other factors that may lead to a deviation between Γ_m and Γ_m^s are i) rupture of vesicles, ii) deformation of the vesicles, iii) contribution of aqueous solution that is enclosed between the vesicles, and iv) incomplete surface coverage. In case of rupture of the vesicles, the maximum adsorbed mass would correspond to the mass of a single bilayer, which is in the order of only 5 mg m^{-2}. Since the total adsorbed mass is substantially higher and depends on the vesicle radius, we can rule this out (also in the adsorption kinetics no indications of vesicle rupture have been found). Deformation of vesicles, on the other hand, will undoubtedly play a role. The vesicles will not remain spherical when they are adsorbed to the gold surface. To increase the interaction energy between the vesicle and the surface the vesicles will flatten to some degree, which results in a decrease of the adsorbed mass per unit area. Solution enclosed between the vesicles would increase Γ_m, but we do not expect that this is a major effect, especially not in view of the vesicle deformation. Incomplete coverage would of course lead to lower Γ_m values.

Combination of the QCM results with SPR results gives more insight into the way the vesicles are adsorbed on the gold surface. SPR results are shown in figure 5.4a, which gives the shift in the SPR angle $\Delta\Theta$ as a function of the free vesicle size. It shows that $\Delta\Theta$ increases from approximately 800 m$^\circ$ for $R = 25$ nm to approximately 1400 m$^\circ$ for $R = 70$ nm. For larger values of R $\Delta\Theta$ starts to decrease again to approximately 1200 m$^\circ$ when $R = 125$ nm. The angle shift $\Delta\Theta$ is a measure for the adsorbed lipid mass, although the interpretation of the data is not straightforward as already discussed. Since the sensitivity of the SPR decreases when the distance between the mass and the surface increases, deformation (flattening) of
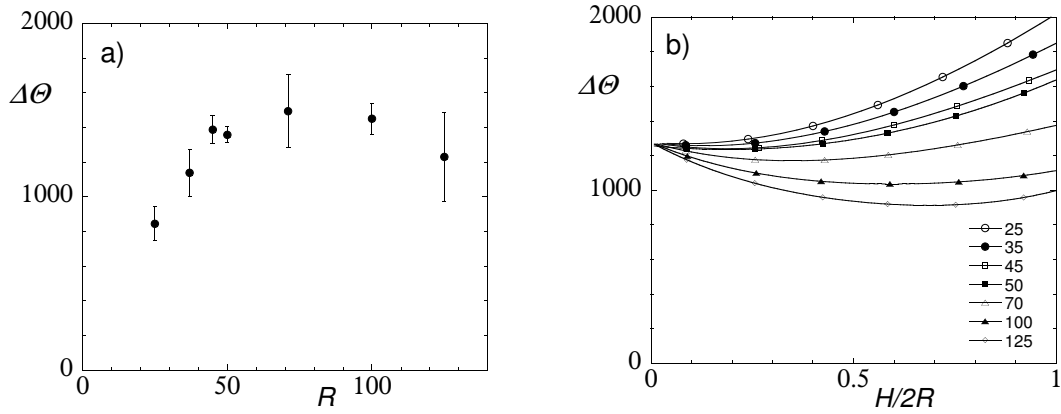
Figure 5.4: a) The shift in the SPR angle $\Delta\Theta$ in m° resulting from the adsorption of DOPC vesicles as a function of vesicle radius R in nm b) Theoretical shift in SPR angle versus the degree of deformation of the adsorbed vesicles $H/2R$ for the various vesicle radii R used in the experiments. Note that $H/2R = 1$ implies that the adsorbed vesicles are not deformed at all.

the vesicles contributes to the angle shift in two different manners: the lipid mass per surface area decreases, which results into a smaller angle shift, but also the average distance of the bilayer with respect to the surface decreases, which gives an increase in angle shift. In order to quantify these opposite effects we calculated the shift in SPR angle for various degrees of deformation with the Huygens program as described before (see Materials and methods section / SPR measurements). The parameters in the program were chosen in such a way that the sensitivity was the same as in the experimental setup, i.e., $\kappa = 7.2 \times 10^{-6}/m°$. The effect of flattening on the lipid mass per unit area has been given by equation 5.4.

In figure 5.4b the calculated values for $\Delta\Theta$ are plotted for vesicle sizes used in the experiments as a function of deformation, which is expressed as $H/2R$. What can be seen immediately is that $\Delta\Theta$ depends on the size and deformation of the vesicles. The decrease of $\Delta\Theta$ with increasing vesicle size can be attributed to the increased average distance between the vesicles' bilayer and the surface. An interesting feature is that the dependence of $\Delta\Theta$ on de vesicle deformation becomes stronger with decreasing vesicle size. For the three smallest vesicles the SPR angle monotonically decreases with increasing vesicle deformation (i.e., decreasing value of $H/2R$). Here the decrease of the lipid mass per unit area is on $\Delta\Theta$ is dominant over the increased SPR sensitivity. For the three largest vesicles these counteracting effects result in a minimum in $\Delta\Theta$ at a certain $H/2R$. All curves coincide at $H/2R = 0$ where the vesicles are completely flattened.

Comparison of the measured $\Delta\Theta$ values for the three largest vesicles with the calculated values shows that they are in the same range, although the measured $\Delta\Theta$ values tend to be somewhat larger than what is theoretically expected. This may be due to the relatively simple model used for the deformation of the vesicles and
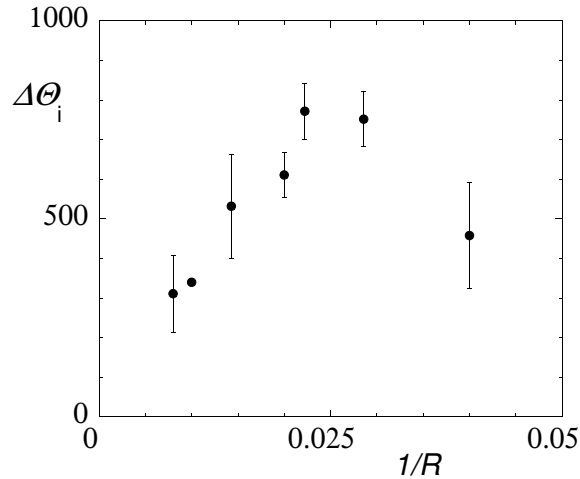
Figure 5.5: The initial adsorption rate, given by the SPR angle shift between injection of the vesicle dispersion and the first measurement, $\Delta\Theta_i$ (m°), versus the vesicle curvature $1/R$.

the calculation of $\Delta\Theta$. Anyway, the rather good agreement between the theoretical shifts in the SPR angle and the measured values shows that in the case of the larger vesicles a closely packed monolayer of deformed liposomes is formed.

Knowing that these larger vesicles, i.e., $R > 50$nm, are approximately closely packed on the gold surface gives us the opportunity to retrieve to some extend the deformation of the adsorbed vesicles. In figure 5.3b the ratio between the measured QCM mass Γ_m and the ideal theoretical QCM mass Γ_m^s is depicted as a function of R. In the case of the largest vesicle, i.e., $R \approx 125$nm, Γ_m/Γ_m^s is approximately 0.4. The underestimation of Γ_m, caused by the viscoelasticity of the adsorbed layer, is approximately 15 percent as discussed earlier. This means that the deformation of the vesicles $H/2R \approx 0.5$, depending on the additional water mass. This deformation becomes smaller with decreasing vesicle size, i.e., when $R \approx 50$nm, $H/2R \approx 0.8$.

For the smaller vesicles, $R < 50$nm, the dependence of the theoretical SPR angle (fig. 5.4b) on $H/2R$ is rather large. However, the measured $\Delta\Theta$ in the case of these small vesicles is smaller then all these theoretically possible SPR angles. This suggests that these small vesicles are not densely packed on the surface, but show a lower degree of surface coverage. Assuming that $H/2R \approx 0.8$ a rough estimate of the surface coverage can be made. This gives a surface coverage of approximately 0.5, 0.7 and 0.9 for vesicles with $R = 25$nm, $R = 35$nm and $R = 45$nm, respectively.

This smaller degree of surface coverage, i.e., less attractive interaction, in the case of the smaller vesicles is supported by the initial adsorption rate shown in figure 5.5 as a function of $1/R$. The initial adsorption rate is indicated by $\Delta\Theta_i$ (m°, i.e., the SPR angle shift between the injection of the vesicle dispersion and the first measurement approximately 7 seconds later.

The figure shows that in the range from $1/R = 0.008$ nm^{-1}, i.e., $R = 125$nm,

to $1/R \approx 0.025$ nm^{-1}, i.e., $R > 40$nm, the initial adsorption rate is inversely proportional to size of the vesicles. This is strong evidence that in this region the adsorption rate is transport limited. When $1/R$ becomes larger than 0.025 nm^{-1} this proportionality is lost, which indicates that attachment to the surface becomes the limiting factor. This can be attributed the fact that these small vesicles, i.e., with large curvature, do have a small initial interaction area with the gold surface and consequently do not have enough adhesion energy to stay attached to the surface. They have to deform to some extend in order to stay attached and as a consequence the number of vesicles that sticks to the surface decreases.

5.3.2 Theory

In this section we present the results of SCF calculations that were selected such that they can be compared to or assist in the interpretation of the experimental result. Of course from the SCF calculations one get supplementary information, e.g. on the thermodynamic and structural properties of adsorbed vesicles (as compared to free vesicles in solution). We focus on the effects of vesicle size, interaction energy between the lipid headgroup segments and the surface, and the bilayer elasticity. In addition, we address the stability of the adsorbed vesicles by comparison with the thermodynamic properties of adsorbed bilayer patches composed of the same number of lipid molecules.

It is generally believed that the questions whether a vesicle adsorbs or not and if it stays intact when it adsorbs, is determined by the interplay of several factors, which have been described by Seifert and Lipowsky [92]. These are the interaction energy between the hydrophilic lipid headgroup segments H and the surface S, which is in our model determined by the Flory-Huggins interaction parameter χ_{SX} ($=\chi_{SH}$), the elastic properties of the bilayer which are described by the bending modulus k_c, the lateral tension of the bilayer γ and the pressure difference between the vesicle exterior and interior $P = P_e - P_i$. The latter contribution is in our calculations automaticallyset to zero because we consider equiibrium only. In other words we are considering a bound vesicle that has been adsorbed for a period of time in which it was capable of reducing the pressure to $P = 0$ by adjusting its volume and/or surface area. This implies that the volume and the surface area of the free and the bound vesicle may differ, but the number of lipids N in the two vesicles is the same in all cases.

The strength of the interaction between the vesicles and the surface is varied by varying the Flory-Huggins interaction parameter χ_{SH} between the lipid hydrophilic head segments H and the surface S. However this parameter only gives the (free) energy for having a head-surface contact. More important is the free energy of interaction which also involves conformational degrees of freedom of the lipids. Therefore, in this section we will not always use χ_{SH}, but will sometimes present the results as a function of the bilayer-surface interaction (free) energy ΔG (in units $k_B T/l^2$),
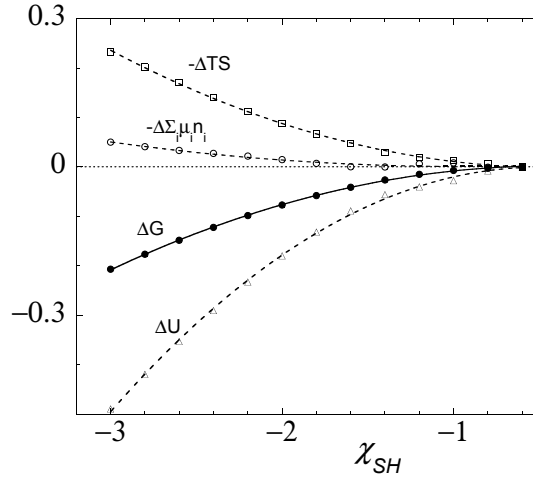
Figure 5.6: a) The relation between the lipid-surface interaction energy ΔG (in $k_B T/l^2$) and the Flory-Huggins interaction parameter χ_{SH}.

which is defined as

$$\Delta G = \Omega_{BS} - \Omega_S - \Omega_B \qquad (5.11)$$

Here Ω_{BS} is the grand potential of a flat bilayer adsorbed to a flat surface and Ω_S is the grand potential of a free surface (both in units $k_B T$ and per unit area). Both have been determined at the cmc of the lipids, i.e., at the chemical potential of the lipids where the free bilayer is tensionless, i.e., the grand potential $\Omega_B = 0$. The grand potential Ω can be described with

$$\Omega = U - TS - \Sigma_i \mu_i N_i \qquad (5.12)$$

where U is the contact interaction energy between the segments in the system, TS is the entropic contribution, with T the temperature and S the entropy and $\Sigma_i \mu_i N_i$ is the total chemical potential of all the segments present in the system, with μ_i the chemical potential of a molecue of type i and N_i the number of molecules of type i. This means that ΔG can also be described with

$$\Delta G = \Delta U - \Delta(TS) - \Delta \sum_i \mu_i N_i \qquad (5.13)$$

with $\Delta U = U_{BS} - U_S - U_B$, $\Delta(TS) = (TS)_{BS} - (TS)_S - (TS)_B$ and $\Delta \Sigma_i \mu_i N_i = (\Sigma_i \mu_i N_i)_{BS} - (\Sigma_i \mu_i N_i)_S - (\Sigma_i \mu_i N_i)_B$. The dependence of ΔG and its contributions ΔU, ΔTS and $\Delta \Sigma_i \mu_i N_i$ on χ_{SH} are shown in figure 5.6.

The figure clearly shows that the dependence of ΔG on χ_{SH} is stronger when χ_{SH} is more negative. For $\chi_{SH} \approx -0.7$ the effective adsorption energy $\Delta G = 0$, suggesting that the bilayer does not adsorb when $\chi_{SH} > -0.7$. The decrease of ΔG with decreasing χ_{SH}, can be attributed to a decrease of ΔU, which is mainly caused by an increased number of favourable interactions between the hydrophilic headgroup
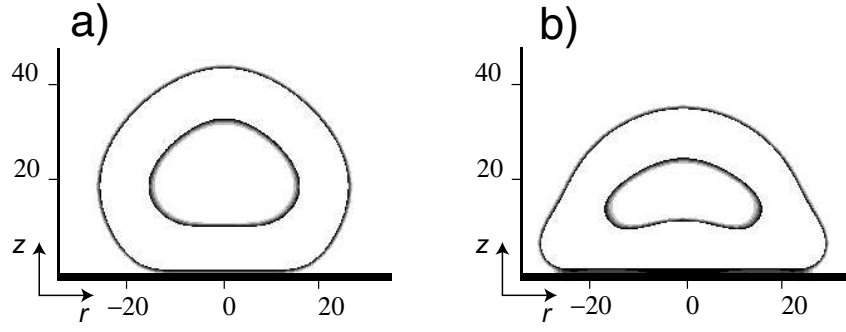
Figure 5.7: Equal volume fraction contour plots of interfacial vesicles for two different bilayer-surface interaction energies ΔG. The lines indicate the volume fraction of lipids of 0.5 (which occurs just beneath the head groups; it thus points to the edge of the membrane core). Both vesicles consists of 1000 lipids, with a tail length of $t = 18$. The dimensions of the r and z axes are in lattice layers l. a) $\Delta G = -7.65 \times 10^{-2} k_B T / l^2$ ($\chi_{SH} = -2$) b) $-2.06 \times 10^{-1} k_B T / l^2$ ($\chi_{SH} = -3$)

segments and the surface and the increased energy gain per interaction. There are also two opposing effects. The entropic contribution $\Delta(TS)$ increases because the water molecules adjacent to the surface are replaced by lipid molecules when χ_{SH} becomes larger, resulting in more conformational restrictions of these lipids. The chemical potential contribution $\Delta\Sigma_i \mu_i N_i$ is only small and can be attributed to the increased number of lipids in the system when χ_{SH} is large.

In figure 5.7 two examples of equal volume fraction contour plots for the adsorbed vesicles are presented. From this figure one can easily retrieve the overall shape of the adsorbed vesicle. The inner and outer boundaries of the bilayer, arbitrarily positioned where the lipid volume fraction $\varphi_l = 0.5$, are depicted as black lines. Between these two boundaries φ_l increases to approximately 0.9, and the volume fraction profile is quite comparable to that of the flat tensionless bilayer, which is shown in figure 5.2. In both cases the vesicle consist of $N = 1000$ lipids and each lipid has two tails of 18 segments, i.e., $t = 18$. When these vesicles are in the free state they have a radius $R = 18.4l$. The bilayer-surface interaction energies $\Delta G = -7.65 \times 10^{-2} k_B T / l^2$ (a) and $-2.06 \times 10^{-1} k_B T / l^2$ (b), respectively.

From figure 5.7 it is obvious that the degree of deformation or flattening of the adsorbed vesicle becomes larger when the interaction between the vesicle and the surface increases. However, besides this increased flattening, figure 5.7b shows that the bilayer topology at the edges of the adsorbed vesicle close to the surface is a function of the adsorption energy. This means that the bending at the edges is not caused by simple change in curvature of the bilayer, but involves rather drastic structural changes.

In figure 5.8a the dependence of vesicle deformation on ΔG is depicted. The deformation is given by $H/2R$, with H the distance between the surface and the
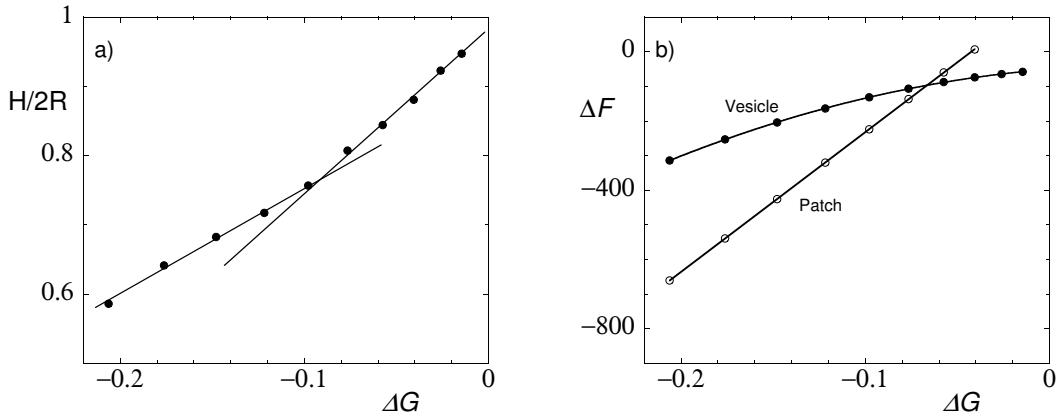
Figure 5.8: a) The relation between the deformation of the adsorbed vesicle, $H/2R$, and the bilayer-surface interaction energy ΔG. b) Total adsorption energy as a function of ΔG for adsorption of an intact vesicle and for adsorption of a vesicle in the form of a bilayer patch. In both cases the number of lipids in the vesicle $N = 1000$ and the tail length of the lipids $t = 18$.

centre of the (upper) lipid bilayer part at $r = 0$ that is not in contact with the surface, minus half the thickness of the flat adsorbed bilayer. R is the radius of the free vesicle ($R = 18.4l$). The figure proves that there are two regimes with different dependencea of $H/2R$ on ΔG. The transition between these two regimes is approximately at $\Delta G = -0.1k_BT/l^2$. In the range $-0.1k_BT/l^2 < \Delta G < 0$ the deformation of the adsorbed vesicle can be regarded to be elastic (i.e., the density of the bilayer is locally adjusted, but the volume fraction profiles do not change drastically), while in the range $\Delta G < 0.1k_BT/l^2$ structural changes as seen in fig 5.7b of the bilayer play an important role.

The total adsorption energy ΔF, i.e., the free energy difference between the free and the adsorbed state of a vesicle (intact or as a bilayer patch), is defined as

$$\Delta F = (\Omega_{SV} + \sum_i N_i\mu_i)_{bv} - (\Omega_S + \Omega_V + \sum_i N_i\mu_i)_{fv} \qquad (5.14)$$

with Ω_{SV}, Ω_S and Ω_V the grand potential (per unit area) of a bound vesicle, a bare surface and a free vesicle, respectively. The term $\sum_i N_i\mu_i$ denotes the total chemical potential of the system, and N the number of molecules per type and μ_i the chemical potential. The subscripts bv and fv denote the bound vesicle state and the free vesicle state, respectively. It is noted that the number of molecules N_i is the same in both states, as well as the temperature T and pressure difference P over the bilayer, i.e., $P = 0$.

In figure 5.8b the dependence of the adsorption energy ΔF on the bilayer-surface interaction energy ΔG is depicted for both the adsorption of an intact vesicle and the adsorption of a bilayer (with the same number of lipids) as a flat bilayer patch. The bilayer patch has a flat disk-like bilayer next to the surface, similarly as an adsorbed

bilayer, but on top of this, it has a rim. The rim is the sourse of some excess energy. It is possible to analyse the disk in large detail and extract the edge-energy as well as the membrane tension of the bilayer body. However, we will not do his here because it will distract us from the main line. It thus comes to no surprise that in the case of the bilayer patch there is a linear relation between ΔF and ΔG. However, in the case of the adsorbed intact vesicle, there is a deviation from this linearity and the slope of the curve is always smaller than that of the line for the adsorbed patch. The non-linearity must be attributed to the increasing deformation of the vesicle with increasing lipid-surface interaction energy, which diminishes the energy gain by adsorption. From our calculations we see that in the present model of the lipid surface interactions the adsorption-transition of the vesicles is a continuous phase transition; there is no evidence for hysterisis in the adsorption process. This means that as soon as ΔG is negative the vesicles will adsorb. At $\Delta G \approx -0.07 k_B T/l^2$, ΔF for the vesicle and the bilayer patch are equal. This signals an abrupt transition. For $\Delta G < -0.07 k_B T/l^2$ the bilayer patch is energetically more favourable and for $\Delta G > -0.07 k_B T/l^2$ the vesicles are energetically more favourable. As the two lines cross each other, we may trap a system in a meta stable state, i.e., that a patch is found whereas the vesicle is more preferred and the other way around. This effect is the natural consequence of an abrupt first-order transition.

From the above it follows that the vesicle adsorption can be divided in three different ΔG regimes. The weak interaction regime is from $-0.07 k_B T l^{-2} < \Delta G < 0$. In this regime the adsorbed vesicle is stable with respect to the adsorbed bilayer patch resulting in intact vesicle adsorption. The number of adsorbed vesicles per unit area decreases with increasing ΔG. The intermediate regime, i.e, $-0.1 k_B T l^{-2} < \Delta G < -0.07 k_B T l^{-2}$, is the regime where adsorption of an intact vesicle is slightly less favourable than formation of a bilayer patch. However, because the vesicles show only elastic deformation in this regime they may still adsorb intact and not fuse with other adsorbed vesicles. The third regime is the strong interaction regime, i.e., $\Delta G < 0.10 k_B T l^{-2}$, where the adsorbed vesicles have a strong tendency to rupture and fuse with other adsorbed vesicles, because staying intact is energetically highly unfavourable compared to forming a bilayer patch. As shown in figure 5.7b, in this regime the adsorbed vesicles are strongly deformed, having a highly energetic ridge, and this can be relaxed by a joint structural reorganisation of neighbouring vesicles, i.e., fusion. If the lipid-surface interaction is very strong it is even possible that the vesicles rupture without having interactions with other vesicles. From the calculations we do not get information about the way the metastable vesicles evolve to the more stable adsorbed bilayers.

In figure 5.9a, the relation between the vesicle deformation and radius of the free vesicle R is depicted. The figure shows that there is a linear relation between $H/2R$ and R. This is in agreement with the experimental results, from which it was concluded that the deformation of the lipid vesicles increases when the vesicles size becomes larger. For the QCM results the ratio Γ_m/Γ_m^s (fig. 5.3b) can be used as a
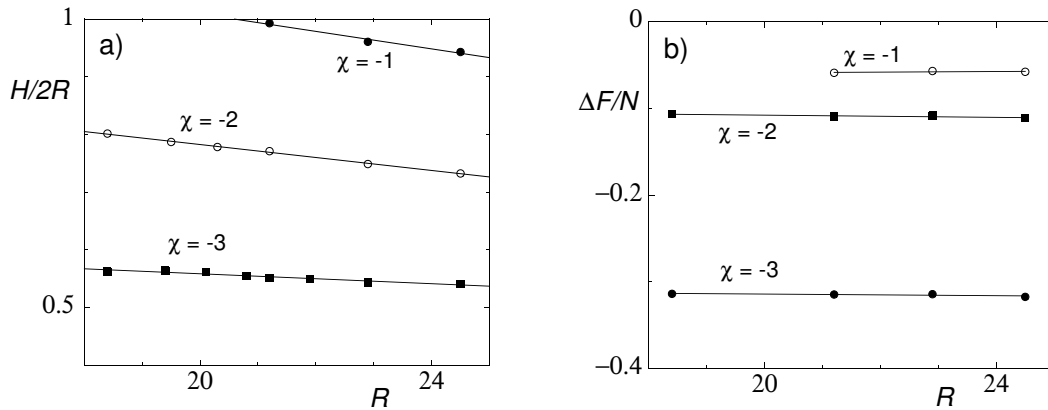
Figure 5.9: a) Dependence of the deformation of the adsorbed vesicle, expressed as $H/2R$, on R. b) The relation between the adhesion energy per lipid molecule (in k_BT) and R.

measure for the degree of deformation of the adsorbed vesicles, assuming that the surface is fully covered by vesicles. The SPR results show that this assumption is justified for the larger vesicle sizes. Although the ratio Γ_m/Γ_m^s gives just a qualitative indication, because the exact additional water mass in the adsorption layer is unknown as well as the dissipation due to the visco-elastic response, it is clear that it linearly depends on R for $R > 25$ nm. This is also the case if we correct for the (estimated) visco-elastic effect and additional mass (not shown).

The slope of the lines in figure 5.9 increases with decreasing vesicle-surface interaction. Thus not only the deformation itself, but also the change of deformation with the vesicle size gives information about ΔG. Another interesting phenomenon can be observed at $\chi_{SH} = -1$ and $R = 21l$ (corresponding to $N \approx 1250$): here $H/2R = 1$, i.e., the vesicle is not deformed, which results in a very small vesicle-surface interaction area and it is likely that at this χ_{SH} value a smaller vesicle does not adsorb. It can thus be concluded that when $\Delta G = 6.73 \times 10^{-3} k_BT/l^2$ the minimal radius for vesicles to adsorb is $R_{min} \approx 21l$. Likewise, for $\chi_{SH} = -1.2$ or $\Delta G = 1.46 \times 10^{-2} k_BT/l^2$ we found that this minimal radius $R_{min} \approx 18l$ (not shown). Comparison of R_{min} with the minimal adsorption radius R_a calculated according to the model of Seifert and Lipowski [92], i.e., for $P = 0$, $R_a = (2k_c/W)^{1/2}$, shows a rather large difference. Using for W the ΔG values mentioned above and k_c as given by equation 5.9, this gives R_a values of $48l$ and $70l$, respectively. The most plausible reason for this difference is the fact that Lipowski and Seifert assumed an infinitely thin sheet with certain elasticity, while in reality the bilayer has a finite thickness and the headgroup region is a substantial part of it. This means that this headgroup region can adjust itself in order to increase the interaction area between the bilayer.

In figure 5.9b the relation between $\Delta F/N$, that is the adsorption energy normalised by the number of lipids in the system and R is shown. Two interesting
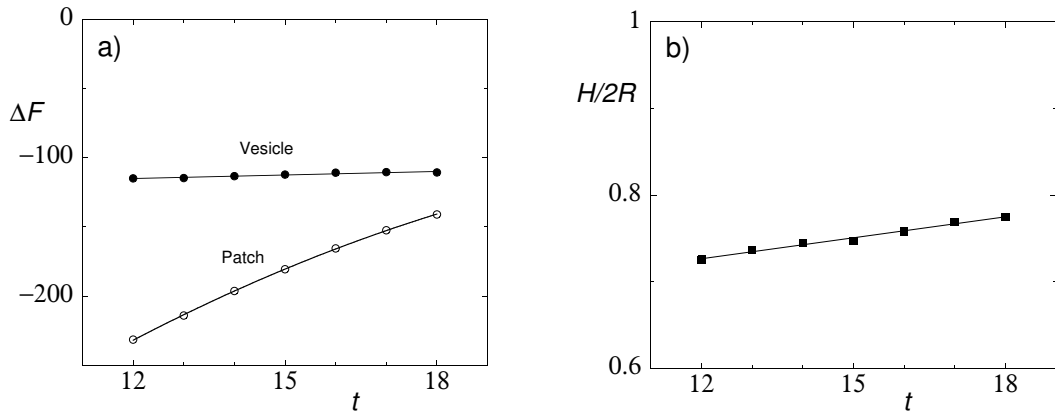
Figure 5.10: a) Adhesion energy ΔF as function of the lipid tail length t. b) Vesicle deformation $H/2R$ as a function of the lipid tail length t. In both cases $\Delta G = -0.077k_BT/l^2$ and $N = 1000$.

features can be observed, namely that for a certain χ_{SH} the value of $\Delta F/N$ is constant with vesicle size and that $\Delta F/N$ becomes larger when the headgroup-surface interaction becomes stronger. This size-independency of $\Delta F/N$ indicates that the interaction area between the vesicle and the surface A_i is proportional to the total bilayer area of the vesicle A.

Figure 5.10a shows that the energy change upon adsorption ΔF for a vesicle does surprisingly not depend on the elastic properties of the lipid bilayer. The tensionless bilayer thickness d_l^0 shows a linear relation on t (equation 5.7) and ranges from $d_l^0 = 8.17l$ when $t = 12$ to $d_l^0 = 10.7l$ when $t = 18$. This is also the case for the bending modulus k_c (equation 5.9), which ranges from $12.8k_BT$ when $t = 12$ to $16.6k_BT$ when $t = 18$. The independency of ΔF on t shows that there is a balance between the total lipid-surface interaction energy and the bending and stretching energy of the bilayer of an adsorbed vesicle, which is determined by the vesicle size and ΔG.

Even though ΔF does not vary with k_c, it is clear that the manner of vesicle adsorption is influence by k_c, because the balance between the elastic and interaction contribution results in a decreased interaction area with increasing k_c which results in less interaction area and as a consequence less deformation $H/2R$. In figure 5.10a this linear dependence of $H/2R$ on the lipid tail length t and thus k_c is shown. In contrast to intact vesicle adsorption, the adsorption as a bilayer patch gives a ΔF that increases (i.e., becomes less negative) almost linearly with increasing t. This is attributed to the fact that when t becomes larger the lipids at the edge of the patch have more problems to organise in such a way that no hydrophobic tails are exposed to the aqueous environment. For decreasing t it becomes more likely that the adsorbed vesicle ruptures in order to form a bilayer patch.

5.3.3 Outlook

Above we have presented the very first SCF predictions for adsorbed lipid vesicles. In agreement with predictions in the literature we collected evidence that the size of vesicles matters for the adsorption process. Although the experimental verification of this effect is far from trivial, we believe that our experimental data also point to this direction. More work is needed however to come to a complete picture. In experiments one should be able to tune the interactions of the vesicles with the surface (work of this type is in progress) as well as modify the membrane bending modulus (e.g. with additives) and from the theoretical point of view it would be worthwhile to take more realistic lipid surface interactions into account, e.g. electrostatic interactions, etc. A combined effort of experiments and theoretical modelling is in our opinion necessary because of the huge parameter space that presents itself in this problem. We showed that it is possible to combine theory and experiments and we therefore hope that the present paper will inspire other works of this type.

5.4 Conclusions

The combination of QCM and SPR results show that DOPC vesicles adsorb intact to the gold surface in the range 25 nm $< R <$ 125 nm. In this size range the adsorption can roughly be divided into two regimes, i.e., for 40 nm $< R <$ 125 nm the DOPC vesicles completely cover the gold surface, but below $R = 40$ nm the surface area covered with adsorbed vesicles decreases to approximately 50 percent when $R = 25$ nm. We furthermore found that the deformation of the DOPC vesicles becomes more pronounced with increasing vesicle size. For vesicles of $R = 125$ nm the adsorbed mechanical mass (as measured with QCM) was approximately 50 percent of the mass expected for spherical vesicles, which indicates that the adsorbed vesicles are flattened to ca half of their original height.

The results of the SCF model calculations on a single DOPC vesicle are in line with the experimental results. We found a linear relation between the degree of deformation (expressed as $H/2R$, with H the height of the adsorbed vesicle) and the vesicle size. The calculations also demonstrated that at a certain radius, which depends on the lipid-surface interaction and the bilayer elasticity, the adsorbed vesicle is not deformed anymore. This radius is assumed to be the minimal radius for vesicle adsorption. Besides this size-dependent effect we also found that the lipid-surface interaction can be divided into different regimes. There is a weak interaction regime where the adhesion of an intact vesicle is energetically favourable over adsorption as a bilayer patch. In this regime vesicle deformation does not lead to major changes in the lipid bilayer structure and therefore may be described as an elastic deformation. Furthermore, there is a strong interaction regime in which it is likely that adsorbed vesicles fuse and rupture in order to from bilayer patches, caused by extensive deformation of the vesicles, including drastic local changes in the bilayer

structure, and by the large energy difference between the adsorbed vesicle and the bilayer patch. Between these regimes there is an intermediate interaction regime in which the deformation of adsorbed vesicles still does not include drastic changes in bilayer structure, but where the adsorbed bilayer patch is already energetically somewhat favourable with respect to the vesicle.

From the calculations we also found that for the adsorption of intact vesicles the total adsorption energy per vesicle remarkably does not depend on bilayer elasticity, although the degree of vesicle deformation decreases with increasing bending modulus k_c. This suggests a balance between the penalty for bilayer deformation and the energy gain by bilayer-surface interaction.

Overall we can concluded that it is important to implement molecular detail in a model for vesicle adsorption, in particular for describing cases of strong bilayer-surface interaction, because local structural changes in the bilayer itself, which are not described in simple elasticity models, are important.

Chapter 6

Adhesion of phospholipid vesicles to gold: Effect of ionic strength, pH and applied potential

Abstract

The adhesion of lipid vesicles to surfaces is of interest, generically as well as in view of possible applications. Until now the principles behind it are poorly understood. Why, for instance, is it that on some surfaces vesicles do adsorb intact, while on other surfaces adsorbed vesicles transform into a supported bilayer? We address this question experimentally, by studying the adsorption of dioleoyl phosphatidylcholine (DOPC) and dioleoyl phosphatidylglycol (DOPG) vesicles to a gold surface, as well as theoretically, by using a self-consistent field (SCF) model that takes into account molecular details of the lipid bilayer. Adsorption studies were performed using a quartz crystal microbalance (QCM), which gives the adsorbed mechanical mass, and by surface plasmon resonance (SPR) measurements of the adsorbed lipid mass. We specifically investigated the contribution of the electrostatic interactions by varying the pH, ionic strength and by applying an external potential to the gold substrate. In the case of DOPG the pH shows a small but obvious effect on the adsorbed amount, which is attributed to the variation of the charge density on the gold surface. Variation of the ionic strength has a rather pronounced effect on the adsorbed DOPG amount, while in the case of DOPC this effect is absent. According to SCF calculations the difference between the adsorbed amounts of DOPG and DOPC can be attributed to a much stronger dependence of the headgroup density of the DOPG bilayer on the ionic strength than found for the DOPC bilayer. Somewhat unexpectedly, variation of the electric potential of the gold surface by an external circuit does significantly affect neither the adsorption of DOPG nor that of DOPC vesicles. This can be understood from the limited dependence of the surface and double layer potential of the gold substrate on the externally applied potential in the experimentally accesible potential range (i.e., where no redox reactions occur).

6.1 Introduction

When vesicles come into contact with a surface there are, roughly speaking, three possibilities, i.e., the vesicles do not adsorb to the surface, they do adsorb to the surface and stay intact thus forming a supported vesicular layer (SVL), or they adsorb to the surface and transform into a supported lipid bilayer (SLB). In an earlier study we showed that DOPC vesicles do adsorb intact on a gold surface [101]. Above a radius of approximately 40 nm the vesicles completely cover the surface, while below this radius the surface is only partly occupied. In addition, it was found experimentally that the deformation of the adsorbed vesicles increases with increasing vesicle size, which was confirmed by self-consistent field (SCF) calculations. Apart from the vesicle size, the interaction energy between bilayer and surface also influences the deformation of the adsorbed vesicle. The SCF calculations revealed three separate regimes i) the bilayer-surface interaction is repulsive and no adsorption takes place; ii) the interaction is weakly attractive and vesicles adsorb intact and partly or completely cover the surface; iii) the attractive interaction is rather strong and an adsorbed bilayer patch is energetically favourable over an adsorbed intact vesicle. The SCF method gives a more complete picture of vesicle adsorption compared to previously used theoretical methods [92–95, 102, 103], because it reveals structural adaptations of the bilayer on a molecular scale, which are not accounted for in the other models.

The variation of the bilayer-surface interaction explains why on some substrates, for example Au, Pt and TiO_2, phospholipid vesicles do adsorb intact while on others, for example SiO_2 and Si_3N_4, the vesicles transform into a supported lipid bilayer [37, 89, 90]. Since most surfaces in contact with an aqueous solution are charged, it is expected that electrostatic interactions between surface and vesicles play a role, especially in the case of the adsorption of charged lipid vesicles.

Several studies tried to elucidate the importance of electrostatic interactions between lipid vesicles and various substrates. Richter et al. [104, 105] systematically studied the relation between the vesicle charge and the adhesion on negatively charged surfaces. They found that varying the vesicle charge by changing the lipid composition determined whether the vesicles formed a supported lipid bilayer, stayed intact upon adsorption or did not adsorb at all. Also other studies investigated the importance of electrostatic interactions [106–108] by comparing the adsorption of positively and negatively charged vesicles on both positively and negatively charged substrates. Interpretation problems remain as in these studies either the lipids are changed or the substrate is changed in order to vary the charge characteristics of the systems. This implies that besides electrostatic interactions also other interactions, such as van der Waals or specific chemical interactions were varied.

In this study we investigate the importance of electrostatic interactions between the gold surface and lipid vesicles consisting of DOPC, DOPG or a mixture of these two. By varying the pH, ionic strength and an externally applied potential to the

gold substrate we try to get insight into the role of electrostatic interactions. Gold has been chosen because it is known that DOPC lipid vesicles do adsorb intact to its surface and also because over a relatively large potential range no electrochemical surface reactions occur in contact with an aqueous solution. The third reason is its ideal surface for use in the quartz crystal microbalance (QCM) and the surface plasmon resonance (SPR) apparatus. By varying the pH the degree of protonation of the oxide groups, which are present at the gold surface [1], is changed resulting in variation of the surface charge density. Barten et al. [1] showed that the isoelectric point of gold is at pH $\approx$ 4.9. It is noted here that variation of the pH and especially the ionic strength also influences the lipid bilayer properties, like the headgroup density and bilayer rigidity [25]. Because this might affect the adhesion of the lipid vesicles we also studied the adhesion as a function of an externally applied potential, which does not alter the vesicles in solution. In former studies [1, 109] the relation between the solution pH or an externally applied potential and the double layer potential of gold has been determined with colloidal probe AFM (atomic force microscopy). There has been a limited number of studies [110–116] where the adhesion of various molecules like polymers and proteins have been studied as a function of an externally applied potential. However, to our best knowledge until now no studies have been conducted where the adhesion of lipid vesicles is investigated as a function of an externally applied potential. The experimental results are complemented by a detailed self-consistent field analysis of lipid bilayers adsorbed onto a gold-like surface.

6.2   Materials and methods

6.2.1   Vesicle preparation

The lipids that were used in this study are dioleoyl phosphatidylcholine (DOPC) and dioleoyl phosphatidylglycol (DOPG), which were purchased from Avanti Polar Lipids (Alabaster, AL, USA). Furthermore we used KNO_3 from Merck (Darmstad, Germany). Water was purified with a Milli-Q water purification system (Millipore, Sweden) and had a resistance > 17 MΩ/cm. For the confocal fluorescent microscope measurements also the fluorescent probe β-bodipy fl C_{12}-HPC from Molecular Probes was used. The lipids were dissolved in chloroform and in the case of the confocal fluorescent microscope measurements the fluorescent probe was added with a probe/lipid molar ratio of 0.01. The chloroform was evaporated under nitrogen or in a roto-evaporator and the lipids were placed in vacuum for at least 2.5 hours to dry them completely. Subsequently, they were resuspended in a KNO_3 solution to a lipid concentration between 10 and 15 mg/ml. The resulting polydisperse multi-lamellar vesicle dispersion was freeze-thawed three to five times to dissolve all the lipids and to obtain unilamellar vesicles. The freeze-thawed dispersion was pushed at least 41 times through a polycarbonate filter with a pore radius R_p of 50 nm

or 200 nm by using a mini-extruder (LiposoFast, Avestin, Ottawa, Canada). The number of extrusions is an odd number, since in order to minimise contamination it is better to have the final vesicle solution in the other chamber than the initial solution. With dynamic light scattering (DLS) and using cumulant analysis and Contin fit the mean vesicle size and the size distribution of the vesicles was determined. The mean radius of the vesicles R extruded through the filter with $R_P = 50$ nm was found to be 45 nm and for $R_p = 200$ nm it was 100 nm.

6.2.2 QCM measurements

To monitor the adhesion of the lipids to gold, a quartz crystal microbalance was used from Maxtek, Inc (Santa Fe Springs, California USA), with plano-plano AT-cut polished quartz plates (1 inch in diameter) with a fundamental resonance frequency of 5 MHz, on both sides coated with an inner layer of chrome and an outer layer of gold (149273-1). The quartz plates were placed in a Teflon crystal holder (CHT-100), which was connected to a plating monitor (PM-710). The flow cell used was home-made with an inlet and an outlet that allows for the supply of the vesicles.

Before the measurements the plates were rinsed extensively with chloroform, ethanol and millipore water, followed by cleaning in a plasma cleaner PDC-32G from Harrick (Ithaca, New York) for at least 3 minutes. After this the plates were placed overnight in the same solution (without vesicles) as used in the adsorption measurements. Prior to each measurement a plate was shortly rinsed with millipore water and dried under nitrogen. Then it was placed in the Teflon cell holder with the flow cell. The flow of solution through the cell was created by using gravity, because the use of a pump resulted in an oscillating flow that interfered with the measurements.

The QCM measures the change in frequency of a gold-coated quartz piezo crystal. From this frequency shift the adsorbed mass can be calculated with the Sauerbrey relation [38]. Detailed information about the QCM technique and the interpretation of the data can be found in a previous paper [101].

6.2.3 Surface plasmon resonance measurements

The adhesion of lipids to gold was also measured with a surface plasmon resonance (SPR) instrument (Autolab ESPRIT SPR instrument, Eco Chemie B.V., Utrecht). It uses a laser with a fixed wavelength of 670 nm. The instrument contains two cuvettes which both were used to study the adsorption of the lipid vesicles. In order to do this the substrate was first calibrated at least 10 times for 60 seconds with solution and a baseline was measured. Then $100\mu l$ of the vesicles solution was injected in each cuvette. During the measurement in both cuvettes the solution was mixed continuously by aspirating and dispensing 30 μl it with a flow of 33 $\mu l/s$. The adsorbed amount of vesicles was determined by measuring the shift of the angle

where the reflection of the incident light beam was minimal. The cleaning procedure of the gold plates before measurements was the same as for the QCM gold plates.

Detailed information about the surface plasmon resonance technique and the interpretation of the data can be found in a previous paper [101].

6.2.4 Confocal fluorescent microscopy measurements

Images were collected with a Cell Map IC Bio-Rad (MicroScience Division, Hemel Hampstead, UK) confocal laser-scanning microscope, coupled to a Nikon Eclipse TE $2000-S$ microscope. Vesicles were imaged with a 63x, 1.4 NA DIC lens. Bodipy was excited with 488 nm line of the argon laser. Images were collected by Kalman averaging of $2-3$ full scans and acquired with LaserSharp 2000 software. The same crystal/gold plates were used as in the QCM measurements.

6.2.5 Self-consistent field (SCF) theory

The SCF theory has been discussed in detail in previous papers [79, 117], so we will discuss it only briefly in this section. The self-consistent field approximation uses a discrete lattice consisting of layers in which the volume fraction of the molecules is averaged. The molecules that are used in the model are coarse-grained and consist of segments which represent small atom groups, for instance a CH_2 or CH_3 group in a lipid tail. All segments have the same size as a lattice site. The lattice represents a three dimensional system, but because of the averaging one or two relevant coordinates remain. This dimensional reduction is achieved by making use of the symmetry in a system and by applying appropriate lattice geometry, e.g., flat, spherical or cylindrical. The advantage of this approach is a decrease of calculation time, but a drawback is that the geometry of the self-assembled structures is constrained. An important feature of the model is that the pair interactions of a segment with all other segments are replaced by the interaction of this segment with an external potential field $u_A(z)$:

$$u_A(z) = u'(z) + k_B T \sum_B \chi_{AB}(<\varphi_B(z)> -\varphi_B^b) + \nu_A e\psi(z) - \frac{1}{2}\epsilon_0\epsilon_A E(z)^2 \quad (6.1)$$

where $u'(z)$ represents the energy that is needed to generate a vacant site at position z to insert a segment A. The second term represents the non-ideal interactions between segment A and all other segments, with φ_B the volume fraction of the other segments and the superscript b refers to the bulk solution. The angular brackets represent a local average. The Flory-Huggins nearest-neighbour exchange energy parameter is denoted by χ_{AB}. If this parameter is negative the AB interaction is energetically favourable over the AA and BB interactions. The third term, i.e., $\nu_A e\psi(z)$, represents the electrostatic interactions between the segments, with $\psi(z)$ the electrostatic potential at z and ν_A the valency of segment A. The fourth term,

i.e., $\frac{1}{2}\epsilon_0\epsilon_A E(z)^2$, accounts for the polarization of the segments as a consequence of the electrostatic potential gradient, denoted by the electric field $E(z) = -\partial\psi/\partial z$, and their polarisability represented by the dielectric permittivity ϵ_A. In the SCF approach we compute the electrostatic potential by using a discrete version of the Poisson equation. The input for this is the charge density and dielectric constant profiles. Both can be computed from the volume fraction profiles. The volume fraction of a free segment A at position z, $\varphi_A(z)$, can be retrieved from the potential $u_A(z)$.

$$\varphi_A(z) \propto G_A(z) = \exp\left(\frac{-u_A(z)}{k_B T}\right) \qquad (6.2)$$

Here $G_A(z)$ is the Boltzmann factor, which as indicated is proportional to the number $n_A(z)$ of segments A at position z.

When a segment is not free, but part of a chain-like molecule, the possible conformations of the chain have to be taken into account. By generating all possible self-avoiding random walk conformations the statistical weight of all these possible chain conformations can be retrieved. However, for larger chains this becomes a very time-consuming job. This is the reason why we make use of a first-order Markov approximation, which allows positioning of a chain segment on a site which is occupied by another segment of the same chain. Such Markov model leads to freely jointed chains. An efficient propagator formalism relates the potentials to the volume fraction distribution and implements equation 6.2 for the lipid molecules. The normalisations of the volumefraction profiles depends from case to case. For exemple for freely-floating bilayer the normalisation involves a given number of lipids per unit area, which are chosen such that the membrane tension vanishes. For adsorbed lipids the normalisation is such that a fixed number of molecules exists in the system. These molecules are either adsorbed in typically an adsorbed bilayer or remain in solution. Some nonadsorbed lipids give rise to a low but finite bulk concentration. As a result adsorption isotherms can be computed. Typically we will be interested in the structure of the adsorbed bilayer at the CMC, i.e., the lipid concentration where the freely-floating bilayers are free of tension.

In the present work the SCF theory is used to study the thermodynamic and structural aspects of the adsorption of a flat lipid bilayer to a flat surface (resembling a gold surface). The adhesion of a flat bilayer to a flat surface implies one significant gradient, namely perpendicular to the surface. For this reason the lattice can be reduced to a one-dimensional flat system as shown in figure 6.1.

Various molecules are present in the system, which are shown in figure 6.1. The most abundant one is the water molecule, which consist of one segment W that can adopt three different states, corresponding to H_2O, OH^- and H_3O^+. The dissociation constant of water $k_w^\varphi = 10^{-17.5}$. The superscript φ means that this dissociation constant is retrieved from dimensionless volume fractions φ instead of molar concentrations, which means that $pH^\varphi - 1.75 \approx pH$. The salt present in the system is presented by the cation K and anion A, having a charge of $+e$ and
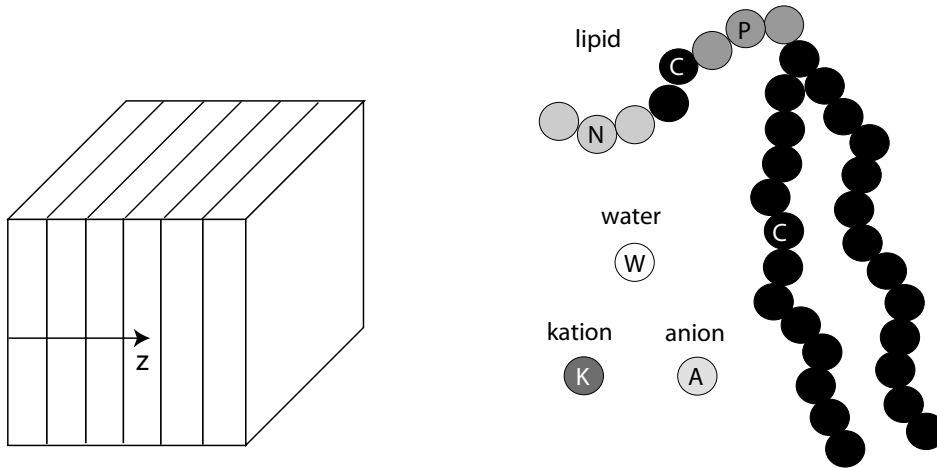
Figure 6.1: On the left side an example of the one-dimensional flat lattice is shown, which is used in the self-consistent field calculations. The size of the lattice sites is l. On the right side the various molecules are depicted. The lipid consist of 45 segments. In the case of the DOPG-like lipid the P-segments have a charge of $-1/3e$ and the N-segments are uncharged. In the case of the DOPC-like lipid the P-segments have a charge of $-1/3e$ and the N-segments have a charge of $+1/3e$. The charge of the cation (K) is $+e$ and the charge of the anion (A) is $-e$. The water molecule (W) can have a charge of $-e$, 0 or $+e$.

$-e$, respectively, with e the unit charge. The Flory-Huggins interaction parameters between the various segments are shown in table 6.1.

The lipid molecule representing DOPG or DOPC has two tails, each consisting of $t = 18$ hydrophobic segments connected with each other and the headgroup by one hydrophobic segment. The headgroup consist of three different fragments, i.e., two hydrophilic fragments consisting of three segments, which are spaced by a two segment long hydrophobic fragment. The hydrophilic N-segments are uncharged in the case of the DOPG lipid and have a charge of $1/3e$ in the case of the DOPC lipid. The hydrophilic P-segments have a charge of $-1/3e$ in both the DOPG and DOPC lipid. The repulsive Flory-Huggins interaction parameter between the hydrophobic tail segment C and the water segments W, i.e., $\chi_{CW} = 1.6$, and this, together with the repulsive interaction parameter between the head segments and the tail segments $\chi_{XC} = 2$, drives the formation of the typical bilayer structure.

Figure 6.2 shows two examples of volume fraction density profiles of the lipid segments across a lipid (DOPG) bilayer in aqueous solution. In figure 6.2 the ionic strength is low, i.e., $\varphi_{KA}^b = 0.001$, while in figure 6.2b the ionic strength is higher, i.e., $\varphi_{KA}^b = 0.01$. In both situations pH$^\varphi$ = 5. The figure shows that the bilayer thickness d_l^0 decreases with decreasing ionic strength, which can be attributed to less screening of the negatively headgroup segments by counterions, resulting in an increased repulsive interaction between the headgroups. The bilayer thickness,

χ	W	C	N	P	K	A	S	O
W	0	1.6	0	0	0	0	0	0
C	1.6	0	2	2	2	2	0	0
N	0	2	0	0	0	0	−3	0
P	0	2	0	0	0	0	−3	0
K	0	2	0	0	0	0	0	0
A	0	2	0	0	0	0	0	0
S	0	0	−3	−3	0	0	0	0
O	0	0	0	0	0	0	0	0

Table 6.1: The Flory-Huggins interaction parameters between the various molecular segments, and the molecular segments and the surface sites (S and O). A positive value means that the interaction is repulsive and a negative value represents an attractive interaction with respect to the interaction between identical segments.
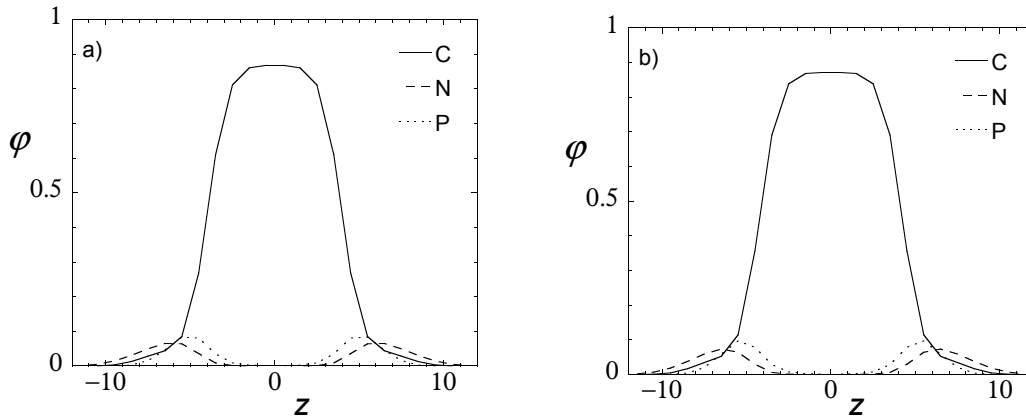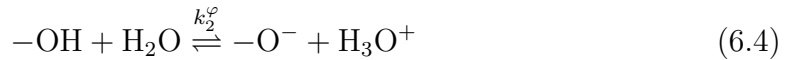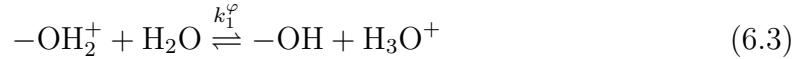

Figure 6.2: Two volume fraction density profiles across tensionless lipid bilayers. The lipids resemble DOPG. The volume fractions of the hydrophobic tail segments C and the hydrophilic N and P segments are shown. In both cases $\text{pH}^{\varphi} = 5$. a) $\varphi_{KA}^{b} = 0.001$. b) $\varphi_{KA}^{b} = 0.01$.

arbitrarily chosen as the distance between the positions where $\varphi_C = 0.5$, $d_l^0 = 8.1l$ when $\varphi_{KA}^b = 0.01$ and $d_l^0 = 7.6l$ when $\varphi_{KA}^b = 0.001$. The tail density in the core of the bilayer $\varphi_C \approx 0.88$ in both cases. The critical micelle concentration (CMC), defined as the lipid bulk volume fraction φ_l^b coexisting with the flat tensionless bilayer, increases with decreasing ionic strength (data is known accurately - not presented).

6.2.6 Modelling of the gold surface

Besides the molecules a surface S is present in the system at $z = 0$. The Flory-Huggins interaction parameters between the surface and the various segments are given in table 6.1. The most important one is the attractive interaction between the hydrophilic lipid headgroup segments and the hydrophilic surface S, i.e., $\chi_{SN} = \chi_{SP} = -3$. For simplicity, the interaction between S and the other segments have been set to $\chi = 0$.

In order to study the adhesion of a lipid bilayer to a gold surface we have to model the surface S in such a way that it exhibits the (electric and electrostatic) properties of the gold surface. To mimic the pH dependence of the double layer potential of gold resulting from the presence of oxide surface groups [1, 109], we attach groups O to the surface. For simplicity we take the Flory-Huggins interaction parameter between these groups and all other components in the system zero. The surface groups can adopt three different states, i.e., they can be negatively charged (-O$^-$), uncharged (-OH) or positively charged (-OH$_2^+$) by accepting or donating protons (H$_3$O$^+$) as shown below.

$$-\text{OH}_2^+ + \text{H}_2\text{O} \overset{k_1^\varphi}{\rightleftharpoons} -\text{OH} + \text{H}_3\text{O}^+ \tag{6.3}$$

$$-\text{OH} + \text{H}_2\text{O} \overset{k_2^\varphi}{\rightleftharpoons} -\text{O}^- + \text{H}_3\text{O}^+ \tag{6.4}$$

Using streaming potential measurements and colloidal probe AFM, Giesbers et al. [109] and Barten et al. [1] have measured the double layer potential ψ^d of a gold surface in equilibrium with aqueous solutions as a function of pH. Both studies showed that at a ionic strength of 1 mM ψ^d varies between approximately 30 mV and -30 mV when the pH increases from 3 to 7, with the isoelectric point (i.e.p) at pH ≈ 5. At pH values above ca 7 ψ^d is virtually constant. Barten et al. determined the number of oxide groups present on the gold surface by fitting the pH dependence of the double layer potential with a model developed by Duval et al. [118]. From this they found a density of approximately $n_s \approx 1 \times 10^{-2}$ sites nm^{-2}, which means that the oxide groups cover only a very small fraction of the surface (less than 0.1%). In order to obtain the same dependency of ψ^d on pH, in our calculations the equilibrium constants k_1^φ and k_2^φ are both set at 10^{-7}, and the group density n_s is in the same order of magnitude as found by Barten et al., i.e., $n_s = 1.5 \times 10^{-3}$ l^{-2}.
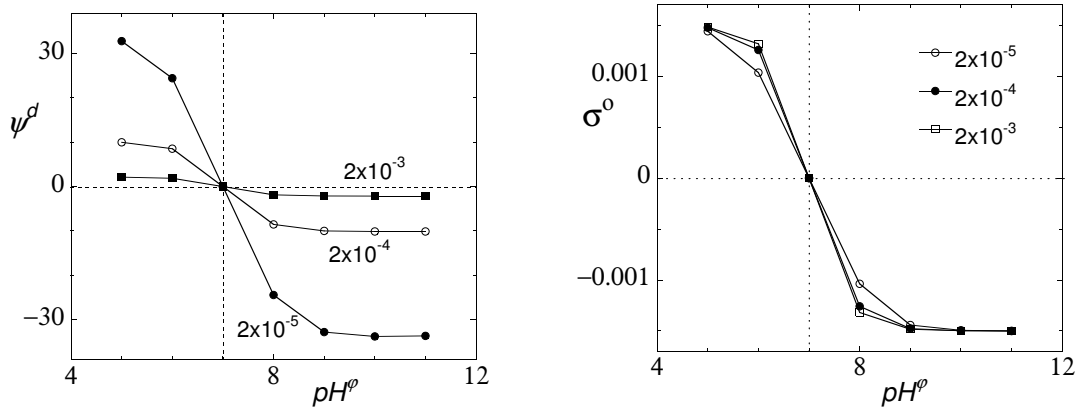
Figure 6.3: The double layer potential ψ^d (in mV) (a) and charge density σ^o in e l^{-2} (b) of the model surface as a function of the pH$^\varphi$ at various salt concentrations, i.e., $\varphi^b_{KA} = 2 \times 10^{-3}$, 2×10^{-4} and 2×10^{-5}. The density of amphoteric O-groups on the surface $n_s = 1.5 \times 10^{-3}$ l^{-2} and the equilibrium constants are $k^\varphi_1 = k^\varphi_2 = 10^{-7}$.

The double layer potential of the surface ψ^d (in mV) is shown in figure 6.3a as a function of pH$^\varphi$, for various values of φ^b_{KA}. In the model the double layer potential is chosen as the potential in the second layer from the surface as depicted in figure 6.4.

Figure 6.3 shows that there is a rather strong ψ^d transition around the i.e.p. and it furthermore shows that ψ^d varies between approximately -30 mV and 30 mV for $\varphi^b_{KA} = 2 \times 10^{-5}$, which is comparable to 1 mM. Figure 6.3b shows the pH$^\varphi$-dependence of the surface charge density σ^o. According to this figure σ^o shows a rather strong transition from completely positively charged to completely negatively charged in the range $5 < $ pH$^\varphi < 9$. Due to the low density of chargeable surface groups this is only weakly influenced by the ionic strength.

Barten et al. [1] also experimentally determined the relation between the double layer potential over the gold/solution interface and the applied potential $\Delta\Phi$ by means of an external electric circuit. In the studied potential range the variation in ψ^d was found to be only a fraction of the variation in $\Delta\Phi$; for example, at pH 5 and 1 mM KNO$_3$ it is only about 10%.

In order to mimic this relation we introduced an outer layer at the gold surface as shown in figure 6.4 with a smaller dielectric constant, resulting in a capacitance $C^e_g \approx 3.5$ μF cm^{-2}. This means that when there is a potential difference between the bulk gold and the solution a part of this difference is bridged in this outer layer. From electro-reflectance measurements on gold [119] there is evidence that such an outer layer with different dielectric constant indeed exists and has a thickness in the range of 0.05 - 0.2 nm. The introduction of such a layer in our model, together with the oxidic surface groups, gives results comparable to the experimental ones. The relation between the applied potential $\Delta\Phi$ and the double layer potential ψ^d is shown in figure 6.5a.
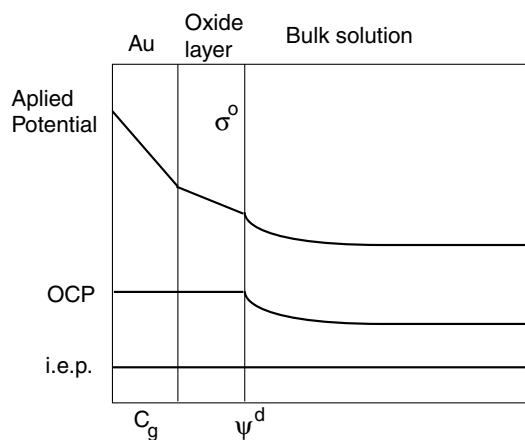
Figure 6.4: The SCF profile of the potential in the electric double layer at the gold surface.
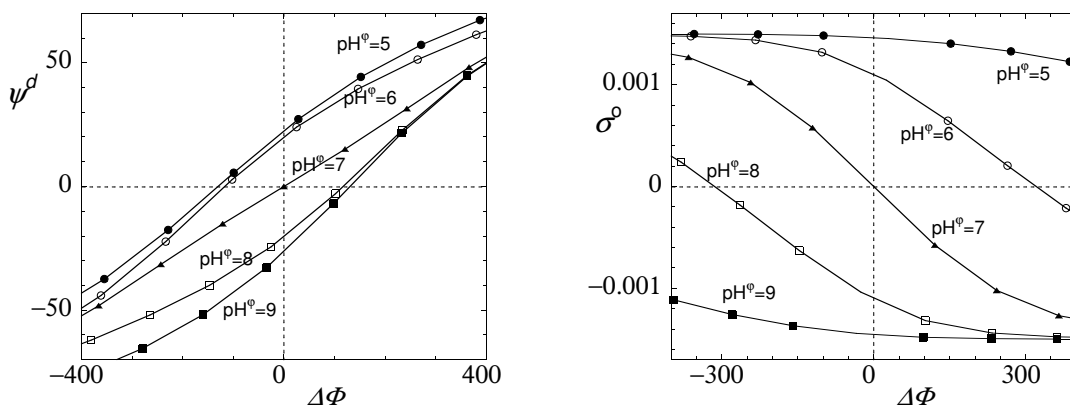

Figure 6.5: The double layer potential ψ^d in mV (a) and the charge density of the surface σ^o in $e\ l^{-2}$ (b) as a function of the applied potential $\Delta\Phi$ for various pH^φ values, at $\varphi^b_{KA} = 2 \times 10^{-5}$. Chargeable group density $n_s = 1.5 \times 10^{-3}\ l^{-2}$ and equilibrium constants the same as in figure 6.3.

The relation between ψ^d and $\Delta\Phi$ closely follows that found by Barten et al. [1]. Only for low pH there is a deviation from the measured data. A possible reason for this discrepancy is that in our case the number of oxidic groups is constant, while for the real gold surface the number of oxidic groups is thought to increase when the pH becomes lower than 5 [1]. Indeed, we find that when we increases the oxidic group density for $\mathrm{pH}^\varphi < 5$ (pH < 3.25) by a factor of two, i.e., $n_s = 3 \times 10^{-3} \ l^{-2}$, that the calculations fit better with the experimental data. However, since in the experiments described in this paper we varied the externally applied potential only at pH 5, for modelling the effect on vesicle adsorption $n_s = 1.5 \times 10^{-3} \ l^{-2}$ is a good choice. In figure 6.5b the relation between σ^o and $\Delta\Phi$ is given for various values of pH^φ. The figure shows that in this potential range the closer the pH is near the isoelectric point, the stronger the surface charge is affected by the applied potential.

In our calculations described in this paper we focus on the bilayer-surface interaction (free) energy ΔG (in units $k_B T/l^2$), which can be described as

$$\Delta G = \Omega_{BS} - \Omega_S - \Omega_B \tag{6.5}$$

Here Ω_{BS} is the grand potential of a flat bilayer adsorbed to a flat surface and Ω_S is the grand potential of a free surface (both in units $k_B T/l^2$)). Both have been determined at the cmc of the lipids, i.e., at the chemical potential of the lipids where the free bilayer is tensionless, i.e., the grand potential $\Omega_B = 0$.

So, here we do not model the adhesion of complete vesicles to the surface as done in a previous paper [101]. In that paper we investigated relation between the bilayer-surface interaction (free) energy ΔG and the total adsorption free energy of the vesicle ΔF. Therefore, by considering here only ΔG sufficient information can be obtained on the effect of electrostatic interactions between vesicles and surface, while the calculations are much less time-consuming. From the variation of ΔG, it is relatively simple to deduce the effect of the electrostatics on the adhesion of a complete vesicle.

6.3   Results and discussion

The importance of electrostatic interactions for the adhesion of DOPC and DOPG vesicles on a gold surface is investigated. To achieve this we first studied the effect of the lipid concentration and thus the vesicle concentration to see if we are at the maximum of the adsorption isotherm. We varied the pH, because this has an effect on the charge of the gold surface. In addition, the ionic strength is varied and we applied an external potential across the gold/solution interface. The effect of these experimental variables is also investigated by SCF modelling.
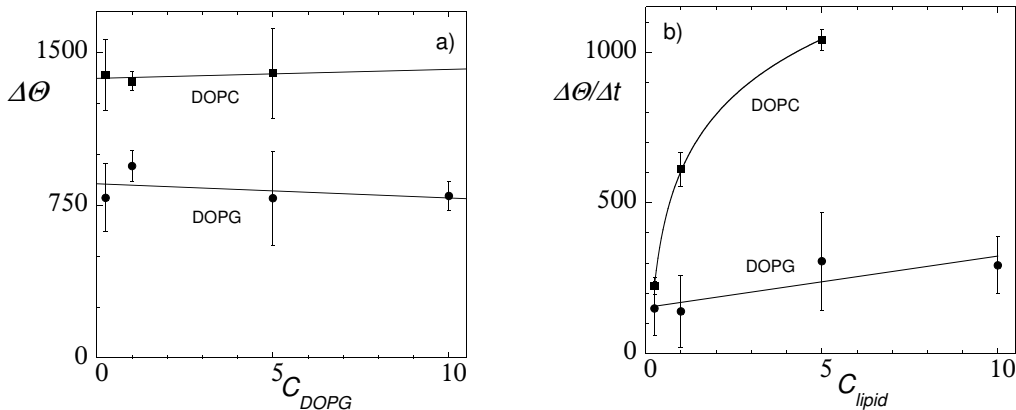
Figure 6.6: a) The total shift in critical angle $\Delta\Theta$ (in m°) as measured by SPR upon adsorption as a function of the lipid concentration C (in units g l^{-1}), for DOPG as well as DOPC vesicles. b) The initial change in critical angle $\Delta\Theta/\Delta t$ ($\Delta t = 6$ s). In all cases the ionic strength of the solution $I = 250$ mM and the pH = 3. Radius of the vesicles: 45 nm.

6.3.1 Lipid concentration effect

Figure 6.6a shows the effect of vesicle concentration on the total shift in critical angle $\Delta\Theta$ as found by SPR upon adsorption of DOPG as well as DOPC vesicles on the gold surface from aqueous solutions of pH 3 and 250 mM KNO$_3$. The radius of the DOPC and the DOPG vesicles R is approximately 45 nm. The shift in critical angle is a measure for the adsorbed lipid mass. In figure 6.6b the initial critical angle shift $\Delta\Theta/\Delta t$ is given, i.e., the difference between injection of the vesicle solution in the SPR cell and the first measurement, with Δt always 6 s. This initial shift in critical angle is an indication for the initial adsorption rate.

We will first discuss the SPR results. In figure 6.6 the vesicle concentration C_s is given in g l^{-1}, which means that the molar concentration of the DOPG and DOPC lipids are approximately the same ($M_{\text{DOPG}} = 797$ g mol^{-1} and $M_{\text{DOPC}} = 786$ g mol^{-1}). For both lipids $\Delta\Theta$ is independent of the vesicle concentration, which means that we are at the plateau level of the adsorption isotherm. In the case of the DOPC vesicles $\Delta\Theta \approx 1400$ m°, which corresponds to full surface coverage of the gold with vesicles as has been shown in our previous paper [101]. In the case of the DOPG vesicles the shift in critical angle is considerably smaller. It is not likely that this difference results from a difference in SPR sensitivity for the DOPC and DOPG lipids, since at a higher KNO$_3$ concentration of 1000 mM, upon adsorption of DOPG vesicles $\Delta\Theta$ also increases to approximately $\Delta\Theta \approx 1400$ m°. (We will come back later to this salt effect.) Therefore, we conclude that at 250 mM and pH 3 the adsorbed lipid mass of DOPG is significantly lower than that of DOPC.

In addition, from figure 6.6b it follows that the adsorption of DOPG vesicles under these conditions is much slower than that of DOPC vesicles. As shown by
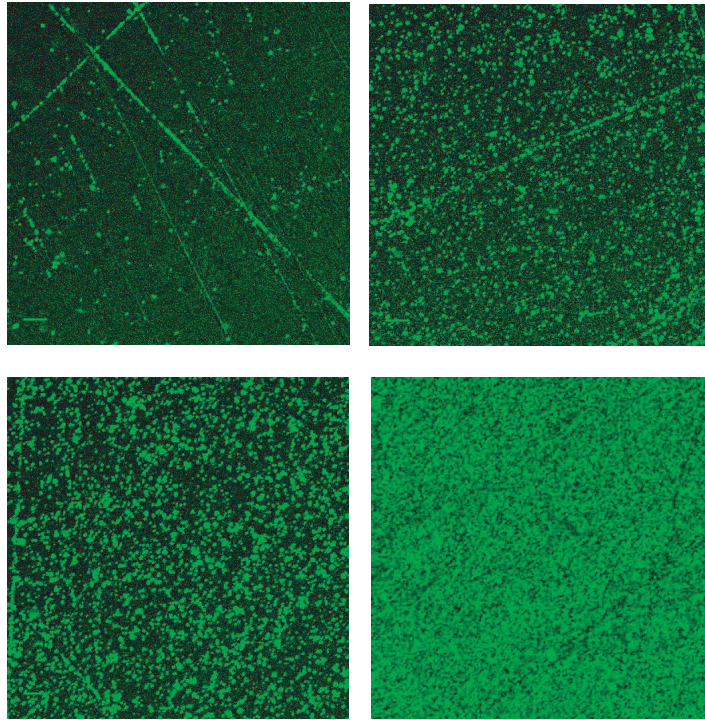
Figure 6.7: DOPG vesicles (containing 1% of fluorescent lipids) at a gold surface, imaged using a confocal fluorescent microscope. The bar in each plot represents 5 μm. The vesicles ($R \approx 100$ nm) were adsorbed from a solution of pH 3 and a KNO$_3$ concentration of a) 10 mM, b) 50 mM, c) 100 mM and d) 250 mM.

previous studies [91,101] the adsorption of DOPC vesicles onto gold is mass transport limited in this concentration range. This means that the initial adsorption rate is proportional to the vesicle concentration. That this proportionality is not found here is probably due to a too long time interval between injection and first measuring (6 s), which means that other factors, like the available surface area, start to play a role. However, it is clear that for the DOPC vesicles $\Delta\Theta/\Delta t$ depends much stronger on vesicle concentration than for the DOPG vesicles. This implies that the initial adsorption rate of the DOPG vesicles is mainly determined by the rate of attachment of the vesicles to the surface. Since the ionic strength is rather high (250 mM) it is not electrostatic repulsion between DOPG vesicles that causes the low adsorption rate and low adsorbed amounts. This implies that the DOPC vesicle would adsorb more strongly than the uncharged DOPG vesicle. Because this is in contradiction with the electrostatic interactions between the vesicles and the surface this difference in adsorption has to come from variations in van der Waals or specific interactions.

6.3.2 Effect of the ionic strength

In figure 6.7 confocal fluoresence microscopy images are presented of DOPG vesicles adsorbed onto a gold surface from solutions with different KNO$_3$ concentrations as
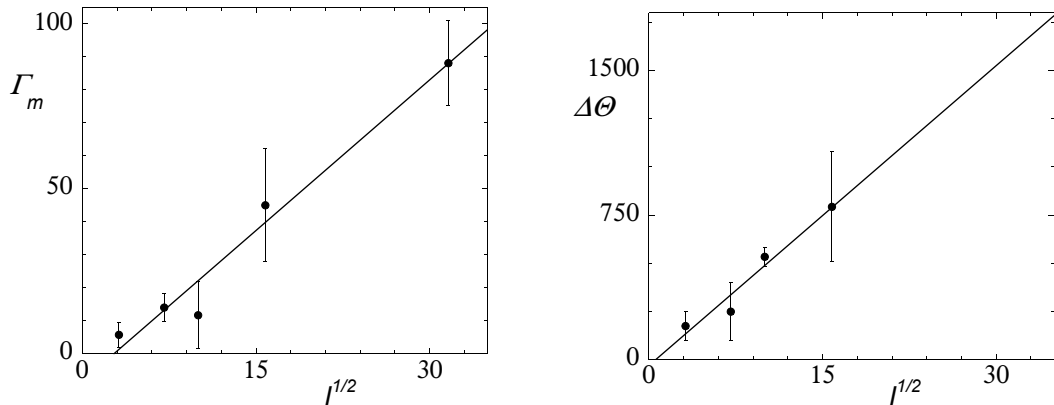
Figure 6.8: Adsorption of DOPG vesicles of radius $R \approx 100$ nm onto gold as a function of the square root of the ionic strength $I^{1/2}$ (in M$^{1/2}$), at pH 3. The vesicle concentration in solution amounts to 0.25 g l^{-1}. a) The total adsorbed mechanical mass Γ_m (in mg m^2) as measured with QCM and b) the total shift of the critical angle (in m°) measured with the SPR.

indicated (pH 3). The figure shows that the number of adsorbed vesicles increases significantly over this range of ionic strengths. However, these images do not reveal whether all vesicles do adsorb intact or that part of the adsorbed vesicles break and fuse to form a supported bilayer. This is because the emitted fluorescence within a distance of approximately 5 nm from the gold surface is almost completely quenched due to Förster energy transfer [120]. Therefore, if a supported bilayer, which has a thickness of approximately 4 nm, would be present at the surface, this would probably not be visible. An interesting feature is that the adsorbed vesicles are distributed randomly and more or less homogeneously over the gold surface, but they seem to have a preference for irregularities (scratches) on the gold surface, which is especially visible at a ionic strength of 10 mM. This preference may have two reasons, i.e., the increased contact area between the vesicles and the surface at these irregularities stimulates the adhesion, and /or the vesicles adsorbed at these irregularities do not have to deform as much as on the smooth surface in order to gain enough interaction energy and therefore have less tendency to fuse or rupture.

In order to find out whether the DOPG vesicles do adsorb intact or partly transform into a flat supported bilayer we studied their adsorption with QCM as well as with SPR. The results as a function of the square root of the ionic strength $I^{1/2}$ are given in figure 6.8. This figure shows that both the adsorbed mechanical mass and the adsorbed lipid mass are proportional to $I^{1/2}$, and thus the ratio of these two quantities is constant. To have an idea of the actual mass ratio, we have to estimate the DOPG mass from the SPR angle shift. It is not straightforward to calculate the lipid mass precisely, since the conversion factor depends on the size as well as the degree of deformation of the vesicles [101]. Assuming that the SPR sensitivity for DOPG is comparable to that for DOPC and that the degree of deformation of the
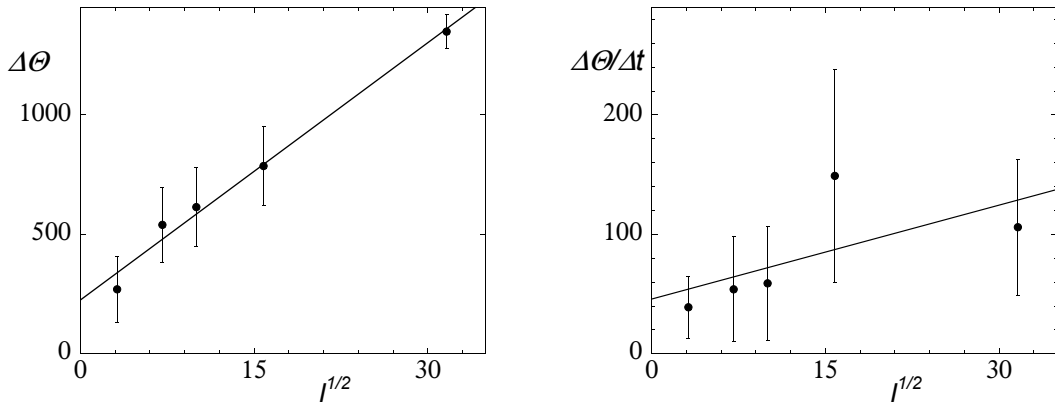
Figure 6.9: Adsorption of DOPG vesicles of radius $R \approx 45$ nm onto gold as a function of the square root of the ionic strength $I^{1/2}$ in M$^{1/2}$, at pH= 3. The vesicle concentration in solution is 1 g l^{-1}. a) The total shift in critical angle (in m°) from SPR upon adsorption, and b) the initial change in critical angle $\Delta\Theta/\Delta t$ (in m° s^{-1}).

DOPG vesicles is comparable to equally sized DOPC vesicles, 100 m° corresponds to approximately 1 mg m^{-2} [101]. This means that the actual lipid vs. mechanical mass ratio is approximately 0.15, and therefore it can be concluded that the vesicles adsorb intact to the gold surface irrespective of the ionic strength. This is further supported by the fact that the adsorbed mechanical mass, measured with the QCM, always increases over a certain time period until it reaches a maximum. If the adhered vesicles would have a tendency to break and form a supported bilayer, the adsorbed mechanical mass would first increase, but then decrease again due to the loss of the internal vesicle volume. This overshoot has been shown experimentally by, e.g., Keller and Kasemo [89].

In figure 6.9 $\Delta\Theta$ and $\Delta\Theta/\Delta t$ are shown as a function of $I^{1/2}$ for adsorption of smaller DOPG vesicles, i.e. with $R \approx 45$ nm, at pH 3. Also for these vesicles there is a linear relation between $\Delta\Theta$ and $I^{1/2}$. The fact that such a relation is found for both vesicle sizes strongly suggests that the effect of salt is related to screening of electrostatic interactions since the Debye length $\kappa^{-1} = \sqrt{c/I}$, with c a constant that is determined by various solution parameters. For the uncharged DOPC vesicles we found that there is no or only a very weak dependence of the adsorbed amount on the ionic strength (results not shown).

The total SPR angle shift $\Delta\Theta$ for these small (45 nm) vesicles is in the same range as for the larger (100 nm) vesicles (figure 6.8b). If the degree of deformation upon adsorption for each of these vesicle sizes is comparable with the deformation of equally sized DOPC vesicles as shown in a previous study [101], the surface coverage is approximately the same for the 45 nm and the 100 nm vesicles. The initial adsorption rate of the 45 nm DOPG vesicles depends only weakly on $I^{1/2}$ as can be seen in figure 6.9b. The initial rates are in all cases well below the adsorption rates of equally sized DOPC vesicles at the same lipid concentration, i.e., $C_{lipid} = 1$
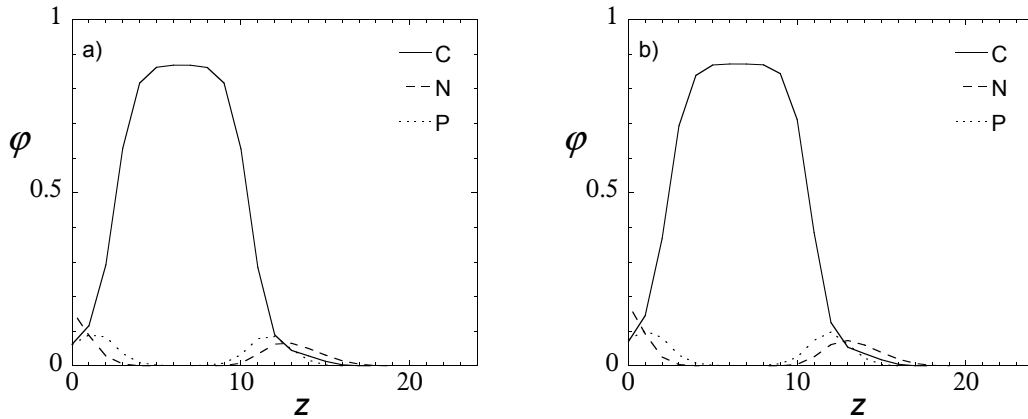
Figure 6.10: Volume fraction density profiles as predicted by SCF modeling across an adsorbed DOPG bilayer at pH$^\varphi$ = 5 and two electrolyte concentrations of a) $\varphi_{KA}^b = 0.001$ and b) $\varphi_{KA}^b = 0.01$ at the CMC. The surface is located at $z = 0$. The volume fractions of the hydrophobic tail segment C and the hydrophilic N and P segments are depicted.

g l^{-1} (see figure 6.6b), again implying attachment limitations.

In the remainder of this section we will present SCF modeling results to gain further insight into the effect of the ionic strength on vesicle adsorption. In figure 6.10 the cross-sectional volume fraction profiles of an adsorbed DOPG bilayer for two different salt concentrations are shown. The bulk concentration of (free) lipids equals the critical micelle concentration (CMC). The volume fraction profiles of the adsorbed bilayer are quite similar to those of the tensionless free bilayer as shown in figure 6.2. However, there are a few important differences. For example, the headgroup density adjacent to the surface is somewhat higher as a result of the favourable interaction between the headgroup segments and the surface. This effect is a bit larger for the higher electrolyte concentration, $\varphi_{KA}^b = 0.01$. As a result of this also the thickness of the adsorbed bilayer d_l (defined before as the distance between the positions where $\varphi_C = 0.5$) is somewhat larger than that of the free bilayer d_l^0.

In figure 6.11a the adsorbed lipid mass θ^{exc} for both DOPG and DOPC bilayers is given as a function of the ionic strength for three different values of the Flory-Huggins interaction parameter between the lipid headgroups and the surface, χ. For the DOPG bilayer θ^{exc} shows a linear dependence on $\sqrt{\varphi_{KA}^b}$. The dependence of θ^{exc} on ionic strength is much stronger for DOPG than for DOPC. This can be attributed to the fact that in the case of the DOPG bilayers increasing the salt concentration has a rather large effect on the headgroup density by screening of the negatively charged headgroup segments (as can be seen in figure 6.10). For the DOPC bilayer, however, this screening effect is limited because the lipid has both positively and negatively charged segments in the headgroup, and at low salt concentrations the headgroups organise in such a way that they counter charge each other [25].
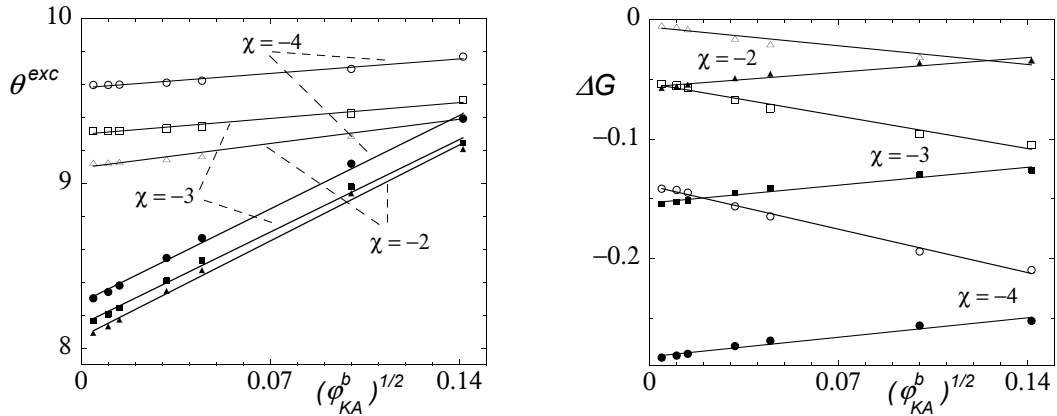
Figure 6.11: a) The adsorbed amounts of DOPG lipids (closed symbols) and DOPC lipids (open symbols) denoted by θ^{exc} per unit area l^2 as a function of the square root of the electrolyte bulk volume fraction $(\varphi^b_{KA})^{1/2}$ for various Flory-Huggins interaction parameters between the hydrophilic headgroup segments and the surface χ. b) The corresponding values for the lipid-surface interaction energy ΔG in $k_B T$ per unit area l^2. pH$^\varphi = 5$.

Because the DOPG headgroup density increases with increasing φ^b_{KA}, the number of favourable Flory-Huggins interactions between the headgroup segments and the surface increases. As a consequence, ΔG becomes more negative at higher electrolyte concentration, which is shown in figure 6.11b. The fact that the dependence of ΔG on $\sqrt{\varphi^b_{KA}}$ is largely determined by the Flory-Huggins interactions is supported by the fact that it becomes more pronounced when χ is set to more negative values. Besides the increase of the Flory-Huggins interaction energy between the bilayer and the surface with increasing ionic strength, there is a small opposite contribution to ΔG due to the decrease of the electrostatic interactions between the positively charged oxide groups and the negatively charged lipid headgroups.

In the experimental study of the ionic strength effect on the adsorption of DOPG vesicles we found a linear dependence of the adsorbed amount of DOPG vesicles on $\sqrt{I}$. It is thus likely that this variation of the adsorbed amount can be attributed to the variation of the adhesion energy as a function of the headgroup density. It should be noted, however, that in the case of vesicle adsorption, the rigidity of the bilayer also has to be taken into account. For DOPG vesicles this rigidity increases with increasing ionic strength when $I > 10$ mM [25] and this would counteract on the increased adsorption of the DOPG vesicles with increasing ionic strength. Apparently, this effect is rather weak compared to the increased bilayer-surface interaction.

For the DOPC bilayer there is a weaker dependence of ΔG on φ^b_{KA}, and it shows a trend opposite of the one found for the DOPG bilayer. In this case the effect of the ionic strength on the adsorption is not related to changes in the headgroup density, but to changes in the headgroup organisation. This results in a small
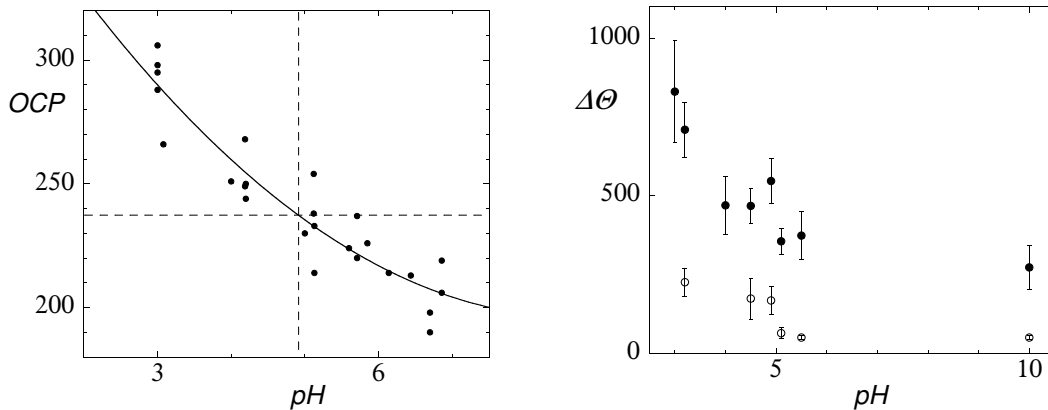
134

Figure 6.12: a) The open circuit potential (OCP, in mV) of the gold substrate with respect to an Ag/AgCl reference electrode as a function of the pH at 10 mM KNO$_3$. Measurement of the OCP was performed in the QCM. b) The total adsorbed lipid mass given as the shift in SPR angle, $\Delta\Theta$ (in m°, closed symbols), and the initial adsorption rate $\Delta\Theta/\Delta t$ (in m° s^{-}1, open symbols) as a function of the pH, for DOPG vesicles of $R \approx 45nm$ and 250 mM KNO$_3$.

decrease of the volume fraction of the negatively charged headgroup segments and a small increase of the positively charged headgroup segments in the layer adjacent to the surface when the ionic strength increases. The overall volume fraction of these two segments in the layer adjacent to the surface decreases slightly when the ionic strength increases resulting in less short-range Flory-Huggins interactions. The electrostatic interactions have a negligible influence in this case. This means that the variation of ΔG is mainly determined by the change of the number of contact (Flory-Huggins) interactions.

6.3.3 pH effect

As discussed before variation of the pH has an effect on the protonation of the oxide groups present on the surface and as a consequence on the charge density of the oxide layer at the gold surface.

In figure 6.12a the open circuit potential (OCP) of the gold substrate with respect to an Ag/AgCl reference electrode is shown as a function of the pH at 10 mM KNO$_3$. The dependence of the OCP reflects to some extent the relation between the double layer potential ψ^d and pH as given in figure 6.3a, and is in line with the OCP values measured by Barten et al. [1]. The intersection of the two dashed lines in figure 6.12 represents the i.e.p. of the gold surface. At the i.e.p. the numbers of the positively and negatively charged groups at the surface are equal and the overall charge of the oxide layer is zero. Assuming that there is no specific adsorption of ions, this implies that the OCP (with respect to the bulk solution) $= \psi^d = 0$, i.e., the potential difference between the bulk solution and the reference electrode amounts to 238 mV.
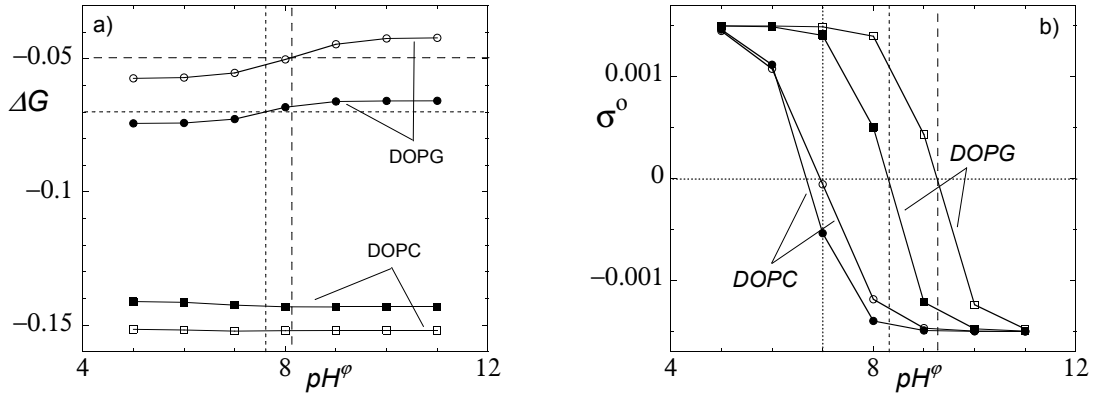
135

Figure 6.13: a) The dependence of ΔG (in units $k_B T/l^2$) on pH^φ for zwitterionic DOPC and anionic DOPG bilayers. b) The charge density of the oxide layer σ^o (in $e\ l^{-2}$) at the substrate surface as a function of the pH^φ when a DOPC or DOPG bilayer is adsorbed. In all cases $\chi = -3$ and in both figures the open symbols represent $\varphi_{KA}^b = 2 \times 10^{-4}$ and the closed symbols $\varphi_{KA}^b = 2 \times 10^{-3}$.

The adsorbed amount of DOPG vesicles of $R \approx 45$ nm (expressed as the SPR angle shift $\Delta\Theta$) as a function of pH at 250 mM KNO_3 is shown in figure 6.12b. The SPR angle shift varies from $\Delta\Theta \approx 700$ m$^\circ$ at pH 3 to $\Delta\Theta \approx 400$ m$^\circ$ at pH 5, which is a decrease of roughly 40 percent. This rather strong dependence of the adsorption on the pH is attributed to variation of the electrostatic interactions between surface and vesicles. The fact that the vesicles do still adsorb above the i.e.p. of the gold surface (in the range pH $5-10$), where the surface is negatively charged, implies that there has to be an attractive interaction apart from the electrostatic repulsion between the vesicles and the surface. (Such an attractive interaction has been accounted for in the SCF modelling.) The figure furthermore shows that the initial adsorption rate is varying in the pH range $3-6$, which again confirms that the DOPG vesicle adsorption is not transport limited. In the case of $R = 100$ nm DOPG vesicles the adsorbed amount at pH 5 is also somewhat smaller with respect to pH 3 for various ionic strengths (not shown). For 100 nm DOPC vesicles the adsorption does not significantly change between pH 3 and pH 5 (only determined at $I = 250$ mM, results not shown).

In order to gain more insight into the factors that determine the adsorption as a function of pH, SCF calculations have been executed and the results will be discussed in the remaining of this section. In figure 6.13a the bilayer adhesion energy in $k_B T$ per unit area l^2, ΔG, is depicted as a function the pH^φ for zwitterionic (DOPC) lipids as well as anionic (DOPG) lipids.

Figure 6.13a shows that at low ionic strength, i.e., $\varphi_{KA}^b = 2 \times 10^{-4}$ and 2×10^{-3}, ΔG for the DOPG bilayer is influenced by pH^φ, while ΔG of the DOPC bilayer is independent of pH^φ. It seems obvious that for the DOPG bilayer the variation of ΔG can be attributed to a change in electrostatic interaction between surface
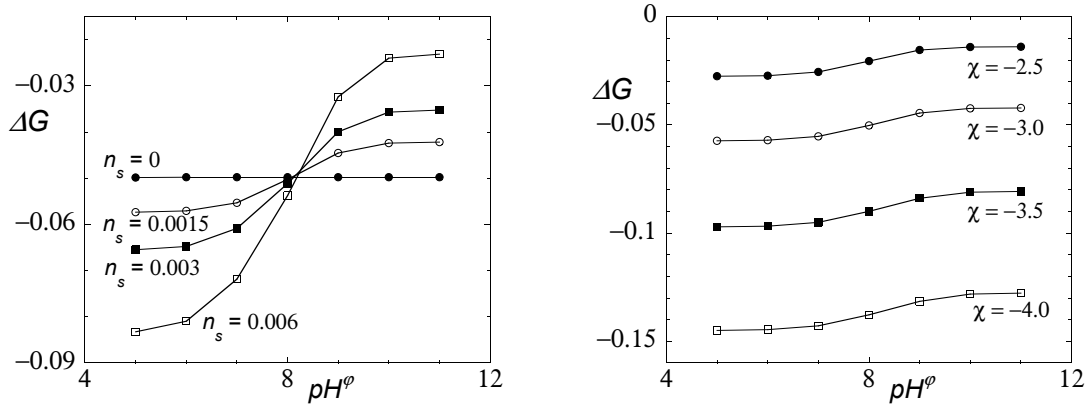
Figure 6.14: a) The dependence of ΔG (in units $k_B T/l^2$) on pH^φ when DOPG bilayers are adsorbed to the surface. The oxide group surface density n_s ranges from 0 to $0.06 l^{-2}$ and $\chi = -3$. b) The dependence of ΔG on pH^φ for the adhesion of anionic DOPG bilayers. The oxide group surface density $n_s = 0.0015\ l^{-2}$ and χ ranges between -2.5 and -4. In both figures $\varphi_{KA}^b = 2 \times 10^{-4}$.

and bilayer, resulting from the change in the charge density of the surface with pH. The protonation of the oxide groups on the surface is affected by the adsorption of the negatively charged DOPG bilayer, which is reflected by a shift of the centre of the transition range of ΔG to a pH^φ value higher than the i.e.p, depending on ionic strength: for $\varphi_{KA}^b = 2 \times 10^{-4}$ the transition point has shifted to approximately $\mathrm{pH}^\varphi = 8.2$ and for $\varphi_{KA}^b = 2 \times 10^{-3}$ it has shifted to $\mathrm{pH}^\varphi = 7.7$. In figure 6.13b this is further elaborated. When a DOPG bilayer is adsorbed the pH^φ where the surface charge density $\sigma^o = 0$ has shifted from $\mathrm{pH}^\varphi = 7$ to $\mathrm{pH}^\varphi \approx 8.3$ for $\varphi_{KA}^b = 2 \times 10^{-3}$, and for $\varphi_{KA}^b = 2 \times 10^{-4}$ even to $\mathrm{pH}^\varphi \approx 9.2$. When a DOPC bilayer is adsorbed to the surface, the protonation of the surface groups is only marginally affected. There is only a small negative shift of pH^φ for $\sigma^o = 0$, which can be attributed to the fact that the outside of the DOPC headgroup region is slightly positively charged, since the density of the positively charged headgroup segments is slightly higher in this region.

The relation between ΔG and pH^φ for several oxide surface group densities n_s is shown in figure 6.14a for DOPG bilayers adsorbed to the surface at $\varphi_{KA}^b = 2 \times 10^{-4}$. The dependence of ΔG on n_s is rather strong and the density of oxide groups is mainly determining the variation of the of ΔG with pH^φ. This is clearly demonstrated by the fact that when $n_s = 0$ there is no effect of the pH on the adsorption energy ΔG. A closer look at the figure furthermore shows that the lines for the various values of n_s do not all intersect at the same point. This results from the fact that the affinity between the oxide groups and the lipid headgroups differs from the affinity between the other surface sites and the headgroups. In figure 6.14b, we show the effect of the interaction energy between the hydrophilic headgroup segments N and P and the surface S on ΔG when DOPG bilayers are adsorbed.

The interaction parameter χ is varied between -2.5 and -4 for $n_s = 0.0015 \ l^{-2}$ and $\varphi^b_{KA} = 2 \times 10^{-4}$. As expected the variation of ΔG with pH^φ is not influenced by χ. However, χ determines to a large extent whether a vesicle adsorbs over the whole pH range or whether more DOPG vesicles do adsorb at low pH compared to high pH. When χ is too small it might be possible that the DOPG vesicles do not adsorb at all.

It can be concluded that the effect of pH on the adsorption of DOPG vesicles is rather small, due to the low density of oxide groups at the gold surface. However, it is clearly present as shown both by our experimental en theoretical studies. In this respect it has to be mentioned that the experimentally pH dependence may not only result from variations in the charge of the oxide groups, but possibly also from the pH-dependence of the density of these groups, as discussed by Barten et al [1].

6.3.4 Applied potential effect

Using the QCM we measured the adsorption of DOPG vesicles of different size and at various ionic strengths as a function of an externally applied potential $\Delta\Phi$ at the gold substrate. In addition, we measured the adsorption of DOPC vesicles containing 1% DOPG. Figure 6.15a shows a compilation of the results. The adsorbed amount Γ_m of DOPG is very low in all cases and approximately constant over the whole $\Delta\Phi$ range. Surprisingly, in the case of the mixed vesicles, there seems to be a transition between no adsorption and adsorption in the $\Delta\Phi$ range 100-300mV vs Ag/AgCl, which is the range where the double layer potential of the gold substrate changes from a negative to a positive value (see figure 6.12a). It is not clear why vesicles with only a small fraction of charged lipids would be more sensitive to an applied potential than vesicles completely consisting of charged lipids. Measurements with pure small DOPC lipid vesicles at low salt concentrations had approximately the same Γ_m at all applied potentials upto 300mV vs Ag/AgCl. This rules out the possibility that the variation of Γ_m for the mixed vesicles is caused by the interaction between the surface and the DOPC lipid.

We did not attempt to model the adsorption of bilayers composed of two lipids using SCF theory. Instead we theoretically studied the adsorption of a bilayer consisting of one type of lipids with a small negative charge. These lipids had a P-segment with a charge $-0.33e$ and an N-segment with a charge of $0.30e$, i.e., they have an effective charge of $-0.03e$. This means that this modeled bilayer has the same overall charge as the mixed bilayer. This results in the same ΔG for all $\Delta\Phi$ and was thus not providing an explanation for our observation. May be the variation of Γ_m in the range 100 mV$< \Delta\Phi <$ 300 mV results from the fact that the negatively charged DOPG lipids can translate along the leaflets of the mixed bilayer to accumulate at high energy surface sites, thus giving rise to some extra adsorption.

The adsorption of DOPC and DOPG bilayers as a function of $\Delta\Phi$ has been further investigated by performing SCF calculations. In the section Materials and
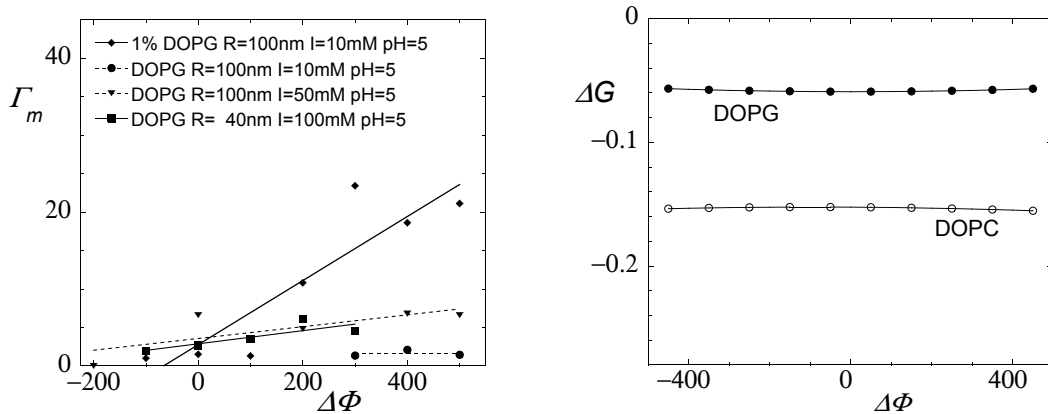
Figure 6.15: a) The maximum adsorbed mechanical mass Γ_m (in mg m^{-2}) as a function of an applied potential $\Delta\Theta$ (in mV vs. an Ag/AgCl 3 M KCl reference electrode) at pH 5, for different types of vesicles and ionic strengths as indicated. b) The adhesion energy per unit area ΔG as a function of the applied potential $\Delta\Phi$ (in mV vs. solution) for both DOPG and DOPC bilayers.

methods we already explained (figure 6.5) how we modelled the gold surface in order to mimic the relation between ψ^d and $\Delta\Phi$ as found by Barten et al. [1].

In figure 6.15b the relation between the adhesion energy per unit area ΔG is shown as a function of $\Delta\Phi$ for a DOPC and for a DOPG bilayer. (It should be noted that in the calculations the reference point for $\Delta\Phi$ is the bulk solution.) The ionic strength $\varphi_{KA}^b = 2 \times 10^{-4}$, which corresponds to ca 10 mM. For both lipids ΔG hardly varies over the whole $\Delta\Phi$ range, which seems to be in agreement with the experimental results. Also at a higher ionic strength ($\varphi_{KA}^b = 2 \times 10^{-3}$, (not shown) no significant dependence of ΔG on $\Delta\Phi$ was found. In order to gain some insight into the effect of $\Delta\Phi$ on the adsorption of vesicles, four different systems were modelled, which only differ with respect to the capacitance C_g of the outer gold layer. This results in a different relation between the applied potential and the double layer potential ψ^d. The four systems, which we will call A, B, C and D, have a capacitance C_g that is respectively 1, 3, 33, and 333 times the C_g that was needed to fit the experimentally determined relation between ψ^d and $\Delta\Phi$. With increasing C_g the dependence of ψ^d on $\Delta\Phi$ becomes stronger, which is shown in figure 6.16a. A detailed explanation of the dependence of ψ^d on $\Delta\Phi$ is given by Duval et al. [118].

By increasing the capacitance C_g in fact the range of ψ^d is enlarged for a given range over which the externally applied potential $\Delta\Phi$ is varied. In figure 6.16b the consequences of increasing C_g for the bilayer-surface interaction energy ΔG is shown. In the cases A and B, in which the ψ^d range is small (figure 6.16a), ΔG is practically constant over the whole range of applied potentials. In cases C and D on the other hand, ΔG shows a strong and complicated dependence on $\Delta\Phi$. We will not go into to the full molecular origin, but point out that it is the consequence of several different processes, like te organisation of the lipid headgroups and the
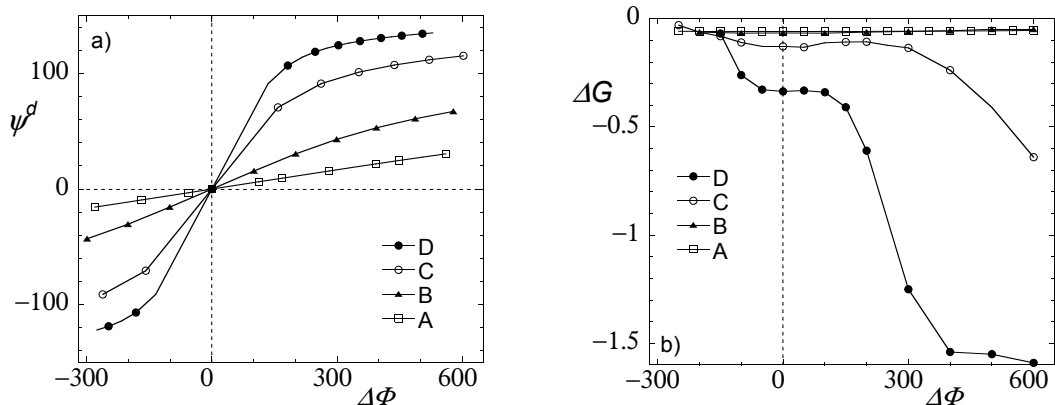
Figure 6.16: a) The double layer potential ψ^d dependence on the applied potential $\Delta\Phi$ for various values of the capacitance C_g of the outer gold layer. The capacitance C_g are 1 (A), 3 (B), 33 (C) and 333 times (D) the C_g that has been chosen in order to fit with the experimental data [1]. The increase of C_g results in the increase of the surface potential and ψ^d at a certain $\Delta\Phi$. b) The dependence of the adhesion energy per unit area ΔG of a DOPG bilayer as a function of the applied potential $\Delta\Theta$ is shown for the four different C_g.

variation of the number of cations and anions in the region between the surface and the bilayer. Indeed in scenario's C and D it is possible that the adsorption of lipids is so strong that vesicle rupture can take place. Clearly the cases C and D do not apply to the experimental situation (gold), and we refrain from a further analysis. In the case of gold (case A) the relatively large potential drop across the outer gold layer leads to a relatively small range over which ψ^d can be varied, with corresponding small response in terms of vesicle adsorption.

6.4   Conclusions

In this study we investigated experimentally and theoretically the contribution of electrostatic interactions to the adsorption of negatively charged and zwitterionic lipid bilayers (vesicles) on gold. This is done by varying the ionic strength, pH and by applying an external potential to the gold substrate.

We found that variation of the ionic strength has a rather strong influence on the adhesion of negatively charged DOPG vesicles, while in the case of zwitterionic DOPC vesicles it has hardly any effect. SCF model calculations show that for the DOPG bilayer the variation in the adhesion can be attributed to the headgroup density dependence on the ionic strength, resulting in a variation of bilayer-surface interaction energy. In the case of the DOPC bilayer such an effect is negligible.

Variation of the pH also has an effect on the adhesion of DOPG vesicles to the gold surface. In this case the variation is directly related to electrostatic interactions between the bilayer and the surface and is a consequence of the pH-dependency of

the double layer potential of the gold (due to the presence of oxide groups at the surface). Because the DOPC bilayer is zwitterionic the electrostatic interaction with the gold surface is negligible and the adsorption is independent of pH.

An externally applied potential did not affect the adsorption of DOPC and DOPG vesicles. The reason is that the experimentally accessible range of externally applied potentials is too small to induce changes in the double layer potential of the gold surface that are large enough to affect the adhesion of the bilayer. In the case of mixed DOPG/DOPC vesicles we found a dependence on the adsorption which is not entirely understood.

Overall it can be concluded that the electrostatic interactions do play a role in the adhesion of DOPG vesicles to the gold surface. The DOPG vesicles are weakly bound to the gold surface and the electrostatic interactions are strong enough to influence the adsorption of intact vesicles. However, they are not strong enough to induce transition of the adsorbed vesicles to a flat supported bilayer. In the case of the DOPC vesicles the electrostatic interactions have no effect on their adsorption and in all cases the adsorbed amount of intact vesicles is the same.

Bibliography

[1] D. Barten, J.M. Kleijn, J. Duval, H.P.v. Leeuwen, J. Lyklema, and M.A. Cohen Stuart. Double layer of a gold electrode probed by AFM force measurements. *Langmuir*, 19:1133, 2003.

[2] R.A. Kik, J.M. Kleijn, and F.A.M. Leermakers. Bending moduli and spontaneous curvature of the monolayer in a surfactant bilayer. *J. Phys. Chem. B*, 109:14251–14256, 2005.

[3] E. Overton. über die osmotische eigenshaften der lebenden planzen und dierzellen. *Vjschr. naturforsch. Ges. Zürich*, 40:159–201, 1895.

[4] E. Overton. über die allgemeinen osmotische eigenshaften der zellen, ihre vermutlichen ursachen und ihre bedeutung für die physiologie. *Vjschr. naturforsch. Ges. Zürich*, 44:88–135, 1899.

[5] I. Langmuir. The constitution and fundamental properties of solids and liquids. ii. liquids. *J. Am. Chem. Soc.*, 39:1848–1906, 1917.

[6] E. Gorter and F. Grendel. On bimolecular layers of lipoids on the chromocytes of the blood. *J. Exp. Med.*, 41:439–443, 1925.

[7] J.F. Danielli and E.N. Harvey. The tension of the surface of the mackerel egg oil, with remarks on the nature of the cell surface. *J. Cell. Physiol.*, 5:483–494, 1935.

[8] J.F. Danielli and H. Davson. A contribution to the theory of permeability of thin films. *J. Cell. Physiol.*, 5:495–508, 1935.

[9] J.D. Robertson. New observations on the ultrastructure of the membranes of frog peripheral nerve fibers. *J. Biophys. Biochem. Cytol.*, 3:1043–1047, 1957.

[10] D.E. Green and R.F. oldberger, editors. *Molecular insights into the living process*, page 195. Academic press, New York, London, 1967.

[11] J. Lenart and S.J. Singer. Protein conformation in cell membrane preparations as studied by optical rotatory dispersion and circular dichroism. *Proc. Natn. Acad. Sci. U.S.A.*, 56:1828–1835, 1966.

[12] S.J. Singer and G.L. Nicolson. The fluid mosaic model of the structure of cell membranes. *Science*, 175:720–731, 1972.

[13] R.L. Cornea and D.D. Thomas. Effects of membrane thickness on the molecular dynamics and enzymatic activity of reconstituted ca-ATPase. *Biochem.*, 33:2912–2920, 1994.

[14] A. Johannsson, C.A. Keightley, G.A. Smith, C.D. Richards, T.R. Hesketh, and J.C. Metcalfe. The effect of bilayer thickness and n-alkanes on the activity of the (Ca^{2+} + Mg^{2+})-dependent ATPase of sarcoplasmic reticulum. *J. Biol. Chem.*, 256:1643–1650, 1981.

[15] A. Johannsson, G.A. Smith, and J.C. Metcalfe. The effect of bilayer thickness on the activity of (Na^+ + K^+)-ATPase. *Biophys. Biochim. Acta.*, 641:416–421, 1981.

[16] J.R. Elliot, D. Needham, J.P. Dilger, and D.A. Haydon. The effect of bilayer thickness and tension on gramicidin single-channel lifetime. *Biophys. Biochim. Acta.*, 735:95–103, 1983.

[17] F.A.M. Leermakers and J.M.H.M. Scheutjens. Statistical thermodynamics of association colloids. i. lipid bilayer membranes. *Biophys. J.*, 89:3264–3274, 1988.

[18] S.M. Oversteegen and F.A.M. Leermakers. Thermodynamics and mechanics of bilayer membranes. *Phys. Rev. E*, 62:8453–8461, 2000.

[19] W. Helfrich. Elastic properties of lipid bilayers: Theory and possible experiments. *Z. Naturforsch*, 28:693–703, 1973.

[20] R. Lipowsky and E. Sackmann, editors. *Handbook of biological physics volume 1*, pages 213–303. Elsevier, Amsterdam, 1995.

[21] C. Nielsen and O.S. Andersen. Inclusion-induced bilayer deformations: Effects of monolayer equilibrium curvature. *Biophys. J.*, 79:2583–2604, 2000.

[22] R. Lipowsky and E. Sackmann, editors. *Handbook of biological physics volume 1*, pages 403–460. Elsevier, Amsterdam, 1995.

[23] C.-H. Lee, W.-C.Lin, and J. Wang. All-optical measurements of the bending rigidity of lipid-vesicle membranes across structural phase transitions. *Phys. Rev. E*, 64:020901, 2001.

[24] R.E. Waugh, J. Song, S. Svetina, and B. Žekš. Local and nonlocal curvature elasticity in bilayer-membranes by tether formation from lecithin vesicles. *Biophys. J.*, 611:974–982, 1992.

144

[25] M.M.A.E. Claessens, B.F. van Oort, F.A.M. Leermakers, F.A. Hoekstra, and M.A. Cohen Stuart. Charged lipid vesicles: Effects of salt on bending rigidity, stability, and size. *Biophys. J.*, 87:3882–3893, 2004.

[26] S. Marčelja. Lipid-mediated protein interaction in membranes. *Biophys. Biochim. Acta*, 455:1–7, 1976.

[27] P. Lagüe, M.J. Zuckermann, and B. Roux. Lipid-mediated interactions between intrinsic membrane proteins: A theoretical study based on intergral equations. *Biophys. J.*, 79:2867–2879, 2000.

[28] P. Lagüe, M.J. Zuckermann, and B. Roux. Lipid-mediated interactions between intrinsic membrane proteins: Dependence on protein size and lipid composition. *Biophys. J.*, 81:276–284, 2001.

[29] M.B. Partenskii and P.C. Jordan. Membrane deformation and the elastic energy of insertion: Perturbation of membrane elastic constants due to peptide insertion. *J. Chem. Phys.*, 117:10768–10776, 2002.

[30] S. May and A. Ben-Shaul. A molecular model for lipid-mediated interaction between proteins in membranes. *Phys. Chem. Chem. Phys.*, 2:4494–4502, 2000.

[31] S. May. Membrane perturbations induced by integral proteins: Role of conformational restrictions of the chains. *Langmuir*, 18:6356–6364, 2002.

[32] N. Dan, P. Pincus, and S.A. Safran. Membrane induced interactions between inclusions. *Langmuir*, 9:2768–2771, 1993.

[33] N. Dan, A. Berman, P. Pincus, and S.A. Safran. Membrane-induced interactions between inclusions. *J. Phys. II France*, 4:1713–1725, 1994.

[34] T. Sintes and A Baumgärtner. Protein attraction in membranes induced by lipid fluctuations. *Biophys. J.*, 73:2251–2259, 1997.

[35] P Biscari and F. Bisi. Membrane-mediated interactions of rod-like inclusions. *Eur. Phys. J. E*, 7:381–386, 2002.

[36] K. Bohinc, V. Kralj-Iglič, and S. May. Interaction between two cylindrical inclusions in a symmetric lipid bilayer. *J. Chem. Phys*, 119:7435–7444, 2003.

[37] E. Reimhult, F. Höök, and B. Kasemo. Intact vesicle adsorption and supported biomembrane formation from vesicles in solution: influence of surface chemistry, vesicle size, temperature and osmotic pressure. *Langmuir*, 19:1681–1691, 2003.

[38] G. Sauerbrey. Verwendung von schwingquarzen zur wagung dunner schichten und zur mikrowagung. *Z. Physik*, 155:206, 1959.

145

[39] J.A. Killian. Synthetic peptides as models for intrinsic membrane proteins. *FEBS Lett.*, 555:134–138, 2003.

[40] C. Montecucco, G.A. Smith, F. Dabbeni-sala, A. Johannsson, Y.M. Galante, and R. Bisson. Bilayer thickness and enzymatic activity in the mitochondrial cytochrome c oxidase and ATPase complex. *FEBS Lett.*, 144:145–148, 1982.

[41] R.J. Froud, C.R.A. Earl, J.M. East, and A.G. Lee. Effect of lipid fatty acyl chain structure on the activity of the $(Ca^{2+} + Mg^{2+})$-ATPase. *Biophys. Biochim. Acta.*, 860:354–360, 1986.

[42] F. Michelangi, E.A. Grimes, J.M. East, and A.G. Lee. Effects of phospholipids on the function of $(Ca^{2+}\text{-}Mg^{2+})$-ATPase. *Biochem.*, 30:342–351, 1991.

[43] M. Criado, H. Eibl, and F.J. Barrantes. Functional properties of the acetylcholine receptor incorporated in model lipid membranes. *J. Biol. Chem.*, 259:9188–9198, 1984.

[44] M.R.R. de Planque, E. Goormaghtigh, D.V. Greathouse, R.E. Koeppe II, J.A.W. Kruijtzer, R.N.J. Liskamp, B. de Kruijff, and J.A. Killian. Sensitivity of single membrane-spanning α-helical peptides to hydrophobic mismatch with a lipid bilayer: Effects on backbone structure, orientation and extend of membrane incorporation. *Biochem.*, 40:5000–5010, 2001.

[45] H.A. Rinia, R.A. Kik, R.A. Demel, M.M.E. Snel, J.A. Killian, J.P.J.M. van der Eerden, and B. de Kruijff. Visualization of highly ordered straited domains induced by transmembrane peptides in supported phosphatidylcholine bilayers. *Biochem.*, 39:5852–5858, 2000.

[46] J.C. Owicki, M.W. Spinggate, and H.M. McConnel. Theoretical study of protein-lipid interactions in bilayer membranes. *Proc. Natl. Acad. Sci. USA.*, 75:1616–1619, 1978.

[47] J.C. Owicki and H.M. Mc.Connel. Theory of protein-lipid and protein-protein interactions in bilayer membranes. *Proc. Natl. Acad. Sci. USA.*, 76:4650–4754, 1979.

[48] F. Jähnig. Critical effects from lipid-protein interaction in membranes. 1. theoretical description. *Biophys. J.*, 36:329–345, 1981.

[49] F. Jähnig. Critical effects from lipid-protein interaction in membranes. 2. interpretation of experimental results. *Biophys. J.*, 36:347–357, 1981.

[50] H. Schröder. Molecular statistical theory for inhomogeneous nematic liquid crystals with boundary conditions. *J. Chem. Phys.*, 67:16–25, 1977.

[51] O.G. Mouritsen and M. Bloom. Mattress model of lipid-protein interactions in membranes. *Biophys. J.*, 46:141–153, 1984.

[52] H.W. Huang. Deformation free energy of bilayer membrane and it's effect on gramicidin channel lifetime. *Biophys. J.*, 50:1061–1070, 1986.

[53] P. Helfrich and E. Jakobsson. Calculation of deformation energies and conformations in lipid membranes containing gramicidin channels. *Biophys. J.*, 57:1075–1084, 1990.

[54] A. Ring. Gramicidin channel-induced lipid membrane deformation energy: influence of chain length and boundary conditions. *Biophys. Biochim. Acta*, 1278:147–159, 1996.

[55] C. Nielsen, M. Goulian, and O.S. Andersen. Energetics of inclusion-induced bilayer deformations. *Biophys. J.*, 74:1966–1983, 1998.

[56] N. Dan and S.A. Safran. Effect of lipid characteristics on the structure of transmembrane proteins. *Biophys. J.*, 75:1410–1414, 1998.

[57] J.A. Lundbk and O.S. Andersen. Spring constants for channel-induced lipid bilayer deformations estimates using gramicidin channels. *Biophys. J.*, 76:889–895, 1999.

[58] P. Sens and S.A. Safran. Inclusions induced phase separation in mixed lipid film. *Eur. Phys. J. E*, 1:237–248, 2000.

[59] S. Marčelja. Chain ordering in liquid crystals. ii. structure of bilayer membranes. *Biophys. Biochim. Acta*, 367:165–176, 1974.

[60] D.R. Fattal and A. Ben-Shaul. A molecular model for lipid-protein interaction in membranes: The role of hydrophobic mismatch. *Biophys. J.*, 65:1795–1809, 1993.

[61] A. Zemel, D.R. Fattal, and A. Ben-Shaul. Energetics and self-assembly of amphipathic peptide pores in lipid membranes. *Biophys. J.*, 84:2242–2255, 2003.

[62] I. Szleifer, A. Ben-Shaul, and W.M. Gelbart. Chain organization and thermodynamics in micelles and bilayers. ii. model calculations. *J. Chem. Phys.*, 83:3612–3620, 1985.

[63] A. Ben-Shaul, I. Szleifer, and W.M. Gelbart. Chain organization and thermodynamics in micelles and bilayers. i. theory. *J. Chem. Phys.*, 83:3597–3611, 1985.

[64] J. van Male. *Self-consistent-field theory for chain molecules: Extensions, computational aspects and applications*. PhD thesis, Wageningen University, 2003.

[65] H.P. van Leeuwen and W. Köster, editors. *Physicochemical kinetics and transport at biointerfaces*, pages 15–111. Wiley and Sons, Chichester, 2004.

[66] L.A. Meijer, F.A.M. Leermakers, and J. Lyklema. Self-consistent field modeling of complex molecules with united atom detail in inhomogeneous systems. Cyclic and branched foreign molecules in dimyristoylphosphatidylcholine membranes. *J. Chem. Phys.*, 110:6560–6579, 1999.

[67] F.A.M. Leermakers, A.L. Rabinovich, and N.K. Balabaev. Self-consistent-field modeling of hydrated unsaturated lipid bilayers in the liquid-crystal phase and comparison to molecular dynamics simulations. *Phys. Rev. E*, 67:011910, 2003.

[68] R. Benz and K. Janko. Voltage-induced capacitance relaxation of lipid bilayer membranes. *Biophys. Biochim. Acta*, 455:721–738, 1976.

[69] S.B. Hladky and D.W.R. Gruen. Thickness fluctuations in black lipid-membranes. *Biophys. J.*, 38:251–258, 1982.

[70] C. Tandford. *The hydrophobic effect: Formation of micelles and biological membranes.* Wiley and Sons, New York, 1980.

[71] H.P. Duwe, J. Käs, and E. Sackmann. Bending elastic moduli of lipid bilayers: Modulation by solutes. *J. Phys. France*, 51:945–962, 1990.

[72] E. Evans and W. Rawicz. Entropy-driven tension and bending elasticity in condensed-fluid membranes. *Phys. Rev. Lett.*, 64:2094–2097, 1990.

[73] M. Kummrow and W. Helfrich. Deformation of giant lipid vesicles by electric-fields. *Phys. Rev. A*, 44:8356–8360, 1991.

[74] S. Tristam-Nagle, H.I. Petrache, and J.F. Nagle. Structure and interactions of fully hydrated dioleoylphosphatidylcholine bilayers. *Biophys. J.*, 75:917–925, 1998.

[75] D. Needham and R.S. Nunn. Elastic deformation and failure of lipid bilayer membranes containing cholesterol. *Biophys. J.*, 58:997–1009, 1990.

[76] J.C. Shillcock and R. Lipowsky. Equilibrium structure and lateral stress distribution of amphiphilic bilayers from dissipative particle dynamics simulations. *J. Chem Phys.*, 117:5048–5061, 2002.

[77] D. Marsh. Lateral pressure in membranes. *Biochim. Biophys. Acta*, 1286:183–223, 1996.

[78] F.A.M. Leermakers and J.M.H.M. Scheutjens. Statistical thermodynamics of associated colloids. iii. the gel to liquid phase transition of lipid bilayermembranes. *J. Chem. Phys.*, 89:6912–6924, 1988.

[79] R.A. Kik, F.A.M. Leermakers, and J.M. Kleijn. Molecular modeling of lipid bilayers and the effect of protein-like inclusions. *Phys. Chem. Chem. Phys.*, 7:1996–2005, 2005.

[80] J.M. Park and T.C. Lubensky. Interactions between membrane inclusions on fluctuating membranes. *J. Phys. I France*, 6:1217–1235, 1996.

[81] K.S. Kim, J. Neu, and G. Oster. Curvature mediated interactions between membrane proteins. *Biophys. J.*, 75:2274–2291, 1998.

[82] M. Goulian, R. Bruinsma, and P. Pincus. Long-range forces in heterogeneous fluid membranes. *Europhys. Lett.*, 22:145–150, 1993.

[83] L.A. Meijer. *The lipid bilayer membrane and it's interaction with additives.* PhD thesis, Wageningen University, 1994.

[84] M.M.A.E. Claessens. *Size regulation and stability of charged lipid vesicles.* PhD thesis, Wageningen University, 2003.

[85] R.J. Roe. Multilayer theory of adsorption from a polymer-solution. *J. Chem. Phys.*, 60:4192–4207, 1974.

[86] E.A. DiMarzio and R.J. Rubin. Adsorption of a chain polymer between two plates. *J. Chem. Phys.*, 55:4318–4336, 1971.

[87] S. Asakura and F. Oosawa. Interaction between particles suspended in solutions of macromolecules. *J. Polym. Sci.*, 33:183–192, 1958.

[88] H.A.H. Rongen, A. Bult, and W.P. van Bennekom. Liposomes and immunoassays. *J. Immun. Methods*, 204:105, 1997.

[89] C.A. Keller and B. Kasemo. Surface specific kinetics of lipid vesicle adsorption measured with a quartz crystal microbalance. *Biophys. J.*, 75:1397–1402, 1998.

[90] E. Reimhult, F. Höök, and B. Kasemo. Vesicle adsorption on sio_2 and tio_2: dependence on vesicle size. *J. Phys. Chem.*, 117:7401–7404, 2002.

[91] E. Reimhult, M. Zäch, F. Höök, and B. Kasemo. A multitechnique study of liposome adsorption on Au and lipid bilayer formation on SiO_2. *Langmuir*, 22:3313, 2006.

[92] U. Seifert and R. Lipowski. Adhesion of vesicles. *Phys. Rev A*, 42:4768–4771, 1990.

[93] R. Lipowsky and U. Seifert. Adhesion of vesicles and membranes. *Mol. Cryst. Liq. Cryst.*, 202:17–25, 1991.

[94] E.M. Blokhuis and W.F.C. Sager. Helfrich free energy for aggregation and adhesion. *J. Chem. Phys.*, 110:3148–3152, 1999.

149

[95] E.M. Blokhuis and W.F.C. Sager. Vesicle adhesion and microemulsion droplet dimerization: small bending rigidity regime. *J. Chem. Phys.*, 110:3148–3152, 1999.

[96] M.V. Voinova, M. Rodalh, M. Johnson, and B. Kasemo. Viscoelastic acoustic response of layered polymer films at fluid-solid interfaces: Continuum mechanics approach. *Phys. Scr.*, 59:391–396, 1999.

[97] L.S. Jung, C.T. Campbell, T.M. Chinowsky, M.N. Mar, and S.S. Yee. Quantitive interpretation of the response of surface plasmon resonance sensors to adsorbed films. *Langmuir*, 14:5636, 1998.

[98] W.N. Hansen. Electric fields produced by propagation of plane coherent electromagnetic radiation in a stratified medium. *J. Opt. Soc. America*, 58:380–390, 1968.

[99] M. Born and E. Wolf, editors. *Principles of Optics*. Pergamon, Oxford, 1975.

[100] Z. Salamon, S. Devanathan, I.D. Alves, and g. Tollin. Plasmon-waveguide resonance studies of lateral segregation of lipids and proteins into microdomains (rafts) in solid-supproted bilayers. *J. Biol. Chem.*, 280:11175, 2005.

[101] R.A. Kik, F.A.M. Leermakers, and J.M. Kleijn. Effect of size, rigidity and bilayer-surface interaction on the adsorption of lipid vesicles: An experimental study and self-consistent field model calculations. Submitted 2007.

[102] C. Tordeux, J.B. Fournier, and P. Galatola. Analytical characterization of adhering vesicles. *Phys. Rev. E*, 65:041912, 2002.

[103] R. Capovilla and J. Guven. Geometry of lipid vesicle adhesion. *Phys. Rev. E*, 66:041604, 2002.

[104] R.P Richter, A. Mukhopadhyay, and A.R. Brisson. Pathways of lipid vesicle deposition on solid surfaces: A combined qcm-d and afm study. *Biophys. J.*, 85:3035–3047, 2003.

[105] R.P Richter and A.R. Brisson. Following the formation of supported lipid bilayers on mica: A study combining afm, qcm-d, and ellipsometry. *Biophys. J.*, 88:3422–3433, 2005.

[106] N.H. Thomson, I. Collin, M.C. Davies, K. Palin, D. Parkins, C.J. Roberts, S.J.B. Tendler, and P.M. Parkins. Atomic force microscopy of cationic liposomes. *Langmuir*, 16:4813–4818, 2000.

[107] S. Sofou and J.L. Thomas. Stable adhesion of phospholipid vesicles to modified gold surfaces. *Biosensors and Bioelectronics*, 18:445–455, 2003.

[108] E. Lüthgens, A. Herrig, K. Kastl, C. Steinem, B. Reiss, J. Wegener, B. Pignataro, and A. Janshoff. Adhesion of liposomes: a quartz crital microbalance study. *Meas. Sci. Technol.*, 14:1865–1875, 2003.

[109] M. Giesbers, J.M. Kleijn, and M.A. Cohen Stuart. The electrical double layer on gold probed by electrokinetic and surface force measurements. *J. Colloid Interface Sci.*, 248:88–95, 2002.

[110] G.F. Khan and W. Wernet. Adsorption of proteins on electro-conductive polymer films. *Thin solid films*, 300:265–271, 1997.

[111] D. Beaglehole, B. Webster, and S. Werner. Ellipsometry study of the adsorption of molecules at electrolyte interfaces with gold and stainless steel. *J. Colloid Interface Sci.*, 202:541–550, 1998.

[112] N. Holmström, A. Askendal, and P. Tengvall. In vitro studies on blood protein adsorption to gold and pyrolytic carbon at pre-set electrical potentials. *Colloids surf. B*, 11:265–271, 1998.

[113] A. Zhou and N. Xie. Investigation of electrosorption of organic molecules onto gold and nickel electrodes using an electrochemical quartz crystal microbalance. *J. Colloid Interface Sci.*, 220:281–287, 1999.

[114] A. Zhou, N. Xie, Y. Wu, Y. Cai, L. Nie, and S. Yao. Study of the adsorption of glutathione on a gold electrode by using electrochemical quartz crystal impedance, electrochemical impedance spectroscopy, and cyclic voltammetry. *J. Colloid Interface Sci.*, 229:12–20, 2000.

[115] D. Barten, J.M. Kleijn, and M.A.C. Stuart. Adsorption of a linear polyelectrolyte on a gold electrode. *Phys. Chem. Chem. Phys.*, 19:4258–4264, 2003.

[116] D. Barten, J.M. Kleijn, and M.A.C. Stuart. Adsorption of charged macromolecules at a gold electrode. *Langmuir*, 20:9703–9713, 2004.

[117] R.A. Kik, F.A.M. Leermakers, and J.M. Kleijn. Molecular modelling of peptide-like inclusions in lipid bilayers: Lipid-mediated peptide-peptide interactions. Submitted 2007.

[118] J. Duval, J. Lyklema, J.M. Kleijn, and H.P. van Leeuwen. Amphifunctionally electrified interfaces: Coupling of electronic and ionic surface-charging processes. *Langmuir*, 17:7573–7581, 2001.

[119] A. Prostak and W. Hansen. Electroreflectance in metals. *Phys .Rev.*, 160:600–601, 1967.

[120] H. Kuhn. Classical aspects of energy transfer in molecular systems. *J. Chem. Phys.*, 53:101–108, 1970.

[121] P.G. de Gennes, C. Taupin. Micro-emulsions and the flexibility of oil-water interfaces. *J. Phys. Chem.*, 86:2294–2304, 1982.

[122] W. Rawicz, K.C. Olbrich, T. McIntosh, D. Needham, E. Evans. Effect of chain length and unsaturation on elasticity of lipid bilayers. *Biophys. J.*, 79:328–339, 2000.

[123] I. Szleifer, D. Kramer, A. Benshaul, D. Roux, W.M. Gelbart. Curvature elasticity of pure and mixed surfactant films. *Phys. Rev. Lett.*, 60:1966–1969, 1988.

[124] I. Szleifer, D. Kramer, A. Benshaul, W.M. Gelbart, S.A. Safran. Molecular theory of curvature elasticity in surfactant films. *J. Chem. Phys*, 92:6800–6817, 1990.

[125] J.S. Rowlinson. The molecular theory of small systems. *Chem. Soc. Rev.*, 12:251–265, 1983.

[126] A. Ben-Shaul, W.M. Gelbart; *in: "Micelles, Membranes, Microemulsions, and Monolayers"*, W.M. Gelbart, A. Ben-Shaul, D. Roux Eds. Springer N.Y. Chapter 1, (1994).

[127] O.A. Evers, J.M.H.M. Scheutjens, G.J. Fleer. Statistical thermodynamics of block copolymer adsorption .1. Formulation of the model and results for the adsorbed layer structure. *Macromolecules*, 23:5221–5233, 1990.

[128] Y. Lauw, F.A.M. Leermakers, M.A. Cohen Stuart. Self-consistent-field prediction for the persistence length of wormlike micelles of nonionic surfactants. *J. Phys. Chem.*, 107:10912–10918, 2003.

[129] R. Strey, R. Schomäcker, D. Roux, F. Frederic, U. Olsson. Dilute lamellar and L3 phases in the binary water-C12E5 system. *J. Chem. Soc. Faraday Trans.*, 86:2253–2261, 1990.

[130] J.N. Israelachvili, D.J. Mitchell, B.W. Ninham. Theory of self-assembly of hydrocarbon amphiphiles into micelles and bilayers. *J. Chem. Soc Faraday Trans 2*, 72:1525–1568, 1976.

[131] F.A.M. Leermakers, J.C. Eriksson, J. Lyklema. *Fundamentals of Colloid and interface Science*, "Association Colloids and their equilibrium modelling." Elsevier, Amsterdam, Chapter 5 **2005**.

[132] J.A. Killian. Hydrophobic mismatch between proteins and lipids in membranes. *Biochim. Biophys. Acta*, 1376:401–416, 1998.

Summary

In biological systems lipid bilayers are subject to many different interactions with other entities. These can range from proteins that are attached to the hydrophilic region of the bilayer or transmembrane proteins that interact with the hydrophobic region of the lipid bilayer. Interaction between two membranes is also very common. To gain more insight into the thermodynamic, structural and mechanical consequences we experimentally and theoretically investigated the interactions of a lipid bilayer with various types of interfaces. More specifically, we have analysed the transmembrane protein-lipid interaction by a computational self-consistent field method and have studied the adhesion of vesicles onto gold experimentally. Some aspects of the latter problem were also analysed theoretically.

There exists a computationally inexpensive, yet qualitatively accurate and realistic method to molecularly model the bilayer membrane in the presence of surfaces, namely the self-consistent field theory. This approach makes use of a large number of approximations. Important ones are: the discretisation of space by using a lattice, the non-self-avoidance of chains implying freely jointed chains and the replacement of binary interactions by an external potential leading to the (local) mean field ansatz. When a transmembrane hydrophobic inclusion is present in the lipid membrane the bilayer around it is disturbed. The structural perturbation of the lipid bilayer around these inclusions have an exponentially decaying wave-like appearance. There are many factors that influence this. The most important ones are the shape of the inclusion, the hydrophobic length of the inclusion, the local interaction between the inclusion and the bilayer, the hydrophobic bilayer thickness and the mechanical characteristics of the lipid bilayer. At distances larger than the bilayer thickness the wavelength and the decaylength of this exponentially decaying wave are exclusively determined by the mechanical and structural properties of the bilayer. This means that the wavelength and the decaylength can be described by the thickness, the bending modulus and the area compression-expansion modulus of the bilayer. The amplitude and the offset of the perturbation are on the other hand set by the properties of the inclusion. Indeed, the hydrophobic length mismatch, i.e., the difference between the hydrophobic length of the inclusion and the hydrophobic thickness of the lipid bilayer, and the contact interaction between the inclusion and the lipid bilayer are the key variables.

The free energy of insertion is mainly determined by the contact interaction

energy between the inclusion and the lipid bilayer and it shows a parabolic dependence on the hydrophobic length mismatch. The free energy of insertion is minimal at a hydrophobic length mismatch where the bilayer perturbations are minimal. We argued that there is a subtle interplay between the entropy loss of the lipid tails adjacent to the surface and the contact interaction between the inclusion and the lipid tails.

Important for the biological performance, we found that overlap of the perturbed regions of the bilayer around two or more inclusions can cause attractive or repulsive interaction between such inclusions depending on the distance between them. This non-monotonic interaction force with the distance between inclusions, is directely linked to the non-monotonic structural perturbations mentioned already. This lipid mediated free energy of interaction between the inclusions can be divided into three different regimes each with their own length scale. These are the short-range segmental, the intermediate-range conformational and the long-range elastic contributions. The short-range contribution is only present when one or two lipids are in between the inclusions. This interaction depends strongly on the Flory-Huggins interaction between the inclusion and the lipid tails. The intermediate-range contribution is present at separations on the length scale of approximately the bilayer thickness. This interaction shows an exponentially decaying dependence on the separation between these inclusions and is a consequence of the confinement of the lipid tails in between these inclusions. The long-range contribution is determined by the elastic properties of the bilayer and has an exponentially decaying wave-like appearance, with a wavelength that is the same as the perturbation wave length of the bilayer.

Our SCF analysis complements available simulations on the one hand and mesoscopic models on the other. Moreover, they may help to analyse experiments and explain observations in biomembranes.

In the second part of this thesis we examined the adhesion of negatively charged DOPG vesicles and zwitterionic DOPC vesicles to a gold surface using quartz crystal microbalance and surface plasmon resonance techniques. Gold has a hydrophilic surface where lipid vesicles adsorb intact. When the vesicle radius was above approximately 40 nm the DOPC vesicles completely cover the surface, whereas below this radius the surface coverage decreases with decreasing vesicles size. When spherical vesicles adsorb onto a surface they deform. The shape deformation of the adsorbed vesicles increases with increasing vesicles size. The diminished deformation for the smaller vesicles results in a relatively small interaction area between the vesicles and the gold surface resulting in less lipid-surface interactions. Self-consistent field model calculations on a single vesicle are in line with these experimental results. The calculations showed that the relative deformation of the vesicles has a linear dependence on the vesicles radius. They furthermore showed that below a certain minimal vesicle radius the deformation is completely absent resulting in a lipid-surface interaction energy that vanishes.

Self-consistent field calculations further indicate that the lipid-surface interac-

tion can be divided into three different regimes. In the weak interaction regime the adhesion of the vesicles is not accompanied by drastic changes in the bilayer structure and the vesicle is deformed elastically. In this case the adhesion of the vesicles is energetically favourable over the adhesion of an equally sized bilayer patch. The adhesion of lipid vesicles to the gold surface can most likely be categorised in this regime. In the second intermediate interaction regime the adsorbed vesicles are energetically unfavourable compared to equally sized bilayer patches. The deformation of these vesicles remain in the elastic regime and therefore they do not transform into an adsorbed lipid bilayer patch. In the strong interaction regime the adsorption of the vesicles is strongly energetically unfavourable compared to equally sized bilayer patches and this interaction is so strong that local molecular rearrangements take place to increase the bilayer curvature. This results in adsorbed vesicles that are very susceptible to fusion and/or rupture. An interesting prediction is that the adsorption energy of a vesicle does not depend on the bilayer rigidity. This means that the adsorption energy is a constant, and fixed by the interaction energy between the lipid molecules and the surface. At the same time the deformations of the vesicles increase with diminishing rigidity, which means that although the interaction is the same, the vesicles with different rigidity can be present in different interaction regimes.

As already mentioned, lipid vesicles adsorb intact onto a gold surface. However, on many other surfaces lipid vesicles transform after adsorption into a supported lipid bilayer. We studied the importance of electrostatic interactions for the adhesion strength of DOPC and DOPG vesicles to a gold surface. This was done by varying the pH, the ionic strength and an externally applied electrostatic potential. Varying the pH of the solution has an effect on the protonation of the oxide groups present at the gold surface. As a consequence the surface charge ranges from a positive charge below pH= 5 to negative charge above pH= 5. In the case of negatively charged DOPG vesicles, we showed that there is a relation between the adsorbed amount and the pH. The adsorbed amount was larger at low pH compared to high pH and remained approximately constant in the pH range $6 - 10$. There is still some adsorption in this pH range, from which it can be concluded that besides the electrostatic interaction also other interactions, such as the van der Waals or other chemical interactions, play a role.

The ionic strength has a rather strong influence on the adhesion of DOPG vesicles, while the adsorbed amount of DOPC vesicles remains approximately constant. Both experiments and self-consistent field modelling showed that the adsorbed amount decreases with decreasing ionic strength. This relation can be attributed to the fact that the headgroup density of the DOPG vesicle decreases with decreasing ionic strength, which results in less favourable non-electrostatic lipid-surface interactions.

The externally applied potential had no effect on the adsorption DOPG vesicles. This can be attributed to the fact that externally applied potential can only be

varied over a limited range, because otherwise redox reactions reaction at the gold surface start to play a role. This means that the surface potential range is too small to influence the interaction energy of the DOPG and the DOPC bilayer. With self-consistent field modelling it was shown that if redox reaction did not occur and the externally applied potential could be varied over a larger range, the interaction energy between the lipid bilayer and the gold surface could be divided into four different regimes. These regimes vary from weakly attractive to strongly attractive.

It can be concluded that the adhesion of DOPG vesicles onto gold is parly determined by electrostatic interactions. Because the vesicles are weakly bound to the gold surface, the electrostatic interaction can influence the adsorption of intact vesicles. However they are never strong enough to induce transition of the adsorbed vesicles to a flat supported bilayer. In the case of DOPC vesicles the electrostatic interactions have a negligible effect

The organisation of proteins in lipid membranes is identified as one of the central issues in molecular biology. We have tried to unravel the role of the lipid matrix in the protein insertion problem. Our results may be important, for example in the case of transmembrane proteins with multiple transmembrane α-helices, because the short-range lipid-mediated interactions of these transmembrane helices can directly influence the quaternary structure of these proteins. Besides generic issues discussed in the present thesis there are numerous molecular specific aspects. These problems will undoubtelly attract many scientific activities in the years to come. Lipid vesicles at surfaces attracted a lot of attention in the last ten years. Vesicles adhesion is used frequently to generate supported lipid bilayers. Such interfacial layers gives the opportunity to study the properties and interactions of these lipid bilayers and use these layers in biotechnological applications. We tried to unravel some details of the interactions of lipid layers with a gold surface. Our results may be used to understand why in some cases supported bilayers are formed while in other vesicles stay intact at the surface. Understanding this will give us the opportunity to control the fusion of lipid vesicles on a surface. Fusion of vesicles in a plane is also an issue in biological processes such as the formation of the cell plate in plant cell division.

Samenvatting

Alle organismen op aarde bestaan uit cellen die worden omgeven door een membraan. Behalve dat dit membraan zorgt voor een gecontroleerd transport van stoffen in en uit de cel, heeft het nog veel meer functies, zoals het verzorgen van de communicatie tussen cellen, het hechten aan extracellulaire grensvlakken, participatie in enzymactiviteit enz. Ook veel organellen, die je zou kunnen beschouwen als de organen van de cel, zijn omsloten door een membraan.

De belangrijkste moleculen waaruit een membraan is opgebouwd zijn fosfolipiden. De meeste fosfolipiden bestaan uit een kopgroep die van water houdt (hydrofiel), en twee staarten die niet van water houden (hydrofoob). Deze moleculen zullen, als ze in water aanwezig zijn, zich op een zodanige manier organiseren dat de hydrofobe staarten zo min mogelijk en de hydrofiele kopgroepen zo veel mogelijk in contact zijn met het omringende water. Een manier om dit te bereiken is om een lipide bilaag te maken waar de kopgroepen naar buiten en de staarten naar binnen zijn gericht. Deze lipide bilagen kunnen beschouwd worden als een tweedimensionale vloeistof, waarin de moleculen vrij kunnen bewegen in laterale richting. Als het oppervlak van de bilaag groot genoeg is zal deze zich kunnen sluiten waardoor een bolvormig vesikel ontstaat zoals weergegeven in figuur 17. De afmetingen van deze lipide vesikels kunnen variëren van micrometers (duizendste millimeters) tot enkele tientallen nanometers (miljoenste millimeters).

In biologische systemen zal een lipide bilaag door vele verschillende externe factoren beïnvloed en verstoord worden. Een voorbeeld hiervan is dat een biologisch membraan niet volledig uit lipiden bestaat maar dat er vanwege zijn functionaliteit ook membraaneiwitten in het membraan aanwezig zijn. Deze eiwitten kunnen vastgeplakt zijn aan de buitenkant van de membraan (periferische membraaneiwitten), maar ze kunnen een membraan ook volledig doorboren (integrale membraaneiwitten). De interactie van deze eiwitten met de lipiden waar ze mee in contact zijn, zorgt ervoor dat de bilaag zich aanpast. Een ander voorbeeld is de verstoring van een celmembraan wanneer de cel zich vastzet aan een bepaald grensvlak, wat bijvoorbeeld gebeurt wanneer cellen zich groeperen in celweefsel. Deze aanhechting zorgt ervoor dat het membraan zich lokaal moet aanpassen, wat weer effect heeft op naastliggende gebieden van het membraan. Ook de ophoping van kleine vesikels in het equatoriale vlak van een delende plantencel, waarbij de vesikels fuseren tot een vlak membraan dat de scheiding vormt tussen de twee dochtercellen, geeft verstoorde
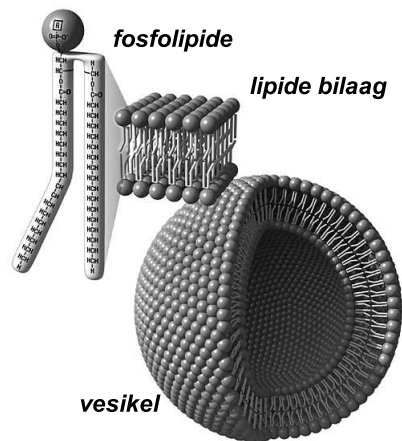
Figure 17: Schematische weergave van een fosfolipide molecuul, een lipide bilaag en een lipide vesikel. De lipide staarten zitten in het binnenste van de bilaag, terwijl de kopgroep aan de buitenkant aanwezig is.

bilagen in de tussenstadia.

In dit proefschrift hebben we twee gevallen bestudeerd waarbij een lipide bilaag een interactie heeft met een oppervlak. In het eerste geval hebben we de gevolgen van de aanwezigheid van integrale membraaneiwitten in een lipide bilaag bestudeerd door het systeem te modelleren gebruik makend van de zogenaamde zelf-consistente veld theorie (self-consistent field, SCF). Dit is een techniek waarbij door middel van computerberekeningen de organisatie van moleculen en de energie in een systeem berekend kan worden. In deze methode worden de moleculen opgebouwd uit deeltjes (segmenten) die allemaal even groot zijn. Het watermolecuul bestaat bijvoorbeeld uit maar een segment, terwijl een lipide molecuul uit zo'n 45 segmenten bestaat, waarvan er negen in de hydrofiele kop zitten en de hydrofobe staarten elk uit 18 segmenten bestaan. De SCF theorie maakt verder gebruik van een rooster om de ruimte op te delen in een beperkt aantal plaatsen waar de segmenten kunnen zitten. Elk segment is precies even groot als een roosterplaats. Door middel van verschillende algoritmes wordt nu de energie berekend voor een bepaalde organisatie van de moleculen in het systeem. Hoe hoger nu de energie hoe kleiner de kans dat een systeem die organisatie aanneemt. Door nu de energie van al die mogelijke organisaties te vergelijken kun je uitrekenen hoe groot de kans is dat een bepaald segment op een bepaalde rooster plaats zit. Het grote voordeel van deze methode is dat het een snelle rekenmethode is met goede resultaten.

In het tweede geval dat in dit proefschrift behandeld wordt, bestuderen we de aanhechting (adsorptie) van lipide vesikels aan een goud oppervlak. Ook hier maken we gebruik van de SCF methode, maar daarnaast hebben we ook gebruik gemaakt van experimentele methoden waarvan de twee belangrijkste de QCM (quartz crystal microbalance) en de SPR (surface plasmon resonance) techniek waren.

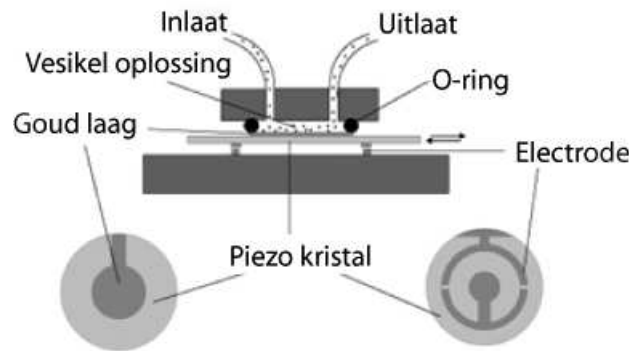De QCM techniek is een methode waarbij een dun laagje goud is aangebracht

Figure 18: Een schematische weergave van de QCM (quartz crystal micobalance). Via de inlaat wordt met constante snelheid een vesikeloplossing langs het goudplaatje geleid. Over het piezo-elektrische kristal wordt via de elektroden een potentiaal aangelegd waardoor het met een bepaalde frequentie trilt. Wanneer de vesikels adsorberen op het goudlaagje verandert de frequentie. Deze frequentieverandering is een maat voor de geadsorbeerde massa.

op een piezo-elektrisch kristal (figuur 18). Door over dit kristal een wisselspanning aan te leggen gaat het trillen met een bepaalde frequentie. Als er nu iets adsorbeert aan het goud zorgt dit voor een verandering van deze frequentie omdat de massa verandert. Door nu de verandering van deze frequentie te meten is het mogelijk om de totale massa van de geadsorbeerde stof te berekenen.

De SPR techniek is een optische techniek en werkt op een totaal andere manier (figuur 19). Hier wordt een dun laagje goud van ongeveer 50 nm op een prisma aangebracht. Door nu via het prisma een gepolariseerde lichtstraal van een bepaalde golflengte te laten reflecteren via de onderkant van het goud en de intensiteit van het gereflecteerde licht te meten kan er een bepaalde hoek gevonden worden waar de intensiteit van de gereflecteerde lichtstraal minimaal is. Deze hoek wordt de kritische hoek genoemd. Wanneer er nu vesikels uit een oplossing adsorberen aan de bovenkant van het goud zal de kritische hoek veranderen omdat de lipiden een andere brekingsindex hebben dan het water. De verandering van de kritische hoek geeft dus informatie over de hoeveelheid lipiden die aan het goud oppervlak aanwezig zijn

Door deze technieken in combinatie met elkaar te gebruiken kun je dus informatie verkrijgen over de hoeveelheid massa lipiden en de totale geadsorbeerde massa die aanwezig is aan het goudoppervlak. Door de verhouding tussen deze twee massa's te bepalen kun je bijvoorbeeld zien of de geadsorbeerde vesikels intact zijn gebleven aan het oppervlak of dat ze zijn getransformeerd in een vlakke geadsorbeerde lipide bilaag.

In de rest van deze samenvatting gaan we dieper in op de twee bestudeerde gevallen, te beginnen met het invoegen van een integraal membraaneiwit in een lipide bilaag. Wanneer een cilindervormig hydrofoob object dwars door een lipide bilaag
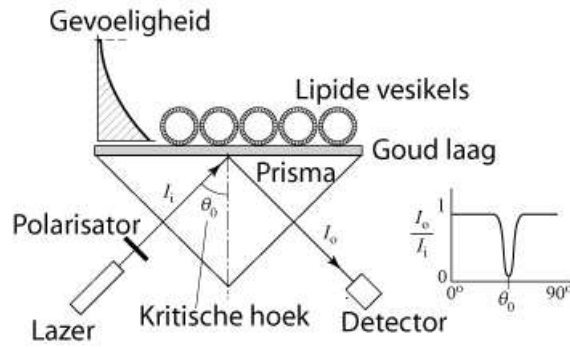
Figure 19: Een schematische weergave van de SPR (surface plasmon resonance) methode. Een gepolariseerde lichtstraal met een bepaalde golflengte wordt via een prisma aan de onderkant van het goudlaagje gereflecteerd. Met een detector wordt de intensiteit van het gereflecteerde licht gemeten. Bij een bepaalde kritische hoek is er een minimale reflectie van het licht, zoals aangegeven in de grafiek. Wanneer er nu lipide vesikels uit een oplossing adsorberen aan de bovenkant van het goud, zal de kritische hoek veranderen omdat de lipiden een andere brekingsindex hebben dan het water. De mate van verandering van deze kritische hoek is een maat voor de hoeveelheid geadsorbeerde lipiden aan het goudoppervlak.

steekt (figuur 20), zal de bilaag om dit object verstoord worden. Vele verschillende factoren hebben een effect op deze verstoring, maar de belangrijkste zijn de vorm van het object, de hydrofobe lengte van het object D, de hydrofobe dikte van de bilaag d_l^0 en de lokale interacties tussen het object en de bilaag.

In alle gevallen heeft de verstoring van de bilaagstructuur om de cilinder een exponentieel afnemende periodieke verschijning. Op grotere afstanden tot de cilinder wordt de golflengte en de exponentiele afname van de verstoring volledig bepaald door de dikte en de mechanische eigenschappen van de bilaag, zoals de stijfheid die wordt beschreven met de buigingsmodulus en de uitrekbaarheid van de bilaag die wordt beschreven met de oppervlaktemodulus. Dit betekent dat de golflengte en

Figure 20: Schematische weergave van een transmembrane hydrofobe cilinder met hydrofiele uiteinden in een lipide bilaag. De cilindervormige staaf heeft een straal R. De lengte Δd is een maat voor het verschil tussen de hydrofobe lengte D van de staaf en de hydrofobe dikte van de bilaag d_l^0.

de afname van de golfamplitude volledig kunnen worden beschreven in termen van de bilaagdikte, de buigingsmodulus en de oppervlaktemodulus. De amplitude en de positie van de golven worden daarentegen ook bepaald door de eigenschappen van het ingesloten object. In het geval van de cilinder zijn de twee belangrijkste factoren die dit bepalen de lokale interactie tussen de cilinder en de bilaag en het verschil tussen de hydrofobe lengte van de cilinder en de hydrofobe dikte van de bilaag.

De verandering van de vrije energie als gevolg van het insluiten van de cilinder in de bilaag wordt voornamelijk bepaald door de contact-interacties tussen de cilinder en de lipide bilaag. Verder vertoont de vrije energie een minimum als functie van het verschil in hydrofobe lengte tussen cilinder en bilaag. In dat minimum is de verstoring van de bilaag het kleinste. In dit proefschrift is beschreven dat de verstoring van de bilaag wordt bepaald door een subtiel samenspel tussen de contact-interacties tussen de cilinder en de bilaag en het entropieverlies van de lipide staarten grenzend aan de cilinder. Met entropieverlies wordt bedoeld dat de verschillende mogelijke conformaties van de lipide staarten wordt beperkt, door de aanwezigheid van de cilinder, wat ongunstig is.

We hebben dus laten zien dat de verstoring van een lipide bilaag om een ingesloten object een periodiciteit heeft en exponentieel afneemt met de afstand tot het object. Als nu twee van zulke objecten bij elkaar in de buurt komen dan zullen de bilaag verstoringen elkaar gaan overlappen. Het interessante is dat door de overlap van deze verstoringen een repulsieve of attractieve interactie tussen de objecten ontstaat, afhankelijk van de afstand tussen hen. Een dergelijke indirecte lipide veroorzaakte interactie zou een rol kunnen spelen in de organisatie van eiwitten in een biologisch membraan.

De indirecte lipide veroorzaakte vrije energie van interactie tussen de ingesloten objecten kan opgedeeld worden in drie verschillende regimes die elk hun eigen lengte schaal hebben. In deze regimes overheersen respectievelijk de bijdrage van wisselwerking tussen de lipide segmenten en de ingesloten objecten, de bijdrage van conformationele restricties van de lipiden die aanwezig zijn tussen de ingesloten objecten en de elastische bijdrage van de lipide bilaag. De segment bijdrage speelt alleen een rol van betekenis wanneer er 1 of 2 lipiden tussen de ingesloten objecten aanwezig zijn. Deze bijdrage wordt sterk bepaald door de contact-interacties tussen ingesloten objecten en de lipide bilaag. De conformatie bijdrage speelt een rol totdat de afstand tussen de ingesloten objecten ongeveer even groot is als de dikte van de bilaag. De interactie heeft een exponentieel afnemende afhankelijkheid van de afstand tussen de ingesloten objecten en is het gevolg van de ruimtelijke beperking van de lipide staarten tussen deze objecten. De elastische contributies die op langere afstanden nog een rol spelen worden bepaald door de structurele en mechanische eigenschappen van de lipide bilaag en laten een exponentieel afnemende periodieke afhankelijkheid zien van de afstand tussen de ingesloten objecten. De golflengte is dezelfde als de golflengte van de structurele bilaagverstoring.

De resultaten die we verkregen hebben uit de SCF analyse complementeren zowel
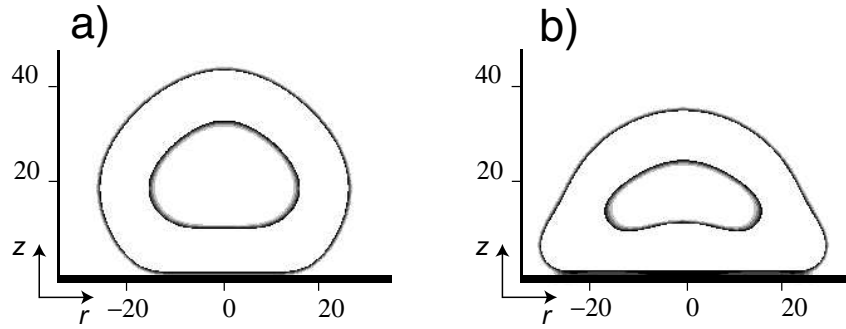
Figure 21: De figuur laat twee even grote geadsorbeerde vesikels zien zoals die zijn berekend met de SCF methode. In het geval van de linker vesikel is de bilaag-oppervlak interactie sterk genoeg om een elastische vervorming van het vesikel te bewerkstelligen waardoor het interactie-oppervlak groot genoeg is om de vesikel te laten adsorberen, maar het blijft waarschijnlijk intact. Voor het rechter vesikel is de interactie met het oppervlak sterk waardoor de bilaag op sommige plaatsen zo sterk wordt verstoord dat het relatief makkelijk zal fuseren met een nabijgelegen vesikel.

eerder gedane moleculaire simulaties als mesoscopische benaderingen. Ze kunnen verder helpen bij de analyse van experimenten en observaties aan biomembranen verklaren.

In het tweede deel van dit proefschrift hebben we gekeken naar de adsorptie van negatief geladen DOPG vesikels en zwitterionische (met een positieve en een negatieve lading in de kopgroep) DOPC vesikels aan een goudoppervlak. Goud heeft een hydrofiel oppervlak waar lipide vesikels intact aan adsorberen. De adsorptie van lipide vesikels wordt bepaald door de bilaag-oppervlak interactie energie en de energie die nodig is voor vervorming van het vesikel. Wanneer een bolvormig vesikel adsorbeert aan het oppervlak moet het enigszins deformeren om genoeg interactie-oppervlak te genereren met het vlakke oppervlak waardoor de adsorptie-energie tussen het oppervlak en de bilaag groot genoeg is. Uit de metingen is gebleken dat DOPC vesikels met een straal groter dan 40 nm het goud volledig bedekken, terwijl beneden deze straal de mate van oppervlaktebedekking met geadsorbeerde vesikels afneemt. Dit heeft te maken met het feit dat de vesikel-deformatie en dus het interactie-oppervlak tussen het vesikel en het oppervlak afneemt met afnemende vesikelgrootte. Hierdoor wordt beneden een straal van 40 nm de interactie-energie tussen het vesikel en het oppervlak zo klein dat de vesikels minder sterk adsorberen. SCF-berekeningen aan een enkel vesikel zijn consistent met deze experimentele resultaten. De berekeningen tonen aan dat de relatieve vervorming van het vesikel recht evenredig is met zijn straal.

De SCF-berekeningen geven verder aan dat de lipide-oppervlak interactie in drie verschillende regimes kan worden verdeeld. In het zwakke interactieregime (figuur 21a) wordt de adsorptie van het vesikel niet vergezeld door drastische veranderingen in de bilaagstructuur en is de vervorming van het vesikel puur elastisch. In dit geval

is de adsorptie van het vesikel energetisch gunstiger dan de adsorptie van een vlakke bilaag die uit evenveel lipiden bestaat als het vesikel. Dit houdt dus in dat wanneer de vesikels adsorberen het energetisch ongunstig is dat ze openbreken en een vlakke bilaag vormen. De adsorptie van de DOPC en DOPG vesikels aan het goudoppervlak valt waarschijnlijk in dit regime. In het tweede tussenliggende interactieregime is een intact geadsorbeerd vesikel energetisch ongunstig vergeleken met de adsorptie van een even grote vlakke bilaag. De vervorming van dit vesikel blijft in het elastische regime en daarom is het niet waarschijnlijk dat het snel spontaan overgaat in een geadsorbeerde vlakke lipide bilaag. In het sterke interactie regime (figuur 21b) is de adsorptie van een intact vesikel energetisch erg ongunstig vergeleken met de vlakke bilaag. Tevens is hier de interactie van de vesikels zo sterk dat plaatselijk drastische moleculaire herschikkingen nodig zijn om de bilaag kromming toe te laten nemen. Dit resulteert in een geadsorbeerd vesikel dat heel ontvankelijk is voor fusie en/of breuk. Een interessant resultaat van de SCF-berekeningen is dat de totale adsorptie-energie van een vesikel niet afhangt van de elasticiteit van de bilaag. Dit betekent dat de totale adsorptie energie een constante is en bepaald wordt door de interactie-energie tussen de lipide moleculen en het oppervlak. De mate van deformatie van het vesikel neemt wel toe met het verminderen van de stijfheid van de bilaag. Dit betekent dat ondanks een gelijke lipide-oppervlak interactie vesikels met verschillende rigiditeit in verschillende interactieregimes kunnen zitten.

Zoals reeds vermeld, adsorberen lipide vesikels intact op een goudoppervlak. Echter op vele andere oppervlakken vormen lipide vesikels een geadsorbeerde lipide bilaag. In deze studie is het belang van de elektrostatische interacties bij de adsorptie van DOPC en DOPG vesikels aan een goudoppervlak onderzocht. Dit werd gedaan door het variëren van de pH, de zoutconcentratie en een op het goud aangelegde elektrische potentiaal.

De pH van de oplossing bepaald de protonatie van de oxidegroepen die aanwezig zijn op het goudoppervlak. De oppervlaktelading is positief bij een pH lager dan 5 en wordt negatief wanneer de pH boven de 5 uitkomt. In het geval van de negatief geladen DOPG vesikels is er een duidelijk meetbaar effect van de pH op de geadsorbeerde hoeveelheid. De geadsorbeerde hoeveelheid neemt toe bij een variatie van pH6 tot pH3, terwijl boven pH6 de geadsorbeerde hoeveelheid gelijk bleef. Ondanks dat boven pH5 het oppervlak negatief is geladen, vindt daar dus toch enigszins adsorptie plaats. Dit betekent dat ook andere interacties, zoals de van der Waals interactie of chemische interacties, een rol spelen.

De ionsterkte heeft een grote invloed op de adsorptie van DOPG vesikels, terwijl de geadsorbeerde hoeveelheid DOPC vesikels niet veranderd bij variatie van de ionsterkte. Zowel experimenten als de SCF-berekeningen tonen aan dat de geadsorbeerde hoeveelheid DOPG vesikels afneemt met het afnemen van de zoutconcentratie in de oplossing. Deze relatie kan worden toegeschreven aan het feit dat de kopgroepdichtheid van de DOPG bilaag afneemt bij een afnemende zout concentratie, wat resulteert in een geringer aantal gunstige lipide-oppervlak interacties.

De extern aangelegde potentiaal heeft geen invloed op de adsorptie van DOPG vesikels. Dit komt doordat er grenzen zijn waarover de externe potentiaal kan worden gevarieerd, omdat anders redoxreacties aan het goudoppervlak een rol gaan spelen. Dit betekent dat het potentiaalbereik aan het goudoppervlak te klein is om een effect te hebben op de adsorptie van DOPG vesikels. Met de SCF-berekeningen hebben we laten zien dat wanneer dit potentiaal bereik groter zou zijn er wel degelijk een variatie van de bilaag-oppervlak interactie zou moeten zijn.

Er kan geconcludeerd worden dat adsorptie van DOPG vesikels op goud gedeeltelijk wordt bepaald door elektrostatische interacties. Omdat de vesikels zwak gebonden zijn aan het goud, kan de elektrostatische interactie effect hebben op de adsorptie van intacte vesikels, maar is nooit sterk genoeg zijn om een overgang van een intact vesikel naar een geadsorbeerde vlakke bilaag te initiëren. In het geval van DOPC vesikels hebben de elektrostatische wisselwerkingen een verwaarloosbaar effect.

De organisatie van eiwitten in lipide bilagen is een belangrijk onderzoeksgebied in de moleculaire biologie. We hebben geprobeerd inzicht te krijgen in de gevolgen van het invoegen van een membraan overspannend object in de lipide bilaag. Onze resultaten kunnen belangrijk zijn met betrekking tot transmembraaneiwitten met verscheidene α-helixen, omdat de bilaag structuur op korte afstanden tussen deze membraanoverspannende helixen rechtstreeks invloed heeft op de quaternaire structuur van deze eiwitten. Natuurlijk moet er wel rekening mee worden gehouden dat er buiten de in dit proefschrift besproken kwesties talrijke andere moleculaire specifieke aspecten een rol spelen.

De adsorptie van lipide vesikels aan een oppervlak heeft de laatste decennia veel aandacht getrokken. Een toepassing is o.a. het maken van een geadsorbeerde vlakke bilaag op een oppervlak omdat deze gebruikt kan worden om een membraan te bestuderen of bijv. in een biosensor.

We hebben door systematisch experimenteren en met behulp van modelberekingen meer inzicht gekregen in de wisselwerking tussen vesikels en een oppervlak en de gevolgen daarvan op de lipide-bilaag structuur. Dit begrip zal bijdragen aan het ontwikkelen van methoden om vesikeladsorptie op een gecontroleerde manier te laten plaatsvinden voor allerlei toepassingen en om de wisselwerking en fusie van vesikels, gecontroleerd in een grensvlak, te bestuderen.

Dankwoord

Dit proefschrift is voortgekomen uit onderzoek dat ik de afgelopen vier jaar met veel plezier heb gedaan aan de leerstoelgroep Fysische chemie en kolloïdkunde. In deze tijd heb ik veel verschillende mensen ontmoet en ik kan zeggen dat het een inspirerende periode uit mijn leven is geweest.

Om te beginnen wil ik mijn copromotor Mieke Kleijn en promotoren Frans Leermakers en Martien Cohen Stuart bedanken voor hun hulp tijdens de afgelopen vier jaar en het feit dat ze altijd voor me klaar stonden. Mieke heeft mij op vele manieren bijgestaan, onder andere door de vele gesprekken en discussies die we hebben gehad. Frans heeft mij in de wereld van het modelleren getrokken. In eerste instantie was ik nogal huiverig om hier in te stappen, maar op aandringen van Frans heb ik deze stap toch gezet en daar ben ik hem achteraf dankbaar voor. Ook wil ik mijn andere promotor Martien bedanken voor zijn bijdrage aan mijn onderzoek. Ondanks dat dit contact een stuk minder frequent was, kwam Martien toch vaak met een verfrissend nieuw idee om een probleem te benaderen.

Verder wil ik Anton, Gert, Remco, Willem, Mara, Ben en Ronald bedanken voor het feit dat ze altijd behulpzaam waren als ik met een vraag of probleem bij ze kwam. Ook de medewerkers van de werkplaats wil ik bedanken voor de hulp bij het ontwerpen en maken van verschillende onderdelen die ik nodig had om te meten.

Tevens wil ik enkele mensen van het laboratorium van Plantencelbiologie bedanken voor de discussies die we regelmatig met elkaar hadden. De gespekken met Agnieszka, Andre, Henk, en natuurlijk Anne Mie waren altijd iets om naar uit te kijken.

Zoals eerder gezegd was het altijd erg gezellig op de leerstoelgroep. Het zou een erg lange lijst worden als ik iedereen zou moeten opnoemen, maar bij deze wil ik iedereen bedanken voor een periode in mijn leven waar ik met zeer warme gevoelens op terugkijk. Door de vele tripjes, activiteiten en borrels hing er altijd een zeer vriendschappelijke sfeer die ik niet snel vergeten zal.

Ook wil ik Jan bedanken voor het feit dat ik in de laatste maanden van mijn promotie onderzoek lekker kon ontspannen en mijn gedachten verzetten door lekker samen te gaan stappen of tot diep in de nacht te pokeren. Rutger, jouw positieve instelling en de vele goede gesprekken die we hebben gehad zijn mij zeer dierbaar. Ook Nique wil ik noemen omdat we elkaar zo lekker voor de gek kunnen houden omdat we elkaar zo goed begrijpen. Tenslotte wil ik ook Richard, die ik al zo

ongeveer mijn hele leven ken, bedanken voor de vele ervaringen die we samen hebben gehad. We zien elkaar de laatste tijd niet zo vaak, maar dat komt wel weer.

Anita wil ik speciaal bedanken omdat zij de afgelopen vier jaar een erg belangrijke rol in mijn leven heeft gespeeld. We hebben een relatie gehad met ups en downs, maar het was nooit saai. Wat ik wel weet is dat zij een heel bijzonder mens is. Ongelofelijk positief, heerlijk eigenwijs en een echte levensgenieter die enorm veel warmte geeft aan de mensen om haar heen. Kortom een diamantje zoals er maar weinig zijn met ook nog eens twee kleine diamantjes, namelijk Lotte en Anouk.

Natuurlijk wil ik Patrick bedanken omdat hij altijd een belangrijke rol heeft gespeeld in mijn leven. Ondanks dat we elkaar momenteel niet zo heel vaak zien is hij een van de weinige zekerheden in mijn leven waar ik altijd van op aan kan en van wie ik weet dat hij mij echt begrijpt en altijd achter me staat.

Tenslotte wil ik mijn ouders, Leen en Anneke, bedanken voor al hetgeen ze mij hebben gegeven in het leven. Er zijn maar weinig mensen die zoveel over hebben voor hun kinderen als jullie en daar ben ik erg dankbaar voor. Ondanks dat ik het jullie niet altijd even gemakkelijk heb gemaakt, hebben jullie mij altijd gesteund en zijn jullie er altijd voor mij geweest. Ik had me geen betere ouders kunnen wensen. Ik hou van jullie.

List of publications

Visualization of highly ordered striated domains induced by transmembrane peptides in supported phosphatidylcholine bilayers.
H.A. Rinia, R.A. Kik, R.A. Demel, M.M.E. Snel, J.A. Killian, J.P.J.M. van der Eerden and B. de Kruijff *Biochem.* 39 (19): 5852-5858 2000

Domain formation in phosphatidylcholine bilayers containing transmembrane peptides: Specific effects of flanking residues.
H.A. Rinia, J.W.P. Boots, D.T.S. Rijkers, R.A. Kik, M.M.E. Snel, R.A. Demel, J.A. Killian, J.P.J.M. van der Eerden and B. de Kruijff *Biochem.* 41 (8): 2814-2824 2002

Bending moduli and spontaneous curvature of the monolayer in a surfactant bilayer.
R.A. Kik, J.M. Kleijn and F.A.M. Leermakers *J. Phys. Chem. B* 109 (30): 14251-14256 2005

Molecular modeling of lipid bilayers and the effect of protein-like inclusions.
R.A. Kik, F.A.M. Leermakers and J.M. Kleijn *Phys. Chem. Chem. Phys.* 7 (9): 1996-2005 2005

Molecular modelling of peptide-like inclusions in lipid bilayers: Lipid-mediated peptide-peptide interactions.
R.A. Kik, F.A.M. Leermakers and J.M. Kleijn *Submitted*

Effect of size, rigidity and bilayer surface interaction on the adsorption of lipid vesicles: Experimental study and self-consistent field model calculations.
R.A. Kik, F.A.M. Leermakers and J.M. Kleijn *Submitted*

Adhesion of phospholipid vesicles to gold: Effect of ionic strength, pH and applied potential.
R.A. Kik, F.A.M. Leermakers, J.M. Kleijn and M.A. Cohen Stuart *To be submitted*

Curriculum vitae

Richard Kik werd geboren op 19 augustus 1971 te Eindhoven. Nadat hij in 1989 aan het Augustinianum te Eindhoven zijn HAVO diploma in ontvangst nam, begon hij de studie HLO chemie aan de Hogeschool Eindhoven. Deze werd in 1995 afgerond en in het jaar daarop ging hij scheikunde studeren aan de Universiteit Utrecht. Zijn afstudeeronderzoek deed hij bij de sectie biochemie en membranen van de faculteit Scheikunde, waar hij de insertie van synthetische peptiden in lipiden bestudeerde met behulp van de atomaire krachten microscoop. Na het afronden van deze studie in 2000 was hij ongeveer twee jaar werkzaam als programmeur bij Spherion Technology. Hier hield hij zich bezig met het ontwikkelen en onderhouden van mainframes bij verschillende bedrijven. In 2002 begon hij aan de Wageningen Universiteit met een promotie onderzoek bij het Laboratorium voor Fysische Chemie en Kolloïdkunde. Hier hield hij zich bezig met de interactie van lipiden bilagen met oppervlakken. Zowel theoretisch als experimenteel onderzoek over dit onderwerp heeft geresulteerd in dit proefschrift.

Education activities

- Colloquia (WUR), Wageningen, The Netherlands, 2002-2006

- Workgroup meetings (WUR-PCC), Wageningen, The Netherlands, 2002-2006

- Molecular modelling (WUR-PCC), Wageningen, The Netherlands, 2003

- Colloïd chemistry (WUR-PCC), Wageningen, The Netherlands, 2003

- Physical chemistry winterschool 'Dynamics', Han sur Lesse, Belgium, 2003

- AMC Conference (AMC), Amsterdam, The Netherlands, 2003

- Physical chemistry winterschool "Statics', Han sur Lesse, Belgium, 2004

- Dutch polymer days (PTN), Lunteren, The Netherlands, 2004-2006

- Vloeistoffen en Grensvlakken (NWO), Lunteren, The Netherlands, 2004-2006

- Julich Soft Matter Days (IFF), Kerkrade, The Netherlands, 2004

- Molecular and cellular biophysics meeting (ALW/FOM/VvBF&BT), Lunteren, The Netherlands, 2004

- Seminar series plant cell biology (WUR-PCB), Wageningen, The Netherlands, 2005

- Caput college (WUR-PCC), Wageningen, The Netherlands, 2005

- Liquid matter conference (EPS), Utrecht, The Netherlands, 2005

- European student conference (WUR-PCC), Biezenmortel, The Netherlands, 2005

- ECIS conference (ECIS), Oslo, Norway, 2005